2004

Development of superconducting magnesium diboride conductors

Saeid Soltanian
University of Wollongong, saeid@uow.edu.au

DEVELOPMENT OF SUPERCONDUCTING MAGNESIUM DIBORIDE CONDUCTORS

A thesis submitted in fulfillment of the requirements for the award of the degree

DOCTOR OF PHILOSOPHY

from

UNIVERSITY OF WOLLONGONG

by

SAEID SOLTANIAN, B. Sc., M. Sc.

Institute for Superconducting & Electronic Materials

Faculty of Engineering

2004

DECLARATION

This is to certify that the work presented in this thesis was carried out by the candidate in the laboratories of the Institute for Superconducting and Electronic Materials (ISEM), at the University of Wollongong, NSW, Australia, and has not been submitted for a degree to any other institution for higher education.

Saeid Soltanian

2004

ACKNOWLEDGMENTS

I would like to express my most sincere appreciate and gratitude to my supervisors, Prof. S. X. Dou and Dr. X. L. Wang for their unceasing academic guidance, encouragement and support during my PhD study in ISEM at the University of Wollongong.

I would also like to give my sincere thanks to Prof. H. K. Liu for her kind supports, Dr. J. Horvat, Dr. M. J. Qin for their continuing contribution to measurements, and to Dr. M. Ionescu, Dr. A. V. Pan and Dr. K. Konstantinov for their useful discussion and suggestions.

I would also like to express my gratitude to Prof. E. W. Collings, Prof. E. Babić, Prof. D. Larbalestier, Dr. I. Kušević, Dr. M. Sumption, Dr. V. Braccini, Dr. S. Li, Dr. P. R. Munroe, Prof. J. A. Ahn and Mr. M. Tomsic for their great collaboration and contribution to transport and magnetic measurements and to providing TEM images, as well as providing chemicals.

My special thanks are given to Dr. T. Silver for her kind help in proofreading and correcting the English in the manuscripts of my papers and this thesis.

Great thanks go to all my friends at ISEM and all the members and technicians at the Faculty of Engineering especially Mrs. B. M. Allen, Mr. R. Kinnell, Mr. G. Tillman and Mr. N. Mackie for their friendly help and assistance in using the facilities.

I would also like to acknowledge the University of Kurdistan in Sanandaj and the Ministry of Science, Research and Technology of Iran for providing my PhD scholarship.

Finally I wish to thank my wife Mino and my sons Amin and Hossain for their patience, support and encouragement.

CONTENTS

ABSTRACT

The work in this thesis concentrates on the fabrication and characterization of MgB_2 superconducting bulk wire and tape. An overview of the research on MgB_2 superconductor during the last three years is also provided.

High transport and magnetic critical current density values above 10^5 A/cm^2 have been obtained for metal-clad wires and tapes. Fe-clad MgB_2 tapes were fabricated using a powder-in-tube technique. The tape shows a sharp transition with a transition width ΔT_c of 0.2 K and a T_{c0} of 37.5 K. An high transport critical current value of 1.7×10^4 A/cm^2 for both 29.5 K in 1 Tesla and 33 K in zero applied field has been achieved. The effects of sintering time and temperature on the formation and critical current densities of Fe-clad MgB_2 wires is also investigated. MgB_2 wires were sintered for different periods of time at predetermined temperatures. In contrast to the common practice of sintering for several hours, results show that there is no need for prolonged heat treatment in the fabrication of Fe/MgB_2 wires. A total time in the furnace of several minutes is enough to form nearly pure MgB_2. J_c of 4.5×10^5 A/cm^2 in zero field and above 10^5 A/cm^2 in 2 T at 15 K has been achieved for Fe/MgB_2 wires sintered for a short time. These findings substantially simplify the fabrication process, making it possible to have a continuous process for fabrication and reducing the costs for large-scale production of MgB_2 wires.

Ag and Cu clad MgB_2 wires were also fabricated using an *in-situ* reaction method. The effects of a shorter than usual sintering on the critical current densities of Ag and Cu clad MgB_2 wires were studied. For Ag clad wire J_c is improved by more than two times after the short period sintering process. J_c values of 1.2×10^5 A/cm^2 in zero field and above 10^4 A/cm^2 in 2 T at 20 K have been achieved for Ag clad MgB_2 wire which is only sintered for a few minutes at 800 ^{o}C. However, a remarkable degree of reaction has been found between the superconducting cores and the sheath materials, leading to the formation of Cu_2Mg and Ag_3Mg for copper and silver clad wires, respectively. The results show that the short sintering causes less reaction between the magnesium and the sheath materials and markedly improves the critical current density. Our results also show that iron is still the best sheath material for MgB_2 superconductor wire and tape. Sixteen-filament stainless steel/Fe/MgB_2 wires were fabricated by the powder-in-tube method followed by groove rolling. Magnetic critical current densities of 3.4×10^5 A/cm^2

in 0.5 T and about 1.9×10^5 A/cm^2 in 1 T at 5 K were achieved. Results on transport J_c of solenoid coils up to 100 turns fabricated with Cu-sheathed MgB_2 wires using a *wind-reaction in-situ* technique are reported. Despite the low density of the single core and some reaction between the Mg and the Cu-sheath, our results demonstrate that the decrease in transport J_c with increasing length of MgB_2 wires is insignificant. Solenoid coils with diameters as small as 10 mm can be readily fabricated using a wind-reaction in-situ technique. The J_c of coils is essentially the same as for straight wires. J_c values of 133,000 A/cm^2 and 125,000 A/cm^2 at 4 K and self field have been achieved for small coil wound using Cu-sheathed tape and Cu-sheathed wire respectively. The results indicate that the MgB_2 wires have potential for large scale applications.

The effect of chemical doping on the superconductivity and critical current density of MgB_2 superconductor is investigated. Enhancements in the J_c field performance as well as the irreversibility field were obtained due to chemical doping with both C and SiC nano-particles.

Doping $MgB_{2-x}(SiC)_{x/2}$ with x = 0, 0.2 and 0.3 and a 10 wt% nano-SiC doped MgB_2 sample, led to slight decrease in T_c and significantly enhanced H_{c2}, H_{irr} and J_c at high magnetic fields. Compared to the non-doped sample, J_c for the 10 wt% doped sample increased by a factor of 32 at 5 K and 8 T, 42 at 20 K and 5 T, and 14 at 30 K and 2 T. At 20 K, which is considered to be a benchmark operating temperature for MgB_2, the best J_c for the doped sample was 2.4×10^5 A/cm^2 at 2 T, which is comparable to J_c of the best Ag/Bi-2223 tapes. At 20 K and 4 T, J_c was 36,000 A/cm^2, which is an order of magnitude higher than for the Fe/MgB_2 tape. Our results show that there are two distinguishable but closely related mechanisms: increase of H_{c2} and improvement of flux pinning that control the performance of $J_c(H)$ in the samples. SiC-doping introduced many nano-scale precipitates and disorders at B and Mg sites, provoking a high resistivity of ρ(40K) = 300 μΩ-cm (RRR = 1.75) for the SiC-doped sample, leading to significant enhancement of both H_{c2} and H_{irr} with only minor effects on T_c. EELS and TEM analysis revealed impurity phases: Mg_2Si, MgO, MgB_4, BO_x, $Si_xB_yO_z$, and BC at a scale below 10 m and an extensive domain structure of 2-4nm domains in the doped sample which serve as strong pinning centers. The effect of nano-SiC doping on the critical current density and flux pinning of Fe/MgB_2 wires is also investigated. The depression of T_c with increasing SiC doping level remained rather small. High level

SiC doping resulted in a substantial enhancement in the $J_c(H)$ performance. The transport J_c for all the wires is comparable to the magnetic J_c at higher fields despite the low density of the samples. The transport I_c for the 10 wt% doped Fe/MgB_2 wire reached 675 A at 24 K and 1 T (J_c = 140,000 A/cm^2) and 500 A at 20 K and 2T (J_c = 103,000A/cm^2). The transport J_c for the 10wt% SiC doped MgB_2 wire is 30 times higher than for the undoped wire. SiC doped MgB_2 polycrystalline samples were fabricated using different grain sizes (20 nm, 100 nm, and 37 μm) of SiC and different doping levels (0, 8, 10, 12, 15 wt %) in order to investigate the effect of the particle size of the starting SiC powder on the properties of samples. Results show that grain sizes of the starting precursors of SiC have a strong effect on the critical current density and its field dependence. The smaller the SiC grains are, the better the J_c field performance is. Significant enhancement of J_c and the irreversibility field H_{irr} were revealed for all the SiC doped MgB_2 with additions up to 15 wt%. A J_c as high as 20,000 A/cm^2 in 8 T at 5 K was achieved for the sample doped with 10 wt% SiC with a grain size of 20 nm. Results indicate that the nano-inclusions and substitution inside MgB_2 are responsible for the enhancement of flux pinning.

Polycrystalline $MgB_{2-x}C_x$ samples with x=0.05, 0.1, 0.2, 0.3, 0.4 nano-particle carbon powder were prepared using an *in-situ* reaction method under well-controlled conditions to limit the extent of C substitution. It was found that both the *a*-axis lattice parameter and the T_c decreased monotonically with increasing doping level. However, for the sample doped with the highest nominal composition of x=0.4 the T_c dropped only 2.7 K. The nano-C doped samples showed an improved field dependence of the J_c compared with the undoped sample over a wide temperature range. The enhancement by C-doping is not as strong as for nano-SiC doped MgB_2. X-ray diffraction results indicate that C reacted with Mg to form nano-size Mg_2C_3 and MgB_2C_2 particles.

A study of ac susceptibility, magnetic shielding and the sample size effect is presented in Chapter 6. Systematic ac susceptibility measurements were performed on MgB_2 bulk samples. It is shown that the flux creep activation energy is a nonlinear function of the current density $U(J) \propto J^{-0.2}$, indicating a nonlogarithmic relaxation of the current density in this material. The dependence of the activation energy on the magnetic field is determined to be a power law $U(B) \propto B^{-1.33}$, showing a steep decline in the activation

energy with magnetic field, which accounts for the steep drop in the critical current density with magnetic field that is observed in MgB_2.

Magnetic shielding was investigated by means of transport critical current measurements for Fe-sheathed MgB_2 round wires. Strong magnetic shielding by the iron sheath was observed, resulting in a decrease in I_c by only 15% in a field of 0.6 T at 32 K. In addition to shielding, interaction between the iron sheath and the superconductor resulted in a constant I_c between 0.2 and 0.6 T. This was well beyond the maximum field for effective shielding of 0.2 T. This effect can be used to substantially improve the field performance of MgB_2/Fe wires at fields at least 3 times higher than the range allowed by mere magnetic shielding by the iron sheath. The dependence of I_c on the angle between the field and the current showed that the transport current does not flow straight across the wire, but meanders between the grains.

The effect of sample size on the critical current density and the flux pinning of pure and SiC doped MgB_2 bulk samples has been investigated. At high fields a systematic degradation of magnetic J_c and H_{irr} was observed as the sample size decreased. However, J_c remarkably increased on decreasing the sample volume at low magnetic fields below 1 T. The SiC doped samples show less sample size effect than the pure samples, indicating a larger n-factor and therefore a stronger pinning effect due to SiC doping.

List of Figures

List of Tables

CHAPTER 1: INTRODUCTION

Superconductivity has been an exciting, fascinating and challenging topic for almost one century. This phenomenon was observed for the first time by a brilliant Dutch physicist. Heike Kamerlingh Onnes, a professor of physics at the University of Leiden, successfully liquefied Helium in 1908 and was subsequently able to reduce the temperature of liquid helium down to as low as 0.9 K. He had intended to measure the resistivity of metals as a function of temperature at very low temperatures. By measuring the resistivity of Mercury, as a high purity metal at the time, he found in 1911 that the electrical resistivity of Mercury abruptly dropped to zero, the lowest measurable value, when the sample was cooled below 4.2 K [1]. Onnes realized that the new phenomenon represented a new physical state and termed it the *superconductive state*. In 1913, he won a Nobel Prize in Physics for his research in this field. His further investigation showed that other metals such as tin and lead also enter the superconducting state if they are cooled below 3.8 K and 7.2 K, respectively [2]. The temperature at which the transition from the normal state to the superconducting state occurs was called the *critical temperature* (T_c). Onnes also observed that although it was possible to pass a huge electric current through the superconducting mercury sample, there was a threshold value for the current density above which the sample would return to the normal state [3]. This threshold value, which is extremely important for practical applications is called the *critical current density* (J_c). Moreover, Onnes also discovered that magnetic fields higher than H_c, the *critical magnetic field*, can similarly destroy the superconducting state.

For many years the study of the low temperature properties of materials led to the observation of the superconductivity in many metals and alloys.

In 1933, Walther Meissner and his student Robert Ochsenfeld discovered an important magnetic property of superconductors. They observed that a magnetic field lower than H_c was suddenly expelled by superconductor specimens on cooling below T_c [4]. In other words, the material becomes fully diamagnetic in the superconducting state. This is called the *Meissner effect* and was found to be an intrinsic property of superconductors. It has been widely used for the testing the superconducting state. Due

to the Meissner effect, if an external magnetic field is applied to a sample which is in the superconducting state, an electric current is produced near the surface of sample, in such a way as to create a magnetic field that exactly cancels the external magnetic field.

In 1935, Fritz and Heinz London theoretically explained the Meissner effect by positing two groups of electrons in a superconducting material, the superconducting electrons and the normal state electrons. They employed the Maxwell equations to develop a set of electrodynamics equations, called the *London equations* [5]. According to the London equations, the magnetic field exponentially falls off with increasing distance from the surface of a superconducting sample. The characteristic decay length is called the *London penetration depth* (λ).

In 1950 V. Ginzburg and L. Landau developed a theoretical explanation for superconductors based on general symmetry properties [6]. Although the *Ginzburg-Landau theory* explained the macroscopic properties of superconductors, the microscopic properties remained unsolved.

Seven years later, three physicists at the University of Illinois in Urbana, John Bardeen, Leon Cooper and Robert Schrieffer, presented a theoretical explanation for the superconducting state [7]. This theory was widely accepted and is well known as the *BCS theory*. Based on this theory, despite the Coulomb repulsive forces between the electrons, due to distortion in the crystal structure (phonon mediation), slight attraction between pairs of electrons located near the Fermi surface leads to the production of bonded pairs of electrons, called *Cooper pairs* [8]. The size of a Cooper pair in a superconductor is known as the *coherence length* (ξ). The BCS theory explained superconductivity in the low temperature and low magnetic field regime. Soon after that, the BCS theory was extended and become useful for high magnetic fields as well [9].

Alexei Alekseevich Abrikosov theoretically investigated the properties of superconductors in external magnetic fields. In 1957 he discovered that superconducting materials can be separated into two groups, *type-I* and *type-II superconductors* [10]. His brilliant predictions were experimentally confirmed about three years later. In type-II superconductors there are two critical fields, the *lower critical field* (B_{c1}) and the *upper critical field* (H_{c2}). If the external magnetic field is lower than B_{c1}, the field is

completely expelled and the material behaves the same as a type-I superconductor. By increasing the field above B_{c1} up to B_{c2}, the flux partially penetrates into the superconductor as *vortices*. As the field increases above B_{c2}, the flux totally penetrates the whole sample, and it returns to the normal state.

In 1962 Brian D. Josephson, a 22 years old British student at Cambridge University, predicted that via a tunneling process, electric current could flow between two superconducting materials separated by a thin (a few nano-meter thick) insulating layer or weak link [11]. Later, his prediction was experimentally confirmed and became known as the *Josephson effect*. This phenomenon is widely used in applications of superconductors.

A significant breakthrough was made in 1986 by Georg Bednorz and Alex Müller, at the IBM Laboratory in Rüschlikon, Switzerland, when they made a ceramic superconductor from lanthanum, barium, copper, and oxygen with a transition temperature of 35 K [12]. Subsequently, by substitution of yttrium for lanthanum another ceramic superconductor with a transition temperature of 92 K was discovered [13]. This was significant because it now became possible to use cheap liquid nitrogen as the refrigerant. Since the transition temperature of the material was considerably higher than those of the old superconductors, they called these materials the *High Temperature Superconductors* (HTS).

Further investigation led to the synthesis of a new Tl-Ca-Ba-Cu-O superconductor with a T_c value of 120 K in 1988 [14]. In 1993 the mercury based oxide superconductor $HgBa_2Ca_2Cu_3O_8$ with a T_c of 133 K was discovered [15]. By the partial substitution of thallium for mercury in this material, the T_c value increased to 138 K for a superconductor with the nominal composition of $Hg_{0.8}Tl_{0.2}Ba_2Ca_2Cu_3O_{8+x}$ [16].

In terms of applications of high temperature superconductors in polycrystalline form, most efforts to date have been concentrated on two main groups of materials, YBCO [13] and BSCCO [17]. In the first group, $YBa_2Cu_3O_7$ (Y123) has a T_c value of 93 K. The superconducting materials in the second group can be synthesized in three different phases, $Bi_2Sr_2CuO_x$ (Bi-2201), $Bi_2Sr_2CaCu_2O_x$ (Bi-2212) and $Bi_2Sr_2Ca_2Cu_3O_x$ (Bi-2223).

Although a single crystal of YBCO has quite an high critical current density and strong flux pinning, it was very soon confirmed that the polycrystalline form of this superconductor cannot be used due to *weak links*. Grain boundaries between grains that are misaligned by more that 10 degrees are not effectively transparent to current flow and act as strong barriers to current [18]. In the BSCCO group, so far Bi-2223 with a T_c value of 110 K has been the most promising compound. The grains in this material can be very well aligned by careful mechanical and thermal processing.

The discovery of superconductivity at 39 K in MgB_2 was first announced by Prof. J. Akimitsu in Jan. 2001 at the Symposium on Transition Metal Oxides in Sendai, Japan and published in *Nature* [19]. For the first few months of 2001, groups all over the world attempted to understand the properties of this new intermetallic superconductor. T_c was interestingly high compared to the other binary superconductors, almost twice as high as the highest T_c previously reported, 23 K in Nb_3Ge. Such a high T_c attracted great interest in clarifying the mechanism of superconductivity in this material, since some theorists proclaimed that a transition temperature higher than 23 K was not possible [20]. On the other hand, although the transition temperature of MgB_2 was only 39 K, indeed much lower than the T_c of 134 K attained by mercury based high-T_c superconducting cuprates (HTS), MgB_2 superconducting wire and tape were quickly prepared by many groups. The biggest motivation to use MgB_2 conductors for power applications is the cost of this superconductor [21]. Despite the low cost of cooling the HTS with liquid nitrogen, the available HTS conductors, made from BSCCO, consume a large amount of expensive silver, about 70% by volume [21]. However MgB_2 is a quite simple compound made of relatively low cost elements. It also can be cooled to a practical temperature by inexpensive and readily available closed-cycle cryocooler systems. In addition, the large coherence length, low anisotropy, strong grain connectivity, and high critical current density of MgB_2 make this superconductor a good candidate for practical applications.

In this thesis, we study the preparation and characterization of MgB_2 superconductor bulk, wire and tape. Our main focus is on possible ways to improve its properties to push it toward practical applications. We have developed techniques to prepare high quality MgB_2 samples. The standard powder-in-tube technique was used to prepare mono-and multi-filamentary wire and tape. Cu, Ag, Fe and stainless steel were used as

sheath materials. Fe appears to be the most suitable sheath material among them, not only because of less reaction with the superconducting core, but also because it partially shields the superconducting core against an external magnetic field. It was found that pure MgB_2 superconductor is not very suitable for practical applications due to low flux pinning and low upper critical field. The poor flux pinning in pure MgB_2 samples that leads to steep decreases in J_c as the magnetic field increases was also confirmed by ac susceptibility measurements. However, we show that the high field critical current density, the upper critical field, and H_{irr} can be improved by chemical doping. Both C and SiC nano-particle doping are shown to significantly improve the J_c field performance, making the materials suitable for practical applications. We have also shown that the H_{irr} and zero field J_c are strongly dependent on the sample size in both pure and SiC-doped polycrystalline samples. However, SiC-doped sample show a much lower sample size effect compared to pure samples.

References.

1. Kamerlingh Onnes, H., *The Superconductivity of Mercury.* Comm. Phys. Lab. Univ. Leiden, 1911. **122 and 124**: p. 1226.

2. Kamerlingh Onnes, H., *The sudden disappearance of the ordinary resistance of tin, and the super-conductive state of lead.* Comm. Physical Lab. Leiden, 1913. **133d**: p. 51.

3. Kamerlingh Onnes, H., *The potential difference necessary for the electric current through mercury below 4.19 K.* Comm. Physical Lab. Leiden, 1913. **133b**: p. 29.

4. Meissner, W. and R. Ochsenfeld, *Ein neuer Effekt bei Eintritt der supraleitfähigkeit.* Naturwissenschaften, 1933. **21**: p. 787-788.

5. London, F. and H. London, *The electromagnetic equations of the supraconductor.* Proc. Roy. Soc., 1935. **A149**: p. 71-88.

6. Ginzburg, V.L. and L.D. Landau, *On the theory of superconductivity.* Zhurnal Eksperimental'noi I Teoreticheskoi Fiziki, 1950. **20**: p. 1064-1082.

7. Bardeen, J., L.N. Cooper and J.R. Schreiffer, *Theory of superconductivity.* Physical Review, 1957. **108**: p. 1175-1204.

8. Cooper, L.N., *bound electron pairs in a degenerate Fermi gas.* Physical Review, 1956. **104**: p. 1189-1190.

9. Gorkov, L.P., *Theory of superconducting alloys in a strong magnetic field near the critical temperature.* Soviet Physics JETP, 1960. **10**: p. 998-1004.

10. Abrikosov, A.A., *On the Magnetic Properties of Superconductors of the Second Group.* Soviet Physics JETP, 1957. **5**: p. 1174-1182.

11. Josephson, B.D., *Possible new effects in superconductive tunnelling.* Phys. Lett., 1962. **1**: p. 251-253.

12. Bednorz, G. and K.A. Müller, *Possible high T_c superconductivity in the Ba-La-Cu system.* Z. Phys. B, 1986. **64**: p. 189-197.

13. Wu, M.K., J.R. Ashburn, C.J. Torng, P.H. Hor, R.L. Meng, L. Gao, Z.J. Huang, Y.Q. Wang and C.W. Chu, *Superconductivity at 93 K in a new mixed-phase Yb-Ba-Cu-O compound system at ambient pressure.* Physical Review Letters, 1987. **58**(9): p. 908-910.

14. Sheng, Z.Z. and A.M. Hermann. *90 K Tl-Ba-Cu-O and 120 K Tl-Ca-Ba-Cu-O bulk superconductors, Proc.* in *1988 World Congress on Superconductivity*. 1988. Singapore: World Scientific.

15. Cantoni, M., A. Schilling, H.U. Nissen and H.R. Ott, *Characterisation of superconducting Hg-Ba-Ca-Cu-oxides. Structural and physical aspects.* Physica C-Superconductivity and Its Applications, 1993. **215**(1-2): p. 11-18.

16. Dai, P., B.C. Chakoumakos, G.F. Sun, K.W. Wong, Y. Xin and D.F. Lu, *Synthesis and neutron powder diffraction study of the superconductor $HgBa_2Ca_2Cu_3O_{8+d}$ by Tl substitution.* Physica C-Superconductivity and Its Applications, 1995. **243**(3-4): p. 201-206.

17. Maeda, H., Y. Tanaka, M. Fukutomi and T. Asano, *A new high-T_c oxide superconductor without a rare earth element.* 1988. **27**: p. L209-L210.

18. Dimos, D., P. Chaudhari and J. Mannhart, *Superconducting transport properties of grain boundaries in $YBa_2Cu_3O_7$ bicrystals.* Physical Review B, 1990. **41**(7): p. 4038-4049.

19. Nagamatsu, J., N. Nakagawa, T. Muranaka, Y. Zenitani and J. Akimitsu, *Superconductivity at 39 K in magnesium diboride.* Nature, 2001. **410**(6824): p. 63-64.

20. Canfield, P. and G. Crabtree, *Magnesium diboride: Better late than never.* Physics Today, 2003. **56**(3): p. 34-40.

21. Grant, P., *Rehearsals for prime time.* Nature, 2001. **411**: p. 532.

CHAPTER 2: LITERATURE REVIEW

2-1 Introduction

Magnesium diboride is an old material, synthesized and very well known since 1954 [1]. The discovery of superconductivity at 39 K in MgB_2 was first announced by Prof. J. Akimitsu in Jan. 2001 at the Symposium on Transition Metal Oxides in Sendai, Japan. Soon after that many groups all over the world attempted to work on this this new intermetallic superconductor. From an experimental point of view, different aspects have been studied, such as preparation of this superconductor, including the preparation of samples in the form of bulk, wire, tape and thin film, as well as the characterization of samples. At the same time many groups have tried to theoretically explain the properties of this superconductor. Papers daily appear on the cond-mat website providing rapid communications between all groups. More than 900 papers have been submitted to the cond-mat website during the last three years. Also according to the ISI Current Contents Database, until Jan 2004 more than 1300 papers with the title or subject of MgB_2 or magnesium diboride have been published in the international journals. The large amount of published research results reveals the great interest of the research community in this newly discovered material. In this chapter we provide general information about this superconductor and present a brief overview of the research progress in this field.

2-2 Crystal Structure and Superconductivity in MgB_2

MgB_2 has a layered structure with the P6/mmm space group, as shown in Fig. 2-1. It contains graphite-type boron layers that are separated by hexagonal close-packed magnesium layers. Each magnesium atom is located at the center of hexagons of boron atoms. The hexagonal unit cell has the in plane and out of the plane lattice parameters of a = 3.086 Å and c = 3.524 Å, respectively. Both transport and magnetic measurements show that MgB_2 is a superconductor with a transition temperature of about 39 K Fig. 2.

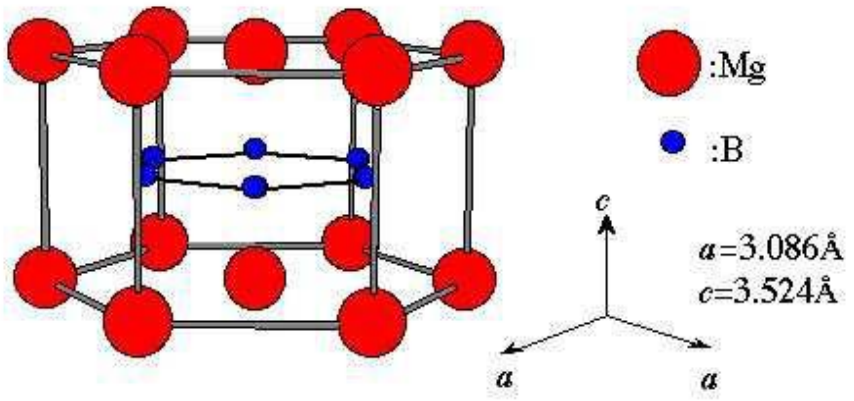

Figure 2- 1: The crystal structure of MgB_2.

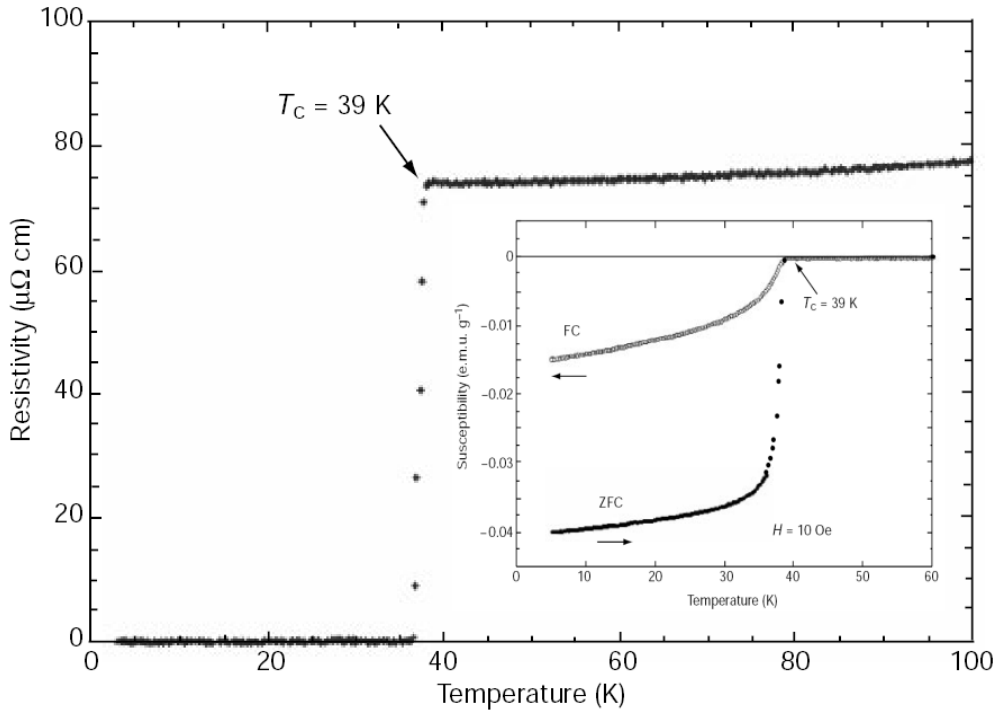

Figure 2- 2: Temperature dependence of the resistivity of MgB_2 under zero magnetic field [2]. Inset is the field dependence of the susceptibility under zero field cooling (ZFC) and field cooling (FC) conditions.

2-3 Overview of Progress on MgB_2

2-3-1 Superconducting Energy Gap

According to the BCS model the value of the superconducting gap is given by $\Delta=1.76 K_B T_c$ [3]. Taking the T_c value of 39 K into account, we obtain a value of Δ=5.9 meV for MgB_2 superconductor. Soon after the discovery of MgB_2 superconductor, the energy band structure of this superconductor near the Fermi energy was theoretically calculated from first principles [4-13]. The band structure of this compound is shown in Fig. 2-3.

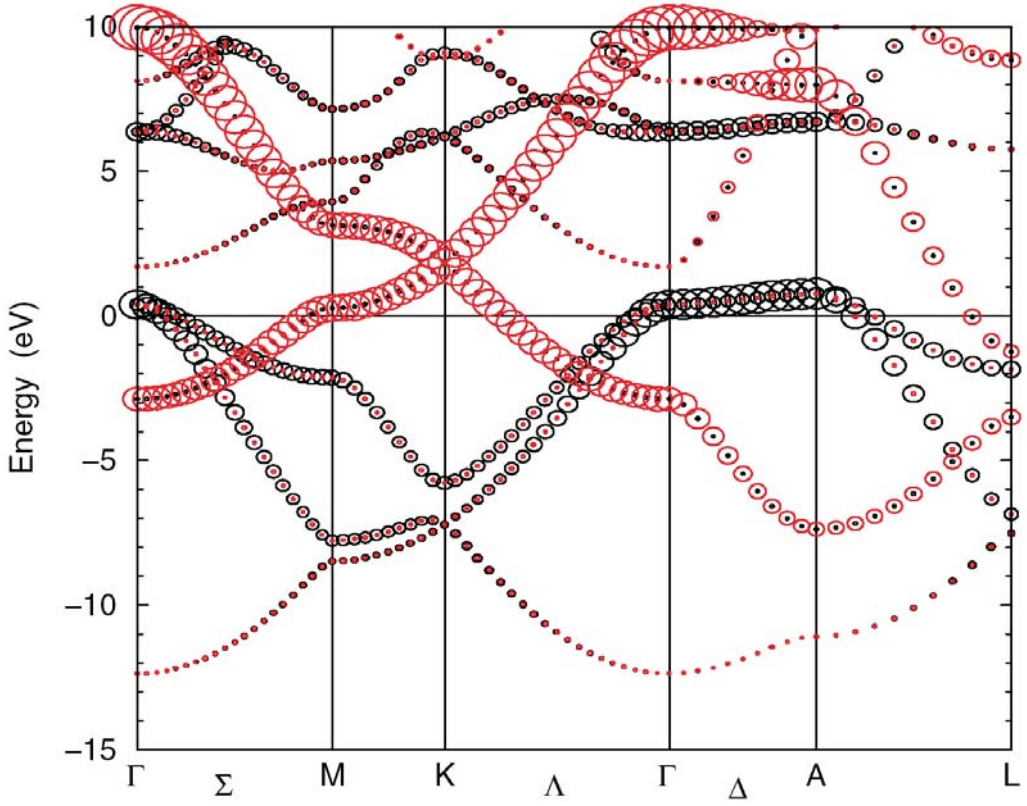

Figure 2- 3: Band structure of MgB_2 superconductor with the B *p* character. The radii of the gray and black circles are proportional to the B p_z and B $p_{x,y}$ character respectively [4].

An early scanning tunneling spectroscopy experiment by Karapetrov et al shows that the value of the superconducting gap in MgB_2 at 4.2 K is 5 meV [14] with a temperature dependence of the BCS form.

Rubio-Bollinger et al. also reported a tunneling spectroscopy experiment [15] in small grains of MgB_2 and a good fit to the BCS model with a gap value of 2 meV was

obtained. To explain such a large discrepancy from the expected value of 5.9 meV they supposed that this value was due to the deviation of the DOS at the surface of superconductor with respect to the bulk. Therefore they supposed that this value of gap corresponded to a critical temperature at the surface of about 13.2 K.

Further experimental studies with different techniques such as specific heat measurements, point contact spectroscopy, Raman spectroscopy, tunneling spectroscopy and Andreev reflection spectroscopy indicate that in contrast to the conventional superconductors, MgB_2 has two different sized superconducting gaps of about $\Delta(0) = 7$ meV for the σ sheets and $\Delta(0) = 2$meV for the π sheets [16-56]. The superconductor gaps decrease with temperature, and both gaps equally become zero at $T=T_c$ as is shown in Fig. 2-4. These results are also supported by theoretical studies [8, 57-60]. It has been shown that the Fermi surface of this compound consists of four bands, two σ-type two-dimensional cylindrical hole sheets and two π-type three-dimensional tubular networks [4, 61, 62] as is shown in Fig. 2-5. This Fermi surface topology is very well confirmed by de Hass-van Alphen experiments as well [63, 64].

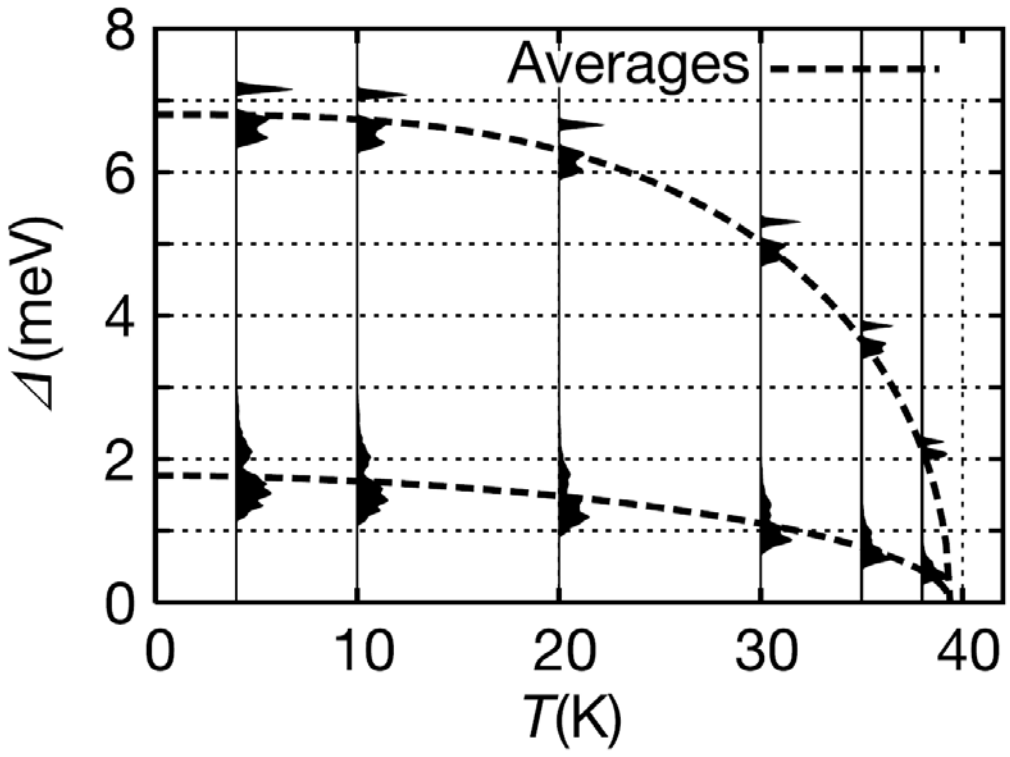

Figure 2- 4: Temperature dependence of superconducting gaps in MgB_2. Vertical solid curves represent the distribution of the superconducting gap values at various temperatures from 4 K to 38 K [60].

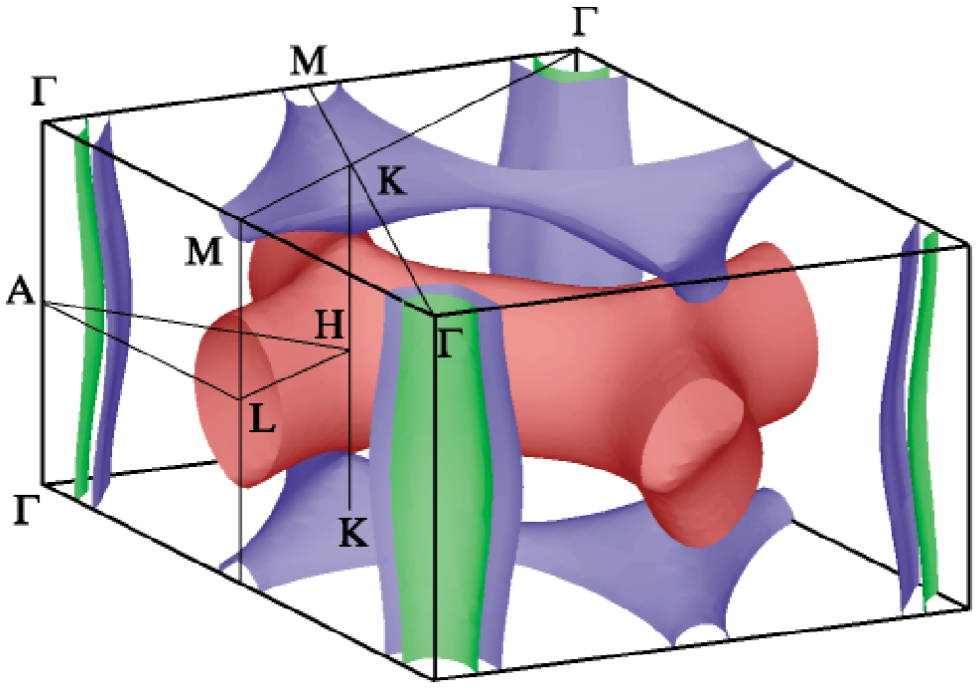

Figure 2- 5: The Fermi surface of the MgB_2 superconductor. The green and blue surface (holelike) comes from the bonding $p_{x,y}$ bands, the blue tubular network (holelike) from the bonding p_z bands, and the red (electronlike) tubular network from the antibonding p_z band. The last two surfaces touch at the *K* point [4].

2-3-2 Hall Effect

The first measurement to evaluate the longitudinal resistivity (ρ_{xx}) and Hall coefficient (R_H) of the polycrystalline MgB_2 sample by Kang et al. shows that R_H is positive in this superconductor for all temperatures above T_c [65], indicating that the charge carriers in MgB_2 are holes. According to their results R_H decreases with decreasing temperature with the value of $R_H = 4.1 \times 10^{-11}$ m^3/C at 100 K (Fig. 2-6). They also showed that $Cot\ \theta_H$ is proportional to $T^{1.8}$ as shown in the inset of Fig. 2-6.

The hole carrier density calculated by this group at this temperature is 1.5×10^{23} $/cm^3$, which is about one order of magnitude larger than the charge carrier density in Nb_3Sn [66] and about two orders of magnitude larger than $YBa_2Cu_3O_y$ [67] at the same temperature. An Hall coefficient measurement of a *c*-axis oriented thin film by the same group confirmed that holes are the charge carriers [68, 69] (Fig. 2-7). In addition, it was found that $Cot\ \theta_H$ linearly increases as a function of T^2 instead of $T^{1.8}$. However a deviation from linearity occurred in the temperature range below 130 K (T^* in Fig. 2-7) [69].

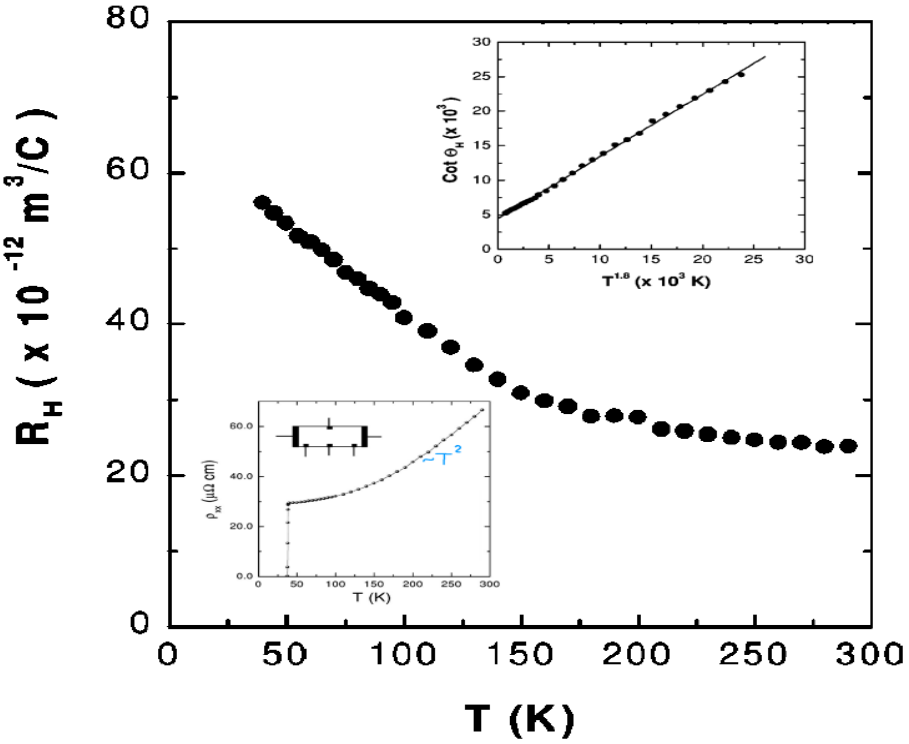

Figure 2- 6: Hall coefficient at 5 K. Top inset is the cotangent of the Hall angle measured at 5 T. The curve shows a nearly $T^{1.8}$ behavior. Bottom inset is the temperature dependence of the ρ_{xx} curve which shows an overall T^2 behavior and a sharp transition near T_c [65].

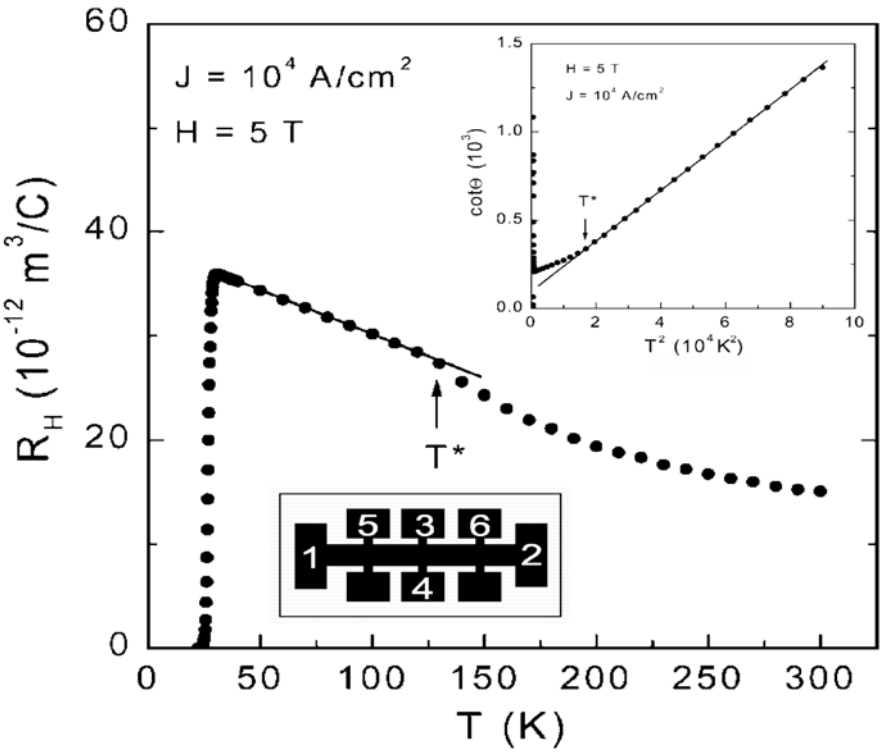

Figure 2- 7: R_H versus temperature of MgB_2 thin films at 5 T. Distinct temperature dependencies of the R_H are evident below and above 130 K. The upper inset is the temperature dependence of $Cot\ \theta_H$ at 5 T. A clear T^2 law was observed above 130 K. The lower inset is a schematic diagram of the Hall-bar pattern. [68, 69]

More measurements by Kang et al. showed no Hall sign anomaly in the mixed state (Fig. 2-8) [68]. Other results reported by this group also indicated a universal scaling law of $\rho_{xy} \propto \rho^{\beta}_{xx}$ with β~2 in the mixed state and ρ_{xy} and ρ_{xx} the longitudinal and Hall resistivities, respectively. These results were in agreement with the experimental results for $Bi_2Sr_2CaCu_2O_8$ single crystal [70] and $Tl_2Ba_2Ca_2Cu_3O_{10}$ thin film[71]. It is also in agreement with the universal Hall scaling theory proposed by Vinokur et al. [72].

However, experimental results reported by Jin et al. showed an unusual Hall effect in the mixed state in superconducting MgB_2 films [73]. In contrast to Kang et al., Jin et al. observed a sign reversal in the measured Hall resistivity versus temperature over a wide range of applied magnetic field up to 8 T, as we can see in Figs. 2-9 and 2-10. An anisotropy in the normal state Hall effect was also observed in the MgB_2 single crystal by Eltsev et al. (Fig. 2-11) [74, 75]. They found a positive in-plane Hall constant (H parallel to the c axis) in agreement with the previous experiments, while they found that the out-of-plane Hall constant (H parallel to *ab* plans) is negative, indicating n-type charge carriers.

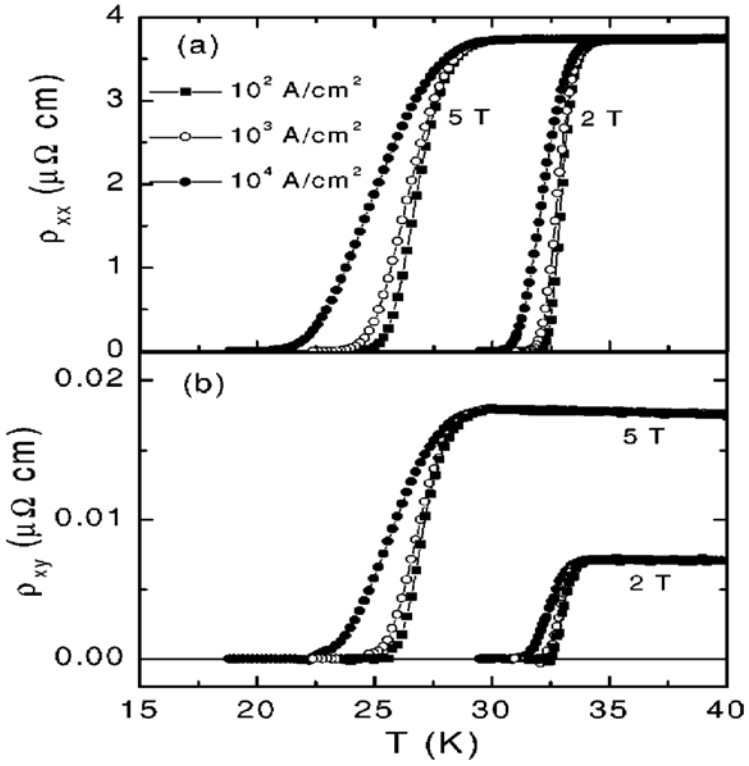

Figure 2- 8: ρ_{xx} (a) and ρ_{xy} (b) measured at applied current densities of 10^2, 10^3, and 10^4 A/cm^2 and for *H*=2 and 5 T. No sign change was observed in the mixed-state, which is in contrast to the HTS case [68].

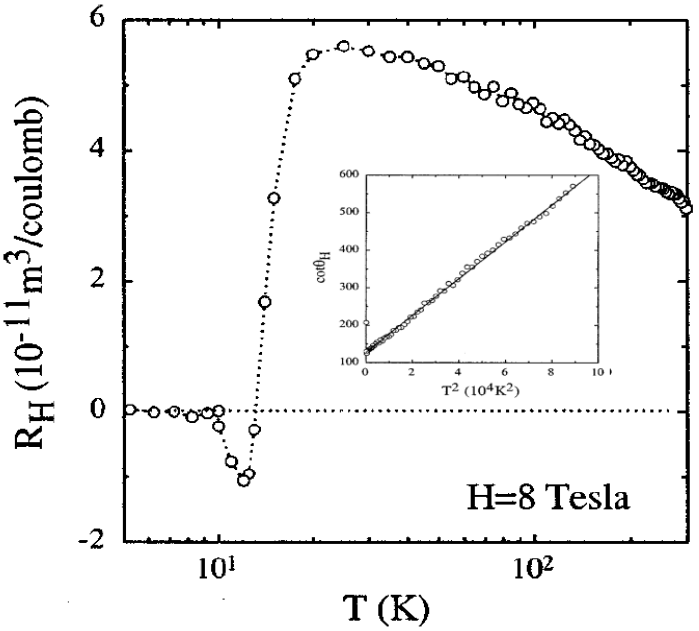

Figure 2- 9: Temperature dependence of R_H (H=8T) of a MgB_2 film plotted on a logarithmic temperature scale. The sign change of R_H in the mixed state can be clearly seen. The inset is the Hall angle $Cot\ \theta_H$ versus the temperature between T_c and 300 K at H=8 T [73].

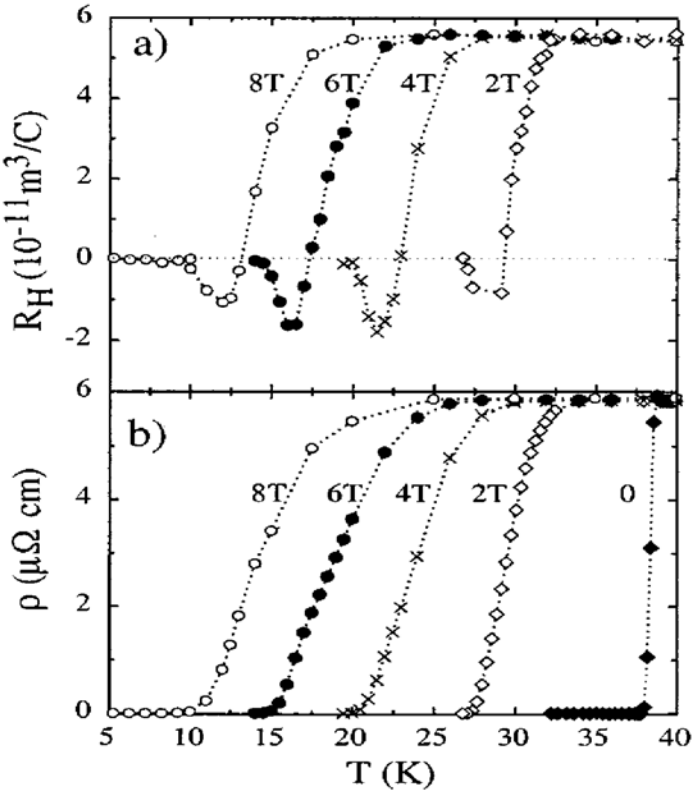

Figure 2- 10: Temperature dependence of (a) R_H and (b) longitudinal resistivity ρ at H=2, 4, 6, and 8 T [73].

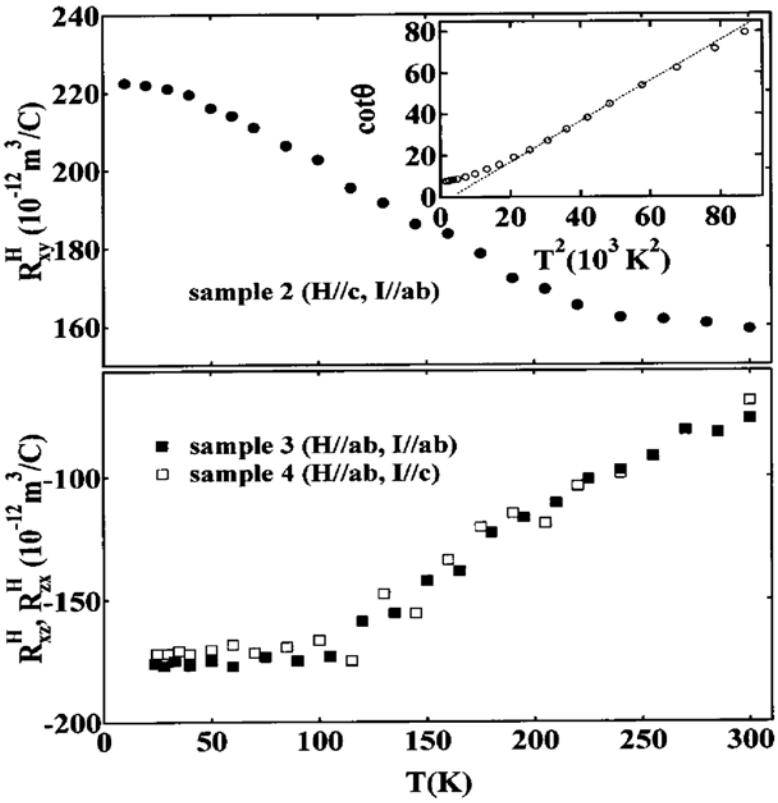

Figure 2- 11: The in- and the out-of-plane Hall constants, as a function of temperature in the normal state of MgB_2 single crystals (top and bottom panels, respectively). Inset: Temperature dependence of *Cot* θ_H at 5 T. The line is a linear fit at intermediate temperatures of 150–220 K [74].

This result was in agreement with the numerical calculations of the independent Hall components of the resistivity tensor for MgB_2 performed by Eltsev et al. (Fig. 2-12) [76]. The anisotropy in the Hall coefficient can be explained as follow: as we saw earlier, the Fermi surface of MgB_2 consists of four bands, two hole-like σ-bands in the form of 2D cylindrical Fermi surfaces and two hole- and electron-like 3D π-bands [4, 8, 9]. In the in plane case (*H* parallel to c), the hole-like carriers dominate the behavior of R_H, resulting in positive values of R_H. On the other hand when *H* is parallel to the *ab* plane (out-of-plane), the σ-bands become less important, and the electron-like carriers dominate the R_H [75-77].

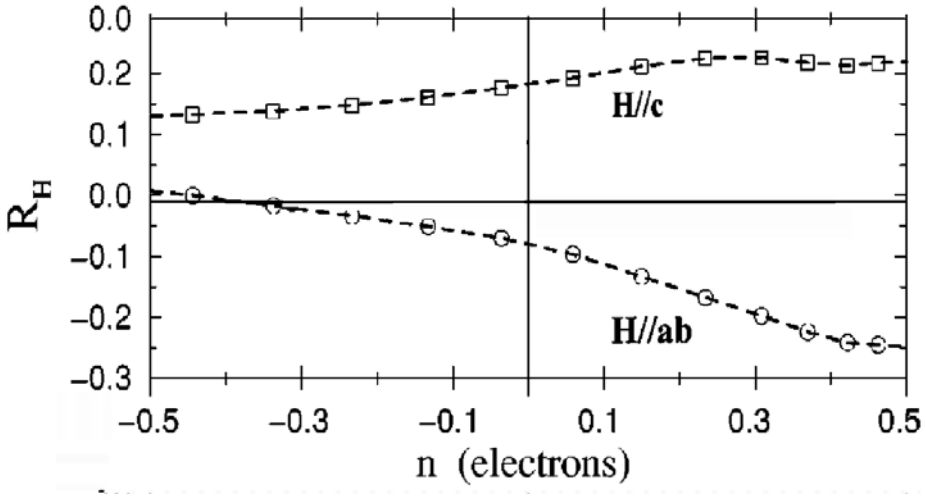

Figure 2- 12: The numerical calculation of transport properties of MgB_2 as a function of doping in a rigid-band scheme [76].

2-3-3 Pressure Effect

Study of the superconducting properties under high pressure is one of the first experiments usually performed after the discovery of a new superconductor. The effect of pressure on the MgB_2 superconductor has been examined by many groups in terms of either change in the transition temperature or change in lattice parameters. Table 2-1 shows a summary of experimental results of the effects of pressure on the T_c of MgB_2 superconductor [78]. As we can see, the experiments have been carried out at pressures as high as 44 GPa. Also, different materials such as He, Fluorinert, NaF and Silicon oil have been utilized as a pressure medium. The experimental results of a few groups are also presented in Fig. 2-13 [79]. It can be seen that T_c monotonically decreases as the pressure is increased, with the measured dT_c/dP values between –0.35 K/GPa [80, 81] and –2 K/GPa [82, 83]. However, a dT_c/dP value of about –1.1 K/GPa is mostly confirmed by experiments. The reduction of T_c under pressure is consistent with a BCS-type pairing interaction mediated by high-frequency boron-boron modes. This indicates that the reduction of the density of states at the Fermi energy, due to the contraction of B-B and B-Mg bonds, dominates the hardening phonon frequencies that can cause an increase in T_c as external pressure is applied [79].

Table 2- 1: Summary of the experimental results of the pressure effects on MgB_2 superconductor single crystal (first 5 rows) and polycrystalline (remaining rows) samples [78].

P_{max} (GPa)	T_c (0) (K)	$(dTc/dP)_0$ (K/GPa)	Measurement	Pressure medium	Sample	Ref.
0.63, 23	38.24	-1.10(3)	χ_{ac}	He	SC	[78]
0.61	38.27	-1.14(3)	χ_{ac}	He	SC	[78]
0.4	37.16	-1.17(4)	χ_{ac}	He	SC	[78]
0.58	37.88	-1.12(3)	χ_{ac}	He	SC	[78]
1.4	38	-2	ρ	Fluorinert	SC	[82]
0.66	39.1	-1.11(2)	χ_{ac} ^{11}B	He	PC	[84]
0.63	39.1	-1.09(4)	χ_{ac} ^{11}B	He	PC	[85]
0.61	39.2	-1.11(3)	χ_{ac} ^{11}B	He	PC	[85]
0.64	40.5	-1.12(3)	χ_{ac} ^{10}B	He	PC	[85]
0.4	37.5	-1.13	χ_{ac}	He	PC	[86]
0.84	39.2	-1.07	χ_{ac}	He	PC	[87]
0.84	37.4	-1.45	χ_{ac}	He	PC	[87]
0.6	37.3	-1.2	χ_{ac}	He	PC	[78]
32.3	39.1	-1.1	χ_{ac} ^{11}B	He	PC	[78]
33	40.2	-1.1	χ_{ac}^{mod} ^{11}B	He	PC	[88]
44	39.2	-1.6	χ_{ac}^{mod} ^{10}B	He	PC	[88]
15	39.1	-1.6	χ_{ac}^{mod} ^{11}B	Fluorinert	PC	[78]
1.84	37.4	-1.6	χ_{ac}	Fluorinert	PC	[89]
28	37.3	-2	χ_{ac}	4:1 methanol/ethanol	PC	[83]
1.46	38.2	-1.36	ρ	1:1 dephne/kerosene	PC	[90]
1.35	37.5	-1.9	ρ	Fluorinert	PC	[91]
1.1	38.3	-1.5(1)	X_{dc}	Kerosene/mineral oil	PC	[92]
9	39	-1.03	ρ	Fluorinert	PC	[93]
40	39	-1.1	X_{dc}		PC	[94]
7.6	37.5	-1.6(increasing)	X_{ac}	NaF	PC	[86]
7.6	37.5	-1.13(decreasing)	X_{ac}	NaF	PC	[86]
11	39	-1.20(9)	ρ	Steatite	PC	[95]
33	~35	-0.35 to –0.8	ρ	Steatite	PC	[80, 81]
0.8	38	-1.18(6)	X_{dc}	Silicon oil	PC	[95]

Changes in the crystal structure and lattice parameters of MgB_2 superconductor under pressure have been studied by many groups [81, 86, 93, 96-100]. Experimental results confirm that MgB_2 remains hexagonal and keeps its crystal structure even at high pressures up to 40 GPa [81]. It is also confirmed by all experimental results that an anisotropy in the compressibility of MgB_2 occurs, with the *c*-axis lattice parameter decreasing faster than the *a*-axis lattice parameter as the hydrostatic pressure increases, indicating that the Mg-Mg (in-plane) bonds are stronger than the Mg-B (out-of-plane) bonds (Fig 2-14) [79]. This anisotropy in the compressibility decreases with pressure as revealed in the inset of Fig. 2-14 [79, 81].

The differences in dT_c/dP as well as in the compressibility values reported by different groups might be due to the different materials utilized in different experiments as the pressure medium, as we can see in Table 2-1 and Figs. 2-13 and 2-14 [78, 79].

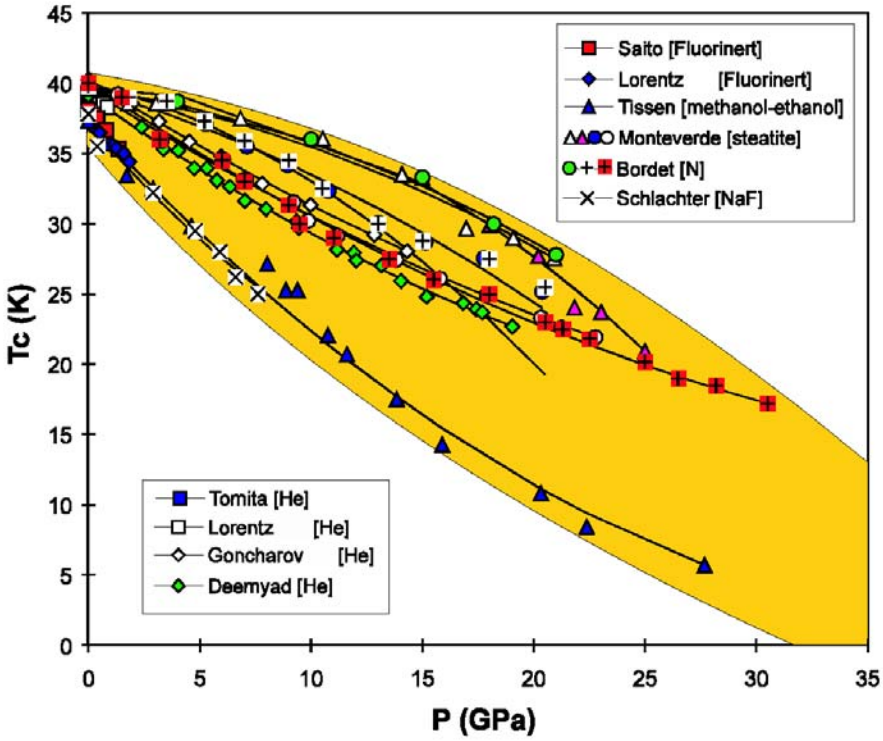

Figure 2- 13: The pressure dependence of T_c of the MgB_2 superconductor [79]. The legends indicate the pressure medium used by each author, Saito [91], Lorentz [87, 89], Tissen [83], Monteverde [80], Bordet [81], Schlachter [86], Tomita [84], Goncharov [100], and Deemyad [85].

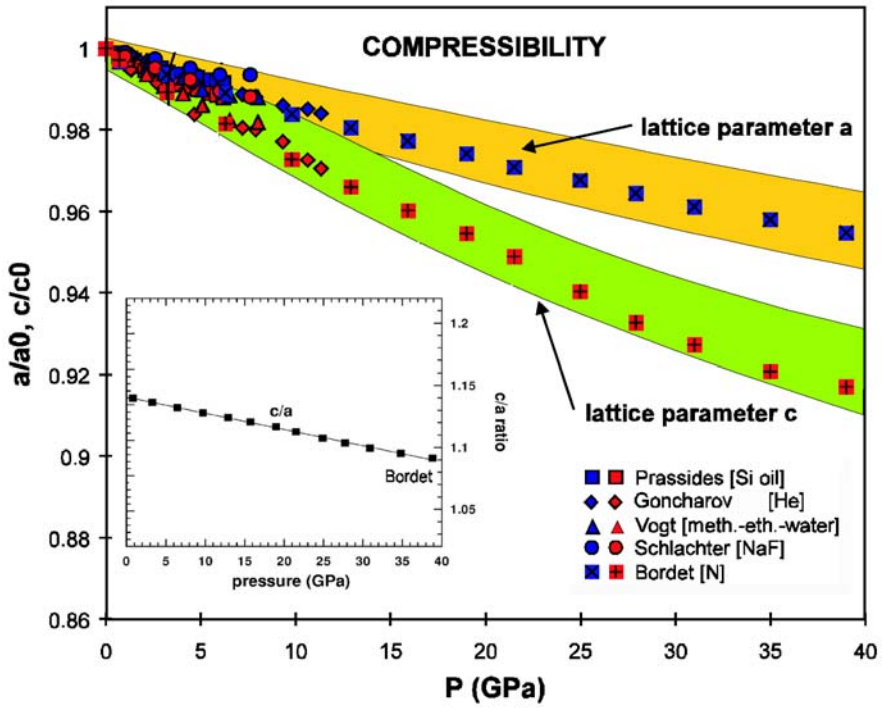

Figure 2- 14: The pressure dependence of the normalized lattice parameters of MgB_2 superconductor. The lattice parameters are normalized to zero pressure values [79]. The legends indicate the pressure medium used by each author, Prassides [98], Goncharov [100], Vogt [96], Schlachter [86], and Bordet [81]. Inset shows the pressure dependence of the ratio between the c-axis lattice parameters and a-axis lattice parameters [81].

2-3-4 Isotope Effect

An isotope effect on a superconductor transition temperature indicates the phonon mediation of superconductor coupling. MgB_2 is a special system with two elements which both have different isotope masses that can change T_c due to substitution of different isotopes. For a single element superconductor, the isotope effect coefficient (α) is defined as $\alpha = d\ln T_c / d\ln M$ or $T_c \propto M^{\alpha}$ [101, 102]. M is an atomic mass, which is different for different isotopes of this superconductor.

For a multi-element superconductor the total isotope effect coefficient is the sum over the individual isotope effects for different masses M_i:

$$\alpha_t = \sum \alpha_i = \sum -\partial \ln T_c / \partial \ln M_i$$

Soon after the discovery of the MgB_2 superconductor, the effect of B isotopes on this superconductor was measured by Bud'ko et al. [103]. They found that measurements of both temperature dependent magnetization and specific heat reveal a 1 K shift in T_c from 39.2 K for $Mg^{11}B_2$ to 40.2 K for $Mg^{10}B_2$ (Figs. 2-15 and 2-16). Also, using the above equation they calculated the boron isotope coefficient to be $\alpha_B = 0.26$ (3), where 3 indicates the error in the last decimal place. These results strongly support the idea that MgB_2 is a phonon mediated BCS superconductor.

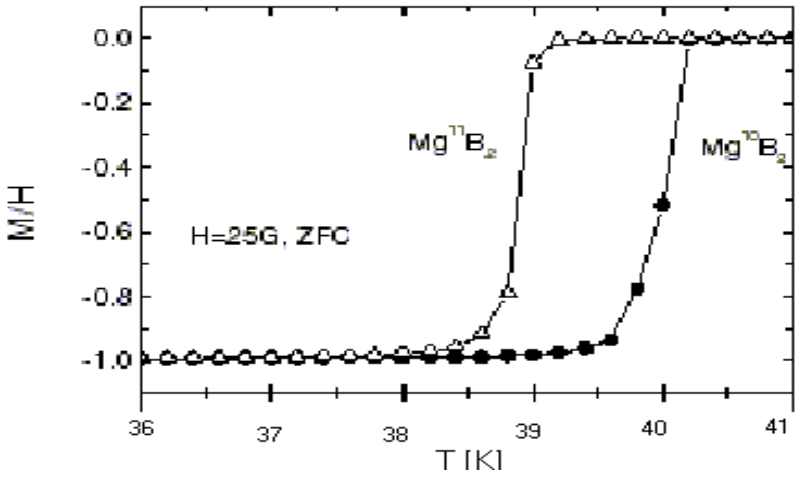

Figure 2- 15: Magnetization divided by applied magnetic field as a function of temperature for $Mg^{10}B_2$ and $Mg^{11}B_2$ [103].

Further studies of the isotope effects of both the Mg and B elements were performed by Hinks et al. [104]. They measured six different samples prepared using ^{10}B, ^{11}B, ^{24}Mg, ^{25}Mg and ^{26}Mg isotopes. Fig. 2-17 shows the superconducting transition for the isotopically substituted MgB_2 samples reported by Hinks et al. [104]. According to their experimental results, the B isotope effect coefficient is $\alpha_B = 0.3$ (1), which was in good agreement with the measurements of Bud'ko et al. On the other hand, they found that Mg isotope has very little effect on T_c. T_c increases by about 0.1 K on substitution of ^{24}Mg with ^{26}Mg. The estimated Mg isotope effect coefficient is $\alpha_{Mg} = 0.02$ (1). Therefore the total isotope effect is $\alpha_t = \alpha_B + \alpha_{Mg} = 0.32$. These results clearly indicate that the phonons involved in the superconductivity of MgB_2 are mainly B phonons, while Mg phonons make very little contribution to the overall pairing.

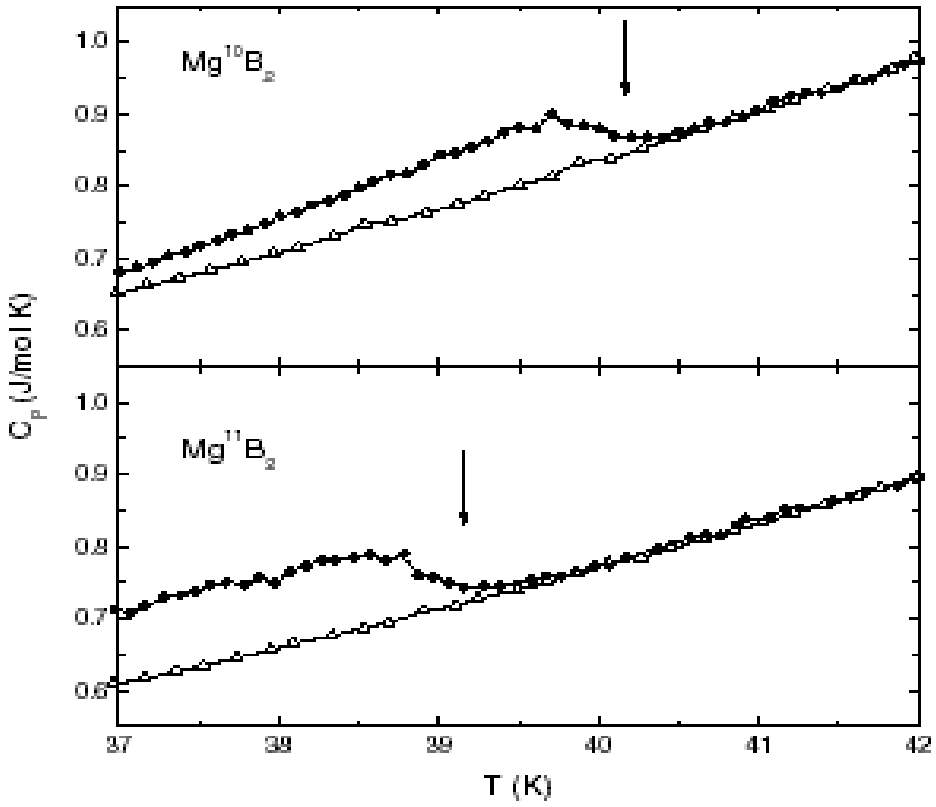

Figure 2- 16: Temperature dependent specific heat of $Mg^{10}B_2$ and $Mg^{11}B_2$ in zero and 90 kG (filled circle and open triangles, respectively) applied magnetic field for temperatures near T_c. Arrows show the transition temperatures [103].

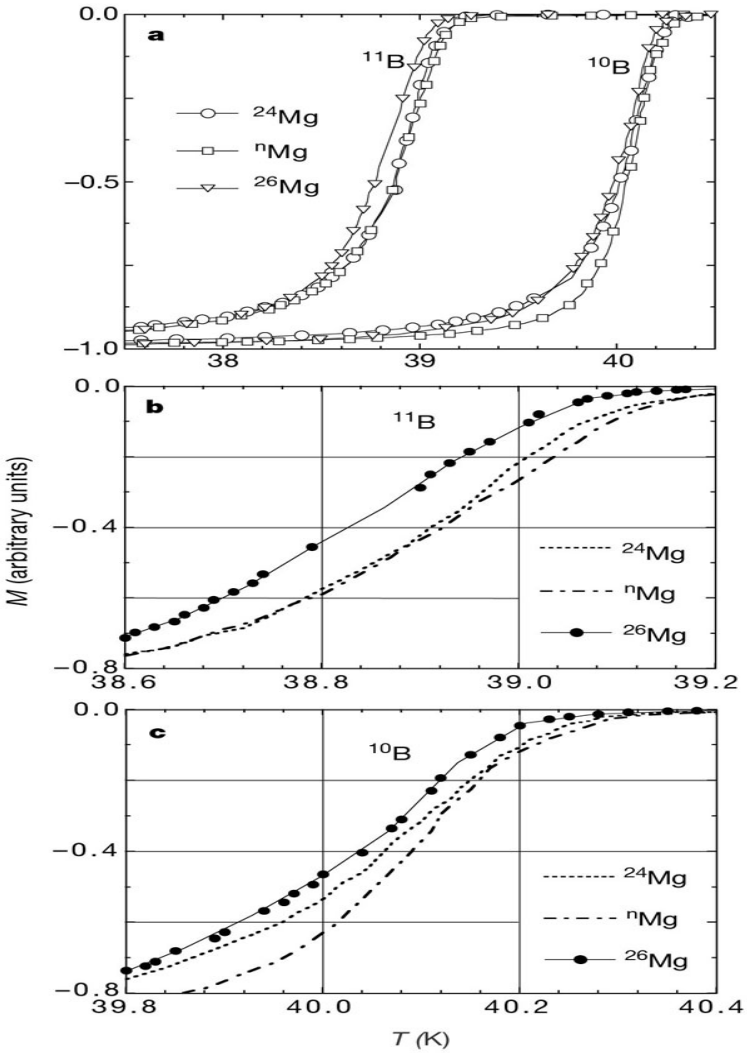

Figure 2- 17: Superconducting transition for the MgB_2 samples substituted by Mg and B isotopes (reported by Hinks et al.) [104]. The magnetization for all samples is shown in (a) (^{n}Mg indicates a sample with natural Mg). (b) and (c) show the small change in superconducting transition due to the substitution of Mg isotopes (the temperature scale is expanded).

The total isotope effect for MgB_2 is much lower than the expected value of 0.5 for a conventional BCS superconductor. Recent calculations [105] show that the reduced isotope effect can be due to the anharmonicity of the planar B optic mode. This idea was confirmed by Choi et al. [59]. By calculation of the isotopic-effect exponent coefficient from the anisotropic Eliashberg equation with anharmonic phonon frequencies, they obtained $\alpha_B = 0.32$ and $\alpha_{Mg} = 0.03$ which are very close to the experimental values. However without anharmonicity they obtained $\alpha_B = 0.46$ and $\alpha_{Mg} = 0.02$, indicating that the low isotope effect exponent coefficient is mainly due to phonon anharmonicity.

2-3-5 Fabrication of MgB_2 Thin Film

Superconducting films are important for electronics applications such as Josephson junctions and superconducting quantum interference devices (SQUID). Many groups have attempted to prepare MgB_2 thin films. However, the high sensitivity of Mg to oxidation, the high volatility of Mg and the large difference between the vapor pressures of Mg and B are the main obstacles to preparation of superconducting MgB_2 films.

MgB_2 thin films have been prepared using the different techniques as listed in Table 2-2. Pulsed laser deposition (PLD) seems to be the most common method for film fabrication among them. High quality films have been prepared using a one step preparation (*in-situ*) or a two step preparation (*ex-situ*) technique. *Ex-situ* techniques consist of deposition of amorphous B (or Mg-B composite) precursors on substrates, then heating the film in a rich Mg vapor. This method has been widely used and has been quite successful in growing high-quality films [106-112]. A few groups have also fabricated MgB_2 film using the *in-situ* or one step technique [113-116].

Each method has its benefits and disadvantage. The two step method gives good crystalline films and good superconducting properties, but cannot be used to fabricate Josephson junctions or multi-layer films. On the other hand, although the *in-situ* method gives films with poorer crystallinity and lower T_c, this method is applicable for multi-layer fabrication. The one step method gives films with a more smooth surface than films made via the two step method, but generally speaking, MgB_2 films have a rough surface morphology compared to $YBa_2Cu_3O_7$ thin films. Therefore, methods need to be improved to be suitable for electronic device applications. However, recently Zeng et al. [117] reported *in-situ* growth of high-quality MgB_2 thin films by using a newly developed technique of hybrid physical–chemical vapor deposition. This is expected to be a very promising growth technique in terms of applications for superconducting electronics.

Different substrates have been used for the deposition of MgB_2 thin films. Appropriate substrate selection is important in order to achieve better lattice matching and less reaction with the superconductor film. It has been reported that MgB_2 reacts with many common substrate materials such as Si, SiO_2, Al_2O_3, SiC and $SrTiO_3$, but no reaction

occurs with ZrO_2 and MgO [118]. To date, various substrates such as sapphire (Al_2O_3) – R and -C, $SrTiO_3$ (100) and (111), SiC (0001), $LaAlO_3$, MgO (100) and Si (100) and (111) have been used to prepare MgB_2 film. Al_2O_3 seems to be the most common substrate used to prepare high quality films. For this substrate, films prepared by Mg diffusion show higher T_c with a sharper transition than other films[79]. Fig. 2-18 which is extracted from reference [79] shows the critical temperature of thin films prepared on different substrates.

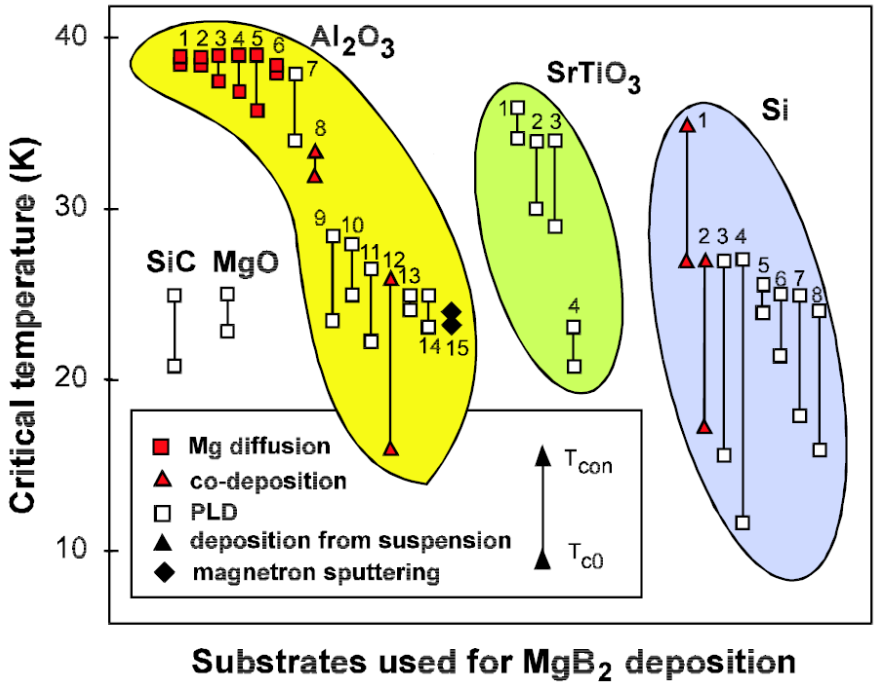

Figure 2- 18: Critical temperature and critical temperature width for MgB_2 films deposited on different substrates. Figure is extracted from ref. [79]. Data are from the references: Al_2O_3 1 [107, 111], 2 [109], 3 [106], 4, 8, 12 [112], 5 [119], 6, 10, 13 [111], 7 [120], 9, 14 [121], 11 [122], 14 [123]; $SrTiO_3$- 1,2,3 [108],4 [124]; Si-1,2 [112], 3,4 [125],5, 6, 7 [111], 8 [124]; MgO- [124] ; SiC [124].

2-3-6 Fabrication of MgB_2 Single Crystal

The physical properties of a superconductor especially the anisotropy properties, have to be studied on a single crystal. Many groups have attempted to grow single crystals after the discovery of MgB_2 superconductor. However, the formation of MgO phase, the high

Table 2- 2: Summary of the experimental results on MgB_2 superconductor thin film prepared by different techniques.

Preparation technique	T_c (K)	Substrate	Reference
PLD	29-34	Al_2O_3	[126]
PLD	22-24	Si, $SrTiO_3$, MgO	[124]
PLD	27	Si	[127]
PLD	31-36	$SrTiO_3$	[108]
PLD	36	Al_2O_3, MgO	[128]
PLD	25	MgO, Al_2O_3	[114]
PLD	39	Al_2O_3	[106]
EBE[1]	39	Al_2O_3, MgO	[110]
PLD	22, 39	$SrTiO_3$	[129]
MBE[2]	36	Si, $SrTiO_3$, Al_2O_3	[113]
PLD	39	Al_2O_3	[119]
PLD	38.6, 38.1	Al_2O_3, MgO	[130]
PLD	34	Al_2O_3	[120]
EBE	26, 38	Al_2O_3	[131]
rf MS[3]	35	Al_2O_3	[132]
PLD, MS	34	Al_2O_3, MgO, STO	[133]
EBE	29	Si, Al_2O_3	[134]
PLD	31.4, 36.2, 37.5	Al_2O_3, MgO	[135]
PLD	31.5, 37.4	MgO	[136]
CVD	39	Al_2O_3	[137]
PLD	25, 37.5	Al_2O_3	[138]
PLD	20, 30, 37	$SrTiO_3$	[139]
MBE	34.5	Al_2O_3	[115]
PLD	39.2	Al_2O_3	[140]
Vacuum co-deposition	29	Kapton-E polyamide foil!	[141]
PLD	20-24	Si, $SrTiO_3$, MgO, SiC	[142]
HPCVD[4]	39.3	Al_2O_3, SiC	[117]
MTS[5]	28	Al_2O_3	[143]
MBE	32-36	Si, $SrTiO_3$, Al_2O_3	[144]
MS	35	MgO	[145]
MBE	35.2	Si, MgO	[146]
CVD	35	Al_2O_3	[147]
PLD	34	Al_2O_3	[148]
Rf MS	24	$SrTiO_3$, Al_2O_3	[149]
Rf Sputtering	15-20	$SrTiO_3$, Al_2O_3	[150]
d.c. PMS[6]	35	Al_2O_3, MgO	[151]
PLD	38	Al_2O_3, MgO	[152]
PLD	24-30	AlB_2, ZrB_2, CaB_6, Al_2O_3	[153]
PLD	39.2	Al_2O_3	[69]
MS	35	MgO, Al_2O_3	[154]
rf MD	27	MgO	[155]
Ion implantation	11-18	Mg	[156]
HPCVD	41.8	SiC	[157]
MEB	15-37.5	Si, $SrTiO_3$, Al_2O_3e, Glass	[158]
CVD	37.5	$LaAlO_3$	[159]
HPCVD	40	SiC	[160]
PLD, EBE	25-39	Al_2O_3, Si	[111]
PLD	25	Al_2O_3, MgO	[121]
PLD	24	Al_2O_3	[122]
MS	24	Al_2O_3	[123]
PLD	28	Al_2O_3	[116]

[1] electron-beam evaporation
[2] molecular beam epitaxy
[3] magnetron sputtering
[4] hybrid physical–chemical vapour deposition (HPCVD)
[5] multiple-target sputtering
[6] planar magnetron sputtering

reactivity of Mg in the vapor and melt phases with containers and flux materials, the low solubility of MgB_2 in Mg, and the high Mg vapor pressure and incongruent melting of Mg cause difficulties in the crystal growth procedure of MgB_2 [161, 162].

A thermodynamic analysis of the Mg-B system using the calculation of phase diagrams modeling technique is presented by Liu et al. [163]. They calculated three phase diagrams of temperature–composition (Fig. 2-19), pressure–composition (Fig. 2-20), and pressure–temperature (Fig. 2-21) for this superconductor based on the known data on the MgB_2, MgB_4 and MgB_7 phases. According to their results, MgB_2 is stable only under high Mg overpressure. If the Mg overpressure is too low MgB_2 tends to decompose to MgB_4 +Mg (gas) [163]. For example under 1 atm and 1 Torr pressure, MgB_2 is decomposed to MgB_4 and Mg gas at 1545 ^oC and 912 ^oC, respectively [161].

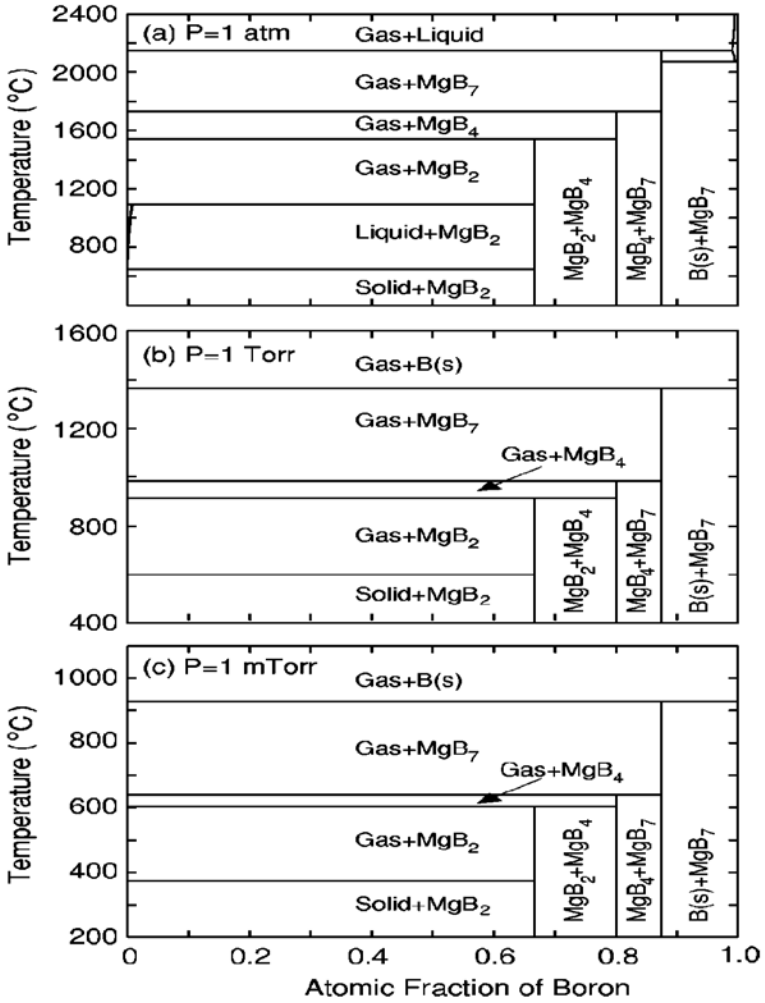

Figure 2- 19: Temperature–composition phase diagrams of the Mg–B system under pressures of (a) 1 atm, (b) 1 Torr, and (c) 1 mTorr [163].

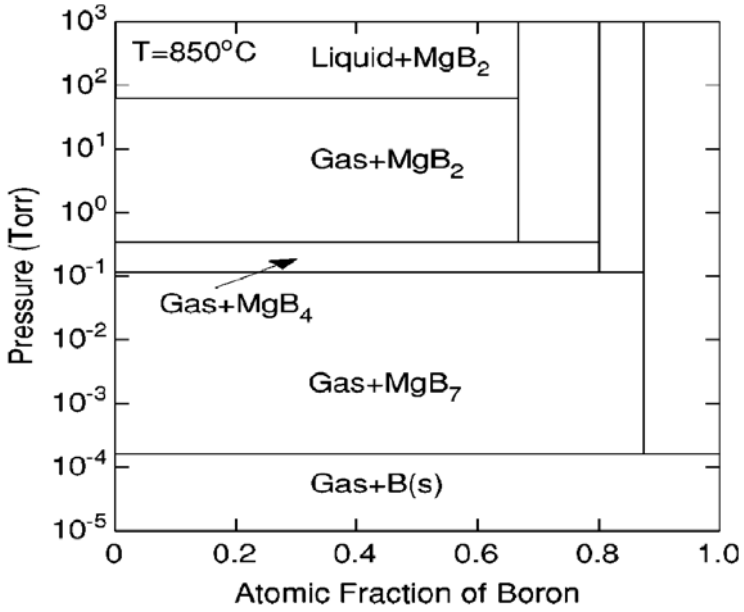

Figure 2- 20: Pressure–composition phase diagram of the Mg–B system at 850 °C.

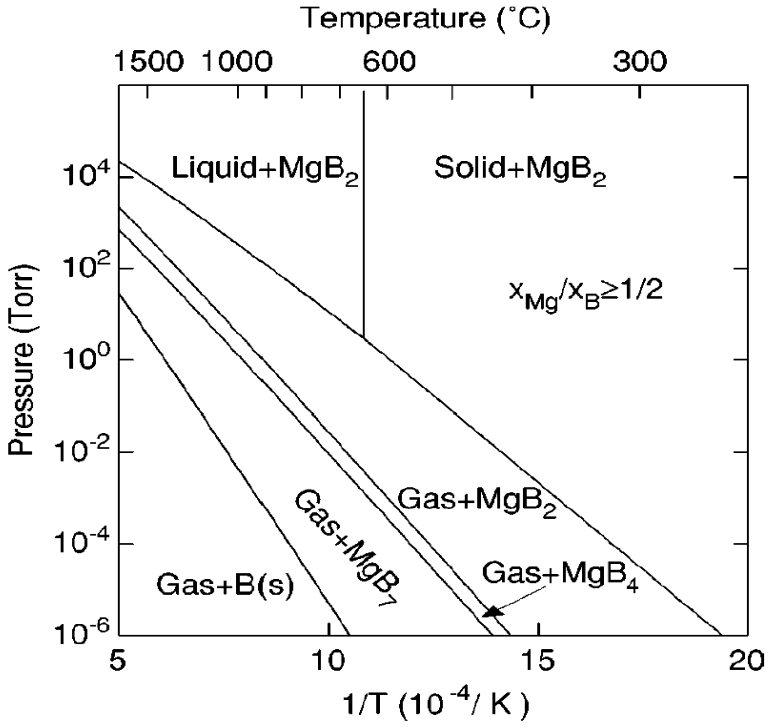

Figure 2- 21: The phase diagram (pressure–temperature) for the Mg:B atomic ratio x_{Mg} /x_B>1/2. The thermodynamic stability window for the deposition of MgB_2 thin films is region of Gas+MgB_2 [163].

So far, two different methods have been developed to prepare sub-millimeter MgB_2 single crystal; one is crystal growth by encapsulation and the other is the high-pressure method. In this method a mixture of Mg and B is heated at high temperature up to 1700 ^oC in a closed metal container of stainless steel, Nb or Mo [164-166] under an Ar gas

pressure of $1 < P_{Ar} < 14$kbar. With this method, crystals have been made using techniques such as vapor transformation [167, 168], using a mixture of MgB_2 and other flux materials, i.e. Na [166], Mg [164, 165, 169-171], Cu[171, 172], and Al [171]. The other method is sintering at high-pressures and temperatures in BN[162, 171, 173-177] or Ta reaction cells[169]. For experiments in the Mg-B-N system, the BN powder is used as a source of boron and nitrogen. The powder is put in a BN container as a reaction cell and sintered under high pressure, mostly by using the cubic-anvil press as shown in Fig. 2-22 [171]. Fig. 2-23 shows optical microscope images of MgB_2 single crystal prepared using the BN system.

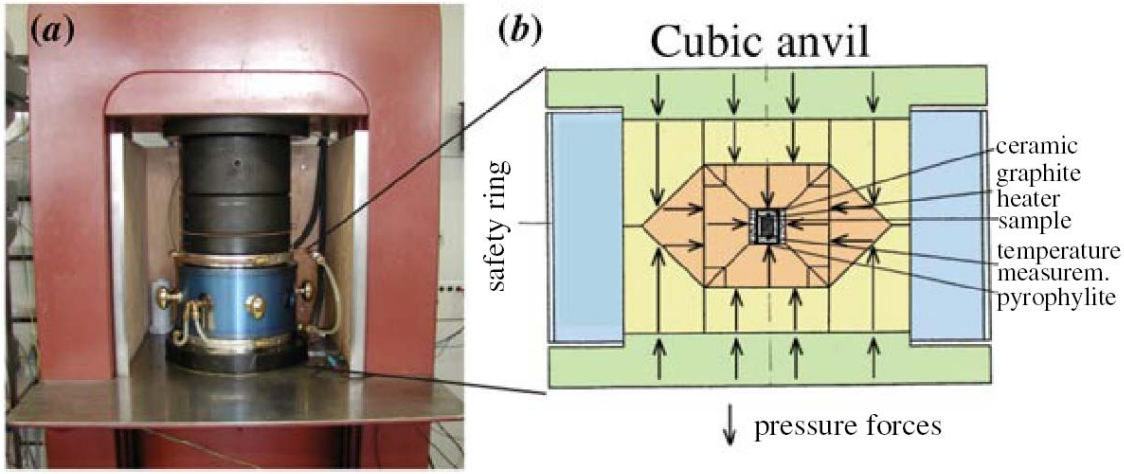

Figure 2- 22: a) The image of the cubic anvil apparatus including the hydraulic press to provide the necessary force. b) A schematic of the cubic anvil cell. Steel pieces are arranged so as to provide forces from all sides onto the sample located in the middle. A 400 A current passes through a graphite tube inside the pyrophylite cube to provide the heat. The sample is placed in a BN container which is located inside the graphite heater [171].

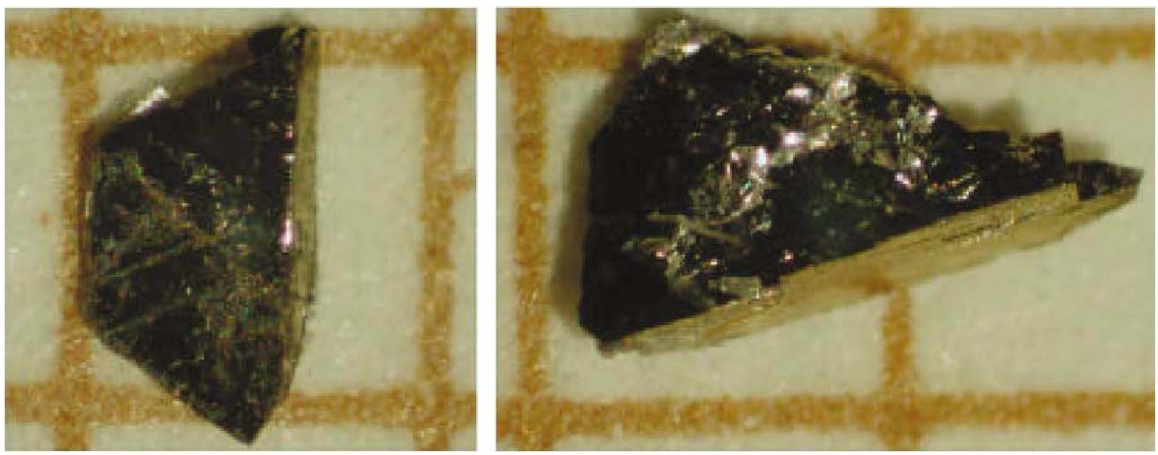

Figure 2- 23: Optical microscope picture of MgB_2 single crystals prepared using the Mg-B-N system under high pressure. Scale size is 1 mm [162].

2-3-7 Fabrication of MgB_2 Wire and Tape

Preparing and developing superconducting wires and tapes is essential for practical applications such as applications in the cable and magnet industries. MgB_2 superconductor wire was produced very soon after the discovery of this superconductor. The first wire was produced by Canfield et al. [178] by diffusing Mg vapor into boron fibers with a tungsten wire core. This wire showed a quite high J_c value of above 10^5 A/cm^2 at 5 K and zero field. The results were promising and many groups have attempted to make wires and tapes using different methods.

2-3-7-1 Preparation of Wire and Tape

Since MgB_2 is mechanically hard and brittle, it is impossible to directly draw it into a fine wire. Different techniques have been developed to prepare MgB_2 conductors. Although the powder in tube technique is widely used, other techniques have also been tried by a few groups. The powder-in-tube technique will be explained in detail in the next chapter. However, the continuous tube forming and filling technique (CTFF) will be explained in this chapter.

2-3-7-1-1 Powder in Tube Technique

The conventional powder-in-tube technique, using a metal tube as a stabilizer, has become a major method for the preparation of wires and tapes due to the relatively low cost and high quality of the products, as well as the suitability of this technique for large scale industrial production.

2-3-7-1-2 Continuous Tube Forming and Filling (CTFF) Technique

This technique has been used to prepare MgB_2 wires and tapes by the High-Tech Company in US. In fact it has been adapted to wire fabrication from pre-existing technologies used in the tobacco industry. In this technique, a continuous metal strip (Fe, Cu,) is first produced as a sheath material. As the ribbon enters and moves through the tube shaping dies they gradually form it into a U shape as shown in the Fig. 2-24. After the powder is inserted, the closing dies gradually close off the tube. After the tube

has been closed, it passes through subsequent dies to reduce the diameter to a fine wire of approximately 2mm in diameter. Numerous long lengths of wire have been made using this technique.

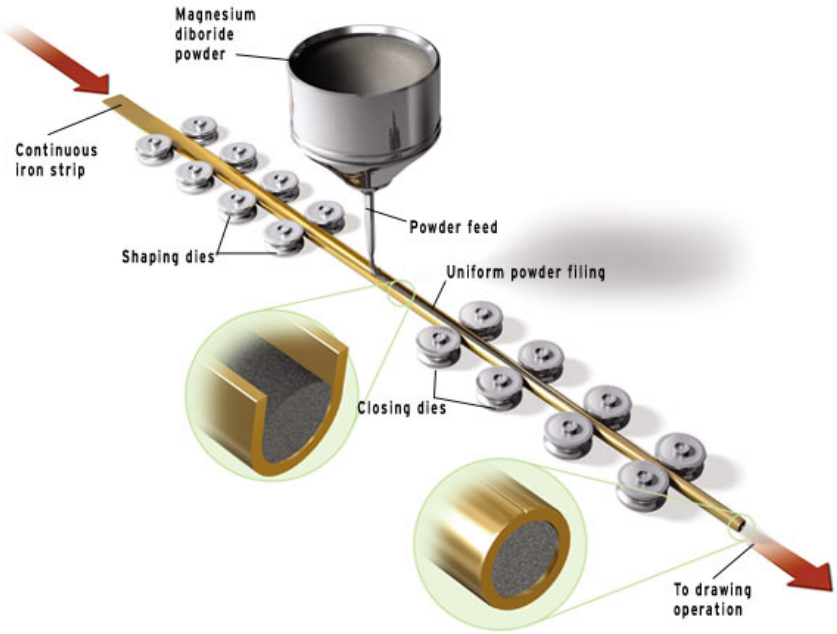

Figure 2- 24: Schematic of apparatus for continuous tube forming and filling (CTFF) for MgB_2 wire and tape fabrication.

2-3-7-2 Effect of the Sheath Material

Using the proper metal as a sheath material has been found to be critical in preparing high performance wire. Iron was found to be a suitable sheath material for MgB_2 wire [179] or tape [180-182] as Mg tends to react with many metals such as Cu and Ag even at temperatures lower than its melting point [181].

2-3-7-2-1 WIRE

Iron has been widely used by many groups as a sheath material for wire [179, 181, 183-212]. However other metals, such as Cu [185, 195, 200, 206, 213-227], Ag [213, 215, 218, 220, 221, 223], Ni [189, 228-230], and Ta[195, 231] have also been used for this purpose. In addition multi-layers of metals or metallic alloys, such as stainless steel (SS) [185, 204, 215, 232-237], carbon steel (CS) [206], Fe/Cu [181, 188, 203, 219, 238], Fe/SS [186, 201, 239-241], NbZr [195], Cu/Ni [185, 206, 232], Cu/Ta [214, 242-244],

Ag/SS [213], Ta/Cu/SS [245], Nb/Cu/SS [239, 245], Ta/SS [186], and Nb/SS [186], have been reported by many groups as metal cladding for MgB_2 wire.

2-3-7-2-2 Tape

Fe is also most commonly used as a sheath material for MgB_2 superconducting tape [180, 182, 186, 188-190, 195, 197-199, 201, 206, 209, 211, 241, 246-254]. However, similar to the wire situation, other metals and alloys, such as Cu [195, 206, 215, 217, 219, 252, 255-259], Ag[215, 252, 257], SS [206, 215, 232, 258, 260-264], Ni [182, 189, 228, 257, 265-270], Ta[195], Nb[271], Fe/Cu[219, 272], Ni/Cu[206, 232, 258], NbZr[195], Fe/SS[186, 201], Ta/Cu[244, 273], Cu/NbZr[274], Monel[271], and CS[206, 275-277], have also been used as the metal cladding.

It was found that mechanical hardness of the sheath material results in densification as well as improving the grain connectivity in the superconducting core[185, 186, 206, 258, 277]. Therefore, hard sheath materials such as SS [186, 258] and CS [277] have been used. Experimental results reveal that critical current density and its field dependence are significantly enhanced due to the hardness of sheath materials.

Multi-filamentary wires and tapes are also prepared using different sheath materials [188, 191, 194, 198, 200, 203, 209, 229, 240, 274, 278].

2-3-7-3 Effect of the Precursor Material

In terms of precursor material, to prepare MgB_2 superconductor two different methods are mainly used. In the so-called *in situ* reaction method a mixture of Mg and B is used as a starting material. The mixture is packed into a metallic tube, and then MgB_2 is formed inside the tube by heat treatment. However, commercially available and pre-reacted MgB_2 powder is used as a starting material in the *ex situ* reaction method. The *in situ* reaction method is widely used both for wire [180, 187, 190, 191, 200, 207, 210, 211, 213, 218, 220, 221, 223-227, 238, 244, 248-250, 275, 279-281] and for tape [180, 187, 190, 191, 200, 207, 210, 211, 221, 238, 244, 248-250, 273, 275, 279, 280]. The *ex situ* reaction method is also used both for wire [194, 197, 199, 203, 207, 213, 219, 220, 222, 275, 282] and for tape [194, 197, 199, 203, 207, 219, 222, 231, 275]. Apart from

these methods a mixture of Mg+2B and MgB_2 was also used by Schlachter et al. to prepare wire and tape [208], as well as by Pan et al. [207].

In the *ex situ* reaction method it has been shown that the quality of the starting powder has a significant effect on the critical current density of Cu clad tape [256].

Fujii et al. used MgH_2 instead of Mg as a precursor powder to prepare MgB_2 tape. They claimed that the J_c values of the tapes prepared using mixture of MgH_2 + B were about twice as large as those prepared using the mixture of Mg + B [251, 275, 276].

Using the pre-reacted powder, the influence of the initial MgB_2 grain size on critical current density, upper critical and irreversibility fields has been studied by Flukiger et al. [198]. They employed ball milling to reduce the grain size of MgB_2 starting material leading to an enhancement of J_c [198].

The porosity of samples has been one of the main weaknesses of MgB_2 samples so far. Samples with higher mass density have been prepared using pre-reacted and very fine powders in the reaction *ex situ* technique [198] or by sintering under pressure (hot press technique) in the reaction *in situ* method [283-286]. The hot isostatic pressing (HIP) method has also been employed to make dense samples, resulting in improvements in the microstructure and superconducting properties of the material, thereby improving the J_c field performance [235, 287].

2-3-7-4 Magnetic Shielding and ac Loss in Fe/MgB_2 Conductors

Studies on two other physical aspects of Fe sheath MgB_2 superconductor, ie. magnetic shielding [183, 187, 192, 202, 205, 288] and ac loss [187, 288] have also been reported. Results indicate that the presence of Fe in MgB_2/Fe composite shields the superconductor core against an external field of 2 kOe; at higher fields a fixed ΔH was observed (partial shielding) [183, 187]. It also results in suppression of ac loss due to shielding of the core against an externally applied field [187]. Therefore, using Fe as a sheath material may be beneficial for power applications.

2-3-7-5 Long Conductors and Coil

Ni coil [230] has been produced using *ex situ* reaction, and Cu coil [227] has been produced using the wind-reaction *in situ* technique (to be explained in chapter 4). Ni clad conductor in the shape of a helix about 1.5 m long and in a pancake shape about 2 m long have also been successfully prepared and measured by Grasso et al. [270]. These results confirm the suitability of this superconductor for practical applications.

2-3-7-6 Effect of Heat Treatment in MgB_2 Tape and Wire

On the one hand, heat treatment is an essential step in the *in situ* technique. For post annealing, a wide range of temperatures have been used, from as low as just above the Mg melting point [179, 227] to as high as 1100 ^{o}C [204]. It was found that even lower sintering temperatures of 500 ^{o}C [289] or 600 ^{o}C [225] are enough to form the MgB_2 phase if mechanically pre-alloyed powder is employed.

On the other hand, even in the *ex situ* reaction methods, post annealing is essential as it has been found to enhance the J_c and its magnetic field performance [185, 194, 201, 204, 208, 229, 270, 277]. This enhancement is reported to be up to one order of magnitude [201, 208].

The effects of sintering time on the critical current density of MgB_2 wires prepared by the reaction *in situ* method have also been studied (it will be explained in chapter 4). We have found that prolonged heat treatment is not necessary in the fabrication of Fe clad wires. MgB_2 phase can be formed quickly. Several minutes sintering gives almost the same performance as a longer sintering time. This finding substantially simplifies the fabrication procedure for wire. Short sintering of wires with other sheath materials, such as Cu and Ag, avoid a high reaction rate between the magnesium powder and the sheath, resulting in an enhancement in J_c (see Chapter 4).

2-3-7-7 Other Techniques Have Been Used for Preparation of MgB_2 Conductors

Other techniques, such as Reactive Liquid Mg Infiltration to make hollow wires as used by Giunchi et al. [278] and diffusion of magnesium vapor into boron fibers with

tungsten cores [178, 290-292], as well as the suspension spinning method [293, 294], were also tried by a few groups to prepare MgB_2 superconducting wire.

Two more different techniques, boron diffusion into Mg tape [295] and deposition of MgB_2 film on a Hastelloy tape buffered with an yttria-stabilized-zirconia layer [296], have also been used to prepare different types of MgB_2 tape.

2-3-8 Chemical Doping

Attempts have been made to accomplish substitutions in the MgB_2 superconductor lattice. Substitutions are important because they can lead to increases in T_c or to the discovery of a related compound with higher T_c, or to enhancement in the physical properties by such means as producing pinning centers. They can also clarify the mechanism of superconductivity.

Many elements have been tried as substitutes for Mg or B, such as C [297-305], Al [306-311], Mn [309, 312], Zr [309, 313-315], Na [310, 316], Li [306, 316-318], Si [306, 319], Be [320], Ag [309, 310, 321], Ti [212, 244, 309, 315, 322, 323], Mg [324], B [324], Sn [325], Fe [309, 325, 326], Co [325, 326], F [327], Cu [309, 310, 328, 329], Mo [309], Ca [309, 310], Y [309], Pb [330], Ir [331], Zn [310], V [323], Nb [323] and O [108]. In addition to the above elements, many compounds have also been tried as dopants in MgB_2, such as SiC [193, 211, 251, 332-335], Y_2O_3 [336], WSi_2 [250], $ZrSi_2$ [250] and SiO_2 [251].

Although many of the above reports declared the Mg and B had been partially replaced by other elements, Cava et al. [337] have recently claimed that most of them are incorrect and that just three elements, C, Al and Mn are really substituted, while the others cannot meet the criteria for successful chemical doping.

Unfortunately, all chemical dopants lead to decreases in the T_c value. It has been shown by many groups that C can substitute in the B position up to about x=0.1 in the MgB2-xCx composition. All reports show a serious decrease in the in-plane lattice parameter. There are some disagreements between the results in term of the rate of decrease in T_c, which is probably due to incomplete incorporation of C in different experiments. Al has also been found to be very well substituted in the Mg site. The higher the doping, the

larger the decreases in T_c and the wider the transition. The decrease in T_c is significant as at about x=0.4 in Mg1-xAlxB_2 the superconducting phase disappears [338]. Doping also leads to a contraction in both lattice parameters. However, the in-plane lattice parameter decreases faster than the out-of-plan lattice parameter as the doping level increases. It has also been found that there are two phases for doping levels between x=0.1 and x=0.25 having different *c* axis lattice parameters with different AlB_2 base structures [337] (Fig. 2-25). In the case of Mn, it has been shown that the solubility of Mn in MgB_2 is very low; Mn can successfully substitute into the Mg site to the maximum value of 5%. The substitution causes a great suppression in T_c at the rate of dT_c/dx=-159 [312].

In contrast to doping with elements, a slight reduction of T_c has been found in the samples doped with large amount of SiC, Y_2O_3, WSi_2, $ZrSi_2$ and SiO_2. Also, the J_c values of samples doped with these compounds were significantly enhanced in high magnetic fields and increases in H_{irr} and H_{c2} occurred, a promising development for practical applications.

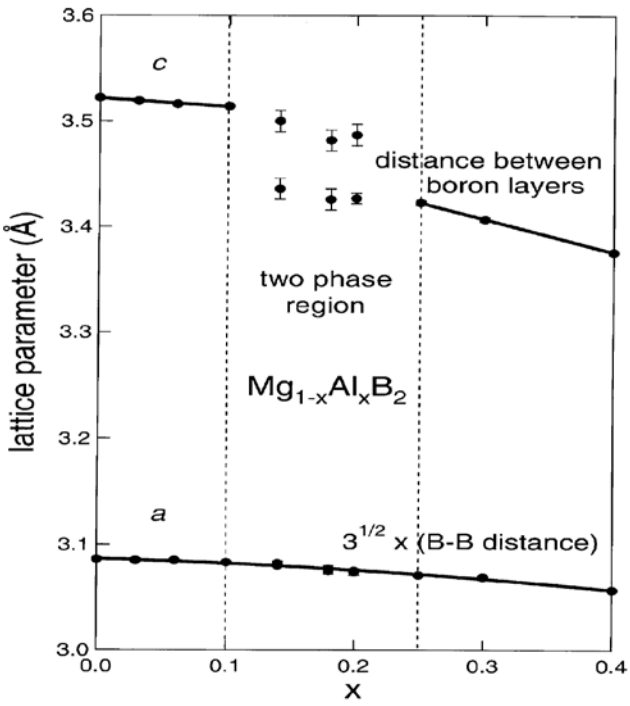

Figure 2- 25: Partial collapse of the spacing between the boron layers in Mg_{1-x} Al_xB_2. The figure shows variation of the in-plane (a) and between-plane (c) lattice parameters as a function of aluminium concentration. In the two-phase region, c-axis values for both phases are shown [337, 338].

2.3.9 Critical Fields

MgB_2 is a type II superconductor, therefore two different critical field have to be measured.

2-3-9-1 Upper Critical Field (H_{c2})

To have a potential application, it is essential to have a high H_{c2}, as it shows the ability of superconductor to sustain superconductivity at high magnetic fields. A wide range of H_{c2} values has been reported for different samples so far. Even for the same sample there are two different values for H_{c2} due to anisotropy in this superconductor. For clean single crystal samples, relatively low values of the upper critical fields about $H_{c2}^{\parallel ab}(0) \approx 18$ T and $H_{c2}^{\perp ab}(0) \approx 3.5$ T have been reported parallel and perpendicular to the *ab* plan, respectively [174, 339-343]. However, the higher value of the upper critical fields varies considerably up to about $H_{c2} \approx 29$ T for bulk samples containing impurities [344, 345] and up to about $H_{c2}^{\parallel ab}(0) \approx 48$ T for thin film according to recent measurements [344, 346, 347]. Such high values of H_{c2} also suggest that MgB_2 is a suitable candidate for practical applications.

2-3-9-2 Lower Critical Field (H_{c1})

By characterizing single and polycrystalline MgB_2 superconductors, different values of the lower critical field ranging between $H_{c1}(0) \approx 150$ Oe to 480 Oe have been reported [79, 164, 348-351]. However, according to recent measurements in a high purity single crystal sample, the lower critical field has been found to be $H_{c1}^{\parallel ab}(5K) \approx 120$ mT and $H_{c1}^{\perp ab}(5K) \approx 250$ mT [342].

2.3.10 Penetration Depth

Using the data for the lower critical field, the value of the penetration depth can be calculated, ranging between 85-203 nm [79] with the average value of $\lambda \sim 140$ nm [340, 352]. However, recent measurements in a high purity single crystal sample shows the penetration depth to be $\lambda_{ab}(0) \approx 22 \pm 2$ nm and $\lambda_c(0) \approx 100 \pm 10$ nm [342].

2-3-11 Coherence Length

In the CGS system the coherence length can be calculated using H_{c2} as $\xi^2 = \Phi_0 / 2\pi H_{c2}$ [353]. Using the value of H_{c2}, $\xi(0)$ has been estimated to be ~ 5 nm in polycrystalline samples [178]. Considering the different values of H_{c2} in single crystal, the values of the coherence length have been reported to be $\xi_{ab}(0) \approx 7$ nm and $\xi_c(0) \approx 4$ nm for aligned MgB_2 crystallites, using the $\xi_{ab}^2(0) = \Phi_0 / 2\pi H_{c2}^{\perp ab}$ and $\xi_{ab}\xi_c = \Phi_0 / 2\pi H_{c2}^{\parallel ab}$ formulas [354]. However, different values of $\xi_{ab}(0) = 10 \pm 0.2$ nm and $\xi_c(0) = 5 \pm 0.2$ nm were recently reported for single crystal, which are relatively higher than other values in the literature [342].

2-3-12 Mean Free Path

The electronic mean free path can be roughly calculated from the experimental data of resistivity (ρ) and carrier density, as well as the average Fermi velocity, using the classical Drude model. The value of l is estimated to be approximately 60 nm[178] for high purity polycrystalline samples and 80 nm for single crystal samples [33].

2-3-13 Anisotropy

The study of anisotropy is important for practical applications as well as for understanding the physical properties. The layered structure of MgB_2 results in an anisotropy property in the superconducting parameters. Many groups have measured the anisotropy parameter by using either the upper critical field $\gamma = H_{c2}^{\parallel ab} / H_{c2}^{\perp ab} = \xi_{ab} / \xi_c$ or the critical current density $\gamma = J_c^{ab} / J_c^c$.

2-3-13-1 Anisotropy in MgB_2 Powder

The anisotropy in H_{c2} has been measured for MgB_2 powder. The very large values of γ=6 [355] and γ= 6-9 [356] were determined using different techniques.

2-3-13-2 Anisotropy in Bulk MgB_2

A small, but distinct anisotropy of the upper critical field $\gamma = H_{c2}^{\parallel ab} / H_{c2}^{\perp ab} = 1.2$ was found for hot deformed and high density samples [357-359]. However an upper critical field anisotropy of $\gamma = 1.7$ as well as an almost temperature independent ratio J_c^{ab}/J_c^{c} similar to 1.5 were found in an aligned bulk MgB_2 crystallite sample [354, 360].

2-3-13-3 Anisotropy in MgB_2 Thin Film

Different values of the anisotropy parameter were found for MgB_2 thin film samples. Different values of $\gamma = 1.8$-2 [347], 1.2-1.8 [135], 1.4-1.8 [136], 1.25 [346], 2 [361] and 3 [132] have been reported for the upper critical field anisotropy. By measuring the critical current density $\gamma = 2.55$ was determined from the scaling behavior of J_c [362].

2-3-13-4 Anisotropy in MgB_2 Single Crystal

In single crystal samples a wide range for the anisotropy parameter from $\gamma = 2$ to $\gamma = 6$ has been reported by many groups [164, 165, 170, 171, 174, 175, 339, 341-343, 363-372]. Although many people found a constant anisotropy parameter over the temperature range measured [339, 342, 363], despite the anisotropic Ginzburg-Landau theory that predicts temperature independent anisotropy, it has been found by many groups that γ is temperature dependent and decreases with increasing temperature [171, 174, 343, 365-368, 371].

2-3-13-5 Anisotropy in MgB_2 Tape

It has been found from x-ray diffraction studies, that *c*-axis texturing appears in the core of MgB_2 tapes during the cold working procedure [198, 199, 206, 215, 228, 258, 275]. This texturing increases with the sheath strength [215, 258] and has been found to be larger in tapes made by the *ex situ* technique than in tapes made by the *in situ* technique [275]. The anisotropy ratio was determined to be 1.3 for H_{c2} parallel and perpendicular to the surface of the tape [198, 199]. However an unusual larger anisotropy factor of 10 was also reported by Kumakura et al. [258].

2-3-14 Strong Grain Connectivity

It has been confirmed by transport and magnetic measurements that unlike the HTS superconductors [373, 374], MgB_2 does not show any weak links, therefore grain boundaries are highly transparent to current flow [375, 376]. This is an advantage of MgB_2 compared to the HTS superconductors so far as practical applications are concerned, since high values of critical current density have been observed in MgB_2 thin film, bulk, and tapes and wires with no weak links.

Fig. 2-26 reveals the temperature dependence of J_c at different magnetic fields [377]. A good agreement between the J_c values obtained by transport measurements and the magnetic J_c values estimated from hysteresis loops using the Bean model confirms inductive current flows throughout the sample with no grain boundary barrier.

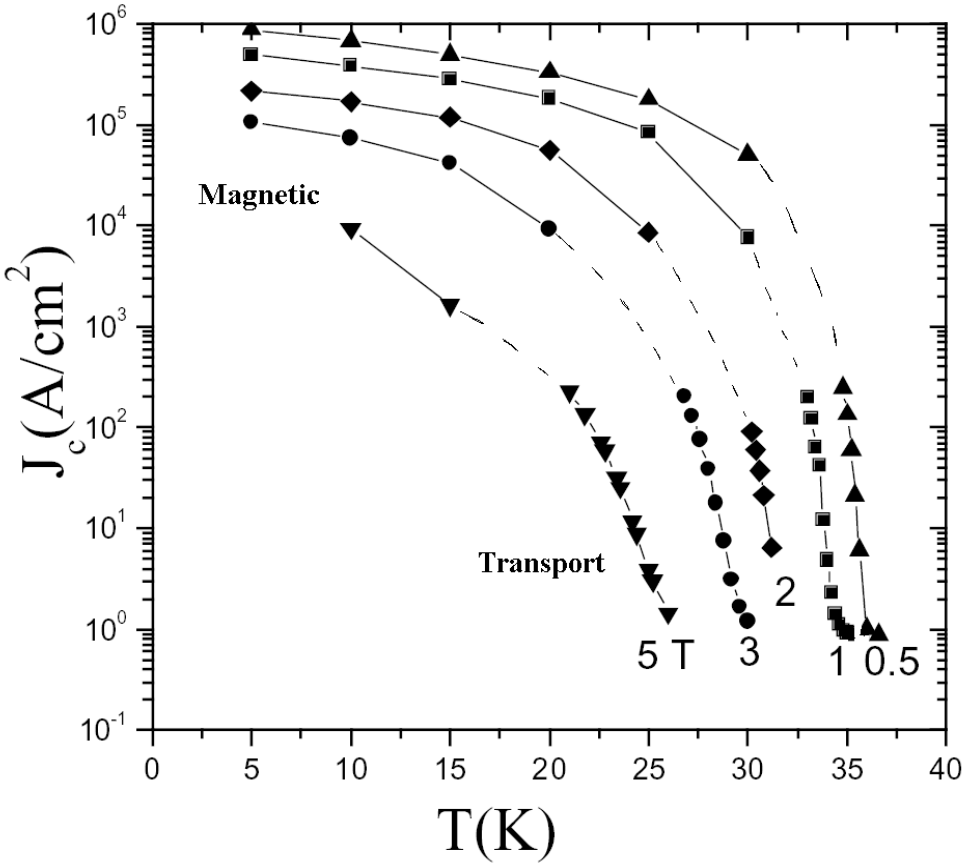

Figure 2- 26: Temperature dependence of the critical current density of polycrystalline MgB_2 sample for H = 0.5, 1, 2, 3, and 5 T. The values for $J_c > 10^3$ A/cm^2 were estimated from magnetic measurements, while those for $J_c < 10^3$ A/cm^2 were estimated from transport measurements [377].

References

1. Jones, M. and R. Marsh, *The preparation and structure of magnesium boride, MgB_2.* Journal of American Chemical Society, 1954. **76**: p. 1434.

2. Nagamatsu, J., N. Nakagawa, T. Muranaka, Y. Zenitani and J. Akimitsu, *Superconductivity at 39 K in magnesium diboride.* Nature, 2001. **410**(6824): p. 63-64.

3. Wolf, E.L., *Principle of Electron Tunneling Spectroscopy*. 1985, New York: Oxford University Press.

4. Kortus, J., Mazin, II, K.D. Belashchenko, V.P. Antropov and L.L. Boyer, *Superconductivity of metallic boron in MgB_2.* Physical Review Letters, 2001. **86**(20): p. 4656-4659.

5. An, J.M. and W.E. Pickett, *Superconductivity of MgB_2: Covalent bonds driven metallic.* Physical Review Letters, 2001. **86**(19): p. 4366-4369.

6. Bohnen, K.P., R. Heid and B. Renker, *Phonon dispersion and electron-phonon coupling in MgB_2 and AlB_2.* Physical Review Letters, 2001. **86**(25): p. 5771-5774.

7. Yildirim, T., O. Gulseren, J.W. Lynn, C.M. Brown, T.J. Udovic, Q. Huang, N. Rogado, K.A. Regan, M.A. Hayward, J.S. Slusky, T. He, M.K. Haas, P. Khalifah, K. Inumaru, and R.J. Cava, *Giant anharmonicity and nonlinear electron-phonon coupling in MgB_2: A combined first-principles calculation and neutron scattering study - art. no. 037001.* Physical Review Letters, 2001. **8703**(3): p. 7001-NIL_119.

8. Liu, A.Y., I. Mazin and J. Kortus, *Beyond Eliashberg superconductivity in MgB_2: Anharmonicity, two-phonon scattering, and multiple gaps - art. no. 087005.* Physical Review Letters, 2001. **8708**(8): p. 7005.

9. Kong, Y., O.V. Dolgov, O. Jepsen and O.K. Andersen, *Electron-phonon interaction in the normal and superconducting states of MgB_2 - art. no. 020501.* Physical Review B, 2001. **6402**(2): p. 501.

10. Choi, H.J., D. Roundy, H. Sun, M.L. Cohen and S.G. Louie, *First-principles calculation of the superconducting transition in MgB_2 within the anisotropic Eliashberg formalism - art. no. 020513.* Physical Review B, 2002. **6602**(2): p. 513-513.

11. Ravindran, P., P. Vajeeston, R. Vidya, A. Kjekshus and H. Fjellvag, *Detailed electronic structure studies on superconducting MgB_2 and related compounds - art. no. 224509.* Physical Review B, 2001. **6422**(22): p. 4509.

12. Papaconstantopoulos, D.A. and M.J. Mehl, *Precise tight-binding description of the band structure of MgB_2 - art. no. 172510.* Physical Review B, 2001. **6417**(17): p. 2510.

13. Harima, H., *Energy band structures of MgB_2 and related compounds.* Physica C-Superconductivity and Its Applications, 2002. **378**: p. 18-24.

14. Karapetrov, G., M. Iavarone, W.K. Kwok, G.W. Crabtree and D.G. Hinks, *Scanning tunneling spectroscopy in MgB_2.* Physical Review Letters, 2001. **86**(19): p. 4374-4377.

15. Rubio-Bollinger, G., H. Suderow and S. Vieira, *Tunneling spectroscopy in small grains of superconducting MgB_2.* Physical Review Letters, 2001. **86**(24): p. 5582-5584.

16. Bouquet, F., R.A. Fisher, N.E. Phillips, D.G. Hinks and J.D. Jorgensen, *Specific heat of $Mg^{11}B_2$: Evidence for a second energy cap - art. no. 047001.* Physical Review Letters, 2001. **8704**(4): p. 7001.

17. Wang, Y.X., T. Plackowski and A. Junod, *Specific heat in the superconducting and normal state (2-300 K, 0-16 T), and magnetic susceptibility of the 38 K superconductor MgB_2: evidence for a multicomponent gap.* Physica C, 2001. **355**(3-4): p. 179-193.

18. Bouquet, F., R.A. Fisher, N.E. Phillips, D.G. Hinks and J.A. Jorgensen, *Specific heat of $Mg^{11}B_2$, a two-gap superconductor.* Journal of Superconductivity, 2002. **15**(5): p. 469-473.

19. Bouquet, F., R.A. Fisher, N.E. Phillips, D.G. Hinks and J.D. Jorgensen, *Specific heat of $Mg^{11}B_2$: evidence for two energy gaps.* Physica C-Superconductivity and Its Applications, 2003. **388**: p. 109-110.

20. Bouquet, F., Y. Wang, R.A. Fisher, D.G. Hinks, J.D. Jorgensen, A. Junod and N.E. Phillips, *Phenomenological two-gap model for the specific heat of MgB.* Europhysics Letters, 2001. **56**(6): p. 856-862.

21. Bouquet, F., Y. Wang, I. Sheikin, T. Plackowski, A. Junod, S. Lee and S. Tajima, *Specific heat of single crystal MgB_2: A two-band superconductor with two different anisotropies - art. no. 257001.* Physical Review Letters, 2002. **8925**(25): p. 7001-7001.

22. Yang, H.D., J.Y. Lin, H.H. Li, F.H. Hsu, C.J. Liu, S.C. Li, R.C. Yu and C.Q. Jin, *Order parameter of MgB_2: A fully gapped superconductor - art. no. 167003.* Physical Review Letters, 2001. **8716**(16): p. 7003.

23. Szabo, P., P. Samuely, J. Kacmarcik, T. Klein, J. Marcus, D. Fruchart, S. Miraglia, C. Marcenat and A.G.M. Jansen, *Evidence for two superconducting energy gaps in MgB_2 by point-contact spectroscopy - art. no. 137005.* Physical Review Letters, 2001. **8713**(13): p. 7005.

24. Szabo, P., P. Samuely, J. Kacmarcik, T. Klein, J. Marcus and A.G.M. Jansen, *Point-contact spectroscopy of MgB_2 in high magnetic fields.* Physica C-Superconductivity and Its Applications, 2003. **388**: p. 145-146.

25. Giubileo, F., D. Roditchev, W. Sacks, R. Lamy, D.X. Thanh, J. Klein, S. Miraglia, D. Fruchart, J. Marcus and P. Monod, *Two-gap state density in MgB_2: A true bulk property or a proximity effect? art. no. 177008.* Physical Review Letters, 2001. **8717**(17): p. 7008.

26. Giubileo, F., D. Roditchev, W. Sacks, R. Lamy and J. Klein, *Strong coupling and double-gap density of states in superconducting MgB_2.* Europhysics Letters, 2002. **58**(5): p. 764-770.

27. Giubileo, F., D. Roditchev, W. Sacks, R. Lamy and J. Klein, *Two gap signature in magnesium diboride.* International Journal of Modern Physics B, 2002. **16**(11-12): p. 1577-1583.

28. Chen, X.K., M.J. Konstantinovic, J.C. Irwin, D.D. Lawrie and J.P. Franck, *Evidence for two superconducting gaps in MgB_2 - art. no. 157002.* Physical Review Letters, 2001. **8715**(15): p. 7002.

29. Tsuda, S., T. Yokoya, T. Kiss, Y. Takano, K. Togano, H. Kito, H. Ihara and S. Shin, *Evidence for a multiple superconducting gap in MgB_2 from high-resolution photoemission spectroscopy - art. no. 177006.* Physical Review Letters, 2001. **8717**(17): p. 7006.

30. Tsuda, S., T. Yokoya, T. Kiss, A. Chainani, Y. Takano, K. Togano, H. Kito, H. Ihara and S. Shin, *Superconducting gap of MgB_2 observed using ultrahigh-resolution photoemission spectroscopy.* Physica B, 2002. **312**: p. 150-151.

31. Uchiyama, H., S. Tajima, K.M. Shen, D.H. Lu and Z.X. Shen, *Photoemission studies in MgB_2.* Physica C-Superconductivity and Its Applications, 2003. **385**(1-2): p. 85-90.

32. Laube, F., G. Goll, J. Hagel, H. von Hohneysen, D. Ernst and T. Wolf, *Superconducting energy gap distribution of MgB_2 investigated by point-contact spectroscopy.* Europhysics Letters, 2001. **56**(2): p. 296-301.

33. Sologubenko, A.V., J. Jun, S.M. Kazakov, J. Karpinski and H.R. Ott, *Thermal conductivity of single-crystalline MgB_2 - art. no. 014504.* Physical Review B, 2002. **6601**(1): p. 4504-4504.

34. Iavarone, M., G. Karapetrov, A.E. Koshelev, W.K. Kwok, G.W. Crabtree, D.G. Hinks, W.N. Kang, E.M. Choi, H.J. Kim and S.I. Lee, *Two-band superconductivity in MgB_2 - art. no. 187002.* Physical Review Letters, 2002. **8918**(18): p. 7002-7002.

35. Iavarone, M., G. Karapetrov, A. Koshelev, W.K. Kwok, D. Hinks, G.W. Crabtree, W.N. Kang, E.M. Chi, H.J. Kim and S.I. Lee, *MgB_2: directional tunnelling two-band superconductivity.* Superconductor Science & Technology, 2003. **16**(2): p. 156-161.

36. Takasaki, T., T. Ekino, T. Muranaka, H. Fujii and J. Akimitsu, *Multiple-gap structure of the binary superconductor MgB_2.* Physica C-Superconductivity and Its Applications, 2003. **388**: p. 147-148.

37. Samuely, P., P. Szabo, J. Kacmarcik, T. Klein and A.G.M. Jansen, *Point-contact spectroscopy of MgB_2.* Physica C-Superconductivity and Its Applications, 2003. **385**(1-2): p. 244-254.

38. Martinez-Samper, P., J.G. Rodrigo, G. Rubio-Bollinger, H. Suderow, S. Vieira, S. Lee and S. Tajima, *Scanning tunneling spectroscopy in MgB_2.* Physica C-Superconductivity and Its Applications, 2003. **385**(1-2): p. 233-243.

39. Karapetrov, G., M. Iavarone, A.E. Koshelev, W.K. Kwok, G.W. Crabtree, D.G. Hinks and S.I. Lee, *Momentum-dependent scanning tunneling spectroscopy in MgB_2.* Physica C-Superconductivity and Its Applications, 2003. **388**: p. 141-142.

40. Ivarone, M., G. Karapetrov, A.E. Koshelev, W.K. Kwok, G.W. Crabtree, D.G. Hinks, R. Cook, W.N. Kang, E.M. Choi, H.J. Kim, and S.I. Lee, *Directional scanning tunneling spectroscopy in MgB_2.* Physica C-Superconductivity and Its Applications, 2003. **385**(1-2): p. 215-220.

41. Eskildsen, M.R., M. Kugler, G. Levy, S. Tanaka, J. Jun, S.M. Kazakov, J. Karpinski and O. Fischer, *Scanning tunneling spectroscopy on single crystal MgB_2.* Physica C-Superconductivity and Its Applications, 2003. **385**(1-2): p. 169-176.

42. Ekino, T., T. Takasaki, H. Fujii, T. Muranaka and J. Akimitsu, *Tunneling spectroscopy of the energy gap in MgB_2 under magnetic fields.* Acta Physica Polonica B, 2003. **34**(2): p. 523-526.

43. Ekino, T., T. Takasaki, T. Muranaka, J. Akimitsu and H. Fujii, *Tunneling spectroscopy of the superconducting gap in MgB_2 - art. no. 094504.* Physical Review B, 2003. **6709**(9): p. 4504-4504.

44. Badr, M.H. and K.W. Ng, *Temperature and field dependence of MgB_2 energy gaps from tunneling spectra.* Physica C-Superconductivity and Its Applications, 2003. **388**: p. 139-140.

45. Schmidt, H., J.F. Zasadzinski, K.E. Gray and D.G. Hinks, *Evidence for two-band superconductivity from break-junction tunneling on MgB_2 - art. no. 127002.* Physical Review Letters, 2002. **8812**(12): p. 7002-7002.

46. Naidyuk, Y.G., I.K. Yanson, L.V. Tyutrina, N.L. Bobrov, P.N. Chubov, W.N. Kang, H.J. Kim, E.M. Choi and S.I. Lee, *Superconducting energy gap distribution in c-axis oriented MgB_2 thin film from point contact study.* Jetp Letters, 2002. **75**(5): p. 238-241.

47. Li, Z.Z., H.J. Tao, Y. Xuan, Z.A. Ren, G.C. Che and B.R. Zhao, *Andreev reflection spectroscopy evidence for multiple gaps in MgB_2 - art. no. 064513.* Physical Review B, 2002. **6606**(6): p. 4513-4513.

48. Lee, S., Z.G. Khim, Y.N. Chong, S.H. Moon, H.N. Lee, H.G. Kim, B. Oh and E.J. Choi, *Measurement of the superconducting gap of MgB_2 by point contact spectroscopy.* Physica C, 2002. **377**(3): p. 202-207.

49. Tajima, S., J. Quilty, H. Uchiyama and S. Lee, *Superconducting gap in the multi-band system MgB_2.* Journal of Low Temperature Physics, 2003. **131**(5-6): p. 1217-1225.

50. Souma, S., Y. Machida, T. Sato, T. Takahashi, H. Matsui, S.C. Wang, H. Ding, A. Kaminski, J.C. Campuzano, S. Sasaki, and K. Kadowaki, *The origin of multiple superconducting gaps in MgB_2.* Nature, 2003. **423**(6935): p. 65-67.

51. Schmidt, H., J.F. Zasadzinski, K.E. Gray and D.G. Hinks, *Break-junction tunneling on MgB_2.* Physica C-Superconductivity and Its Applications, 2003. **385**(1-2): p. 221-232.

52. Koshelev, A.E. and A.A. Golubov, *Mixed state of a dirty two-band superconductor: Application to MgB_2 - art. no. 177002.* Physical Review Letters, 2003. **9017**(17): p. 7002-7002.

53. Gonnelli, R.S., D. Daghero, G.A. Ummarino, V.A. Stepanov, J. Jun, S.M. Kazakov and J. Karpinski, *Independent determination of the two gaps by directional point-contact spectroscopy in MgB_2 single crystals.* Superconductor Science & Technology, 2003. **16**(2): p. 171-175.

54. Plecenik, A., P. Kus, L. Satrapinsky, Y. Xu and R. Sobolewski, *Fabrication and transport properties of MgB_2 thin films and tunnel junctions.* Journal of Superconductivity, 2002. **15**(6): p. 621-625.

55. Gonnelli, R.S., D. Daghero, G.A. Ummarino, V.A. Stepanov, J. Jun, S.M. Kazakov and J. Karpinski, *Direct evidence for two-band superconductivity in MgB_2 single crystals from directional point-contact spectroscopy in magnetic fields - art. no. 247004.* Physical Review Letters, 2002. **8924**(24): p. 7004-7004.

56. Bugoslavsky, Y., Y. Miyoshi, G.K. Perkins, A.V. Berenov, Z. Lockman, L. MacManus-Driscoll, L.F. Cohen, A.D. Caplin, H.Y. Zhai, M.P. Paranthaman, H.M. Christen, and M. Blamire, *Structure of the superconducting gap in MgB_2 from point-contact spectroscopy.* Superconductor Science & Technology, 2002. **15**(4): p. 526-532.

57. Kristoffel, N., T. Ord and K. Rago, *MgB_2 two-gap superconductivity with intra- and interband couplings.* Europhysics Letters, 2003. **61**(1): p. 109-115.

58. Ghosh, A., *Two-gap superconductivity in MgB_2.* International Journal of Modern Physics B, 2003. **17**(13): p. 2589-2598.

59. Choi, H.J., M.L. Cohen and S.G. Louie, *Anisotropic Eliashberg theory of MgB_2: T_c, isotope effects, superconducting energy gaps, quasiparticles, and specific heat.* Physica C-Superconductivity and Its Applications, 2003. **385**(1-2): p. 66-74.

60. Choi, H.J., D. Roundy, H. Sun, M.L. Cohen and S.G. Louie, *The origin of the anomalous superconducting properties of MgB_2.* Nature, 2002. **418**(6899): p. 758-760.

61. Shulga, S.V., S.-L. Drechsler, H. Eschrig, H. Rosner and W.E. Pickett, *The upper critical field problem in MgB_2.* cond-mat/0103154, 2001.

62. Dahm, T. and N. Schopohl, *Fermi surface topology and the upper critical field in two-band superconductors: Application to MgB_2 - art. no. 017001.* Physical Review Letters, 2003. **9101**(1): p. 7001-7001.

63. Carrington, A., P.J. Meeson, J.R. Cooper, L. Balicas, N.E. Hussey, E.A. Yelland, S. Lee, A. Yamamoto, S. Tajima, S.M. Kazakov, and J. Karpinski, *Determination of the Fermi surface of MgB2 by the de Haas-van Alphen effect - art. no. 037003.* Physical Review Letters, 2003. **9103**(3): p. 7003-7003.

64. Carrington, A., J.R. Cooper, N.E. Hussey, P.J. Meeson, E.A. Yelland, S. Lee, A. Yamamoto and S. Tajima, *De Haas-van Alphen effect in single crystal MgB_2.* Physica C-Superconductivity and Its Applications, 2003. **388**: p. 105-106.

65. Kang, W.N., C.U. Jung, K.H.P. Kim, M.S. Park, S.Y. Lee, H.J. Kim, E.M. Choi, K.H. Kim, M.S. Kim and S.I. Lee, *Hole carrier in MgB_2 characterized by Hall measurements.* Applied Physics Letters, 2001. **79**(7): p. 982-984.

66. N.lscher, C. and G. Saemann–Ischenko, *Superconductivity and crystal and electronic structures in hydrogenated and disordered Nb_3Ge and Nb_3Sn layers with A15 structure.* Physical Review B, 1985. **32**(3): p. 1519.

67. Harris, J.M., Y.F. Yan and N.P. Ong, *Experimental test of the T^2 law for the Hall angle from T_c to 500 K in oxygen-reduced $YBa_2Cu^3O_{6+x}$ crystals.* Physical Review B, 1992. **46**(21): p. 14293.

68. Kang, W.N., H.J. Kim, E.M. Choi, K.H.P. Kim, H.S. Lee and S.I. Lee, *Hall effect in c-axis-oriented MgB_2 thin films - art. no. 134508.* Physical Review B, 2002. **6513**(13): p. 4508-4508.

69. Kang, W.N., H.J. Kim, E.M. Choi, K.H.P. Kim, H.S. Lee and S.I. Lee, *Synthesis of c-axis-oriented MgB_2 thin films and the Hall effect.* Superconductor Science & Technology, 2003. **16**(2): p. 237-240.

70. Samoliov, A.V., *Universal behavior of the Hall resistivity of single crystalline $Bi_2Sr_2CaCu_2O_x$ in the thermally activated flux flow regime.* Physical Review Letters, 1993. **71**(4): p. 617.

71. Budhani, R.C., S.H. Liou and Z.X. Cai, *Diminishing sign anomaly and scaling behavior of the mixed-state Hall resistivity in $Tl_2Ba_2Ca_2Cu_3O_{10}$ films containing columnar defects.* Physical Review Letters, 1993. **71**(4): p. 621.

72. Vinokur, V.M., V.B. Geshkenbein, M.V. Feigel'man and G. Blatter, *Scaling of the Hall resistivity in high-T_c superconductors.* Physical Review Letters, 1993. **71**(8): p. 1242.

73. Jin, R., M. Paranthaman, H.Y. Zhai, H.M. Christen, D.K. Christen and D. Mandrus, *Unusual Hall effect in superconducting MgB_2 films - art. no. 220506.* Physical Review B, 2001. **6422**(22): p. 0506.

74. Eltsev, Y., K. Nakao, S. Lee, T. Masui, N. Chikumoto, S. Tajima, N. Koshizuka and M. Murakami, *Anisotropic resistivity and Hall effect in MgB_2 single crystals - art. no. 180504.* Physical Review B, 2002. **6618**(18): p. 504-504.

75. Eltsev, Y., K. Nakao, S. Lee, T. Masui, N. Chikumoto, S. Tajima, N. Koshizuka and M. Murakami, *Anisotropic electrical transport in MgB_2 single crystals.* Journal of Low Temperature Physics, 2003. **131**(5-6): p. 1069-1073.

76. Satta, G., G. Profeta, F. Bernardini, A. Continenza and S. Massidda, *Electronic and structural properties of superconducting MgB_2, $CaSi_2$, and related compounds - art. no. 104507.* Physical Review B, 2001. **6410**(10): p. 4507.

77. Masui, T. and S. Tajima, *Normal state transport properties of MgB_2.* Physica C-Superconductivity and Its Applications, 2003. **385**(1-2): p. 91-97.

78. Deemyad, S., T. Tomita, J.J. Hamlin, B.R. Beckett, J.S. Schilling, D.G. Hinks, J.D. Jorgensen, S. Lee and S. Tajima, *Dependence of the superconducting transition temperature of single and polycrystalline MgB_2 on hydrostatic pressure.* Physica C-Superconductivity and Its Applications, 2003. **385**(1-2): p. 105-116.

79. Buzea, C. and T. Yamashita, *Review of the superconducting properties of MgB_2.* Superconductor Science & Technology, 2001. **14**(11): p. R115-R146.

80. Monteverde, M., M. Nunez-Regueiro, N. Rogado, K.A. Regan, M.A. Hayward, T. He, S.M. Loureiro and R.J. Cava, *Pressure dependence of the superconducting transition temperature of magnesium diboride.* Science, 2001. **292**(5514): p. 75-77.

81. Bordet, P., M. Mezouar, M. Nunez-Regueiro, M. Monteverde, M.D. Nunez-Regueiro, N. Rogado, K.A. Regan, M.A. Hayward, T. He, S.M. Loureiro, and R.J. Cava, *Absence of a structural transition up to 40 GPa in MgB_2 and the relevance of magnesium nonstoichiometry - art. no. 172502.* Physical Review B, 2001. **6417**(17): p. 2502.

82. Masui, T., K. Yoshida, S. Lee, A. Yamamoto and S. Tajima, *Phonon contribution to the transport properties of single-crystal MgB_2 - art. no. 214513.* Physical Review B, 2002. **6521**(21): p. 4513-4513.

83. Tissen, V.G., M.V. Nefedova, N.N. Kolesnikov and M.P. Kulakov, *Effect of pressure on the superconducting T_c of MgB_2.* Physica C, 2001. **363**(3): p. 194-197.

84. Tomita, T., J.J. Hamlin, J.S. Schilling, D.G. Hinks and J.D. Jorgensen, *Dependence of T_c on hydrostatic pressure in superconducting MgB_2 - art. no. 092505.* Physical Review B, 2001. **6409**(9): p. 2505.

85. Deemyad, S., J.S. Schilling, J.D. Jorgensen and D.G. Hinks, *Dependence of the superconducting transition temperature of MgB_2 on pressure to 20 GPa.* Physica C, 2001. **361**(4): p. 227-233.

86. Schlachter, S.I., W.H. Fietz, K. Grube and W. Goldacker. *High pressure studies of T_c and lattice parameters of MgB_2.* in *International Cryogenic Materials Conference - ICMC*. 2001. Madison, Wisconsin (USA).

87. Lorenz, B., R.L. Meng and C.W. Chu, *Hydrostatic Pressure Effect on the Superconducting Transition Temperature of MgB_2.* cond-mat/0104303, 2001.

88. Struzhkin, V.V., A.F. Goncharov, R.J. Hemley, H.K. Mao, G. Lapertot, S.L. Bud'ko and P.C. Canfield, *Phonon-assisted electronic topological transition in MgB_2 under pressure.* cond-mat/0106576, 2001.

89. Lorenz, B., R.L. Meng and C.W. Chu, *High-pressure study on MgB_2 - art. no. 012507.* Physical Review B, 2001. **6401**(1): p. 2507.

90. Choi, E.S., W. Kang, J.Y. Kim, M.-S. Park, C.U. Jung, H.-J. Kim and S.-I. Lee, *Pressure dependent thermoelectric power of MgB_2 superconductor.* cond-mat/0104454, 2001.

91. Saito, E., T. Taknenobu, T. Ito, Y. Iwasa, K. Prassides and T. Arima, *Pressure dependence of T_c in the MgB_2 superconductor as probed by resistivity measurements.* Journal of Physics-Condensed Matter, 2001. **13**(12): p. L267-L270.

92. Kazakov, S.M., M. Angst, J. Karpinski, I.M. Fita and R. Puzniak, *Substitution effect of Zn and Cu in MgB_2 on T_c and structure.* Solid State Communications, 2001. **119**(1): p. 1-5.

93. Tang, J., L.C. Qin, A. Matsushita, Y. Takano, K. Togano, H. Kito and H. Ihara, *Lattice parameter and T_c dependence of sintered MgB_2 superconductor on hydrostatic pressure - art. no. 132509.* Physical Review B, 2001. **6413**(13): p. 2509.

94. Profeta, G., A. Continenza, F. Bernardini, M. Monni and S. Massidda, *Electronic, dynamical and superconducting properties of MgB_2: doping, surface and pressure effects.* Superconductor Science & Technology, 2003. **16**(2): p. 137-142.

95. Razavi, F.S., S.K. Bose and H. Ploczek, *Effect of pressure on the superconductivity of MgB_2.* Physica C, 2002. **366**(2): p. 73-79.

96. Vogt, T., G. Schneider, J.A. Hriljac, G. Yang and J.S. Abell, *Compressibility and electronic structure of MgB_2 up to 8 GPa - art. no. 220505.* Physical Review B, 2001. **6322**(22): p. 0505.

97. Tang, J., L.C. Qin, H.W. Gu, A. Matsushita, Y. Takano, K. Togano, H. Kito and H. Ihara, *Structural and electronic properties of superconductor MgB_2 under*

high pressure. Journal of Physics-Condensed Matter, 2002. **14**(44): p. 10623-10626.

98. Prassides, K., Y. Iwasa, T. Ito, D.H. Chi, K. Uehara, E. Nishibori, M. Takata, M. Sakata, Y. Ohishi, O. Shimomura, T. Muranaka, and J. Akimitsu, *Compressibility of the MgB_2 superconductor - art. no. 012509.* Physical Review B, 2001. **6401**(1): p. 2509.

99. Jorgensen, J.D., D.G. Hinks and S. Short, *Lattice properties of MgB_2 versus temperature and pressure - art. no. 224522.* Physical Review B, 2001. **6322**(22): p. 4522.

100. Goncharov, A.F., V.V. Struzhkin, E. Gregoryanz, J.Z. Hu, R.J. Hemley, H.K. Mao, G. Lapertot, S.L. Bud'ko and P.C. Canfield, *Raman spectrum and lattice parameters of MgB_2 as a function of pressure - art. no. 100509.* Physical Review B, 2001. **6410**(10): p. 0509.

101. Franck, J.P., in *Physical properties of high temperature superconductors IV*, Ginsberg, Editor. 1994, World Scientific: Singapore. p. 189.

102. Kishore, R., in *Studies of high temperature superconductors*, A. Narlikar, Editor. 1999, Nova Scientific Publishers: Commack, NY. p. 23.

103. Bud'ko, S.L., G. Lapertot, C. Petrovic, C.E. Cunningham, N. Anderson and P.C. Canfield, *Boron isotope effect in superconducting MgB_2.* Physical Review Letters, 2001. **86**(9): p. 1877-1880.

104. Hinks, D.G., H. Claus and J.D. Jorgensen, *The complex nature of superconductivity in MgB_2 as revealed by the reduced total isotope effect.* Nature, 2001. **411**(6836): p. 457-460.

105. Hinks, D.G. and J.D. Jorgensen, *The isotope effect and phonons in MgB_2.* Physica C-Superconductivity and Its Applications, 2003. **385**(1-2): p. 98-104.

106. Kang, W.N., H.J. Kim, E.M. Choi, C.U. Jung and S.L. Lee, *MgB_2 superconducting thin films with a transition temperature of 39 kelvin.* Science, 2001. **292**(5521): p. 1521-1523.

107. Kim, H.J., W.N. Kang, E.M. Choi, M.S. Kim, K.H.P. Kim and S. Lee, *High current-carrying capability in c-axis-oriented superconducting MgB_2 thin films - art. no. 087002.* Physical Review Letters, 2001. **8708**(8): p. 7002.

108. Eom, C.B., M.K. Lee, J.H. Choi, L.J. Belenky, X. Song, L.D. Cooley, M.T. Naus, S. Patnaik, J. Jiang, M. Rikel, A. Polyanskii, A. Gurevich, X.Y. Cai, S.D. Bu, S.E. Babcock, E.E. Hellstrom, D.C. Larbalestier, N. Rogado, K.A. Regan, M.A. Hayward, T. He, J.S. Slusky, K. Inumaru, M.K. Haas, and R.J. Cava, *High critical current density and enhanced irreversibility field in superconducting MgB_2 thin films.* Nature, 2001. **411**(6837): p. 558-560.

109. Paranthaman, M., C. Cantoni, H.Y. Zhai, H.M. Christen, T. Aytug, S. Sathyamurthy, E.D. Specht, J.R. Thompson, D.H. Lowndes, H.R. Kerchner, and

D.K. Christen, *Superconducting MgB_2 films via precursor postprocessing approach.* Applied Physics Letters, 2001. **78**(23): p. 3669-3671.

110. Moon, S.H., J.H. Yun, H.N. Lee, J.I. Kye, H.G. Kim, W. Chung and B. Oh, *High critical current densities in superconducting MgB_2 thin films.* Applied Physics Letters, 2001. **79**(15): p. 2429-2431.

111. Zhai, H.Y., H.M. Christen, L. Zhang, A. Paranthaman, C. Cantoni, B.C. Sales, P.H. Fleming, D.K. Christen and D.H. Lowndes, *Growth mechanism of superconducting MgB_2 films prepared by various methods.* Journal of Materials Research, 2001. **16**(10): p. 2759-2762.

112. Plecenik, A., L. Satrapinsky, P. Kus, S. Gazi, S. Benacka, I. Vavra and I. Kostic, *MgB_2 superconducting thin films on Si and Al_2O_3 substrates.* Physica C, 2001. **363**(4): p. 224-230.

113. Ueda, K. and M. Naito, *As-grown superconducting MgB_2 thin films prepared by molecular beam epitaxy.* Applied Physics Letters, 2001. **79**(13): p. 2046-2048.

114. Grassano, G., W. Ramadan, V. Ferrando, E. Bellingeri, D. Marre, C. Ferdeghini, G. Grasso, M. Putti, P. Manfrinetti, A. Palenzona, and A. Chincarini, *As-grown magnesium diboride superconducting thin films deposited by pulsed laser deposition.* Superconductor Science & Technology, 2001. **14**(9): p. 762-764.

115. Jo, W., J.U. Huh, T. Ohnishi, A.F. Marshall, M.R. Beasley and R.H. Hammond, *In situ growth of superconducting MgB_2 thin films with preferential orientation by molecular-beam epitaxy.* Applied Physics Letters, 2002. **80**(19): p. 3563-3565.

116. Zhao, Y., M. Ionescu, A.V. Pan and S.X. Dou, *In situ annealing of superconducting MgB_2 films prepared by pulsed laser deposition.* cond-mat/0310755, 2003.

117. Zeng, X.H., A.V. Pogrebnyakov, A. Kotcharov, J.E. Jones, X.X. Xi, E.M. Lysczek, J.M. Redwing, S.Y. Xu, J. Lettieri, D.G. Schlom, W. Tian, X.Q. Pan, and Z.K. Liu, *In situ epitaxial MgB_2 thin films for superconducting electronics.* Nature Materials, 2002. **1**(1): p. 35-38.

118. He, T., R.J. Cava and J.M. Rowell, *Reactivity of MgB_2 with common substrate and electronic materials.* Applied Physics Letters, 2002. **80**(2): p. 291-293.

119. Wang, S.F., S.Y. Dai, Y.L. Zhou, Z.H. Chen, D.F. Cui, J.D. Xu, M. He, H.B. Lu and G.Z. Yang, *Superconducting MgB_2 thin films with T_c approximate to 39 K grown by pulsed laser deposition.* Chinese Physics Letters, 2001. **18**(7): p. 967-968.

120. Zeng, X.H., A. Sukiasyan, X.X. Xi, Y.F. Hu, E. Wertz, Q. Li, W. Tian, H.P. Sun, X.Q. Pan, J. Lettieri, D.G. Schlom, C.O. Brubaker, and Z.K. Liu, *Superconducting properties of nanocrystalline MgB_2 thin films made by an in situ annealing process.* Applied Physics Letters, 2001. **79**(12): p. 1840-1842.

121. Grassano, G., W. Ramadan, V. Ferrando, E. Bellingeri, D. Marre', C. Ferdeghini, G. Grasso, M. Putti, A.S. Siri, P. Manfrinetti, A. Palenzona, and ChincariniA., *In-situ Magnesium Diboride Superconducting Thin Films grown by Pulsed Laser Deposition.* cond-mat/0103572, 2001.

122. Christen, H.M., H.Y. Zhai, C. Cantoni, M. Paranthaman, B.C. Sales, C. Rouleau, D.P. Norton, D.K. Christen and D.H. Lowndes, *Superconducting magnesium diboride films with T_c approximate to 24 K grown by pulsed laser deposition with in situ anneal.* Physica C, 2001. **353**(3-4): p. 157-161.

123. Ermolov, S.N., M.V. Indenbom, A.N. Rossolenko, I.K. Bdikin, L.S. Uspenskaya, N.S. Stepakov and V.G. Glebovskii, *Superconducting MgB_2 films obtained by magnetron sputtering.* JETP Letters, 2001. **73**(10): p. 557-561.

124. Blank, D.H.A., H. Hilgenkamp, A. Brinkman, D. Mijatovic, G. Rijnders and H. Rogalla, *Superconducting Mg-B films by pulsed-laser deposition in an in situ two-step process using multicomponent targets.* Applied Physics Letters, 2001. **79**(3): p. 394-396.

125. Brinkman, A., D. Veldhuis, D. Mijatovic, G. Rijnders, D.H.A. Blank, H. Hilgenkamp and H. Rogalla, *Superconducting quantum interference device based on MgB_2 nanobridges.* Applied Physics Letters, 2001. **79**(15): p. 2420-2422.

126. Berenov, A., Z. Lockman, X. Qi, J.L. MacManus-Driscoll, Y. Bugoslavsky, L.F. Cohen, M.H. Jo, N.A. Stelmashenko, V.N. Tsaneva, M. Kambara, N.H. Babu, D.A. Cardwell, and M.G. Blamire, *Growth of strongly biaxially aligned MgB_2 thin films on sapphire by postannealing of amorphous precursors.* Applied Physics Letters, 2001. **79**(24): p. 4001-4003.

127. Brinkman, A., D. Mijatovic, G. Rijnders, V. Leca, H.J.H. Smilde, I. Oomen, A.A. Golubov, F. Roesthuis, S. Harkema, H. Hilgenkamp, D.H.A. Blank, and H. Rogalla, *Superconducting thin films of MgB_2 on Si by pulsed laser deposition.* Physica C, 2001. **353**(1-2): p. 1-4.

128. Ferdeghini, C., V. Ferrando, G. Grassano, W. Ramadan, E. Bellingeri, V. Braccini, D. Marre, P. Manfrinetti, A. Palenzona, F. Borgatti, R. Felici, and T.L. Lee, *Growth of c-oriented MgB_2 thin films by pulsed laser deposition: structural characterization and electronic anisotropy.* Superconductor Science & Technology, 2001. **14**(11): p. 952-957.

129. Shinde, S.R., S.B. Ogale, R.L. Greene, T. Venkatesan, P.C. Canfield, S.L. Bud'ko, G. Lapertot and C. Petrovic, *Superconducting MgB_2 thin films by pulsed laser deposition.* Applied Physics Letters, 2001. **79**(2): p. 227-229.

130. Wang, S.F., S.Y. Dai, Y.L. Zhou, Z.H. Chen, D.F. Cui, J.D. Xu, M. He, H.B. Lu, G.Z. Yang, G.S. Fu, and L. Han, *Superconducting MgB_2 thin films grown by pulsed laser deposition on $Al_2O_3(0001)$ and MgO(100) substrates.* Superconductor Science & Technology, 2001. **14**(11): p. 885-887.

131. Andreone, A., A. Cassinese, C. Cantoni, E. Di Gennaro, G. Lamura, M.G. Maglione, M. Paranthaman, M. Salluzzo and R. Vaglio, *Study of the microwave electrodynamic response of MgB_2 thin films.* Physica C, 2002. **372**: p. 1287-1290.

132. Bu, S.D., D.M. Kim, J.H. Choi, J. Giencke, E.E. Hellstrom, D.C. Larbalestier, S. Patnaik, L. Cooley, C.B. Eom, J. Lettieri, D.G. Schlom, W. Tian, and X.Q. Pan, *Synthesis and properties of c-axis oriented epitaxial MgB_2 thin films.* Applied Physics Letters, 2002. **81**(10): p. 1851-1853.

133. Chen, K., P. Ma, R.J. Nie, T. Yang, F.X. Xie, L.Y. Liu, S.Z. Wang, D. Dai and F. Wang, *Growth and superconductivity characteristics of MgB_2 thin films.* Superconductor Science & Technology, 2002. **15**(12): p. 1721-1724.

134. Chromik, S., S. Benacka, S. Gazi, V. Strbik, Z. Oszi and I. Kostic, *Superconducting properties of MgB_2 thin films prepared by sequential deposition of boron and magnesium.* Vacuum, 2002. **69**(1-3): p. 351-354.

135. Ferdeghini, C., V. Ferrando, G. Grassano, W. Ramadan, E. Bellingeri, V. Braccini, D. Marre, M. Putti, P. Manfrinetti, A. Palenzona, F. Borgatti, R. Felici, and C. Aruta, *Anisotropy in c-oriented MgB_2 thin films grown by pulsed laser deposition.* Physica C-Superconductivity and Its Applications, 2002. **378**: p. 56-60.

136. Ferdeghini, C., V. Ferrando, G. Grassano, W. Ramadan, V. Braccini, M. Putti, P. Manfrinetti and A. Palenzona, *Transport properties of c-oriented MgB_2 thin films grown by pulsed laser deposition.* Physica C, 2002. **372**: p. 1270-1273.

137. Fu, X.H., D.S. Wang, Z.P. Zhang and J. Yang, *Superconducting MgB_2 thin films prepared by chemical vapor deposition from diborane.* Physica C-Superconductivity and Its Applications, 2002. **377**(4): p. 407-410.

138. Ionescu, M., J. McKinnon, C. Cai, A. Li, K. Konstantinov, A.V. Pan and S.X. Dou, *Growths of MgB_2 thin films by pulsed laser deposition.* Crystal Engineering, 2002. **5**(3-4): p. 391-400.

139. Ivanov, Z., A. Malisa, L.G. Johansson and P.V. Komissinski, *Superconductivity in magnesium diboride thin films.* Physica C, 2002. **372**: p. 1274-1276.

140. Kang, W.N., H.J. Kim, E.M. Choi, K.H.P. Kim and S.I. Lee, *Growth and transport properties of c-axis-oriented MgB_2 thin films.* Physica C-Superconductivity and Its Applications, 2002. **378**: p. 1246-1251.

141. Kus, P., A. Plecenik, L. Satrapinsky, Y. Xu and R. Sobolewski, *Superconducting properties of MgB_2 thin films prepared on flexible plastic substrates.* Applied Physics Letters, 2002. **81**(12): p. 2199-2201.

142. Mijatovic, D., A. Brinkman, G. Rijnders, H. Hilgenkamp, H. Rogalla and D.H.A. Blank, *Superconducting thin films of MgB_2 by pulsed-laser deposition.* Physica C, 2002. **372**: p. 1258-1261.

143. Saito, A., A. Kawakami, H. Shimakage and Z. Wang, *As-grown MgB_2 thin films deposited on Al_2O_3 substrates with different crystal planes.* Superconductor Science & Technology, 2002. **15**(9): p. 1325-1329.

144. Ueda, K., H. Yamamoto and M. Naito, *Synthesis and photoemission study of as-grown superconducting MgB_2 thin films.* Physica C-Superconductivity and Its Applications, 2002. **378**: p. 225-228.

145. Vaglio, R., M.G. Maglione and R. Di Capua, *High-quality MgB_2 thin films in situ grown by dc magnetron sputtering.* Superconductor Science & Technology, 2002. **15**(8): p. 1236-1239.

146. van Erven, A.J.M., T.H. Kim, M. Muenzenberg and J.S. Moodera, *Highly crystallized as-grown smooth and superconducting MgB_2 films by molecular-beam epitaxy.* Applied Physics Letters, 2002. **81**(26): p. 4982-4984.

147. Wang, D.S., X.H. Fu, Z.P. Zhang and J. Yang, *A new method for preparing superconducting MgB_2 films from diborane.* Chinese Physics Letters, 2002. **19**(8): p. 1179-1180.

148. Xi, X.X., X.H. Zeng, A. Soukiassian, J. Jones, J. Hotchkiss, Y. Zhong, C.O. Brubaker, Z.K. Liu, J. Lettieri, D.G. Schlom, Y.F. Hu, E. Wertz, Q. Li, W. Tian, H.P. Sun, and X.Q. Pan, *Thermodynamics and thin film deposition of MgB_2 superconductors.* Superconductor Science & Technology, 2002. **15**(3): p. 451-457.

149. Ahn, J.R., S.G. Lee, Y.S. Hwang, G.Y. Sung and D.K. Kim, *Fabrication of MgB_2 thin film by rf magnetron sputtering.* Physica C-Superconductivity and Its Applications, 2003. **388**: p. 127-128.

150. Akinaga, M., S. Umeda, H. Hasegawa and T. Shirasawa, *A simple preparation of superconducting MgB_2 thin films by composite-target sputtering system.* Physica C-Superconductivity and Its Applications, 2003. **388**: p. 119-120.

151. Andreone, A., A. Cassinese, F. Chiarella, R. Di Capua, E. Di Gennaro, G. Lamura, M.G. Maglione, M. Salluzzo and R. Vaglio, *In situ sputtering growth and characterization of MgB_2 films for microwave applications.* IEEE Transactions on Applied Superconductivity, 2003. **13**(2): p. 3602-3605.

152. Ferrando, V., S. Amoruso, E. Bellingeri, R. Bruzzese, P. Manfrinetti, D. Marre, R. Velotta, X. Wang and C. Ferdeghini, *Growth methods of c-axis oriented MgB_2 thin films by pulsed laser deposition.* Superconductor Science & Technology, 2003. **16**(2): p. 241-245.

153. Hikita, Y., T. Fukumura, T. Ito, M. Kawasaki and H. Takagi, *Fabrication of MgB_2 thin film on boride substrates by pulsed laser deposition.* Journal of Low Temperature Physics, 2003. **131**(5-6): p. 1187-1191.

154. Maglione, M.G., F. Chiarella, R. Di Capua, R. Vaglio, M. Salvato, L. Maritato and S.L. Prischepa, *High quality fully in-situ MgB_2 thin films obtained by DC*

magnetron sputtering. International Journal of Modern Physics B, 2003. **17**(4-6): p. 779-784.

155. Mori, Z., K. Eitoku, T. Doi, S. Koba and Y. Hakuraku, *MgB_2 thin film fabrication by rf magnetron sputtering.* Physica C-Superconductivity and Its Applications, 2003. **388**: p. 115-116.

156. Peng, N., G. Shao, C. Jeynes, R.P. Webb, R.M. Gwilliam, G. Boudreault, D.M. Astill and W.Y. Liang, *Ion beam synthesis of superconducting MgB_2 thin films.* Applied Physics Letters, 2003. **82**(2): p. 236-238.

157. Pogrebnyakov, A.V., J.M. Redwing, J.E. Jones, X.X. Xi, S.Y. Xu, Q. Li, V. Vaithyanathan and D.G. Schlom, *Thickness dependence of the properties of epitaxial MgB_2 thin films grown by hybrid physical-chemical vapor deposition.* Applied Physics Letters, 2003. **82**(24): p. 4319-4321.

158. Ueda, K. and M. Naito, *In situ growth of superconducting MgB_2 thin films by molecular-beam epitaxy.* Journal of Applied Physics, 2003. **93**(4): p. 2113-2120.

159. Wang, S.F., Y.L. Zhou, Y.B. Zhu, Z. Liu, Q. Zhang, Z.H. Chen, H.B. Lu, S.Y. Dai and G.Z. Yang, *Preparation and properties of MgB2 thin films on LaAlO3 substrates by chemical vapour deposition.* Superconductor Science & Technology, 2003. **16**(7): p. 748-751.

160. Zeng, X.H., A.V. Pogrebnyakov, M.H. Zhu, J.E. Jones, X.X. Xi, S.Y. Xu, E. Wertz, Q. Li, J.M. Redwing, J. Lettieri, V. Vaithyanathan, D.G. Schlom, Z.K. Liu, O. Trithaveesak, and J. Schubert, *Superconducting MgB_2 thin films on silicon carbide substrates by hybrid physical-chemical vapor deposition.* Applied Physics Letters, 2003. **82**(13): p. 2097-2099.

161. Lee, S., *Crystal growth of MgB_2.* Physica C-Superconductivity and Its Applications, 2003. **385**(1-2): p. 31-41.

162. Karpinski, J., S.M. Kazakov, J. Jun, M. Angst, R. Puzniak, A. Wisniewski and P. Bordet, *Single crystal growth of MgB_2 and thermodynamics of Mg-B-N system at high pressure.* Physica C-Superconductivity and Its Applications, 2003. **385**(1-2): p. 42-48.

163. Liu, Z.K., D.G. Schlom, Q. Li and X.X. Xi, *Thermodynamics of the Mg-B system: Implications for the deposition of MgB_2 thin films.* Applied Physics Letters, 2001. **78**(23): p. 3678-3680.

164. Xu, M., H. Kitazawa, Y. Takano, J. Ye, K. Nishida, H. Abe, A. Matsushita, N. Tsujii and G. Kido, *Anisotropy of superconductivity from MgB_2 single crystals.* Applied Physics Letters, 2001. **79**(17): p. 2779-2781.

165. Kim, K.H.P., J.H. Choi, C.U. Jung, P. Chowdhury, H.S. Lee, M.S. Park, H.J. Kim, J.Y. Kim, Z.L. Du, E.M. Choi, M.S. Kim, W.N. Kang, S.I. Lee, G.Y. Sung, and J.Y. Lee, *Superconducting properties of well-shaped MgB_2 single crystals - art. no. 100510.* Physical Review B, 2002. **6510**(10): p. 510-510.

166. Cho, Y.C., S.E. Park, S.Y. Jeong, C.R. Cho, B.J. Kim, Y.C. Kim and H.S. Youn, *Properties of superconducting MgB_2 single crystal grown by a modified flux method.* Applied Physics Letters, 2002. **80**(19): p. 3569-3571.

167. Atsumi, T., M. Tsuji, M.X. Xu, H. Kitazawa and T. Ishida, *Temperature dependence of magnetic torque for a single crystal MgB_2 in 10 kG.* Physica C-Superconductivity and Its Applications, 2003. **388**: p. 165-166.

168. Badr, M.H. and K.W. Ng, *A new heat treatment to prepare high-quality polycrystalline and single crystal MgB_2 in a single process.* Superconductor Science & Technology, 2003. **16**(6): p. 668-671.

169. Jung, C.U., J.Y. Kim, P. Chowdhury, K.H.P. Kim, S.I. Lee, D.S. Koh, N. Tamura, W.A. Caldwell and J.R. Patel, *Microstructure and pinning properties of hexagonal-disc shaped single crystalline MgB_2 - art. no. 184519.* Physical Review B, 2002. **6618**(18): p. 4519-4519.

170. Machida, Y., S. Sasaki, H. Fujii, M. Furuyama, I. Kakeya and K. Kadowaki, *Ambient-pressure synthesis of single-crystal MgB_2 and their superconducting anisotropy - art. no. 094507.* Physical Review B, 2003. **6709**(9): p. 4507-4507.

171. Karpinski, J., M. Angst, J. Jun, S.M. Kazakov, R. Puzniak, A. Wisniewski, J. Roos, H. Keller, A. Perucchi, L. Degiorgi, M.R. Eskildsen, P. Bordet, L. Vinnikov, and A. Mironov, *MgB_2 single crystals: high pressure growth and physical properties.* Superconductor Science & Technology, 2003. **16**(2): p. 221-230.

172. Souptel, D., G. Behr, W. Loser, W. Kopylov and M. Zinkevich, *Crystal growth of MgB_2 from Mg-Cu-B melt flux and superconducting properties.* Journal of Alloys and Compounds, 2003. **349**(1-2): p. 193-200.

173. Lee, S., H. Mori, T. Masui, Y. Eltsev, A. Yamamoto and S. Tajima, *Growth, structure analysis and anisotropic superconducting properties of MgB_2 single crystals.* Journal of the Physical Society of Japan, 2001. **70**(8): p. 2255-2258.

174. Angst, M., R. Puzniak, A. Wisniewski, J. Jun, S.M. Kazakov, J. Karpinski, J. Roos and H. Keller, *Temperature and field dependence of the anisotropy of MgB_2 - art. no. 167004.* Physical Review Letters, 2002. **8816**(16): p. 7004-7004.

175. Pradhan, A.K., Z.X. Shi, M. Tokunaga, T. Tamegai, Y. Takano, K. Togano, H. Kito and H. Ihara, *Electrical transport and anisotropic superconducting properties in single crystalline and dense polycrystalline MgB_2 - art. no. 212509.* Physical Review B, 2001. **6421**(21): p. 2509.

176. Lee, S., A. Yamamoto, H. Mori, Y. Eltsev, T. Masui and S. Tajima, *Single crystals of MgB_2 superconductor grown under high-pressure in Mg-B-N system.* Physica C-Superconductivity and Its Applications, 2002. **378**: p. 33-37.

177. Lee, S., T. Masui, H. Mori, Y. Eltsev, A. Yamamoto and S. Tajima, *Crystal growth and characterization of MgB_2: the relation between structural and*

superconducting properties. Superconductor Science & Technology, 2003. **16**(2): p. 213-220.

178. Canfield, P.C., D.K. Finnemore, S.L. Bud'ko, J.E. Ostenson, G. Lapertot, C.E. Cunningham and C. Petrovic, *Superconductivity in dense MgB_2 wires.* Physical Review Letters, 2001. **86**(11): p. 2423-2426.

179. Wang, X.L., S. Soltanian, J. Horvat, A.H. Liu, M.J. Qin, H.K. Liu and S.X. Dou, *Very fast formation of superconducting MgB_2/Fe wires with high J_c.* Physica C, 2001. **361**(3): p. 149-155.

180. Soltanian, S., X.L. Wang, I. Kusevic, E. Babic, A.H. Li, M.J. Qin, J. Horvat, H.K. Liu, E.W. Collings, E. Lee, M.D. Sumption, and S.X. Dou, *High-transport critical current density above 30 K in pure Fe-clad MgB_2 tape.* Physica C, 2001. **361**(2): p. 84-90.

181. Jin, S., H. Mavoori, C. Bower and R.B. van Dover, *High critical currents in iron-clad superconducting MgB_2 wires.* Nature, 2001. **411**(6837): p. 563-565.

182. Suo, H.L., C. Beneduce, M. Dhalle, N. Musolino, J.Y. Genoud and R. Flukiger, *Large transport critical currents in dense Fe- and Ni-clad MgB_2 superconducting tapes.* Applied Physics Letters, 2001. **79**(19): p. 3116-3118.

183. Horvat, J., X.L. Wang, S. Soltanian and S.X. Dou, *Improvement of critical current in MgB_2/Fe superconducting wires by a ferromagnetic sheath.* Applied Physics Letters, 2002. **80**(5): p. 829-831.

184. Kovac, P., I. Husek and T. Melisek, *Transport currents of two-axially rolled and post-annealed MgB_2/Fe wires at 4.2 K.* Superconductor Science & Technology, 2002. **15**(9): p. 1340-1344.

185. Kumakura, H., A. Matsumoto, H. Fujii and K. Togano, *Development of powder-in-tube processed MgB_2 tapes and wires.* Journal of the Japan Institute of Metals, 2002. **66**(4): p. 214-222.

186. Nast, R., S.I. Schlachter, S. Zimmer, H. Reiner and W. Goldacker, *Mechanically reinforced MgB_2 wires and tapes with high transport currents.* Physica C, 2002. **372**: p. 1241-1244.

187. Sumption, M.D., E.W. Collings, E. Lee, X.L. Wang, S. Soltanian and S.X. Dou, *Reduction and elimination of external-field AC loss in MgB_2/Fe wire by in situ magnetic shielding.* Physica C-Superconductivity and Its Applications, 2002. **378**: p. 894-898.

188. Suo, H.L., C. Beneduce, X.D. Su and R. Flukiger, *Fabrication and transport critical currents of multifilamentary MgB_2/Fe wires and tapes.* Superconductor Science & Technology, 2002. **15**(7): p. 1058-1062.

189. Suo, H.L., C. Beneduce, M. Dhalle, P. Toulemonde and R. Flukiger, *High transport critical currents in dense monofilamentary Fe- and Ni-clad MgB_2*

tapes and MgB_2/Fe wires with 7 filaments. IEEE Transactions on Applied Superconductivity, 2002. **12**(1): p. 1079-1083.

190. Zhou, S.H., A.V. Pan, H.K. Liu, J. Horvat and S.X. Dou, *Effect of various mechanical deformation processes on critical current density and microstructure in MgB_2 tapes and wires.* Superconductor Science & Technology, 2002. **15**(11): p. 1490-1493.

191. Zhou, S.H., A.V. Pan, H.K. Liu and S.X. Dou, *Single- and multi-filamentary Fe-sheathed MgB_2 wires.* Physica C-Superconductivity and Its Applications, 2002. **382**(4): p. 349-354.

192. Collings, E.W., E. Lee, M.D. Sumption, M. Tomsic, X.L. Wang, S. Soltanian and S.X. Dou, *Continuous- and batch-processed MgB_2/Fe strands - transport and magnetic properties.* Physica C-Superconductivity and Its Applications, 2003. **386**: p. 555-559.

193. Dou, S.X., J. Horvat, S. Soltanian, X.L. Wang, M.J. Qin, S.H. Zhou, H.K. Liu and P.G. Munroe, *Transport critical current density in Fe-sheathed nano-SiC doped MgB_2 wires.* Ieee Transactions on Applied Superconductivity, 2003. **13**(2): p. 3199-3202.

194. Fabbricatore, P., M. Greco, R. Musenich, P. Kovac, I. Husek and F. Gomory, *Influence of the sintering process on critical currents, irreversibility lines and pinning energies in multifilamentary MgB_2 wires.* Superconductor Science & Technology, 2003. **16**(3): p. 364-370.

195. Feng, Y., G. Yan, Y. Zhao, C.F. Liu, B.Q. Fu, L. Zhou, L.Z. Cao, K.Q. Ruan, X.G. Li, L. Shi, and Y.H. Zhang, *Superconducting properties of MgB_2 wires and tapes with different metal sheaths.* Physica C-Superconductivity and Its Applications, 2003. **386**: p. 598-602.

196. Feng, Y., G. Yan, Y. Zhao, X.J. Wu, A.K. Pradhan, X. Zhang, C.F. Liu, X.H. Liu and L. Zhou, *High critical current density in MgB_2/Fe wires.* Superconductor Science & Technology, 2003. **16**(6): p. 682-684.

197. Flukiger, R., H.L. Suo, N. Musolino, C. Beneduce, P. Toulemonde and P. Lezza, *Superconducting properties of MgB_2 tapes and wires (vol 385, pg 286, 2003).* Physica C-Superconductivity and Its Applications, 2003. **387**(3-4): p. 419-419.

198. Flukiger, R., P. Lezza, C. Beneduce, N. Musolino and H.L. Suo, *Improved transport critical current and irreversibility fields in mono- and multifilamentary Fe/MgB_2 tapes and wires using fine powders.* Superconductor Science & Technology, 2003. **16**(2): p. 264-270.

199. Flukiger, R., H.L. Suo, N. Musolino, C. Beneduce, P. Toulemonde and P. Lezza, *Superconducting properties of MgB_2 tapes and wires.* Physica C-Superconductivity and Its Applications, 2003. **385**(1-2): p. 286-305.

200. Glowacki, B.A., M. Majoros, M. Eisterer, S. Toenies, H.W. Weber, M. Fukutomi, K. Komori and K. Togano, *MgB_2 superconductors for applications.* Physica C-Superconductivity and Its Applications, 2003. **387**(1-2): p. 153-161.

201. Goldacker, M.W., S.I. Schlachter, J. Reiner, S. Zimmer, A. Nyilas and H. Kiesel, *Mechanical properties of reinforced MgB_2 wires.* IEEE Transactions on Applied Superconductivity, 2003. **13**(2): p. 3261-3264.

202. Horvat, J., S. Soltanian, X.L. Wang and S.X. Dou, *Magnetic shielding in MgB_2/Fe superconducting wires.* IEEE Transactions on Applied Superconductivity, 2003. **13**(2): p. 3324-3327.

203. Kovac, P., M. Dhalle, T. Melisek, H.J.N. van Eck, W.A.J. Wessel, B. ten Haken and I. Husek, *Dependence of the critical current in ex situ multi- and mono-filamentary MgB_2/Fe wires on axial tension and compression.* Superconductor Science & Technology, 2003. **16**(5): p. 600-607.

204. Kovac, P., I. Husek, C. Grovenor and C. Salter, *Properties of as-deformed and post-annealed MgB_2/Fe(Fe-alloy) composite wires.* Superconductor Science & Technology, 2003. **16**(2): p. 292-296.

205. Kovac, P., M. Ahoranta, T. Melisek, J. Lehtonen and I. Husek, *The effect of Fe-magnetization on $I_c(B)$ and $I_c(alpha)$ characteristics of iron-sheathed MgB_2 composite wires.* Superconductor Science & Technology, 2003. **16**(7): p. 793-798.

206. Kumakura, H., A. Matsumoto, H. Fujii, H. Kitaguchi, S. Ooi, K. Togano and H. Hatakeyama, *Fabrication and properties of powder-in-tube processed MgB_2 tapes and wires.* Journal of Low Temperature Physics, 2003. **131**(5-6): p. 1085-1093.

207. Pan, A.V., S.H. Zhou, H.K. Liu and S.X. Don, *Properties of superconducting MgB_2 wires: in situ versus ex situ reaction technique.* Superconductor Science & Technology, 2003. **16**(5): p. 639-644.

208. Schlachter, S.I., W. Goldacker, J. Reiner, S. Zimmer, B. Liu and B. Obst, *Influence of the preparation process on microstructure, critical current density and T_c of MgB_2 powder-in-tube wires.* IEEE Transactions on Applied Superconductivity, 2003. **13**(2): p. 3203-3206.

209. Suo, H.L., P. Lezza, D. Uglietti, C. Beneduce, V. Abacherli and R. Flukiger, *Transport critical current densities and n factors in mono- and multifilamentary MgB_2/Fe tapes and wires using fine powders.* IEEE Transactions on Applied Superconductivity, 2003. **13**(2): p. 3265-3268.

210. Yan, G., B.Q. Fu, Y. Feng, C.F. Liu, P. Ji, X.Z. Wu, L. Zhou, L.Z. Cao, K.Q. Ruan and X.G. Li, *Preparation and transport $J_c(B)$ properties of Fe-clad MgB_2 wires.* Physica C-Superconductivity and Its Applications, 2003. **386**: p. 607-610.

211. Zhou, S.H., A.V. Pan, M.J. Qin, H.K. Liu and S.X. Dou, *Effect of the processing parameters of $MgB_{1.8}(SiC)_{0.1}$/Fe tapes on the critical current density.* Physica C-Superconductivity and Its Applications, 2003. **387**(3-4): p. 321-327.

212. Zhou, S.H., H.K. Liu, J. Horvat and S.X. Dou, *Effect of Ti doping on the superconductivities of MgB_2/Fe wires.* Journal of Low Temperature Physics, 2003. **131**(3-4): p. 687-692.

213. Glowacki, B.A., M. Majoros, M. Vickers, J.E. Evetts, Y. Shi and I. McDougall, *Superconductivity of powder-in-tube MgB_2 wires.* Superconductor Science & Technology, 2001. **14**(4): p. 193-199.

214. Pradhan, A.K., Y. Feng, Y. Zhao, N. Koshizuka, L. Zhou, P.X. Zhang, X.H. Liu, P. Ji, S.J. Du and C.F. Liu, *Transport behavior and critical current densities in MgB_2 wires.* Applied Physics Letters, 2001. **79**(11): p. 1649-1651.

215. Beilin, V., I. Felner, E. Yashchin, E. Dul'kin, M. Roth, I. Lapides and A. Verdyan, *Critical current anisotropy in non-sintered metal-clad MgB_2 tapes.* Physica C, 2002. **377**(1-2): p. 15-20.

216. Eisterer, M., B.A. Glowacki, H.W. Weber, L.R. Greenwood and M. Majoros, *Enhanced transport currents in Cu-sheathed MgB_2 wires.* Superconductor Science & Technology, 2002. **15**(7): p. 1088-1091.

217. Glowacki, B.A. and M. Majoros, *MgB_2 conductors for dc and ac applications.* Physica C, 2002. **372**: p. 1235-1240.

218. Glowacki, B.A., M. Majoros, M.E. Vickers and B. Zeimetz, *Superconducting properties of the powder-in-tube Cu-Mg-B and Ag-Mg-B wires.* Physica C, 2002. **372**: p. 1254-1257.

219. Kovac, P., I. Husek, W. Pachla, T. Melisek, R. Diduszko, K. Frohlich, A. Morawski, A. Presz and D. Machajdik, *Structure, grain connectivity and pinning of as-deformed commercial MgB_2 powder in Cu and Fe/Cu sheaths.* Superconductor Science & Technology, 2002. **15**(7): p. 1127-1132.

220. Majoros, M., B.A. Glowacki and M.E. Vickers, *50 K anomalies in superconducting MgB_2 wires in copper and silver tubes.* Superconductor Science & Technology, 2002. **15**(2): p. 269-275.

221. Martinez, E., L.A. Angurel and R. Navarro, *Study of Ag and Cu/MgB_2 powder-in-tube composite wires fabricated by in situ reaction at low temperatures.* Superconductor Science & Technology, 2002. **15**(7): p. 1043-1047.

222. Pachla, W., A. Presz, R. Diduszko, P. Kovac and I. Husek, *Structural inhomogeneity of superconducting ex situ MgB_2/Cu wires made by the powder-in-tube technique.* Superconductor Science & Technology, 2002. **15**(9): p. 1281-1287.

223. Soltanian, S., X.L. Wang, J. Horvat, A.H. Li, H.K. Liu and S.X. Dou, *Improvement of critical current density in the Cu/MgB_2 and Ag/MgB_2*

superconducting wires using the fast formation method. Physica C-Superconductivity and Its Applications, 2002. **382**(2-3): p. 187-193.

224. Martinez, E., L.A. Angurel, R. Navarro, A. Millan, C. Rillo and M. Artigas, *Study of MgB_2 powders and Cu/MgB_2 powder-in-tube composite wires with Zn addition.* Ieee Transactions on Applied Superconductivity, 2003. **13**(2): p. 3210-3213.

225. Strickland, N.M., R.G. Buckley and A. Otto, *High critical current densities in Cu-sheathed MgB_2 formed from a mechanically-alloyed precursor.* Applied Physics Letters, 2003. **83**(2): p. 326-328.

226. Yang, T.R., G. Ilonca, A.V. Pop, R. Stiufiuc and O. Furdui, *Superconductivity of MgB_2 wires.* Physica C-Superconductivity and Its Applications, 2003. **388**: p. 125-126.

227. Soltanian, S., J. Horvat, X.L. Wang, M. Tomsic and S.X. Dou, *Transport critical current of solenoidal MgB_2/Cu coils fabricated using a wind-reaction in situ technique.* Superconductor Science & Technology, 2003. **16**(1): p. L4-L6.

228. Grasso, G., A. Malagoli, D. Marre, E. Bellingeri, V. Braccini, S. Roncallo, N. Scati and A.S. Siri, *Transport properties of powder-in-tube processed MgB_2 tapes.* Physica C-Superconductivity and Its Applications, 2002. **378**: p. 899-902.

229. Malagoli, A., A. Tumino, V. Braccini, C. Ferdeghini, A.S. Siri, L. Martini, C. Vignola, V. Previtali, G. Volpini and G. Grasso, *Magnetic field dependence of the critical current in MgB_2 and Bi-2223 superconducting tapes fabricated by the powder-in-tube method.* IEEE Transactions on Applied Superconductivity, 2003. **13**(2): p. 3328-3331.

230. Tanaka, K., M. Okada, H. Kumakura, H. Kitaguchi and K. Togano, *Fabrication and transport properties of MgB_2 wire and coil.* Physica C-Superconductivity and Its Applications, 2002. **382**(2-3): p. 203-206.

231. Xu, J.D., S.F. Wang, Y.B. Zhou, Y.L. Zhou, Z.H. Chen, D.F. Cui, H.B. Lu, M. He, S.Y. Dai and G.Z. Yang, *Preparation of MgB_2 superconducting tapes using electrophoresis.* Superconductor Science & Technology, 2002. **15**(8): p. 1190-1192.

232. Kumakura, H., A. Matsumoto, H. Fujii and K. Togano, *High transport critical current density obtained for powder-in-tube-processed MgB_2 tapes and wires using stainless steel and Cu-Ni tubes.* Applied Physics Letters, 2001. **79**(15): p. 2435-2437.

233. Civale, L., A. Serquis, D.L. Hammon, X.Z. Liao, J.Y. Coulter, Y.T. Zhu, T. Holesinger, D.E. Peterson and F.M. Mueller, *High critical currents in powder in tube MgB_2 wires: Influence of microstructure and heat treatments.* IEEE Transactions on Applied Superconductivity, 2003. **13**(2): p. 3347-3350.

234. Liao, X.Z., A. Serquis, Y.T. Zhu, L. Civale, D.L. Hammon, D.E. Peterson, F.M. Mueller, V.F. Nesterenko and Y. Gu, *Defect structures in MgB_2 wires*

introduced by hot isostatic pressing. Superconductor Science & Technology, 2003. **16**(7): p. 799-803.

235. Serquis, A., L. Civale, D.L. Hammon, X.Z. Liao, J.Y. Coulter, Y.T. Zhu, M. Jaime, D.E. Peterson, F.M. Mueller, V.F. Nesterenko, and Y. Gu, *Hot isostatic pressing of powder in tube MgB_2 wires.* Applied Physics Letters, 2003. **82**(17): p. 2847-2849.

236. Serquis, A., L. Civale, D.L. Hammon, J.Y. Coulter, X.Z. Liao, Y.T. Zhu, D.E. Peterson and F.M. Mueller, *Microstructure and high critical current of powder-in-tube MgB_2.* Applied Physics Letters, 2003. **82**(11): p. 1754-1756.

237. Serquis, A., L. Civale, D.L. Hammon, X.Z. Liao, J.Y. Coulter, Y.T. Zhu, D.E. Peterson and F.M. Mueller, *Role of excess Mg and heat treatments on microstructure and critical current of MgB_2 wires.* Journal of Applied Physics, 2003. **94**(6): p. 4024-4031.

238. Glowacki, B.A., M. Majoros, M. Vickers, M. Eisterer, S. Toenies, H.W. Weber, M. Fukutomi, K. Komori and K. Togano, *Composite Cu/Fe/MgB_2 superconducting wires and MgB_2/YSZ/Hastelloy coated conductors for ac and dc applications.* Superconductor Science & Technology, 2003. **16**(2): p. 297-305.

239. Goldacker, W. and S.I. Schlachter, *Influence of mechanical reinforcement of MgB_2 wires on the superconducting properties.* Physica C-Superconductivity and Its Applications, 2002. **378**: p. 889-893.

240. Soltanian, S., X.L. Wang, A.H. Li, E.W. Collings, M.D. Sumption, E. Lee, H.K. Liu and S.X. Dou, *Fabrication and critical current density in 16-filament stainless steel/Fe/MgB_2 square wire.* Solid State Communications, 2002. **124**(1-2): p. 59-62.

241. Eyidi, D., O. Eibl, T. Wenzel, K.G. Nickel, S.I. Schlachter and W. Goldacker, *Superconducting properties, microstructure and chemical composition of MgB_2 sheathed materials.* Superconductor Science & Technology, 2003. **16**(7): p. 778-788.

242. Feng, Y., Y. Zhao, A.K. Dradhan, L. Zhou, X.H. Liu, P. Ji, P.X. Zhang and Y.P. Sun, *High critical current density in powder-in-tube processed MgB_2/Ta/Cu wire.* Chinese Science Bulletin, 2002. **47**(3): p. 251-252.

243. Feng, Y., Y. Zhao, A.K. Pradhan, L. Zhou, P.X. Zhang, X.H. Liu, P. Ji, S.J. Du, C.F. Liu, Y. Wu, and N. Koshizuka, *Fabrication and superconducting properties of MgB_2 composite wires by the PIT method.* Superconductor Science & Technology, 2002. **15**(1): p. 12-15.

244. Fu, B.Q., Y. Feng, G. Yan, Y. Zhao, A.K. Pradhan, C.H. Cheng, P. Ji, X.H. Liu, C.F. Liu, L. Zhou, and K.F. Yau, *High critical current density in Ti-doped MgB_2/Ta/Cu tape by powder-in-tube process.* Journal of Applied Physics, 2002. **92**(12): p. 7341-7344.

245. Goldacker, W., S.I. Schlachter, S. Zimmer and H. Reiner, *High transport currents in mechanically reinforced MgB_2 wires.* Superconductor Science & Technology, 2001. **14**(9): p. 787-793.

246. Fang, H., S. Padmanabhan, Y.X. Zhou and K. Salama, *High critical current density in iron-clad MgB_2 tapes.* Applied Physics Letters, 2003. **82**(23): p. 4113-4115.

247. Fang, H., S. Padmanabhan, Y.X. Zhou, P.T. Putman and K. Salama, *High I_c in iron-clad MgB_2 tape.* IEEE Transactions on Applied Superconductivity, 2003. **13**(2): p. 3207-3209.

248. Fujii, H., K. Togano and H. Kumakura, *Enhancement of critical current density of in situ processed MgB_2 tapes by WB addition.* Superconductor Science & Technology, 2003. **16**(4): p. 432-436.

249. Ma, Y.W., H. Kumakura, A. Matsumoto, H. Hatakeyama and K. Togano, *Improvement of critical current density in Fe-sheathed MgB_2 tapes by $ZrSi_2$, ZrB_2 and WSi_2 doping.* Superconductor Science & Technology, 2003. **16**(8): p. 852-856.

250. Ma, Y.W., H. Kumakura, A. Matsumoto and K. Togano, *Microstructure and high critical current density of in situ processed MgB_2 tapes made by WSi_2 and $ZrSi_2$ doping.* Applied Physics Letters, 2003. **83**(6): p. 1181-1183.

251. Matsumoto, A., H. Kumakura, H. Kitaguchi and H. Hatakeyama, *Effect of SiO_2 and SiC doping on the powder-in-tube processed MgB_2 tapes.* Superconductor Science & Technology, 2003. **16**(8): p. 926-930.

252. Zhou, S.H., A.V. Pan, M. Ionescu, H.K. Liu and S.X. Dou, *Influence of Ag, Cu and Fe sheaths on MgB_2 superconducting tapes.* Superconductor Science & Technology, 2002. **15**(2): p. 236-240.

253. Fischer, C., C. Rodig, W. Hassler, O. Perner, J. Eckert, K. Nenkov, G. Fuchs, H. Wendrock, B. Holzapfel and L. Schultz, *Preparation of MgB_2 tapes using a nanocrystalline partially reacted precursor.* Applied Physics Letters, 2003. **83**(9): p. 1803-1805.

254. Ruan, K.Q., H.L. Li, Y. Yu, C.Y. Wang, L.Z. Cao, C.F. Liu, S.J. Du, G. Yan, Y. Feng, X. Wu, J.R. Wang, X.H. Liu, P.X. Zhang, X.Z. Wu, and L. Zhou, *Transport critical current density of Fe sheath MgB_2 tapes sintered at different temperatures.* Physica C-Superconductivity and Its Applications, 2003. **386**: p. 578-580.

255. Xiao, H., W.H. Song, J.J. Du, Y.P. Sun and J. Fang, *Preparation and superconductivity of MgB_2/Cu tapes.* Physica C-Superconductivity and Its Applications, 2003. **386**: p. 593-597.

256. Fujii, H., H. Kumakura and K. Togano, *Influence of MgB_2 powder quality on the transport properties of Cu-sheathed MgB2 tapes.* Physica C, 2001. **363**(4): p. 237-242.

257. Grasso, G., A. Malagoli, C. Ferdeghini, S. Roncallo, V. Braccini, A.S. Siri and M.R. Cimberle, *Large transport critical currents in unsintered MgB_2 superconducting tapes.* Applied Physics Letters, 2001. **79**(2): p. 230-232.

258. Kumakura, H., A. Matsumoto, H. Fujii, H. Kitaguchi and K. Togano, *Microstructure and superconducting properties of powder-in-tube processed MgB_2 tapes.* Physica C-Superconductivity and Its Applications, 2002. **382**(1): p. 93-97.

259. Hassler, W., C. Rodig, C. Fischer, B. Holzapfel, O. Perner, J. Eckert, K. Nenkov and G. Fuchs, *Low temperature preparation of MgB_2 tapes using mechanically alloyed powder.* Superconductor Science & Technology, 2003. **16**(2): p. 281-284.

260. Ko, J.W., J. Yoo, Y.K. Kim, H.D. Kim, K.H. Oh, S.J. Choe, H. Chung, S.J. Chung, H. Kumakura, A. Matsumoto, and K. Togano, *Influence of Cu addition on microstructure and transport properties in MgB_2 tapes.* IEEE Transactions on Applied Superconductivity, 2003. **13**(2): p. 3214-3216.

261. Matsumoto, A., H. Hatakeyama, H. Kitaguchi, K. Togano and H. Kumakura, *The superconducting properties of MgB_2/(stainless steel) tapes fabricated by the PIT process.* IEEE Transactions on Applied Superconductivity, 2003. **13**(2): p. 3225-3228.

262. Kitaguchi, H., H. Kumakura and K. Togano, *Strain effect in MgB_2/stainless steel superconducting tape.* Physica C, 2001. **363**(3): p. 198-201.

263. Matsumoto, A., H. Kumakura, H. Kitaguchi, H. Fujii and K. Togano, *The annealing effects of MgB_2 superconducting tapes.* Physica C-Superconductivity and Its Applications, 2002. **382**(2-3): p. 207-212.

264. Song, K.J., C. Park, N.J. Lee, H.M. Jang, H.S. Ha, D.W. Ha, S.S. Oh, M.H. Sohn, R.K. Ko, Y.K. Kwon, and J.H. Joo, *Fabrications and properties of MgB_2/stainless-steel tapes by PIT process.* IEEE Transactions on Applied Superconductivity, 2003. **13**(2): p. 3221-3224.

265. Malagoli, A., G. Grasso, A. Tumino, M. Modica, V. Braccini, S. Roncallo, E. Bellingeri, C. Ferdeghini and A.S. Siri, *Fabrication and characterization of Ni-sheathed MgB_2 superconducting tapes.* International Journal of Modern Physics B, 2003. **17**(4-6): p. 461-467.

266. Tachikawa, K., Y. Yamada, M. Enomoto, M. Aodai and H. Kumakura, *Effects of metal powder addition on the structure and critical current of Ni-sheathed PIT MgB_2 tapes.* Ieee Transactions on Applied Superconductivity, 2003. **13**(2): p. 3269-3272.

267. Malagoli, A., V. Braccini, N. Scati, S. Roncallo, A.S. Siri and G. Grasso, *Fabrication and superconducting properties of powder-in-tube processed MgB_2 tapes.* Physica C, 2002. **372**: p. 1245-1247.

268. Tachikawa, K., Y. Yamada, O. Suzuki, M. Enomoto and M. Aodai, *Effects of metal powder addition on the critical current in MgB_2 tapes.* Physica C-Superconductivity and Its Applications, 2002. **382**(1): p. 108-112.

269. Bellingeri, E., A. Malagoli, M. Modica, V. Braccini, A.S. Siri and G. Grasso, *Neutron scattering studies of superconducting MgB_2 tapes.* Superconductor Science & Technology, 2003. **16**(2): p. 276-280.

270. Grasso, G., A. Malagoli, M. Modica, A. Tumino, C. Ferdeghini, A.S. Siri, C. Vignola, L. Martini, V. Previtali and G. Volpini, *Fabrication and properties of monofilamentary MgB_2 superconducting tapes.* Superconductor Science & Technology, 2003. **16**(2): p. 271-275.

271. Sumption, M.D., X. Peng, E. Lee, M. Tomsic and E.W. Collings, *Transport current in MgB_2 based superconducting strand at 4.2 K and self-field.* cond-mat/0102441, 2001.

272. Kovac, P., K. Hense, T. Melisek, I. Husek and H. Kirchmayr, *I-c anisotropy and I_c hysteresis in MgB_2/Fe/Cu tape.* Superconductor Science & Technology, 2002. **15**(7): p. 1037-1039.

273. Fu, B.Q., Y. Feng, Y. Zhao, A.K. Pradhan, C.H. Cheng, P. Ji, X.H. Liu, C.F. Liu, G. Yan and L. Zhou, *Microstructures and superconducting properties in Ti-doped MgB_2/Ta/Cu tape.* Physica C-Superconductivity and Its Applications, 2003. **386**: p. 659-662.

274. Liu, C.F., S.J. Du, G. Yan, Y. Feng, X. Wu, J.R. Wang, X.H. Liu, P.X. Zhang, X.Z. Wu, L. Zhou, L.Z. Gao, K.Q. Ruan, C.Y. Wang, X.G. Li, G.E. Zhou, and Y.H. Zhang, *Preparation of 18-filament Cu/NbZr/MgB_2 tape with high transport critical current density.* Cond-mat/0106061, 2001.

275. Fujii, H., K. Togano and H. Kumakura, *Fabrication of MgB_2 tapes sheathed with carbon steels by ex situ and in situ methods.* IEEE Transactions on Applied Superconductivity, 2003. **13**(2): p. 3217-3220.

276. Fujii, H., K. Togano and H. Kumakura, *Enhancement of critical current densities of powder-in-tube processed MgB_2 tapes by using MgH_2 as a precursor powder.* Superconductor Science & Technology, 2002. **15**(11): p. 1571-1576.

277. Fujii, H., H. Kumakura and K. Togano, *Improved critical current in MgB_2 tapes sheathed with carbon steels.* Journal of Materials Research, 2002. **17**(9): p. 2339-2345.

278. Giunchi, G., S. Ceresara, G. Ripamonti, A. Di Zenobio, S. Rossi, S. Chiarelli, M. Spadoni, R. Wesche and P.L. Bruzzone, *High performance new MgB_2 superconducting hollow wires.* Superconductor Science & Technology, 2003. **16**(2): p. 285-291.

279. Ferdeghini, C., V. Braccini, E. Bellingeri, M.R. Cimberle, V. Ferrando, G. Grasso, A. Malagoli, P. Manfrinetti, D. Marre, M. Modica, A. Palenzona, I. Pallecchi, L. Pellegrino, M. Putti, W. Ramadan, S. Roncallo, A. Tumino, and

A.S. Siri, *Some aspects of material preparation in magnesium diboride: Thin films growth and tapes fabrication.* International Journal of Modern Physics B, 2003. **17**(4-6): p. 400-406.

280. DeFouw, J.D. and D.C. Dunand, *In situ synthesis of superconducting MgB_2 fibers within a magnesium matrix.* Applied Physics Letters, 2003. **83**(1): p. 120-122.

281. Ma, R.Z., Y. Bando, T. Mori and D. Golberg, *Direct pyrolysis method for superconducting crystalline MgB_2 nanowires.* Chemistry of Materials, 2003. **15**(16): p. 3194-3197.

282. Yan, Y.F. and M.M. Al-Jassim, *Solubility, diffusion, and precipitation of oxygen impurities in MgB_2 - art. no. 212503.* Physical Review B, 2003. **6721**(21): p. 2503-2503.

283. Goto, D., T. Machi, Y. Zhao, N. Koshizuka, M. Murakami and S. Arai, *Improvement of critical current density in MgB_2 by Ti, Zr and Hf doping.* Physica C-Superconductivity and Its Applications, 2003. **392**: p. 272-275.

284. Gumbel, A., J. Eckert, G. Fuchs, K. Nenkov, K.H. Muller and L. Schultz, *Improved superconducting properties in nanocrystalline bulk MgB_2.* Applied Physics Letters, 2002. **80**(15): p. 2725-2727.

285. Gumbel, A., O. Perner, J. Eckert, G. Fuchs, K. Nenkov, K.H. Muller and L. Schultz, *High density nanocrystalline MgB_2 bulk superconductors with improved pinning.* IEEE Transactions on Applied Superconductivity, 2003. **13**(2): p. 3064-3067.

286. Viznichenko, R.V., A.A. Kordyuk, G. Fuchs, K. Nenkov, K.H. Muller, T.A. Prikhna and W. Gawalek, *Temperature dependence of the trapped magnetic field in MgB_2 bulk superconductors.* Applied Physics Letters, 2003. **83**(21): p. 4360-4362.

287. Morawski, A., T. Lada and K. Przybylski, *High gas pressure treatments of MgB_2 material.* Physica C-Superconductivity and Its Applications, 2003. **387**(1-2): p. 143-147.

288. Sumption, M.D., E. Lee, X.L. Wang, E.W. Collings and S.X. Dou, *AC (hysteretic) loss by magnetic shielding of MgB_2/Fe superconductors: the pseudo-Meissner effect,.* Advances in Cryogenic Engineering (Materials), 2001. **48**: p. 824.

289. Abe, H., M. Naito, K. Nogi, M. Matsuda, M. Miyake, S. Ohara, A. Kondo and T. Fukui, *Low temperature formation of superconducting MgB_2 phase from elements by mechanical milling.* Physica C-Superconductivity and Its Applications, 2003. **391**(2): p. 211-216.

290. Cunningham, C.E., C. Petrovic, G. Lapertot, S.L. Bud'ko, F. Laabs, W. Straszheim, D.K. Finnemore and P.C. Canfield, *Synthesis and processing of MgB_2 powders and wires.* Physica C, 2001. **353**(1-2): p. 5-10.

291. Canfield, P.C., S.L. Bud'ko, D.K. Finnemore, G. Lapertot, C. Petrovic, C.E. Cunningham, V.G. Kogan, M.H. Jung and A.H. Lacerda, *Basic physical properties of polycrystalline MgB_2 pellets and wires*, in *Superconducting Magnesium Diboride*. 2002, Nova Science Publishers: Hauppauge. p. 1-24.

292. Shen, Q.F., X. Xie, G.H. Zhang, Q.R. Feng, X.L. Xu, C.G. Li, Z.X. Gao, S. Luo, Y.S. He and D. Jin, *Electric transport study of superconducting MgB_2 wire.* Physica C-Superconductivity and Its Applications, 2003. **388**: p. 111-112.

293. Goto, T. and H. Katoh, *Fabrication of MgB_2 superconducting wire by suspension spinning.* Physica C-Superconductivity and Its Applications, 2002. **378**: p. 903-906.

294. Goto, T., H. Katoh and K. Watanabe, *Field dependence of transport J_c for MgB_2 superconducting wire by suspension spinning.* IEEE Transactions on Applied Superconductivity, 2003. **13**(2): p. 3229-3232.

295. Che, G.C., S.L. Li, Z.A. Ren, L. Li, S.L. Jia, Y.M. Ni, H. Chen, C. Dong, J.Q. Li, H.H. Wen, and Z.X. Zhao, *Preparation and superconductivity of a MgB_2 superconducting tape.* cond-mat/0105215, 2001.

296. Komori, K., K. Kawagishi, Y. Takano, H. Fujii, S. Arisawa, H. Kumakura, M. Fukutomi and K. Togano, *Approach for the fabrication of MgB_2 superconducting tape with large in-field transport critical current density.* Applied Physics Letters, 2002. **81**(6): p. 1047-1049.

297. Paranthaman, M., J.R. Thompson and D.K. Christen, *Effect of carbon-doping in bulk superconducting MgB_2 samples.* Physica C, 2001. **355**(1-2): p. 1-5.

298. Maurin, I., S. Margadonna, K. Prassides, T. Takenobu, Y. Iwasa and A.N. Fitch, *Carbon miscibility in the boron layers of the MgB_2 superconductor.* Chemistry of Materials, 2002. **14**(9): p. 3894-3897.

299. Maurin, I., S. Margadonna, K. Prassides, T. Takenobu, T. Ito, D.H. Chi, Y. Iwasa and A. Fitch, *Phase separation in carbon-doped MgB_2 superconductors.* Physica B, 2002. **318**(4): p. 392-397.

300. Mickelson, W., J. Cumings, W.Q. Han and A. Zettl, *Effects of carbon doping on superconductivity in magnesium diboride - art. no. 052505.* Physical Review B, 2002. **6505**(5): p. 2505.

301. Papagelis, K., J. Arvanitidis, S. Margadonna, Y. Iwasa, T. Takenobu, M. Pissass and K. Prassides, *Phase separation in carbon-doped MgB_2 studied by means of alternating current susceptibility measurements.* Journal of Physics-Condensed Matter, 2002. **14**(31): p. 7363-7369.

302. Avdeev, M., J.D. Jorgensen, R.A. Ribeiro, S.L. Bud'ko and P.C. Canfield, *Crystal chemistry of carbon-substituted MgB_2.* Physica C-Superconductivity and Its Applications, 2003. **387**(3-4): p. 301-306.

303. Ribeiro, R.A., S.L. Bud'ko, C. Petrovic and P.C. Canfield, *Carbon doping of superconducting magnesium diboride.* Physica C-Superconductivity and Its Applications, 2003. **384**(3): p. 227-236.

304. Ribeiro, R.A., S.L. Bud'ko, C. Petrovic and P.C. Canfield, *Effects of boron purity, Mg stoichiometry and carbon substitution on properties of polycrystalline MgB_2.* Physica C-Superconductivity and Its Applications, 2003. **385**(1-2): p. 16-23.

305. Soltanian, S., J. Horvat, X.L. Wang, P. Munroe and S. Dou, *Effect of nano-carbon particle doping on the flux pinning properties of MgB_2 superconductor.* Physica C-Superconductivity and Its Applications, 2003. **390**(3): p. 185-190.

306. Cimberle, M.R., M. Novak, P. Manfrinetti and A. Palenzona, *Magnetic characterization of sintered MgB_2 samples: effect of substitution or 'doping' with Li, Al and Si.* Superconductor Science & Technology, 2002. **15**(1): p. 43-47.

307. Luo, H., C.M. Li, H.M. Luo and S.Y. Ding, *Study of Al doping effect on superconductivity of $Mg_{1-x}Al_xB_2$.* Journal of Applied Physics, 2002. **91**(10): p. 7122-7124.

308. Xiang, J.Y., D.N. Zheng, J.Q. Li, L. Li, P.L. Lang, H. Chen, C. Dong, G.C. Che, Z.A. Ren, H.H. Qi, H.Y. Tian, Y.M. Ni, and Z.X. Zhao, *Superconducting properties and c-axis superstructure of $Mg_{1-x}Al_xB_2$ - art. no. 214536.* Physical Review B, 2002. **6521**(21): p. 4536-4536.

309. Cheng, C.H., Y. Zhao, X.T. Zhu, J. Nowotny, C.C. Sorrell, T. Finlayson and H. Zhang, *Chemical doping effect on the crystal structure and superconductivity of MgB_2.* Physica C-Superconductivity and Its Applications, 2003. **386**: p. 588-592.

310. Toulemonde, P., N. Musolino and R. Flukiger, *High-pressure synthesis of pure and doped superconducting MgB_2 compounds.* Superconductor Science & Technology, 2003. **16**(2): p. 231-236.

311. Xiang, J.Y., D.N. Zheng, J.Q. Li, S.L. Li, H.H. Wen and Z.X. Zhao, *Effects of Al doping on the superconducting and structural properties of MgB_2.* Physica C-Superconductivity and Its Applications, 2003. **386**: p. 611-615.

312. Xu, S., Y. Moritomo, K. Kato and A. Nakamura, *Mn-substitution effects on MgB_2 superconductor.* Journal of the Physical Society of Japan, 2001. **70**(7): p. 1889-1891.

313. Feng, Y., Y. Zhao, Y.P. Sun, F.C. Liu, B.Q. Fu, L. Zhou, C.H. Cheng, N. Koshizuka and M. Murakami, *Improvement of critical current density in MgB_2 superconductors by Zr doping at ambient pressure.* Applied Physics Letters, 2001. **79**(24): p. 3983-3985.

314. Feng, Y., Y. Zhao, A.K. Pradhan, C.H. Cheng, J.K.F. Yau, L. Zhou, N. Koshizuka and M. Murakami, *Enhanced flux pinning in Zr-doped MgB_2 bulk superconductors prepared at ambient pressure.* Journal of Applied Physics, 2002. **92**(5): p. 2614-2619.

315. Zhao, Y., Y. Feng, D.X. Huang, T. Machi, C.H. Cheng, K. Nakao, N. Chikumoto, Y. Fudamoto, N. Koshizuka and M. Murakami, *Doping effect of Zr and Ti on the critical current density of MgB_2 bulk superconductors prepared under ambient pressure.* Physica C-Superconductivity and Its Applications, 2002. **378**: p. 122-126.

316. Li, S.Y., Y.M. Xiong, W.Q. Mo, R. Fan, C.H. Wang, X.G. Luo, Z. Sun, H.T. Zhang, L. Li, L.Z. Cao, and X.H. Chen, *Alkali metal substitution effects in $Mg_{1-x}A_xB_2$ (A = Li and Na).* Physica C, 2001. **363**(4): p. 219-223.

317. Zhao, Y.G., X.P. Zhang, P.T. Qiao, H.T. Zhang, S.L. Jia, B.S. Cao, M.H. Zhu, Z.H. Han, X.L. Wang and B.L. Gu, *Effect of Li doping on structure and superconducting transition temperature of $Mg_{1-x}Li_xB_2$.* Physica C, 2001. **361**(2): p. 91-94.

318. Li, H.L., K.Q. Ruan, S.Y. Li, Y. Yu, C.Y. Wang and L.Z. Cao, *Upper critical field and the effect of Li doping on the activation energy in MgB_2.* Physica C-Superconductivity and Its Applications, 2003. **386**: p. 560-564.

319. Wang, X.L., S.H. Zhou, M.J. Qin, P.R. Munroe, S. Soltanian, H.K. Liu and S.X. Dou, *Significant enhancement of flux pinning in MgB_2 superconductor through nano-Si addition.* Physica C-Superconductivity and Its Applications, 2003. **385**(4): p. 461-465.

320. Ahn, J.S., Y.J. Kim, M.S. Kim, S.I. Lee and E.J. Choi, *Structural and superconducting properties of $MgB_{2-x}Be_x$ - art. no. 172503.* Physical Review B, 2002. **6517**(17): p. 2503-2503.

321. Cheng, C.H., Y. Zhao, L. Wang and H. Zhang, *Preparation, structure and superconductivity of $Mg_{1-x}Ag_xB_2$.* Physica C-Superconductivity and Its Applications, 2002. **378**: p. 244-248.

322. Zhao, Y., C.H. Cheng, T. Machi, N. Koshizuka and M. Murakami, *Improved chemical stability of Ti-doped MgB_2 in water.* Applied Physics Letters, 2002. **80**(13): p. 2311-2313.

323. Trociewitz, U.P., P. Sastry, A. Wyda, K. Crockett and J. Schwartz, *Magnetic properties of neutron irradiated and doped MgB_2 superconductors.* IEEE Transactions on Applied Superconductivity, 2003. **13**(2): p. 3320-3323.

324. Hinks, D.G., J.D. Jorgensen, H. Zheng and S. Short, *Synthesis and stoichiometry of MgB_2.* Physica C-Superconductivity and Its Applications, 2002. **382**(2-3): p. 166-176.

325. Kuhberger, M. and G. Gritzner, *Effects of Sn, Co and Fe on MgB_2.* Physica C, 2002. **370**(1): p. 39-43.

326. Kuzmann, E., Z. Homonnay, Z. Klencsar, M. Kuhberger, A. Vertes and G. Gritzner, *Local environments of iron and cobalt in doped MgB_2 superconductors.* Superconductor Science & Technology, 2002. **15**(11): p. 1479-1485.

327. Sekkina, M.M.A. and K.M. Elsabawy, *Fluoride doping and Boron particle size effect on $MgB_{2-x}F_x$ superconductor.* Solid State Communications, 2002. **123**(1-2): p. 1-6.

328. Tampieri, A., G. Celotti, S. Sprio, D. Rinaldi, G. Barucca and R. Caciuffo, *Effects of copper doping in MgB_2 superconductor.* Solid State Communications, 2002. **121**(9-10): p. 497-500.

329. Profeta, G., A. Continenza, A. Floris and S. Massidda, *Cu doping effects in MgB_2 - art. no. 174510.* Physical Review B, 2003. **6717**(17): p. 4510-4510.

330. Gu, D.W., Y.M. Cai, J.K.F. Yau, Y.G. Cui, T. Wu, G.Q. Yuan, L.J. Shen and X. Jin, *Effect of Pb substitution in bulk superconducting MgB_2.* Physica C-Superconductivity and Its Applications, 2003. **386**: p. 643-647.

331. Sekkina, M.M.A. and K.M. Elsabawy, *Narrow range of iridium-substitution on $Mg_{1-x}Ir_xB_2$ superconductor.* Physica C-Superconductivity and Its Applications, 2003. **391**(3): p. 217-222.

332. Dou, S.X., S. Soltanian, J. Horvat, X.L. Wang, S.H. Zhou, M. Ionescu, H.K. Liu, P. Munroe and M. Tomsic, *Enhancement of the critical current density and flux pinning of MgB_2 superconductor by nanoparticle SiC doping.* Applied Physics Letters, 2002. **81**(18): p. 3419-3421.

333. Dou, S.X., A.V. Pan, S. Zhou, M. Ionescu, H.K. Liu and P.R. Munroe, *Substitution-induced pinning in MgB_2 superconductor doped with SiC nano-particles.* Superconductor Science & Technology, 2002. **15**(11): p. 1587-1591.

334. Dou, S.X., A.V. Pan, S. Zhou, M. Ionescu, X.L. Wang, J. Horvat, H.K. Liu and P.R. Munroe, *Superconductivity, critical current density, and flux pinning in $MgB_{2-x}(SiC)_{x/2}$ superconductor after SiC nanoparticle doping.* Journal of Applied Physics, 2003. **94**(3): p. 1850-1856.

335. Soltanian, S., X.L. Wang, J. Horvat, M.J. Qin, H.K. Liu, P.R. Munroe and S.X. Dou, *Effect of grain size and doping level of SiC on the superconductivity and critical current density in MgB_2 superconductor.* IEEE Transactions on Applied Superconductivity, 2003. **13**(2): p. 3273-3276.

336. Wang, J., Y. Bugoslavsky, A. Berenov, L. Cowey, A.D. Caplin, L.F. Cohen, J.L.M. Driscoll, L.D. Cooley, X. Song and D.C. Larbalestier, *High critical current density and improved irreversibility field in bulk MgB_2 made by a scaleable, nanoparticle addition route.* Applied Physics Letters, 2002. **81**(11): p. 2026-2028.

337. Cava, R.J., H.W. Zandbergen and K. Inumaru, *The substitutional chemistry of MgB_2.* Physica C-Superconductivity and Its Applications, 2003. **385**(1-2): p. 8-15.

338. Slusky, J.S., N. Rogado, K.A. Regan, M.A. Hayward, P. Khalifah, T. He, K. Inumaru, S.M. Loureiro, M.K. Haas, H.W. Zandbergen, and R.J. Cava, *Loss of*

superconductivity with the addition of Al to MgB_2 and a structural transition in $Mg_{1-x}Al_xB_2$. Nature, 2001. **410**(6826): p. 343-345.

339. Perkins, G.K., J. Moore, Y. Bugoslavsky, L.F. Cohen, J. Jun, S.M. Kazakov, J. Karpinski and A.D. Caplin, *Superconducting critical fields and anisotropy of a MgB_2 single crystal.* Superconductor Science & Technology, 2002. **15**(7): p. 1156-1159.

340. Canfield, P.C., S.L. Bud'ko and D.K. Finnemore, *An overview of the basic physical properties of MgB_2.* Physica C-Superconductivity and Its Applications, 2003. **385**(1-2): p. 1-7.

341. Zehetmayer, M., M. Eisterer, J. Jun, S.M. Kazakov, J. Karpinski, A. Wisniewski and H.W. Weber, *Mixed-state properties of superconducting MgB_2 single crystals - art. no. 052505.* Physical Review B, 2002. **6605**(5): p. 2505-2505.

342. Caplin, A.D., Y. Bugoslavsky, L.F. Cohen, L. Cowey, J. Driscoll, J. Moore and G.K. Perkins, *Critical fields and critical currents in MgB_2.* Superconductor Science & Technology, 2003. **16**(2): p. 176-182.

343. Lyard, L., P. Samuely, P. Szabo, C. Marcenat, T. Klein, K.H.P. Kim, C.U. Jung, H.S. Lee, B. Kang, S. Choi, S.I. Lee, L. Paulius, J. Marcus, S. Blanchard, A.G.M. Jansen, U. Welp, G. Karapetrov, and W.K. Kwok, *Upper critical magnetic fields in single crystal MgB_2.* Superconductor Science & Technology, 2003. **16**(2): p. 193-198.

344. Gurevich, A., S. Patnaik, V. Braccini, K.H. Kim, C. Mielke, X. Song, L.D. Cooley, S.D. Bu, D.M. Kim, J.H. Choi, L.J. Belenky, J. Giencke, M.K. Lee, W. Tian, X.Q. Pan, A. Siri, E.E. Hellstrom, C.B. Eom, and D.C. Larbalestier, *Very high upper critical fields in MgB_2 produced by selective tuning of impurity scattering.* cond-mat/0305474, 2003.

345. Dou, S.X., V. Braccini, S. Soltanian, R. Klie, Y. Zhu, S. Li, X.L. Wang and D. Larbalestier, *Nanoscale-SiC doping for enhancing Jc and H_{c2} in the superconducting MgB_2.* cond-mat/0308265, 2003.

346. Jung, M.H., M. Jaime, A.H. Lacerda, G.S. Boebinger, W.N. Kang, H.J. Kim, E.M. Choi and S.I. Lee, *Anisotropic Superconductivity in Epitaxial MgB2 Films.* cond-mat/0106146, 2001.

347. Patnaik, S., L.D. Cooley, A. Gurevich, A.A. Polyanskii, J. Jing, X.Y. Cai, A.A. Squitieri, M.T. Naus, M.K. Lee, J.H. Choi, L. Belenky, S.D. Bu, J. Letteri, X. Song, D.G. Schlom, S.E. Babcock, C.B. Eom, E.E. Hellstrom, and D.C. Larbalestier, *Electronic anisotropy, magnetic field-temperature phase diagram and their dependence on resistivity in c-axis oriented MgB_2 thin films.* Superconductor Science & Technology, 2001. **14**(6): p. 315-319.

348. Takano, Y., H. Takeya, H. Fujii, H. Kumakura, T. Hatano, K. Togano, H. Kito and H. Ihara, *Superconducting properties of MgB_2 bulk materials prepared by high-pressure sintering.* Applied Physics Letters, 2001. **78**(19): p. 2914-2916.

349. Li, S.L., H.H. Wen, Z.W. Zhao, Y.M. Ni, Z.A. Ren, G.C. Che, H.P. Yang, Z.Y. Liu and Z.X. Zhao, *Linear temperature dependence of lower critical field in MgB_2 - art. no. 094522.* Physical Review B, 2001. **6409**(9): p. 4522.

350. Sharoni, A., I. Felner and O. Millo, *Tunneling spectroscopy and magnetization measurements of the superconducting properties of MgB_2 - art. no. 220508.* Physical Review B, 2001. **6322**(22): p. 0508.

351. Joshi, A.G., C.G.S. Pillai, P. Raj and S.K. Malik, *Magnetization studies on superconducting MgB_2 - lower and upper critical fields and critical current density.* Solid State Communications, 2001. **118**(9): p. 445-448.

352. Carrington, A. and F. Manzano, *Magnetic penetration depth of MgB_2.* Physica C-Superconductivity and Its Applications, 2003. **385**(1-2): p. 205-214.

353. Schmidt, V.V., *The Physics of Superconductors*, ed. P. Mueller and A.V. Ustinov. 1997, Berlin: Springer-Velag.

354. de Lima, O.F., R.A. Ribeiro, M.A. Avila, C.A. Cardoso and A.A. Coelho, *Anisotropic superconducting properties of aligned MgB_2 crystallites.* Physical Review Letters, 2001. **86**(26): p. 5974-5977.

355. Bud'ko, S.L., V.G. Kogan and P.C. Canfield, *Determination of superconducting anisotropy from magnetization data on random powders as applied to $LuNi_2B_2C$, YNi_2B_2C, and MgB_2 - art. no. 180506.* Physical Review B, 2001. **6418**(18): p. 0506.

356. Simon, F., A. Janossy, T. Feher, F. Muranyi, S. Garaj, L. Forro, C. Petrovic, S.L. Bud'ko, G. Lapertot, V.G. Kogan, and P.C. Canfield, *Anisotropy of superconducting MgB_2 as seen in electron spin resonance and magnetization data - art. no. 047002.* Physical Review Letters, 2001. **8704**(4): p. 7002.

357. Handstein, A., D. Hinz, G. Fuchs, K.H. Muller, K. Nenkov, O. Gutfleisch, V.N. Narozhnyi and L. Schultz, *Fully dense MgB_2 superconductor textured by hot deformation.* Journal of Alloys and Compounds, 2001. **329**(1-2): p. 285-289.

358. Hinz, D., A. Handstein, G. Fuchs, K.H. Muller, K. Nenkov, O. Gutfleisch, V.N. Narozhnyi and L. Schultz, *Observation of texture for fully dense MgB_2 superconductor processed by hot deformation.* Physica C, 2002. **372**: p. 1248-1250.

359. Narozhnyi, V.N., G. Fuchs, A. Handstein, A. Gumbel, J. Eckert, K. Nenkoy, D. Hinz, O. Gutfleisch, A. Walte, L.N. Bogacheva, I.E. Kostyleva, K.H. Muller, and L. Schultz, *Comparative study of dense bulk MgB_2 materials prepared by different methods.* Journal of Superconductivity, 2002. **15**(6): p. 599-601.

360. de Lima, O.F. and C.A. Cardoso, *Critical current density anisotropy of aligned MgB_2 crystallites.* Physica C-Superconductivity and Its Applications, 2003. **386**: p. 575-577.

361. Dulcic, A., M. Pozek, D. Paar, E.M. Choi, H.J. Kim, W.N. Kang and S.I. Lee, *Coherence lengths and anisotropy in MgB_2 superconductor - art. no. 020507.* Physical Review B, 2003. **6702**(2): p. 507-507.

362. Sen, S., A. Singh, D.K. Aswal, S.K. Gupta, J.V. Yakhmi, V.C. Sahni, E.M. Choi, H.J. Kim, K.H.P. Kim, H.S. Lee, W.N. Kang, and S.I. Lee, *Anisotropy of critical current density in c-axis-oriented MgB_2 thin films - art. no. 214521.* Physical Review B, 2002. **6521**(21): p. 4521-4521.

363. Takahashi, K., M.X. Xu, H. Kitazawa and T. Ishida, *Evidence for superconductivity in the boron layers of MgB_2.* Physica C-Superconductivity and Its Applications, 2003. **388**: p. 153-154.

364. Shi, Z.X., A.K. Pradhan, M. Tokunaga, T. Tamegai, Y. Takano, K. Togano, H. Kito and H. Ihara, *Comparative study on the anisotropic properties of MgB_2.* Physica C-Superconductivity and Its Applications, 2003. **388**: p. 157-158.

365. Lee, H.S., K.H.P. Kim, J.H. Choi, C.U. Jung, P. Chowdhury, S. Choi and S.K. Lee, *Transport and magnetic properties in MgB_2 single crystals.* Journal of Low Temperature Physics, 2003. **131**(5-6): p. 1117-1127.

366. Angst, M., R. Puzniak, A. Wisniewski, J. Roos, H. Keller, P. Miranovic, J. Jun, S.M. Kazakov and J. Karpinski, *Anisotropy of the superconducting state properties and phase diagram of MgB_2 by torque magnetometry on single crystals.* Physica C-Superconductivity and Its Applications, 2003. **385**(1-2): p. 143-153.

367. Lyard, L., P. Samuely, P. Szabo, T. Klein, C. Marcenat, L. Paulius, K.H.P. Kim, C.U. Jung, H.S. Lee, B. Kang, S. Choi, S.I. Lee, J. Marcus, S. Blanchard, A.G.M. Jansen, U. Welp, G. Karapetrov, and W.K. Kwok, *Anisotropy of the upper critical field and critical current in single crystal MgB_2 - art. no. 180502.* Physical Review B, 2002. **6618**(18): p. 502-502.

368. Eltsev, Y., S. Lee, K. Nakao, N. Chikumoto, S. Tajima, N. Koshizuka and M. Murakami, *Anisotropic superconducting properties of MgB_2 single crystals.* Physica C-Superconductivity and Its Applications, 2002. **378**: p. 61-64.

369. Masui, T., S. Lee, A. Yamamoto and S. Tajima, *Transport properties of MgB_2 single crystal.* Physica C-Superconductivity and Its Applications, 2002. **378**: p. 216-219.

370. Takahashi, K., T. Atsumi, N. Yamamoto, M.X. Xu, H. Kitazawa and T. Ishida, *Superconducting anisotropy and evidence for intrinsic pinning in single crystalline MgB_2 - art. no. 012501.* Physical Review B, 2002. **6601**(1): p. 2501-2501.

371. Eltsev, Y., S. Lee, K. Nakao, N. Chikumoto, S. Tajima, N. Koshizuka and M. Murakami, *Anisotropic superconducting properties of MgB_2 single crystals probed by in-plane electrical transport measurements - art. no. 140501.* Physical Review B, 2002. **6514**(14): p. 501-501.

372. Pradhan, A.K., M. Tokunaga, Z.X. Shi, Y. Takano, K. Togano, H. Kito, H. Ihara and T. Tamegai, *Angle-resolved magnetotransport studies in anisotropic MgB_2 single crystals - art. no. 144513.* Physical Review B, 2002. **6514**(14): p. 4513-4513.

373. Ekin, J.W., A.I. Braginski, A.J. Panson, M.A. Janocko, D.W. Capone II, N.J. Zaluzec, B. Flandermeyer, d.L.O. F., M. Hong, J. Kwo, and S.H. Liou, *Evidence for weak link and anisotropy limitations on the transport critical current in bulk polycrystalline $Y_1Ba_2Cu_3O_x$.* Journal of Applied Physics, 1987. **62**(12): p. 4821-4828.

374. Mannhart, J., P. Chaudhari, D. Dimos, C.C. Tsuei and T.R. McGuire, *Critical currents in [001] grains and across their tilt boundaries in $YBa_2Cu_3O_7$ films.* Physical Review Letters, 1998. **61**(21): p. 2476-2479.

375. Larbalestier, D.C., L.D. Cooley, M.O. Rikel, A.A. Polyanskii, J. Jiang, S. Patnaik, X.Y. Cai, D.M. Feldmann, A. Gurevich, A.A. Squitieri, M.T. Naus, C.B. Eom, E.E. Hellstrom, R.J. Cava, K.A. Regan, N. Rogado, M.A. Hayward, T. He, J.S. Slusky, P. Khalifah, K. Inumaru, and M. Haas, *Strongly linked current flow in polycrystalline forms of the superconductor MgB_2.* Nature, 2001. **410**(6825): p. 186-189.

376. Kambara, M., N.H. Babu, E.S. Sadki, J.R. Cooper, H. Minami, D.A. Cardwell, A.M. Campbell and I.H. Inoue, *High intergranular critical currents in metallic MgB_2 superconductor.* Superconductor Science & Technology, 2001. **14**(4): p. L5-L7.

377. Kim, K.H.P., W.N. Kang, M.-S. Kim, C.U. Jung, H.-J. Kim, E.-M. Choi, M.-S. Park and S.-I. Lee, *Origin of the high DC transport critical current density for the MgB_2 superconductor.* cond-mat/0103176, 2001.

CHAPTER 3: EXPERIMENTAL PROCEDURE

3-1 Sample Preparation

3-1-1 Preparation of Bulk MgB_2

Polycrystalline samples of MgB_2 were prepared through the conventional solid state reaction using a reaction *in-situ* process. High purity powders (99%) of magnesium (-325 mesh) and amorphous boron (-325 mesh) were used as starting materials. The precursor powders were weighed out according to the nominal atomic ratio and well mixed through grinding using a mortar and pestle. The powders were pressed into pellets 10 mm in diameter and 2-3 mm in thickness using a uniaxial hydraulic press. The pellets were sealed in Fe tubes, then heat treated at different temperature ranged between 680 ^{o}C to 950 ^{o}C. Wide range of sintering time were used from a few minutes to 2h. In order to get the pure phase and suitable results different sintering time and temperature have been used for different experiment. Heat treatment performed in flowing high purity Ar under the ambient pressure using the tube furnace. This was followed by a furnace cooling to room temperature. A temperature profile for the preparation of MgB_2 bulk sample is shown in the Fig. 3-1. Bar-shaped samples in a few millimeter size were cut and dry polished from the sintered pellets.

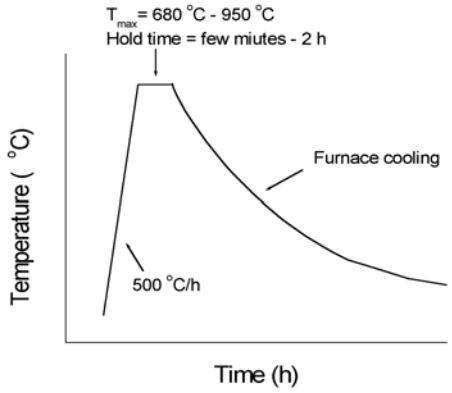

Figure 3- 1: Schematic drawing of the thermal treatment used in the preparation of MgB_2 samples.

3-1-2 Fabrication of MgB_2 Wire and Tape

3-1-2-1 Fabrication of Wire and Tape Using the Powder-in-Tube Technique

During this work Fe, Cu and Ag-clad MgB_2 wires were prepared using a standard powder-in-tube (PIT) method. The procedure is mainly consists of three steps.

I. Preparing the precursor powder and packing the powder into a metal tube.

II. Mechanical deformation process to make green wire or tape.

III. Heat treatment.

In the first step two different powders were used. In the experiments using the *ex situ* reaction technique, commercially available powder supplied by Alfa Acer was employed. However, *in situ* reaction technique was used in the most of the experiments. For these experiments, powders of magnesium and amorphous boron (both in 99% purity and –325 mesh) with the stoichiometry of MgB_2 were well mixed using an agate mortar and pestle. The mixed powder was then loaded into a metal tubes. The tubes used in the experiments have an outside diameter (OD) of 6-9 mm, a wall thickness of 0.5-1.5 mm, and a lenngh of about 10 cm depending on the experiment. One end of the tube was sealed either by a piece of lead or by a piece of aluminum. The tubes were filled in and packed with mixed powders. The remaining ends were crimped mechanically.

Mechanical deformation is the second step. Each tube was drawn to the final diameter of about 1.3 mm. Drawing was carried out by passing the tube through the conical hole of successive round dies at a speed of a few cm/s. For tape making, the thin wire was cold rolled to the flat tape with a thickness of 300-600 μm.

Apart from the above procedure two axial groove rolling was used to prepare the Stainless Steel sheath square wire. A deformation rate of no more than 15% per pass was used in the whole mechanical deformation procedure.

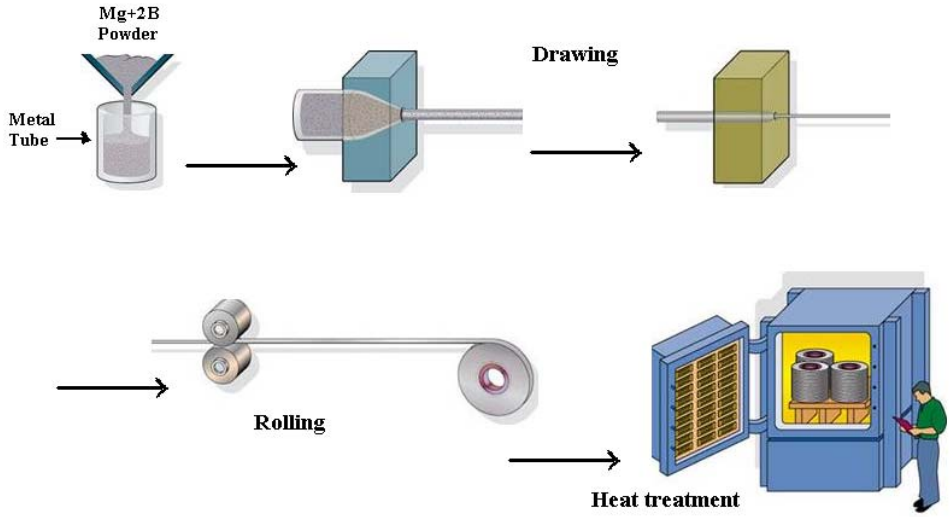

Figure 3- 2: The preparation procedure of the single filament MgB_2 tape.

Sintering the wires and tapes were carried out using a tube furnace by a similar procedure to the heat treatment of pellet samples. Different sintering times and sintering temperatures were used and will be explained for each experiment separately. Fig. 3-2 shows the preparation procedure for single filament MgB_2 tape.

3-1-2-2 Fabrication of Multifilament MgB_2 Wire

To prepare the multifilament wire, numbers of single filament wires with a length of about 10-15 cm were cut from the as drawn wire. This was followed by bundling and restacking the wires, then inserting them into new metal tubes. This tube was then mechanically deformed to a thin wire and heat treated in a similar way to the single wire. Fig. 3-3 shows the fabrication procedure for multifilament tape. The detailed experiments will be presented later.

3-2 Sample Characterization

3-2-1 X-ray Diffraction Pattern (XRD) Technique

The X-ray diffraction pattern technique is the fastest and most convenient method for microstructure characterization of MgB_2 superconductor. This technique has been widely employed to examine the microstructure, phase formation, and study of the

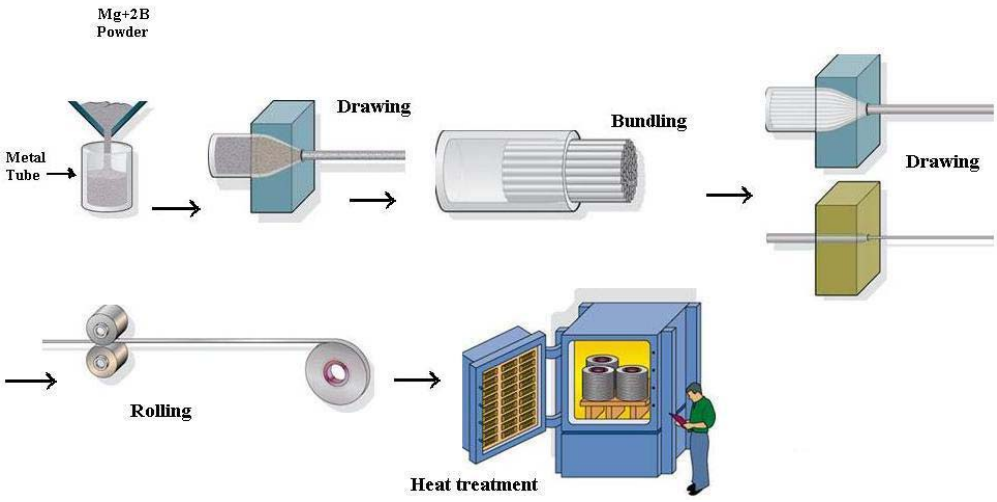

Figure 3- 3: The fabrication procedure of the multifilament tape.

texture, as well as calculation of the lattice parameters. The X-ray examination were carried out using two different instruments: Philips PW1730 and MAC MO3XHF[22]. Both machines were fully automated and configured in a Bragg-Brentano focusing geometry, with a θ-2θ optics. In all X-ray investigations, monochromatized Cu$K\alpha$ radiation from a normal focus X-ray tube was used, having wavelengths $\lambda_{K\alpha 1}$=1.5405 Å and $\lambda_{K\alpha 2}$=1.5443 Å. For the X-ray study of powders and pellets, the samples were ground using a mortar and pestle. For study and phase analysis of MgB_2 tapes or wires, the metal sheaths were mechanically removed simply by dry polishing the sheath to expose the core. A chemical compound or new phase can be determined if the volume ratio exceeds a few percent and if the grain sizes are larger than 1 μ. Peaks were indexed using Bragg's law of $2d\sin\theta = n\lambda$, where n is an integer, λ is the radiation wavelength θ is the diffraction angle and d is the distance between the reflecting parallel planes with same (hkl) Miller's indices. The average grain size can be semi-quantitatively estimated, as the average crystallite is proportional to the width of a reflection peak at half maximum intensity (FWHM) [398, 399]. The lattice parameters were calculated by indexing the peaks using the Rietveld refinement method.

3-2-2 Scanning Electron Microscopy (SEM) and Optical Microscopy (OM)

A direct observation of microstructure as well as the investigation of morphology can be made using the SEM and OM. The SEM was equipped with Electron Dispersive

Analysis (EDS) attachments. The scanning electron microscopy was performed using secondary electron and back-scattered electron (BSE) detectors. The resolution of the optical microscope is 1 μm. However SEM can provide useful information on the structure in the sub-micron range. Specimens were prepared by cold mounting the wires and tapes in the Strues Epofix epoxy resin. The polishing procedure was applied after about 24 h to allow the resin to cure. SiC grinding papers of 600, 800, 1200 and 2400 mesh were used followed by polishing with 5 μm, 3 μm and 1 μm diamond paste. Water cannot be used as a lubricant due to the reaction of MgB_2 with water; therefore to avoid this, Struers blue lubricant was used during the polishing process. A thin layer of gold with a thickness of about 300 Å was deposited on the specimens mounted in resin.

3.2.4 Transmission Electron Microscopy (TEM)

Transmission Electron Microscopy permits a direct observation and characterization of fine microstructure. The TEM images were obtained at the University of New South Wales and the Nanyang Technological University of Singapore. Two different instruments were employed for TEM examination: a Philips CM200 Field Emission Gun Transmission Electron Microscope and a JEOL 3010 High Resolution Transmission Electron Microscope (HRTEM). Specimens were prepared by pulverizing the powder with mortar and pestle, then dispersing it in ethanol. The suspension was then pipetted on to holey-carbon coated copper grids.

3-2-5 Magnetic Measurements

3-2-5-1 AC Susceptibility Measurements

To study the electromagnetic properties of superconductors, a method consisting of generating a harmonically varying magnetic field to probe the sample and registering the magnetic response of the sample, is widely used [400]. The ac susceptibility measurement is one of the common experiments of this type.

A schematic diagram of the instrument for ac susceptibility is shown in Fig. 3-4. For measurement, a piece of MgB_2 in the normal state is placed in a system of coils,

consisting of a large coil for dc magnetic field control, a smaller coil for the ac magnetic field, and pick-up coils which can detect the magnetic response of the specimen. A harmonic magnetic field (H_{ac}) is produced by the ac coil. According to the Faraday's law, the induced voltage in the pick-up coils is:

$$V = -\frac{d\varphi}{dt} \qquad (3\text{-}1)$$

Where φ itself consist of two terms due to H_{ac}, as well as the specimen response, $\varphi = \varphi_{ext} + \varphi_s$. In order to eliminate the φ_{ext}, the pick-up coil set consists of two identical coils, wound in an opposite direction and connected in series together. As long as the sample is in the normal state, the ac magnetic field penetrates the whole sample. When the normal-superconductor transition occurs, the magnetization of the specimen changes due to flux exclusion, therefore φ changes as $\varphi_s = M\mathrm{A}$. Here, A is the cross-sectional area of specimen. Since $\chi = dM/dH$, it follows:

$$\frac{d\varphi}{dt} = A\frac{dM}{dH}\frac{dH}{dt} = \chi A\frac{dH}{dt} \qquad (3\text{-}2)$$

Therefore the voltage induced in the pick-up coil is proportional to the susceptibility of sample:

$$V = -\mathrm{A}\chi\frac{dH}{dt} \qquad (3\text{-}3)$$

Then, any change in the sample susceptibility gives a change in the voltage across the pick-up coil, and this change can be detected by a Lock-in Amplifier.

In this work, the ac susceptibility of MgB_2 samples was measured using the Quantum Design Physical Property Measurement System (PPMS) with a sensitivity of up to 10^{-8} emu. More details as well as experimental results are presented in the subsequent chapters.

3-2-5-2 DC Magnetization Measurements

DC magnetization measurements were carried out on MgB_2 samples using the Quantum Design Physical Property Measurement System (PPMS). In order to measure the absolute value of the dc magnetization, a dc field was applied to the sample, and the sample was moved through the entire detection coil. The pick-up coil detects a waveform signal versus the position of the sample. The dc magnetization was then extracted by fitting the detected signal with the known waveform signal.

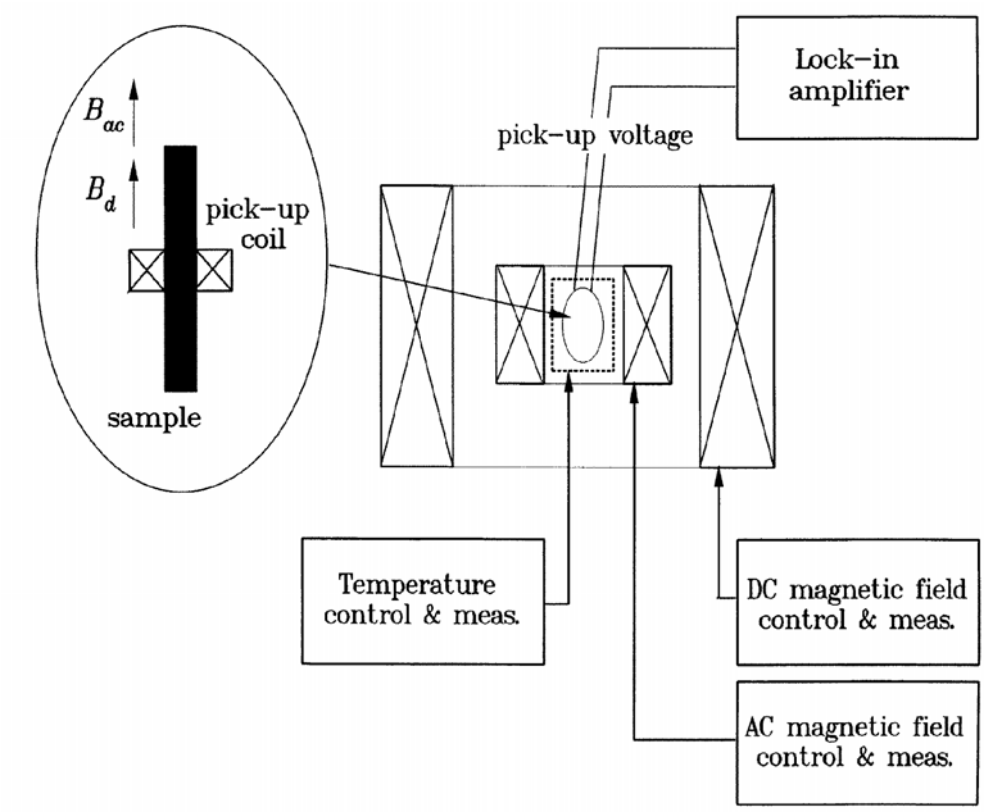

Figure 3- 4: A schematic diagram of the instrument for ac susceptibility.

J_c can be calculated from the measured magnetic hysteresis loop assuming that $J_c \propto \Delta M$, where ΔM is the width of the hysteresis loop (Fig. 3-5). ΔM can be calculated using the relation $\Delta M = M^+ - M^-$, where M^+ and M^- are positive and negative branch of hysteresis loop, respectively. The calculation of J_c from the dc magnetization is based on the *critical state model* [401], applied to a finite sample and usually called the *"modified Bean model"*. For a bar shaped sample, the magnetic critical current density can be calculated using the following relation [402]:

$$J_c = \frac{20\Delta M}{a\left(1-\frac{a}{3b}\right)} \qquad (4\text{-}3)$$

In this relation, a and b are the dimensions of sample in cm, perpendicular to the magnetic field direction with a<b. J_c and ΔM are in A/cm^2 and in emu/cm^3, respectively. For a cylindrical sample parallel to the magnetic field, J_c can be calculated as:

$$J_c = 30\frac{\Delta M}{d},$$

where d is the diameter of the cylinder in cm.

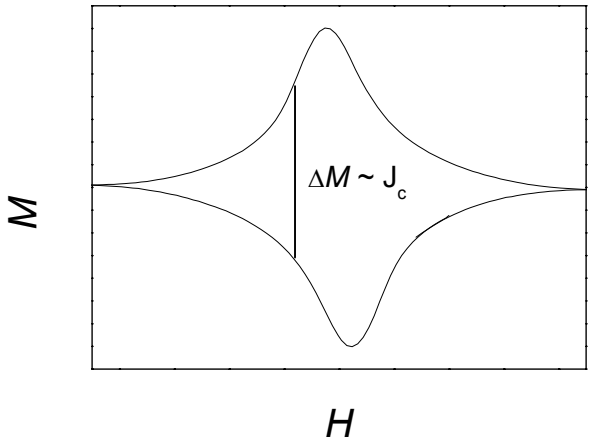

Figure 3- 5: Magnetic hysteresis loop showing the width of the magnetic hysteresis loop (ΔM).

3-2-6 Transport Measurements

Transport measurements of MgB_2 samples were carried out using the so-called four probe technique. This method consists of attaching four contacts to the sample. The two outermost contacts are for the current (I) and the two inner contacts are for the voltage (V). As the current passes trough the sample, a voltage is generated which is proportional to the resistivity. At the normal-superconducting transition, the voltage drops down to a level which is lower than the noise level of the measuring instrument. In the case of critical current (I_c) measurements, the standard value of 1 μV/cm was

used as a criterion for I_c. Therefore, I_c is arbitrarily defined as the value of the current which produces a voltage drop of 1 μV between two voltage contacts separated by 1 cm. In different experiments, contacts were attached to the sample using different materials such as silver epoxy, Woods alloy, or by low temperature soldering with Sn:Pb 50:50 in order to make low resistance contacts. Particular care was taken with the current contacts. Details of the transport measurements are presented in further chapters.

References

1. Azaroff, L.V., *Elements of X-ray crystalography*. 1968: McGraw-Hill. 549.

2. Ionescu, M., *Growth and characterization of Bi-2212 crystals and improvement of Bi-2212/Ag superconducting tapes*, in *ISEM*. 1997, University of Wollongong: Wollongong.

3. Gomory, F., *Characterization of high temperature superconductors by AC susceptibility measurements.* Superconductor Science & Technology, 1997. **10**: p. 523-542.

4. Bean, C.P., *Magnetization of high-field superconductors.* Review of Modern Physics, 1964. **36**: p. 31-39.

5. Chen, D.X. and R.B. Goldfarb, *Kim model for magnetization of type-II superconductors.* Journal of Applied Physics, 1989. **66**(6): p. 2489-2500.

CHAPTER 4: PREPARATION AND CHARACTERIZATION OF MgB_2 WIRE AND TAPE

4-1 Preparation and Characterization of Fe/MgB_2 Wire

4-1-1 Introduction

Efforts have been made to fabricate MgB_2 wires since the discovery of superconductivity at 39 K in this material [19]. A number of techniques have been developed to improve the processing parameters for achieving high critical current densities [198, 201, 233, 252, 277, 291, 315]. Among these, the powder-in-tube (PIT) process appears most promising and practically feasible. Some metals and alloys have been found to be suitable for sheath materials in the PIT process. Iron and its alloys in particular have been found to be non-poisoning to MgB_2 [201, 315, 403]. High transport critical current densities have been reported for Fe and Fe alloy clad-MgB_2 wires by some groups [201, 252, 315].

Heat treatment is applied in most PIT processes used for the fabrication of MgB_2. The times and temperatures that have been used so far for fabricating MgB_2 pellets and wires/tapes range from less than an hour to more than 48 h at sintering temperatures from 600 to 1000 ^oC. All the heat treatments must be under high purity Ar protection from oxidation. High J_c metal-sheathed MgB_2 tapes without any heat treatment were reported using the pre reacted powder [277]. This process has advantages over those with heat treatment as it substantially simplifies the process and hence reduces the cost for wire fabrication. However, the sheath materials need to be of very high hardness in order to densify the MgB_2 core. High toughness metal is easily broken during the cold drawing and rolling process, and very careful and delicate design and control are mandatory [252, 294]. Furthermore, as MgB_2 is very brittle, it would be a formidable task to overcome the cracking problem for long length production without heat treatment.

In order to further improve and simplify the fabrication processes, we have carried out a systematic study on the effects of sintering time on MgB_2 formation and J_c. In this section we present the fabrication procedure as well as the characterization of the Fe-clad MgB_2 wire. The effects of sintering time and temperature on the phase formation and critical current density of Fe-clad MgB_2 wires will also be explained. MgB_2 wires were fabricated using the powder-in-tube process and sintered for different periods of time at predetermined temperatures. In contrast to the common practice of sintering for several hours, the present results show that there is no need for prolonged heat treatment in the fabrication of Fe-clad MgB_2 wires. A total time in the furnace of several minutes is enough to form nearly pure MgB_2 phase with high performance characteristics. The results on T_c, J_c and H_{irr} convincingly show that the samples which were only sintered for 3 minutes have quite good performances. In fact, the J_c field performance for the most rapidly sintered sample is as good as for all the other samples. J_c of 4.5×10^5 A/cm^2 in zero field and above 10^5 A/cm^2 in 2 T at 15 K has been achieved for the best Fe-clad MgB_2 wires. As a result of such a short sintering there is no need for using high purity argon protection and it is possible to carry out the heat treatment in a much less protective atmosphere or in air. These findings substantially simplify the fabrication process, making it possible to have a continuous process for fabrication and reducing the costs for large-scale production of MgB_2 wires.

4-1-2 Experimental Details

The Fe/MgB_2 wire was prepared using the powder-in-tube technique. Powders of magnesium (99%) and amorphous boron (99%) were used as starting materials. The pure Fe tube has 8mm OD, 1.5 mm wall thickness and 10 cm long. The composite tube was drawn from 8 mm to 1.5 mm diameter. Short wire samples of about 2 cm in length were sealed in a small Fe tube and then heat treated at 750 ^oC for 30 min in flowing high purity Ar. Due to a strong shielding effect from the Fe sheath metal [200, 203], bare cores were used for the magnetic characterization. Cylindrical bars of MgB_2 core were obtained by removing the Fe sheath mechanically.

4-1-3 Results and Discussion

4-1-3-1 Phase Formation and Microstructure

Fig. 4-1 shows XRD patterns recorded from the core of the Fe-clad MgB_2 wire after the iron sheath was mechanically removed. The sample is revealed to be single phase with a small amount of MgO (<5%).

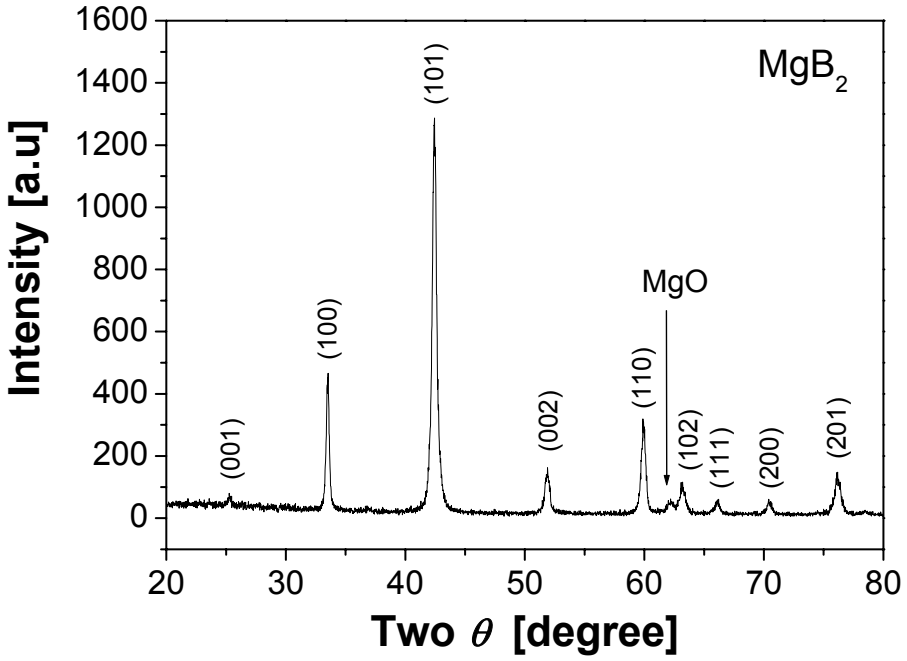

Figure 4- 1: XRD patterns recorded from the core of the Fe-clad MgB_2 wire after the iron sheath was mechanically removed.

Fig. 4-2 shows the more accurate XRD pattern obtained with Rietveld analysis. It also shows a small amount of MgO. The peaks can be very well indexed with the space group *P6/mmm*. SEM examination revealed that the grain size in the superconducting core is smaller than 1 micron. An optical image of a cross-section of a sample is shown in Fig. 4-3. There is a well-defined interface between the Fe sheath metal and the MgB_2 core. No reaction has been found between the sheath and the superconductor. The core is very porous in agreement with the mass density of sample, which is only 1.3 g/cm^3, suggesting that the performance of wire could be further improved if the density of the wires can be increased.

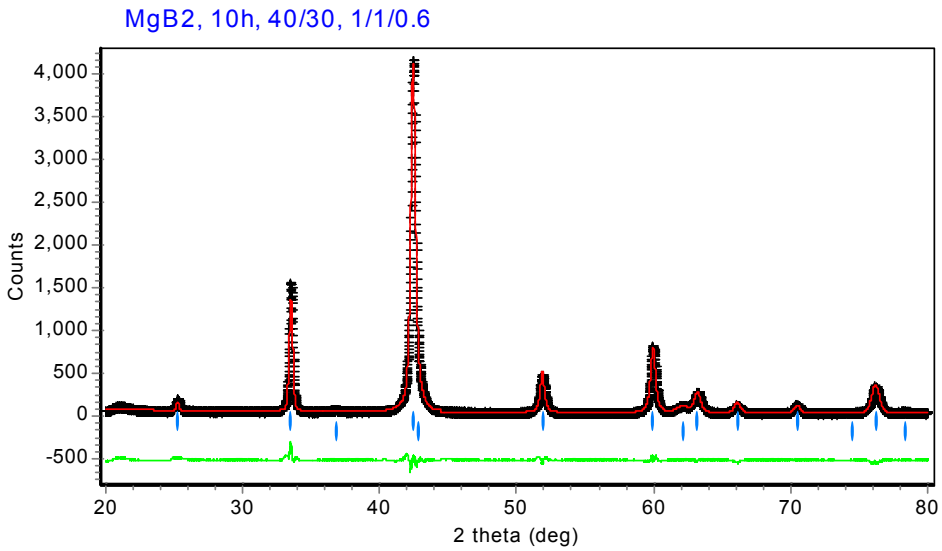

Figure 4- 2: Rietveld analysis of MgB_2 powder. The powder was prepared by grinding the superconducting core of Fe/MgB_2 wire.

4-1-3-2 Superconductivity and Critical Current Density

Fig. 4-4 shows the transition temperature (T_c) for a core sample determined by the ac susceptibility (real part and imaginary part) measurements. The T_c onset for the sample (~ 38.3 K) is almost the same as that reported by a number of groups. The sample also showed a sharp transition with a transition width of less than 1 K.

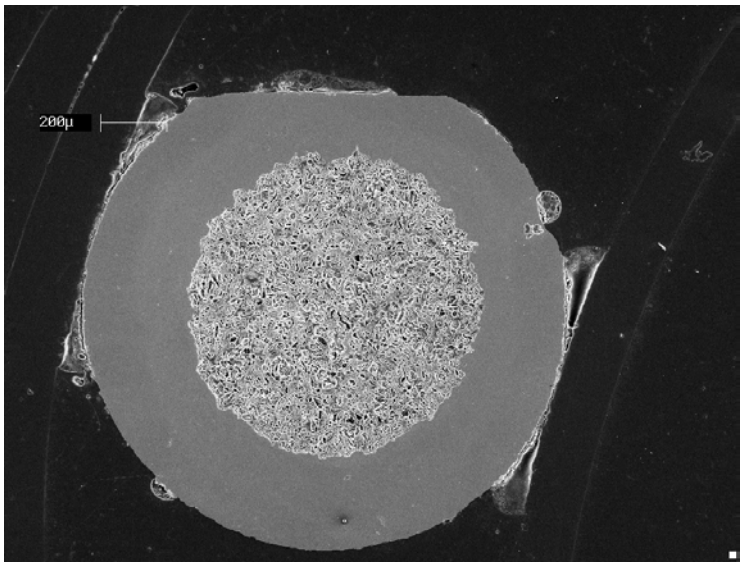

Figure 4- 3: A typical optical microscope image of the transverse cross-section for a Fe/MgB_2 wire sample.

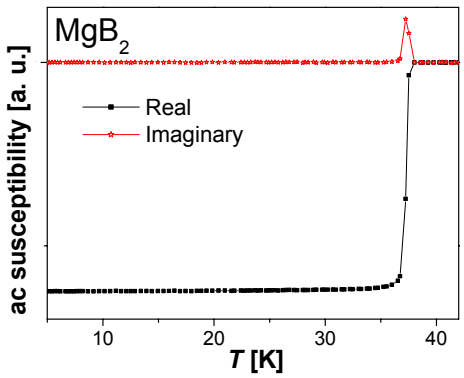

Figure 4- 4: AC susceptibility of the core of the Fe-clad MgB_2 wire after the iron sheath was mechanically removed.

Measurements of the *M-H* loops at different temperatures were carried out on the bare cylindrical bar samples. A typical *M-H* loop of a MgB_2 wire sample is shown in Fig. 4-5. We can see that a typical flux-jumping pattern is present for temperatures below 15 K. This flux jumping was first observed in an MgB_2 bulk samples [404] but occurs in thin films samples as well [405]. The flux jumping has been directly visualized using magneto-optical imaging techniques and explained in terms of phenomena associated with rapid flux penetration[405, 406].The critical current density was calculated from the *M-H* loops using the Bean critical model. J_c versus magnetic field up to 8 Tesla for Fe/MgB_2 wire sample at 5 K, 10 K, 15 K, 20 K, 25 K, and 30 K is presented in Fig. 4-6. It should be noted that J_c of 4.5×10^5 A/cm^2 at 15 K and zero field has been achieved. Because of the flux jumping, the J_c below 15 K cannot be measured.

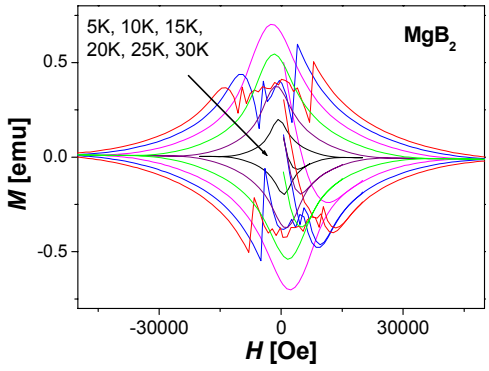

Figure 4- 5: *M-H* loop for Fe/MgB_2 wire sample at different temperatures: 5 K, 10 K, 15 K, 20 K, 25 K, and 30 K.

4-1-3-3 Effect of the Sintering Time

In order to further improve and simplify the fabrication processes of Fe/MgB_2 wire, we have carried out a systematic study on the effect of sintering time on MgB_2 formation and J_c. Short wire samples of about 2 cm in length were sealed in a small Fe tube and then directly heated at a preset temperature (T_{max}) for 3-32 minutes in flowing high purity Ar or nitrogen, or in air (when a very short sintering time is used). This is then followed by a quench in liquid nitrogen.

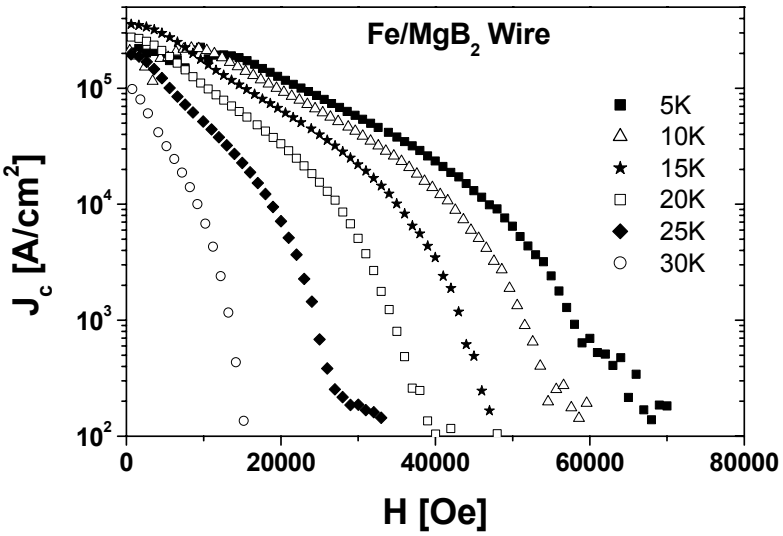

Figure 4- 6: Field dependence of J_c of Fe/MgB_2 wire sample at different temperature 5 K, 10 K, 15 K, 20 K, 25 K, and 30 K.

Fig. 4-7 shows the real temperature of the samples as a function of time, starting from when the wires were loaded into a hot tube furnace held at a constant temperature T_{max} of 745, 840, and 900 ^{o}C. It shows that only a short time (2-3 min.) is required for the samples to reach T_{max}, and that the higher the T_{max}, the shorter the time. Six samples, which were heat treated at different T_{max}, are illustrated and the removal time indicated by open circles as shown in Fig. 4-7. Samples 1, 5 and 6 were removed from the furnace after 3 minutes, having experienced only a few seconds at T_{max}. Samples 2-4 were removed after sintering for 6, 15, and 32 minutes, respectively. The surface of the Fe tube used to seal the wires was slightly oxidized after sintering in air. However, the MgB_2/Fe wire samples sealed inside the Fe tube were as fresh as before sintering,

regardless of the time at T_{max} and regardless of the atmosphere. A longer sintering time only gives rise to more severe surface oxidation of the outside Fe tube.

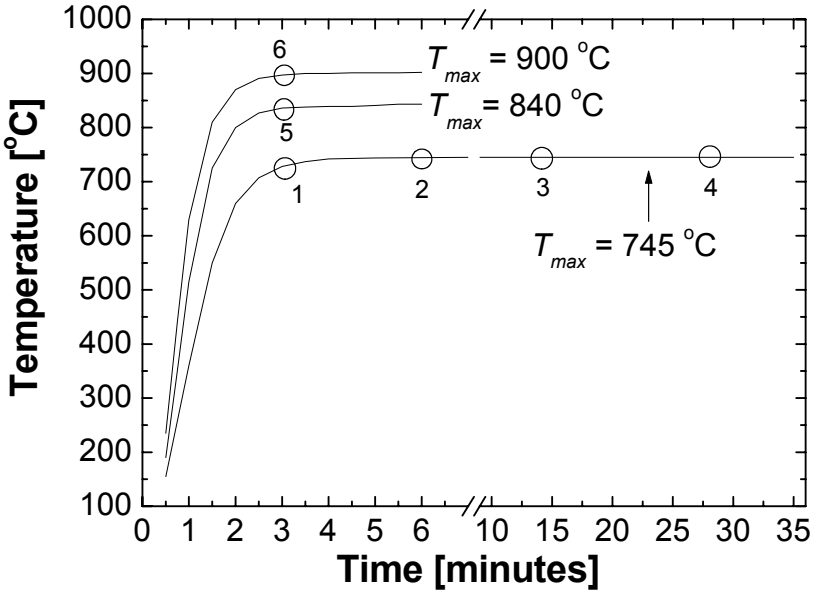

Figure 4- 7: The real temperature of the samples as a function of time, after the wires were loaded into a hot tube furnace held at a constant temperature T_{max}.

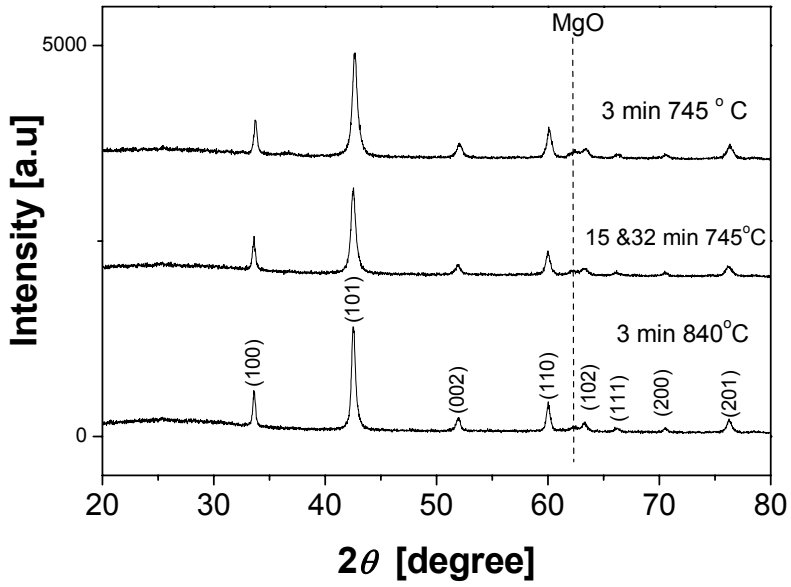

Figure 4- 8: XRD patterns recorded from the powdered core of the Fe-clad MgB_2 wire samples after the iron sheath was mechanically removed.

4-1-3-3-1 Effect of the Sintering Time on the Phase Formation and Microstructure

XRD results show that all the samples have almost the same phase purity (above 90% MgB_2). Fig. 4-8 shows XRD patterns recorded from the core of the Fe/ MgB_2 wires (samples 1, 4 and 5) after the iron sheath was mechanically removed. It is clear that sample 5 has the same high phase purity as sample 4, even though it was only heat treated for 3 min.

SEM examination revealed that the grain size is smaller than 1 micron, and the homogeneity appears to be the same for all the samples. The optical images of cross sections of samples are similar to what has been shown in Fig. 4-3. There is a well-defined interface between the Fe sheath metal and the MgB_2 core. It should also be noted that the density of the wire sample is only 1.3 g/cm^3, suggesting that J_c could be further improved if the density of the wires can be increased.

4-1-3-3-1 Effect of the Sintering time on the Superconductivity, Critical Current Density and Irreversibility Field

Transition temperatures, T_c, and transition widths, ΔT_c, for the 3-15 minute treated samples are all very similar. In fact, T_c is almost the same (~ 38 K) for all the samples, while there is only a small difference in ΔT_c, which decreases with increasing heating time from 3-15 min for samples 1-3 sintered at 745 ^{o}C (Fig 4-9).

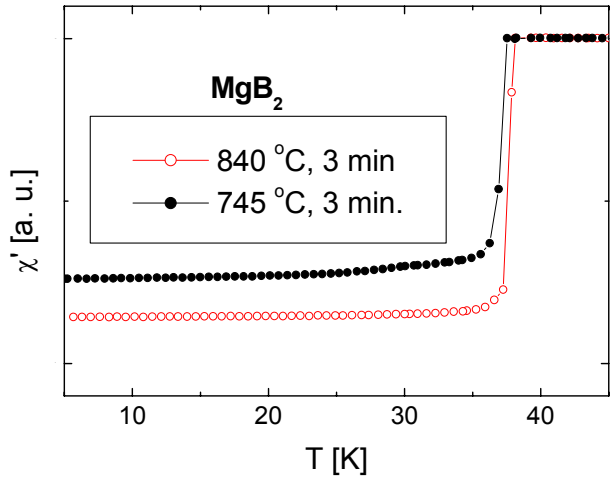

Figure 4- 9: Temperature dependence of the real part of the ac susceptibility.

Measurements of the *M-H* loops at different temperatures were carried out on the bare cylindrical bar samples. J_c versus magnetic field up to 6 Tesla for three samples at 10 K, 15 K, 20 K, and 30 K is shown in Fig. 4-10. Note that J_c of 4.5×10^5 A/cm^2 at 15 K and zero field has been achieved for sample 4. Again the J_c below 15 K cannot be measured because of the flux jumping. For T_{max} = 745 ^{o}C, the J_c increases as the sintering time increases from 3 to 15 min. Fig. 4-11 shows the J_c versus sintering temperature for samples 1, 5 and 6 which were all treated for 3 min. Sample 1, sintered for 3 minutes at 745 ^{o}C, has a markedly lower J_c than the other samples, probably due to poor grain connectivity. However, if T_{max} = 840 ^{o}C , the J_c of the wire treated for just 3 minutes (sample 5) is as good as that of a wire treated for 15 min. at 745 ^{o}C. Furthermore, J_c–field performance of the sample sintered at T_{max} = 840 ^{o}C for 3 min. is the best out of all the samples, as evidenced by the crossover (indicated by arrows) of J_c–H curves in higher fields as shown in Fig. 4-10.

Fig. 4-12 shows the comparison of J_c at 20 K for both zero field and 3 T for sample wires sintered for different times. We can see that the J_c is as high as 3×10^5 A/cm^2 at 20 K zero field for samples 2-5. Noted that J_c for the 3 min sintered sample 5 is the same as for samples 2-4 which were sintered for 6 min to 32 min. For further comparison, J_c data from a Fe-clad MgB_2 tape (described in the next section) are also shown in Fig. 4-12. The sample was prepared by 3 h heating to 800 ^{o}C, holding for 1 h, and then slow cooling down to room temperature. It can be seen that the J_c and field dependence of the wire samples which were sintered for only a very short time are almost as good as the J_c and field performance of this reference tape.

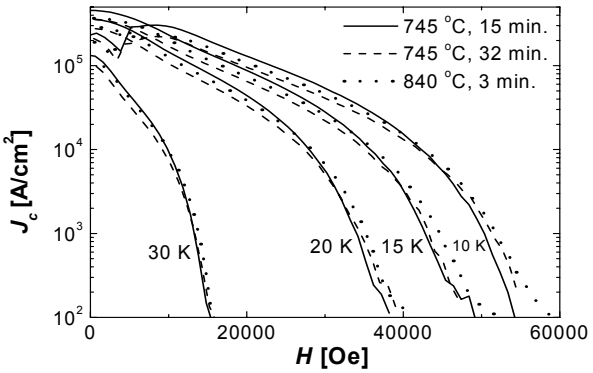

Figure 4- 10: Field dependence of J_c at different temperatures for samples 3, 4 and 5.

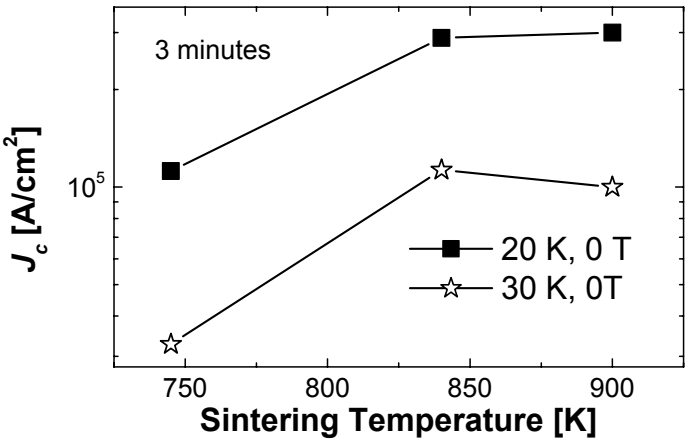

Figure 4- 11: J_c versus sintering temperature of T_{max} for samples 1, 5 and 6 which were all sintered for 3 minutes.

Table 4- 1: Fabrication conditions and J_c for all the samples.

No.	*T*max	Time*	*Jc* (A/cm^2)		
			15 K, 0T	20K, 0T	30 K, 0T
1	745 °C	3 min.	1.5×10^5	1.1×10^5	3.2×10^4
2	745 °C	6 min	2.7×10^5	2.7×10^5	6.5×10^4
3	745 °C	15 min	4.5×10^5	3.5×10^5	1.3×10^5
4	745 °C	32 min	3.5×10^5	2.8×10^5	9.8×10^4
5	840 °C	3 min	3.7×10^5	2.9×10^5	1.1×10^5
6	900 °C	3 min	-	3.0×10^5	1.0×10^5

*Samples were quenched in liquid nitrogen after a total sintering time in a furnace with predetermined T_{max}.

Table 4- 2: Comparison of J_c values.

	J_c (A/cm^2) at 25 K, 1 T	Reference
MgB_2 wire (Sample 4, this work)	5.9×10^4	this work
MgB_2 (HP synthesised pellet)	1.6×10^4	[407]
Bi2223/Ag tape	2.9×10^5	[408]
Bi2212/Ag tape	2.5×10^3	[409]

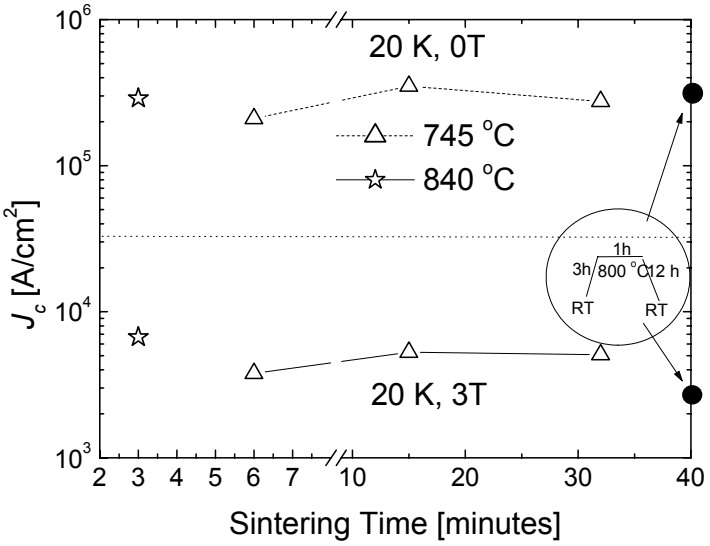

Figure 4- 12: J_c as a function of real sintering time at different $T_{max.}$ J_c data (closed circles) for a normally sintered MgB_2/Fe tape is also shown for comparison.

J_c of sample 4, a typical short-sintered MgB_2 wire is compared with good quality J_c Bi2212/Ag and Bi2223/Ag tapes at 25 K and 1 T [408, 409] (Table 4-2). The J_c of a MgB_2 pellet prepared using Mg+2B powders and sintered at 850 °C for 1 h under a pressure of 45 kbar [407] (HP synthesised MgB_2 pellet) is also shown in the table. It can be seen that our short-sintered sample 4 has a lower J_c than for the Bi2223/Ag tape at 25 K and 1 T, but it has a higher J_c than the HP synthesised MgB_2 pellet, and J_c is more than one order of magnitude higher for the Bi2212/Ag tapes.

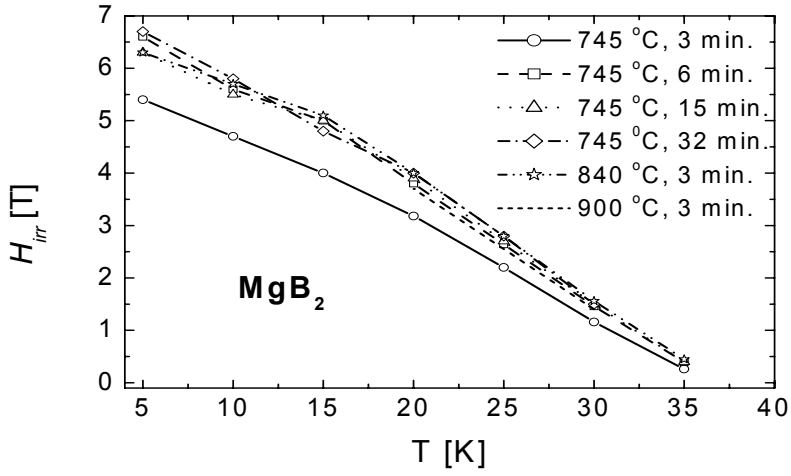

Figure 4- 13: Irreversibility line for all the samples.

Fig. 4-13 shows the irreversibility fields (H_{irr}) versus temperature for all the samples. H_{irr} was determined from J_c–H curves using the criterion of 100 A/cm^2. We can see that all the samples, except sample 1, have approximately the same H_{irr}.

4-1-4 Summary

Fe/MgB_2 wire has been prepared using the powder-in-tube and reaction *in situ* techniques. The effect of sintering time and temperature on the formation and critical current densities of Fe-clad MgB_2 wires has been investigated. It was found that there is no need for prolonged heat treatment in the fabrication of Fe-clad MgB_2 wires. A total sintering time of several minutes is enough to form nearly pure MgB_2. The T_c, J_c and H_{irr} results show convincingly that the samples which were sintered for 3 minutes have quite high performance characteristics. These findings substantially simplify the fabrication process and can reduce the costs for large-scale production of MgB_2 wires.

4-2 Preparation and Characterization of Fe/MgB_2 Tape

4-2-1 Introduction

The high critical current density values observed in bulk samples, regardless of the degree of grain alignment [395], are an advantage for making wires or tapes with no degradation of J_c, in contrast to the degradation due to grain boundary induced weak-links, which is a common and serious problem in cuprate high temperature superconductors. In polycrystalline bulk MgB_2 samples, critical current densities of 10^4 to 10^5 A/cm^2 at 4.2 K have been reported by several groups [368, 404, 410-413]. However, the fabrication of metal clad MgB_2 tapes or wires will be essential to meet the requirements of most such high current applications. Mechanical deformation during the tape making process can increase the density of the superconducting core as well as inducing pinning centres.

For tape fabrication, it is necessary to find a suitable sheath material for MgB_2 which does not degrade the superconductivity. So far, several metal-clad MgB_2 tapes or wires have been fabricated with sheath materials such as Nb [291], Cu, Ag, and Ni [233, 277], as well as Fe. For example, a transport J_c of 10^4 A/cm^2 at 4.2 K has been obtained for Ag/MgB_2 using pre-reacted MgB_2 without any heat treatment [233]. In fact any sort of heat treatment caused a degradation of J_c. A high transport J_c of 10^5 A/cm^2 at 4.2 K has been achieved for an unsintered Ni/MgB_2 tape [277]. Relatively high J_c values were obtained for Cu clad MgB_2 tapes which were sintered for long time (48 h) at 620 ^{o}C [233]. For critical current optimization the proper choice of metal cladding material is essential since the Mg component of the compound tends to react with many metals such as Cu or Ag during sintering or reaction at temperatures around 900-1000 ^{o}C. In a detailed study of material compatibility, Jin et al [201] noted that whereas admixtures as high as 5 mol% of powdered Y, Mo, Cu, Ag, and Ti, to the MgB_2 powder prior to ribbon-forming and sintering at 900 ^{o}C seriously degraded the J_c, the presence of the same amount of Fe powder decreased $J_{c,4.2K}$ only from 1.8×10^5 to 1.5×10^5 A/cm^2 at 0.5 T and not at all at 1.25 T. It has been established that Mg and Fe have meager mutual solubility (about 0.01% Fe in Mg at its M.P. and 0.2 at.% Mg in Fe [414]). This and the

above results suggest that the processing of Mg+B or MgB_2 powders in an Fe tube would be accompanied by little contamination and only slight degradation of J_c, and even then only in fields below about 1 T.

Most of the transport J_c results reported for MgB_2 wires and tapes are limited to 4.2 K so far. To take advantages of the relatively high T_c of 39 K for MgB_2 superconductor it is essential to have high J_c values at temperatures above 20 K. For example, the boiling point of hydrogen at atmospheric pressure is 20.13 K, so that it is possible to use liquid hydrogen or cold hydrogen gas as a cryogen for cooling MgB_2 wires. This requires that the MgB_2 wires have sufficiently high J_c values at around 25 K. In this section we present the fabrication of pure Fe clad MgB_2 tapes with a high transport J_c above 10^4 A/cm^2 at 30 K and 1 T and I_c greater than 150 A.

4-2-2 Experimental Details

Standard powder-in-tube methods were used for the Fe clad MgB_2 tape. The as drawn wire was cold rolled to a ribbon over many steps. Several short samples 2 cm in length were cut from the ribbon. These pieces were then sintered in a tube furnace at 750 K for 30 min in flowing Ar gas. The mass loss after sintering is very small, less than 1%.

4-2-3 Results and Discussion

4-2-3-1 Microstructures

Scanning electron microscopy (SEM) photomicrographs for the Fe clad tape after sintering are shown in Fig. 4-14. The picture on the left is a typical transverse cross section of an Fe clad tape. It clearly shows that the MgB_2 core presents a homogeneous cross section. The picture on the right is the longitudinal cross-sectional micrograph showing good core homogeneity. Fig. 4-15 presents the high magnification microstructure of the core surface after mechanically removal of the Fe sheath material. This micrograph shows a porous microstructure with a clusters of grains of about 100 μm in size. Our results showing large grain sizes are very different from those seen in the reported Cu/Fe/MgB_2 tape which was made using reacted MgB_2 powders with a

starting grain sizes of 3 μm. The final grain size was significantly reduced to 120 nm due to the occurrence of substantial grain refinement during the wire fabrication process [201].

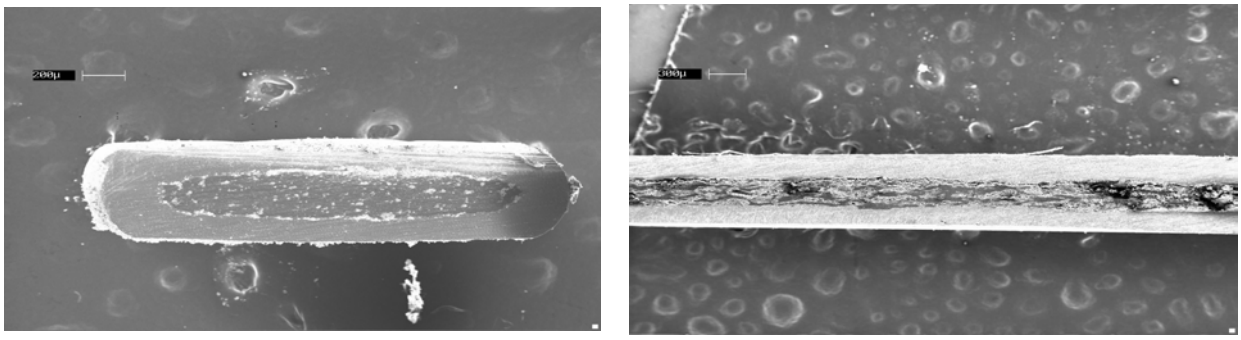

Figure 4- 14: SEM image for a typical transverse (a) and a longitudinal (b) cross-section

4-2-3-2 Transport Properties

The critical current of the Fe clad MgB_2 tape was measured by the standard four-probe method. The sample used for the measurement has a length of 20.5 mm and a width of 3 mm. The MgB_2 core cross-section in this sample is similar to that shown in Fig. 4-14. Its average dimensions are 2.1 × 0.45 mm^2. Therefore, the core cross-section is about 9.45 × 10^{-3} cm^2. The current and voltage contacts were soldered with Wood's alloy (giving a current contact resistance lower than 10 mΩ), and the distance between the voltage contacts was 7.5 mm.

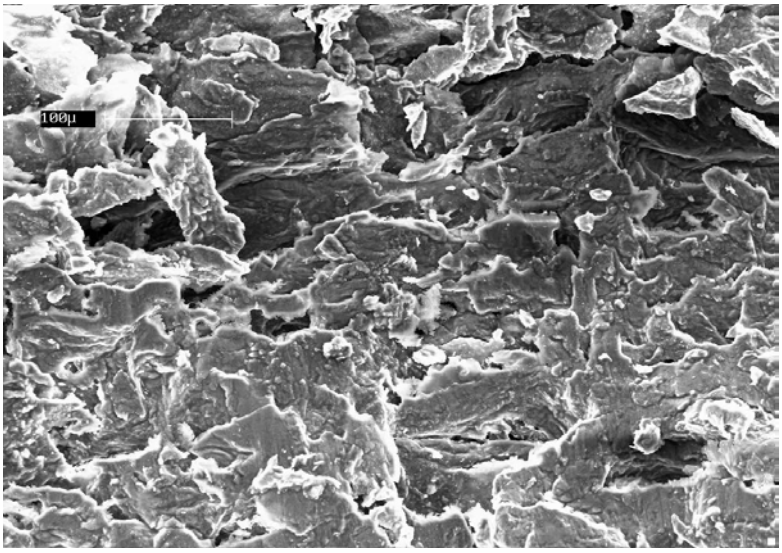

Figure 4- 15: High magnification microstructure of the core surface after the top Fe sheath material has been removed mechanically.

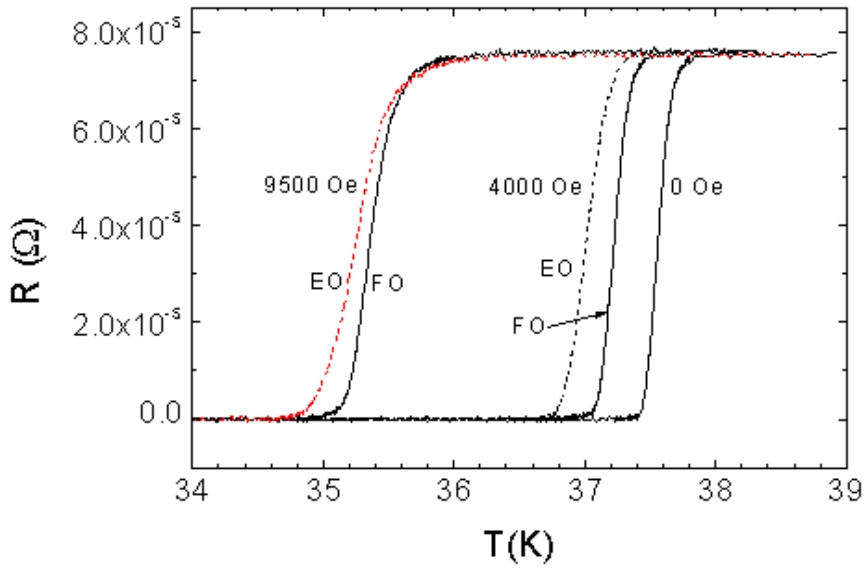

Figure 4- 16: *R-T* curves for Fe/MgB_2 tape measured in fields of 0, 4, and 9.5 kOe in the EO and FO orientation.

The temperature dependence of the resistance (*R-T*) was measured using an AC current (frequency 18.4 Hz, I =1 mA). Fig. 4-16 shows *R-T* measured at zero field over a wide temperature range from 300 to 10 K. It shows a sharp transition with a width, ΔT_c, of 0.2 K and a T_{c0} of 37.8 K. We also measured *R-T* around the transition temperature with applied fields of 4 kOe and 9.5 kOe directed perpendicular to the sample axis and (a) parallel to the broad sample face (the "edge-on" or EO orientation) or (b) perpendicular to it ("face-on", FO). As a result of differences in the degree of magnetic screening (see below) the field-induced decreases in *Tc* were larger for the EO orientation than for the FO orientation.

Critical current measurements were made using a pulse method, with the current pulse linearly rising from zero to maximum current. The pulse duration was 20 ms for T>33 K and 10 ms for T<30 K. The voltage was amplified and recorded on a digital storage oscilloscope together with the voltage across a standard resistor, giving the current flowing through the sample. The temperature of the sample holder was monitored during the measurement with a gold-chromel thermocouple, showing a temperature rise after a pulse of approximately 0.2 K at currents higher than 150 A (the next pulse was applied after the temperature had fallen to denoted values). We estimate that the temperature rise of the sample itself was somewhat higher, but that just means that the critical current obtained is underestimated.

Although the above mentioned procedure for critical current measurements enables the determination of *Ic* with the 1 μV/cm criterion, there were two problems: 1) the current pulse causes magnetization of the iron cladding, which gives a spurious voltage signal V_m superimposed on the voltage of the superconductor V_s. Since V_m was appreciable in fields B<0.4 *T*, I_c in these fields was determined as the current at which the overall voltage starts to increase above the decaying V_m. However, the error in I_c determination is 10% at most, and because of heating, the real I_c is probably higher than the results obtained (especially at lower fields); 2) magnetization depends on the field direction. For that reason, we measured I_c for both field directions (denoted on the figures in the same way as for resistance measurements) at 35 K.

The critical currents measured at temperatures above 29 K and in fields up to 1 T are shown in Fig. 4-17. Again as a result of differences in magnetic screening (see below) $I_{c,FO}$ for a given applied field was greater than $I_{c,EO}$. The critical current, I_c, increased from 10 to 164 A as the temperature decreased from 36.4 to 30 K, and changes of I_c with field were smooth for 32 and 30 K. The critical current density J_c is calculated using the calculated core cross section of 9.45×10^{-3} cm^2, and its value is shown on the right axis of Fig. 4-17 We can see that the Fe clad MgB_2 has a very high transport J_c of above 10^4 A/cm^2 for fields <0.5 T at 33.2K and for fields < 0.8 T at 32 K. The highest J_c is about 1.7×10^4 A/cm^2 at 29.5 K and 1 T.

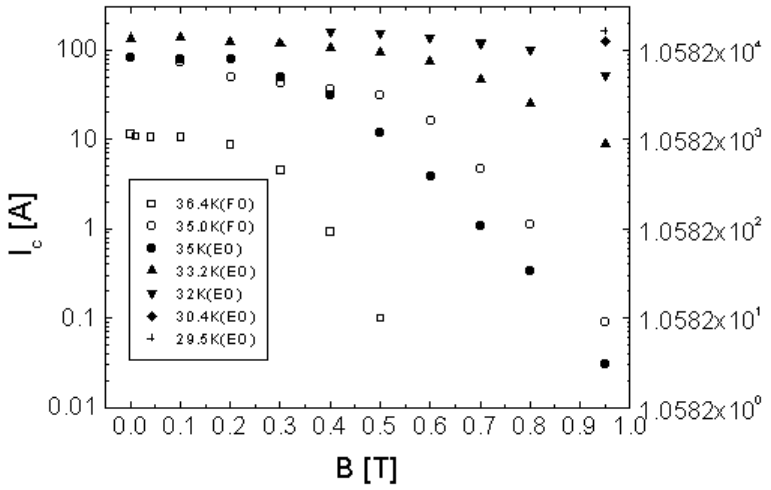

Figure 4- 17: Field dependence of I_c (left axis) and J_c (right axis) at different temperatures with fields perpendicular and parallel to the tape plane.

4-2-3-3 Magnetic Critical Current Density

Magnetic measurements (*M-H* loops) were carried out on a superconducting quantum interference device (SQUID, Quantum Design PPMS 9 T) magnetometer. In order to avoid a large magnetic signal from the Fe clad tape, we measured a MgB_2 core with dimensions of $0.78\times3.95\times0.32mm^3$ taken from one of the Fe-clad tapes. All magnetic measurements were performed in the FO orientation. The magnetic critical current densities were derived from the Bean model: $J_c = 20\Delta M / a(1 - a/3b)$ and are summarized in Fig. 4-18, where $J_c(T)$ curves at B=0 T, 1 T, 2 T are plotted.

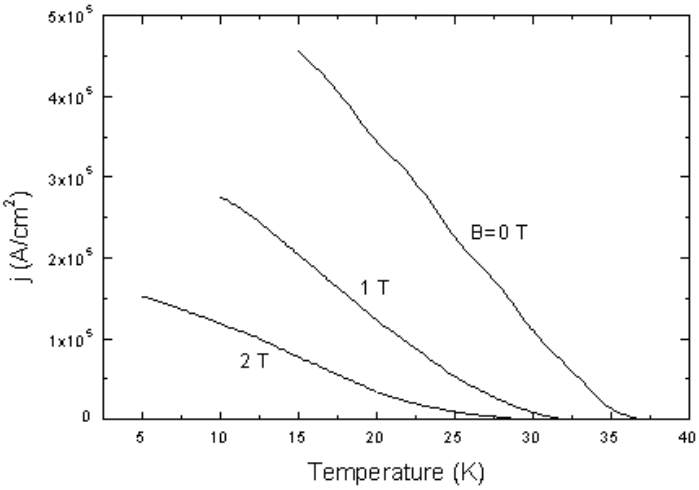

Figure 4- 18: Temperature dependence of J_c at different applied magnetic fields perpendicular to the tape plane (FO orientation).

The magnetic critical current density at B=0 T and T=35 K is about 1.38×10^4 A/cm^2, which is higher than the transport J_c (see fig. 4-17). This is understandable because the transport critical current density was underestimated due to either the heating of the sample or the fast swaping rate of the applied current.

4-2-3-4 Magnetic Screening

Genenko et al. [415] have proposed the use of a surrounding high-permeability medium to enhance a superconductor's transport current density, and Majoris et al [416] have proposed magnetic screening by surrounding ferromagnetic sheaths as a possible way of decreasing transport AC loss in multifilamentary strands. Applicability of the screening

principle to both high-T_c and low-T_c superconductors has been pointed out and its benefits to applications such as power transmission and fault-current limitation suggested [416]. But since Fe or low-alloy steels seem suitable cladding materials for the processing of powder-in-tube MgB_2 strand both from mechanical and chemical-compatibility standpoints, the resulting wires automatically become ideal candidates upon which to explore and exploit the properties of magnetic screening.

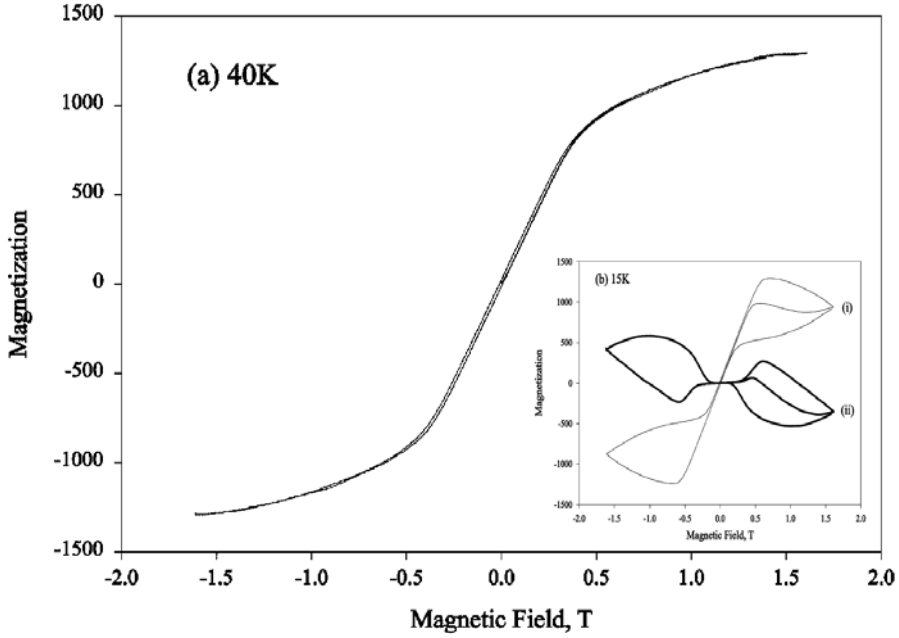

Figure 4- 19: *M*(*H*) loops at *T*=40 K, and *T*=15 K(inset) before (curve i) and after (curve ii) numerically subtracting the *M-H* loop for the Fe sheath as measured at 40 K.

In an Fe-clad wire the influence of magnetic screening can be gauged by comparing its superconductive properties in the sheath-on and sheath-off conditions, provided sheath removal can be successfully achieved without damage to the underlying superconductor. In the case of a rectangular tape screening information can be obtained by comparing its magnetically influenced properties in the FO and EO orientations as in Figs. 4-16 and 4-17, both of which indicate that screening is more effective when the tape is in the FO orientation. Consider Fig. 4-17, for example. This shows that rotating the sample from FO to EO in an applied field of 0.6 T is equivalent to increasing the internal field by 0.13 T. So far, we have not been able to use these data to deduce the actual shielding factors, $S = H_{applied}/H_{internal}$, of the tapes concerned in spite of the existence of some published information on screening by rectangular cylinders [417]. Finally we note that in the context of magnetization measurement an equivalent sheath-off/sheath-on comparison can be achieved using data acquired at 40 K and below T_c,

respectively, as in Fig. 6. The 15K *M-H* loop for an Fe-clad round wire (from the same stock as the tape) is depicted in Fig. 19. That of the superconductive core itself, inset, is obtained by numerically subtracting the *M-H* loop for the Fe sheath as measured at 40 K. Evidently partial screening takes place throughout an applied field range of ±0.6 T and complete shielding within ±0.06 T.

4-2-4 Summary

Fe-clad MgB_2 tapes fabricated by PIT techniques and sintered in pure Ar at 800 ^oC for 1 h at ambient pressure show a superconducting core with large clusters of grains with a size of about 100 μm. They have a sharp transition with a transition width ΔT_c of 0.2 K and T_{c0} at 37.8 K. A transport critical current density of 1.7×10^4 A/cm^2 for both 29.5 K in 1 T and for 33 K in null field has been obtained.

The Fe or low-alloy steel cladding material that seems necessary for successful PIT processing, both from the mechanical- and chemical-compatibility standpoints, also provides magnetic screening, the benefits of which (depending on applied field strength and materials permeability) can be higher I_c and lower ac loss. In low magnetic fields wherein the relative permeability of the sheath material is large the shielding can be very effective, but becomes weaker as the sheath approaches magnetic saturation. It has been pointed out previously [416] that magnetic screening by surrounding ferromagnetic sheaths should decrease transport ac loss in both high-T_c and low-T_c multifilamentary strands and improve the performances of superconductive devices such as power transmission lines and fault-current limiters. Finally we note that the ferromagnetic sheath may have an additional benefit quite apart from screening. In precision field dipole magnets a considerable departure from field uniformity accompanies the use of superconducting strand with its inherent ("persistent-current") magnetization. Among the several techniques available for canceling out the effects of superconductor magnetization [418] is strand coating with a ferromagnetic layer [419-421].

4-3 Preparation and Characterization of Cu/MgB_2 and Ag/MgB_2 Wire

4-3-1 Introduction

As explained in the last section some metals and alloys have been found to be suitable for sheath materials in the PIT process. Iron and its alloys in particular have been found to be not only non-poisoning to MgB_2 [199-201, 315, 403] but also capable of providing magnetic screening to reduce the effect of external applied magnetic fields on the critical current [200, 203, 315]. A high transport J_c on the order of 10^4-10^5 A/cm^2 at 20 K and 4.2 K has been reported for Cu/Fe/MgB_2 tapes where reacted MgB_2 powders were used as the core conductor and sintered at 900-1000 ^{o}C for 0.5 h out of a total heat treatment time of more than 3 h, including the initial heating [404]. Recently Fe and Ni clad wire have been fabricated with quite high J_c values of 2.3x10^5 A/cm2 at 4.2 K and 1.5 T in a Ni/MgB_2 tape and 10^4 A/cm^2 at 4.2 K and 6.5 T in a Fe/MgB_2 tape [202]. By using unreacted Mg+2B powders and sintering at 800 ^{o}C for 1 h, Fe clad MgB_2 tapes with a high transport J_c above 10^4 A/cm^2 at 30 K and 1 Tesla and I_c greater than 150 A also have been successfully fabricated as explained in the previous sections.

Although the high toughness materials have some benefits in achieving high-density samples, these materials are usually very hard to mechanically deform. They are also easily broken. Therefore, easily deformable silver and copper can be better alternatives for sheath materials, especially for some applications such as superconducting magnets, if high critical current density can be achieved. Ag and Cu-clad MgB_2 tapes using in-situ and ex-situ reactions have already been prepared. A magnetic J_c value of above 10^4 A/cm^2 has been reported by Glowacki et al. at 5 K and low magnetic field for Cu clad MgB_2 wire, which was sintered at 620 ^{o}C for 48 h [233]. They have also reported relatively higher J_c values for Cu clad MgB_2 wire that was heat-treated at 700 ^{o}C for 1h [238]. In section 4-1 we have shown that the MgB_2 superconducting phase can be formed in a very short time at any temperature above the melting point of magnesium.

Just a few minutes of heat treatment is enough to achieve high quality Fe/MgB_2 wires with a high J_c value of 4.5×10^5 A/cm^2 at 15 K and 1 T.

As it has been reported that Ag and Cu react with Mg [238], it is proposed that a shorter sintering time would decrease the reaction of Mg with Ag and Cu sheath materials and lead to some improvements in wire performance. In this section we present the fabrication procedure as well as the characterization of the Ag and Cu sheathed MgB_2 superconductor wire. We also study the effect of short period sintering on the J_c of Ag and Cu/MgB_2 wires and compare these results with the performance of Fe/MgB_2 wire that was also prepared with the short sintering.

4-3-2 Experimental Details

The powder-in-tube method was used to fabricate Ag and Cu clad MgB_2 wires using an *in-situ* reaction method. Powders of magnesium (99%) and amorphous boron (99%) with the stoichiometry of MgB_2 were well mixed. The pure Ag and Cu tubes had an outside diameter (OD) of 8 mm, a wall thickness of 1 mm, and were 10 cm long. The fabrication procedure has been explained previously. Short length Ag and Cu-clad wire samples about 2 cm in length were sintered using the fast formation method as described in section 4-1-3-3. One of the Ag-clad samples was also sintered by the normal longer sintering.

For the short sintering, Ag and Cu-clad wire samples were sealed in a small Fe tube and then directly heated at a preset temperature of 800 ^{o}C for 6 minutes in flowing high purity Ar. This was then followed by a quench in liquid nitrogen. In the normal sintering case, one Ag-clad MgB_2 sample was sealed in a small Fe tube and then sintered in a sealed tube furnace in flowing high purity Ar. In this case, the temperature was increased at a heating ramp rate of 600 ^{o}C/h to 800 ^{o}C, then furnace cooled down to room temperature without any holding period at 800 ^{o}C.

Fig. 4-20 shows the real temperature of the normally sintered sample as a function of time. The inset shows the average temperature variation of the fast sintered samples with time, starting from when the samples were loaded into a hot tube furnace held at a constant temperature of 800 ^{o}C.

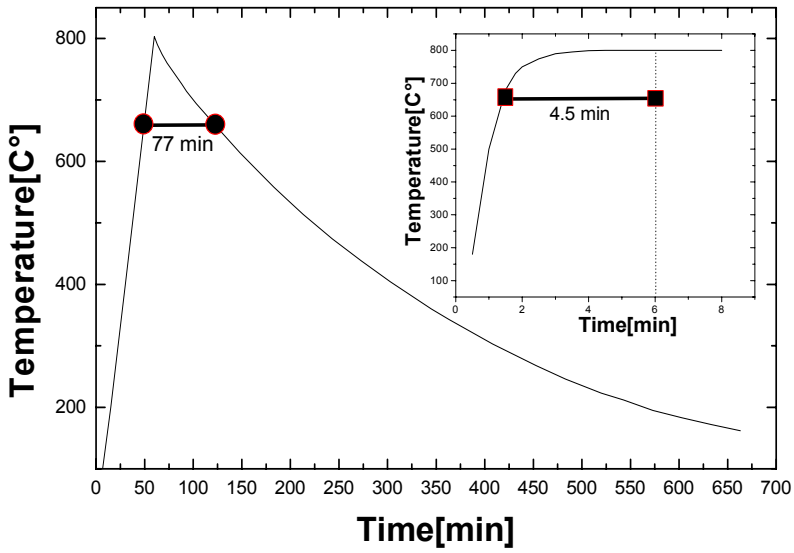

Figure 4- 20: Real temperature that sample has experienced as a function of time for normal sintered sample. The inset shows the time variation of the average real temperature of the short sintered sample, starting from when the wires were loaded into a hot tube furnace held at a constant temperature of 800 °C.

Fig. 4-20 reveals that for the normal sintering case, the sample experienced temperatures higher than 660 °C, which is the magnesium melting point, for about 77 minutes. We thus called this sample the long time-sintered (LS) sample. However, for the fast formation case, this period is only a few minutes (about 4.5 min.) and we call these samples short-time sintered (SS) samples. The surface of the Fe tubes used to seal the wires was slightly oxidized after sintering. However, the MgB_2 wire samples sealed inside the Fe tubes were as fresh as before sintering.

By opening the wires and removing the superconductor cores mechanically, X-ray diffraction of the internal surface of the Ag and Cu sheath materials can be performed. The dc field dependence of the magnetization was measured using the PPMS (Quantum Design) between 5 K and 35 K at different dc fields up to 6 T. For magnetic characterization of Fe clad wire, bare cores were used because of the strong shielding effect of the Fe sheath metal as explained in the last section. Cylindrical bars of MgB_2 core were obtained by mechanically removing the Fe sheath. Ac susceptibility was measured with the amplitude and frequency of the excitation field 1 Oe and 117 Hz, respectively, using the same instrument.

4-3-3 Result and Discussion

The XRD pattern of a typical MgB_2 core separated from the Ag and Cu-clad wires is shown in Fig. 2. It can be seen that the result is relatively single MgB_2 phase with a slight amount of MgO (<5%) and MgB_4. In order to study the reaction between the core and the sheath material at the interface, XRD patterns of the internal surface of the Ag and Cu were obtained after the cores were removed mechanically. The temperature dependence of ac susceptibility for Fe, Ag and Cu-clad samples is shows in the inset of Fig. 4-21. It shown that all samples have a T_c of about 38 K.

The XRD results are shown in Fig. 4-22. The patterns have been recorded from the internal surface of the sheaths of Ag and Cu-clad MgB_2 wire samples when the superconducting core was mechanically removed. It shows that magnesium has reacted

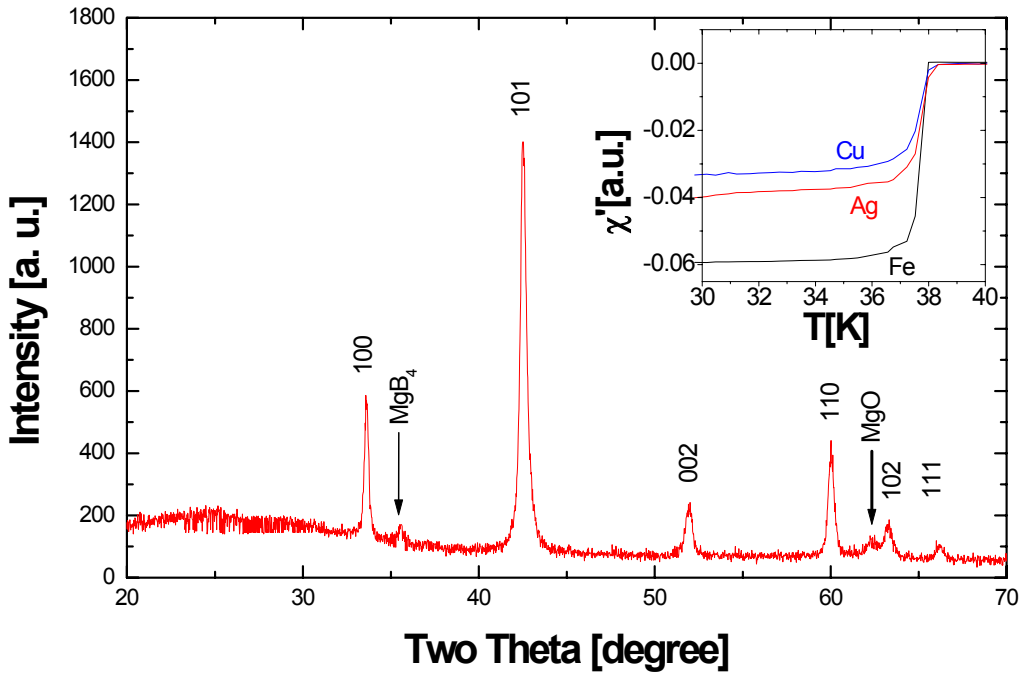

Figure 4- 21: XRD pattern recorded from the superconducting core of one of the MgB_2 samples when the Ag and Cu sheath materials were mechanically removed. The temperature dependence of the ac susceptibility for Fe, Ag and Cu-clad samples is shown in the inset.

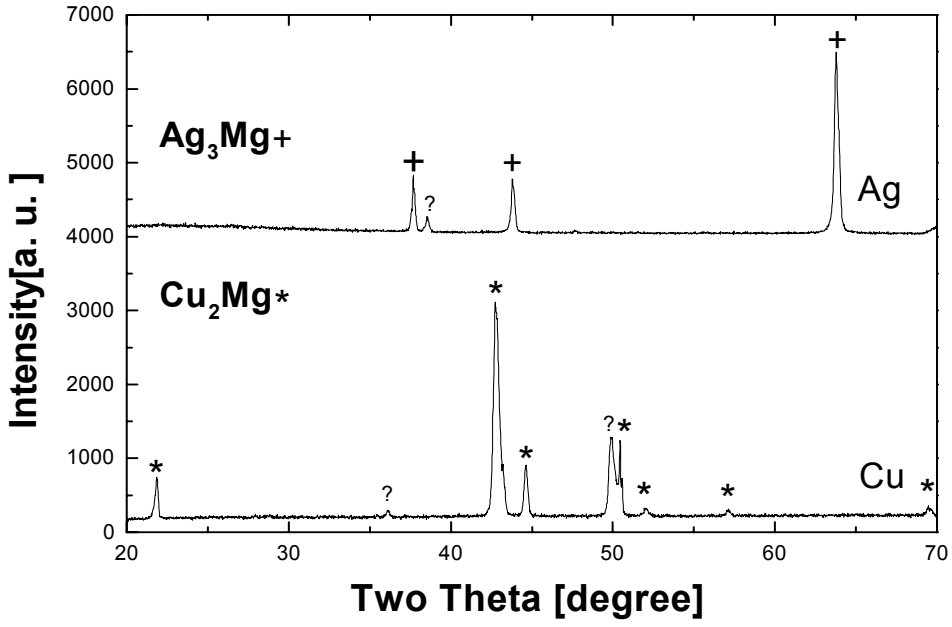

Figure 4- 22: XRD patterns recorded from the internal surface of the sheath of Ag and Cu-clad MgB_2 wire samples when the superconducting core was mechanically removed.

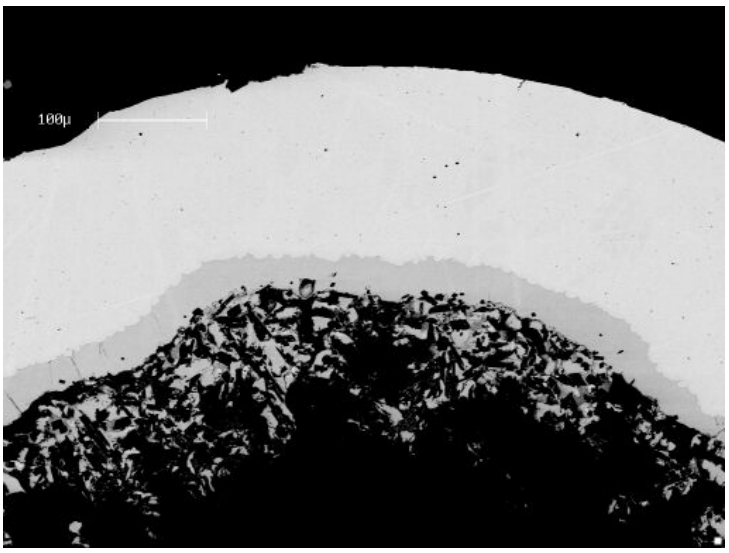

Figure 4- 23: Scanning electron microscope image of a transverse cross-section of SS Cu-clad MgB_2 wire sample using back scattered electron imaging.

with the sheath materials and formed Cu_2Mg and Ag_3Mg phases on the internal sheath surfaces of the Cu and Ag-clad wires, respectively. The unknown peaks that were not matched with PDF database lines are indicated by question marks. For Fe-clad wire

there was not any clear evidence for any reaction between Mg or B and Fe. These results are in agreement with our results in the last sections.

Fig. 4-23 presents a magnified view of a transverse cross section of SS Cu-clad wire using SEM back scattered electron imaging. A well-defined reacted layer about 40 μm in thickness can be clearly seen. It is due to the reaction of magnesium and copper at high temperature in agreement with the XRD pattern (Fig. 4-22). The diffusion of magnesium into the copper sheath is clear in Fig. 4-24, which shows the Electron Dispersive Spectroscopy (EDS) surface analysis result. The magnesium concentration in the central part of the superconductor core is higher than in the area close to the copper sheath. The reacted layer in the SS Ag-clad wire is also about 25 μm (Fig. 4-25). However as we can see in Fig. 4-26, the reacted layer in the LS Ag-clad wire is much thicker, about 90 μm. So increasing the sintering time increases the magnesium deficiency and consequently causes a deficiency in MgB_2 phase in the superconducting core. Longer sintering times could thus lead to a lower J_c in the wire.

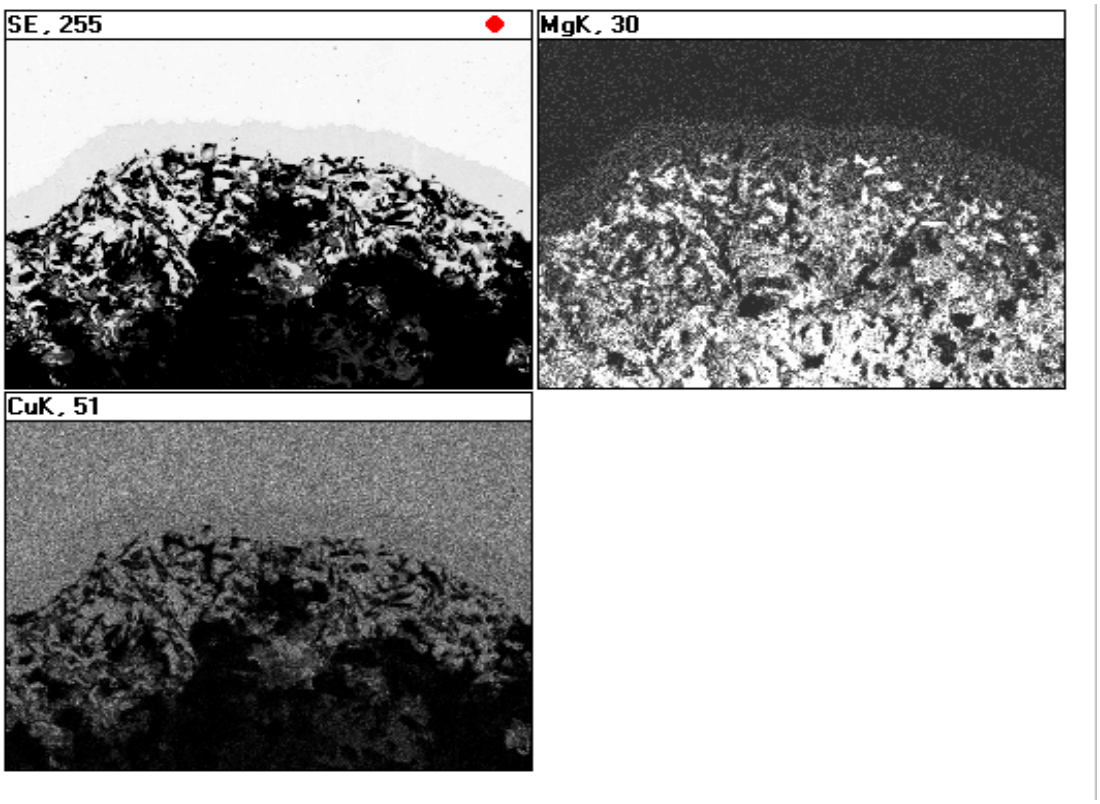

Figure 4- 24: Scanning electron microscope image and EDS surface analysis of a transverse cross-section of SS Cu-clad MgB_2 wire sample.

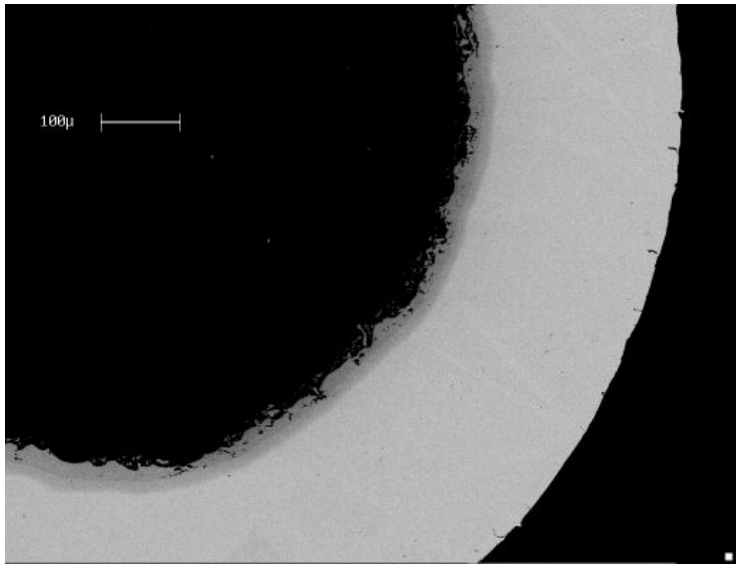

Figure 4- 25: Scanning electron microscope image of a transverse cross-section of the SS Ag-clad MgB_2 wire sample using back scattered electron imaging.

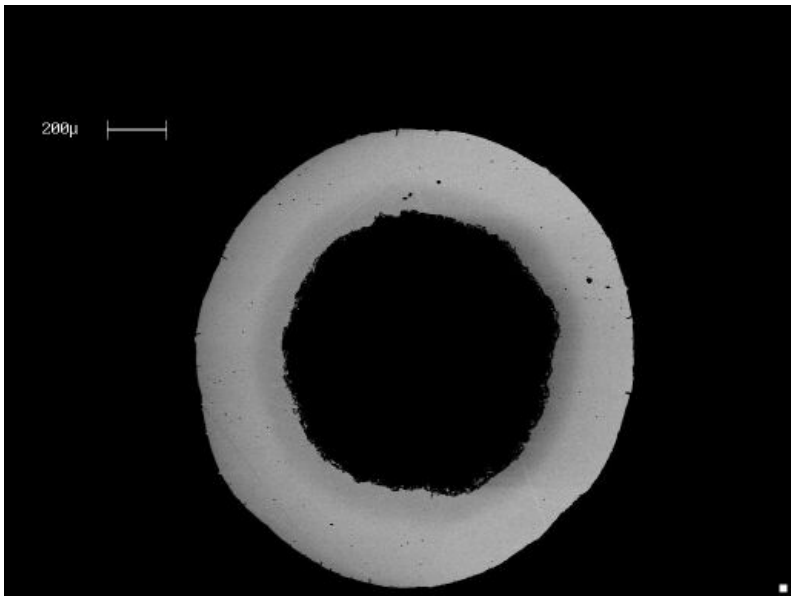

Figure 4- 26: Scanning electron microscope image of a transverse cross-section of the LS Ag-clad MgB_2 sample using back scattered electron imaging.

Measurements of the *M-H* loops at different temperatures were carried out on the Cu, Fe and Ag-clad wires. A typical *M-H* loop of an SS Ag-clad wire sample is shown in Fig. 4-27. We can see that a typical flux-jumping pattern is present for temperatures below 15 K. This flux jumping has been also observed in MgB_2 bulk samples [404].

The critical current density was calculated from the *M-H* loops using the Bean critical model. The field dependence of *Jc* for three samples of Cu and Ag-clad wires at 10 K, 20 K and 30 K are shown in Fig. 4-28. The field dependence of Fe clad wire at 20 K and 30 K is also shown. As we can see, Fe-clad wire has the highest *Jc* and the best *Jc*-field

dependence among all samples at 20 K and 30 K. It should be noted that a *Jc* of 1.3×10^5 A/cm^2 at 20 K and zero field has been achieved for the SS Ag-clad sample. It is not possible to exactly measure the *Jc* at low fields at temperatures below 15 K due to the flux jumping. As we can see the *Jc* in the SS sample is more than two times higher than for the LS sample due to less reaction between the superconducting core and sheath material.

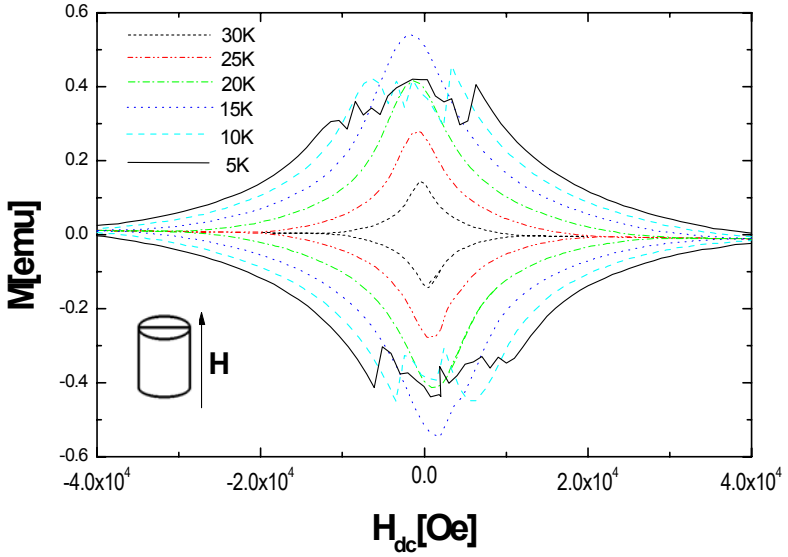

Figure 4- 27: M-H loop of the SS Ag-clad MgB_2 wire sample at different temperatures.

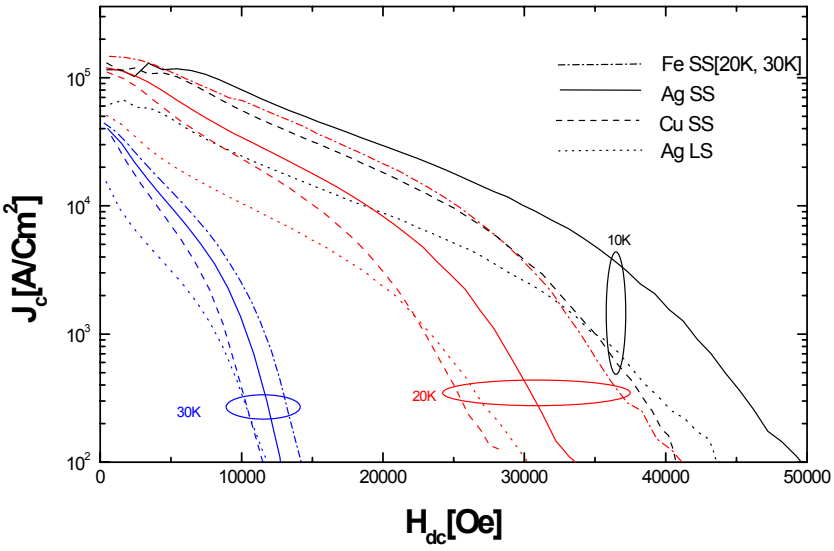

Figure 4- 28: Field dependence of J_c at 5 K, 20 K and 30 K for Ag, Cu and Fe clad wires.

LS Ag-clad wire has the lowest J_c at low fields over the entire temperature range. Although the SS Cu-clad wire has a higher J_c than the LS Ag-clad wire at low field, the J_c-field performance of this sample is not as good as for the LS Ag-clad sample. The LS Ag-clad sample has a slightly higher J_c than SS Cu-clad wire at high fields over the entire temperature range, probably due to poor grain connectivity in the Cu-clad wire.

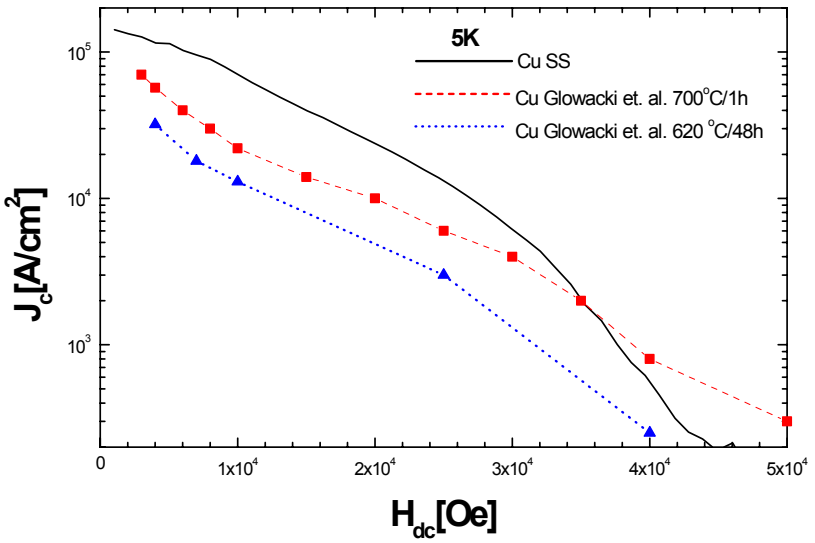

Figure 4- 29: The comparison between Jc field dependence of our SS Cu-clad MgB2 wire and the Cu-clad wires which were reported by Glowacki et al. [14,15] at 5 K.

The field dependence of J_c for the SS Cu-clad wire was compared with the results which were reported by Glowacki et al. [233, 422], as is shown in Fig. 4-29. As we can see, the J_c of wire that was sintered at 700 °C for 1h is about two times higher than for wire that was sintered at 620 °C for 48 h. Our SS Cu-clad wire, which was sintered at 800 °C for 6 min, has better J_c-field performance than wire that was sintered at 620 °C for 48 h. It even has better J_c-field performance at low field (less than 4 T) than wire that was sintered at 700 °C for 1 h. The slightly inferior performance of our SS Cu-clad wire at high fields is probably because the longer sintering time in the 700 °C sample caused stronger grain connectivity.

Fig. 4-30 shows the irreversibility field (H_{irr}) versus temperature for all the samples. H_{irr} was determined from $J_c - H$ curves using the criterion of 100 A/cm^2. We can see that the copper clad wire has the lowest H_{irr} for the whole temperature range. The SS Ag-clad wire also has a higher H_{irr} than the LS wire over the whole temperature range. Fe

has the highest H_{irr} among all the samples. As we can see, the differences between the H_{irr} values are increased by decreasing the temperature.

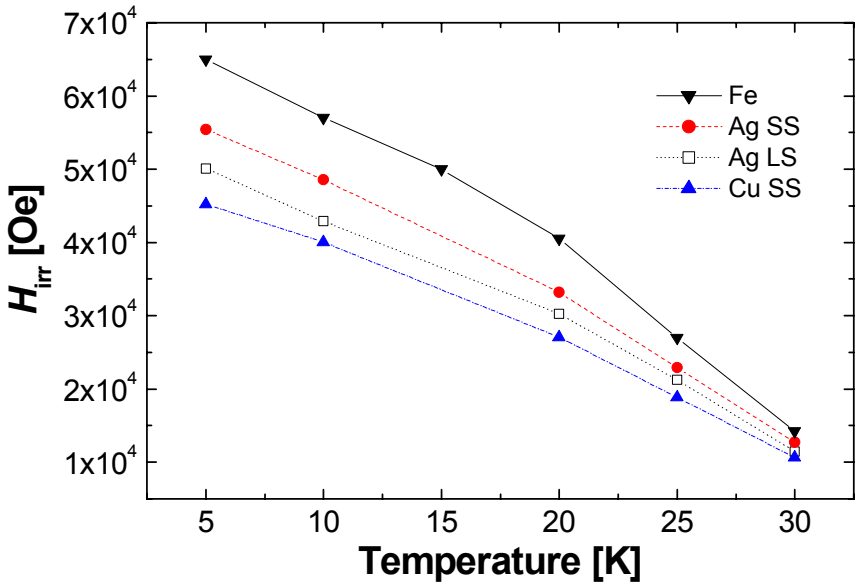

Figure 4- 30: Irreversibility lines for all the samples.

4-3-4 Summary

In this section we have investigated the effects of sintering time and temperature on the critical current densities of Cu, Ag and Fe-clad MgB_2 wires. It was found that a short heat treatment in the fabrication of Cu and Ag clad MgB_2 wires can markedly enhance the critical current density. A total sintering time of several minutes is enough to form nearly pure MgB_2 with high performance characteristics. SEM microanalysis, J_c and H_{irr} results show that the Cu and Ag clad MgB_2 wires samples which were sintered for 6 minutes are better than those sintered for longer times. J_c of 1.2×10^5 A/cm^2 in zero field and above 10^4 A/cm^2 in 2 T at 20 K have been achieved for the SS Ag-clad MgB_2 wire.

4-4 Fabrication and Critical Current Density in 16-Filament Stainless Steel/Fe/MgB_2 Square Wire

4-4-1 Introduction

As we explained in the previous sections the powder-in-tube (PIT) method seems the most promising for practical applications of MgB_2 wires or tapes. Fe and some of its alloys have been found to be suitable for this purpose [200, 203]. Grasso et al. showed that MgB_2 tape or wire can be made from pre-reacted commercially available powder without any heat treatment [277]. Furthermore Suo et al. showed that the critical current density of pre-reacted powder can be improved by a final heat treatment [202]. It has been also shown that increases in the J_c of tapes or wires result from the use of high toughness sheath materials due to mechanical densification of the superconducting core [265]. A 7-filament Cu-Ni/MgB_2 wire prepared by Kumakura et al. [252] had a transport $J_{c,4.2K}$ of about 3×10^4 A/cm^2 in self field and 10^4 A/cm^2 at 1 T. They had used pre-reacted powder and no further heat treatment was applied. An 18-filament Cu/NbZr/MgB_2 tape fabricated by Liu et al. [294] exhibited a transport $J_{c,10K}$ of about 8×10^4 A/cm^2 in self field and 1.36×10^4 A/cm^2 at 1T. They used an *in-situ* reaction method, sintering samples at 600-1000 ^oC for 1-10 h. To prepare dense and compact multifilament wire we used Fe and stainless steel (SS) as a sheath material. In this section we report on the preparation and properties of a 16-filament MgB_2 square wire.

4-4-2 Experimental Details

The SS/Fe/MgB_2 wires were prepared using a standard PIT method. Commercially available MgB_2 powder (Alfa Acer) was loaded into an 8cm long pure Fe tube with an outside diameter of 5 mm and a wall thickness of 0.5 mm. The tube was groove rolled to wire with a square cross section of about 1.5 mm on each side and a length of 50 cm. An empty SS tube was groove rolled to prepare a square cross section tube with a 6 mm inside dimension (each side) and a length of 8 cm. Four pieces of the Fe-clad wire, each about 8 cm in length, were stacked inside this tube which was then groove rolled to a 4-filament wire about 2mm in outside dimension. Fig. 4-31 presents an SEM back

scattered electron image of a transverse cross section of the 4-filament SS/Fe/MgB_2 wire. A well-defined Fe sheath layer fully covered by an SS layer can be clearly seen.

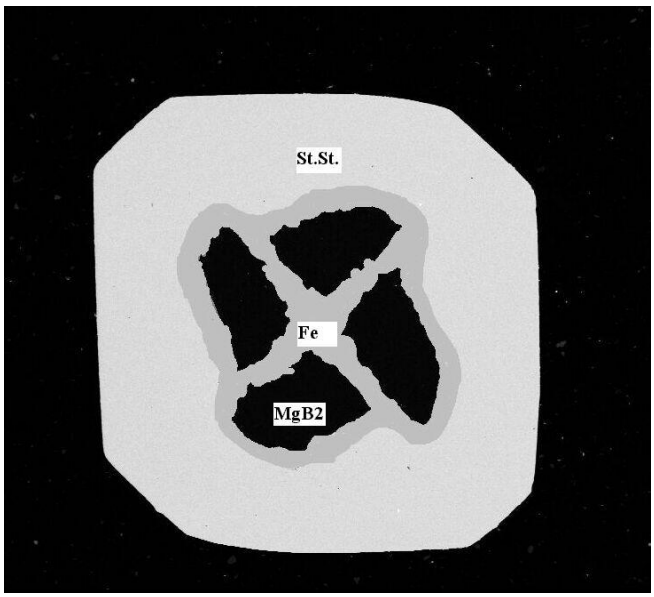

Figure 4- 31: Scanning electron microscope image of a transverse cross-section of 4-filament SS/Fe/MgB_2 wire sample using back scattered electron imaging.

Four pieces of the 4-filament SS/Fe/MgB_2 wire each about 10 cm in length were again stacked inside another SS tube and groove rolled to a tough, high density, 16-filament wire about 2-3 mm in dimension (Fig. 4-32). Fig. 4-32 is an SEM image of a transverse cross section of the 16-filament SS/Fe/MgB_2 wire.

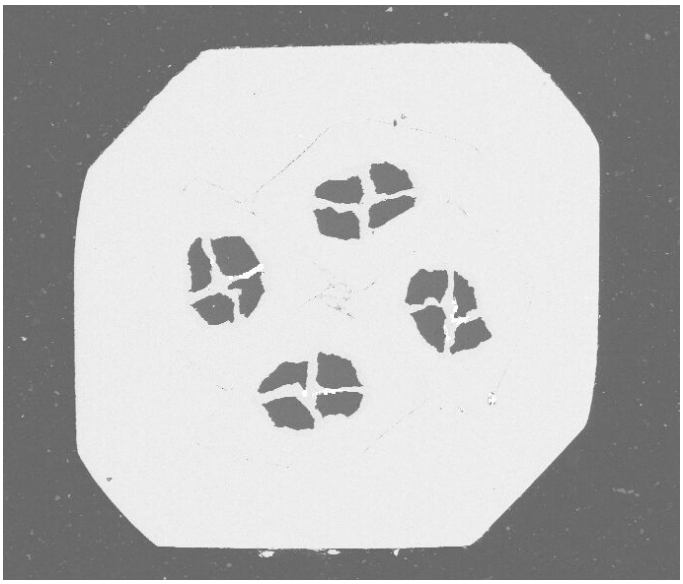

Figure 4- 32: Scanning electron microscope image of a transverse cross-section of 16-filament SS/Fe/MgB_2 wire sample.

Several samples about 2.5cm long were cut and sintered at 950 ^oC in flowing high purity Ar. Fig. 4-33 is an SEM image of a superconducting core from the 16-filament SS/Fe/MgB_2 wire after sintering. Highly packed grains with an average grain size of about 300 nm can be seen.

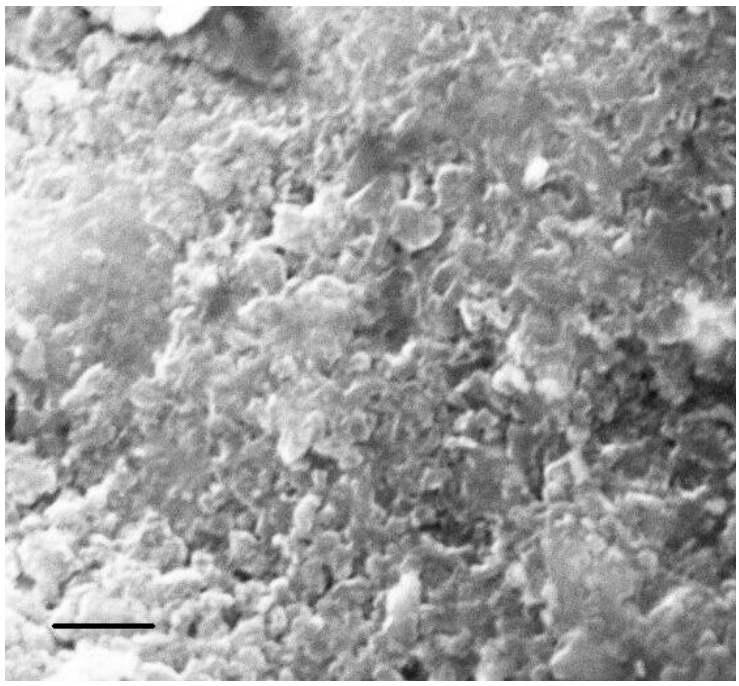

Figure 4- 33: High magnification Scanning Electron Microscope image of a superconducting core for 16-filament SS/Fe/MgB_2 wire sample. The mark indicates 1 micron.

A sample about 6 mm long was taken from the middle of each wire for magnetic measurement. The dc field dependence of the magnetization was measured by VSM using an applied field sweep amplitude of 17 kOe and a temperature range of 4.2 to 40 K, the latter temperature being just above the T_c of MgB_2. In order to obtain the *M-H* loops for the superconductor itself, the Fe contribution (the measurement results at 40 K) was subtracted away from the total *M-H* loop [200, 207]. In the other words, the Fe magnetic contribution was electrically removed. Separate measurement of a small Fe sample sufficed to verify that $(M\text{-}H)_{sheath}$ itself was practically temperature independent within the temperature range of 4 to 40 K, validating the subtraction procedure over the temperature range of interest.

Magnetization loops for the 16-filament wire were measured from 4.2 K to 40 K at 2.5 K temperature intervals. A typical *M-H* loop for a wire sample, with and without the Fe signal, is shown in Fig. 4-34.

4-4-3 Results and Discussion

Fig. 4-35 depicts a representative set of temperature-dependent loops after electrical removal of the sheath material. The paramagnetic slope evident at high temperature is due to the presence of stainless steel. Magnetic J_cs were calculated using the conventional semi-Bean critical-state approach.

The temperature dependences of magnetic J_c of the 16-filament SS/Fe/MgB_2 wire at fields of 5 kOe and 10 kOe are shown in Fig. 4-36. At 5 K, J_cs of 3.4×10^5 A/cm^2 in 5 kOe and 2.4×10^5 A/cm^2 in10 kOe were obtained. The transport J_c temperature dependence of an 18-filament Cu/NbZr/MgB_2 wire [252] in self field and 10 KOe are also included in the figure, as well as the transport $J_{c,4.2K}$ of 7-filament Cu-Ni/MgB_2 wire [294] in self field and 10 kOe. It should be noted that a $J_{c,10K}$ values of 2.3×10^5 A/cm^2 at 5 kOe and 1.3×10^5 A/cm^2 at10 kOe have been achieved for the 16-filament SS/Fe/MgB_2 wire sample. Fig. 4-36 shows that the J_c of our wire at 10 K and 10 kOe is considerably higher than that of the 18-filament Cu/NbZr/MgB_2 tape which had been prepared using unreacted powder and sintered at 600-1000 ^{o}C for 1-10 h.

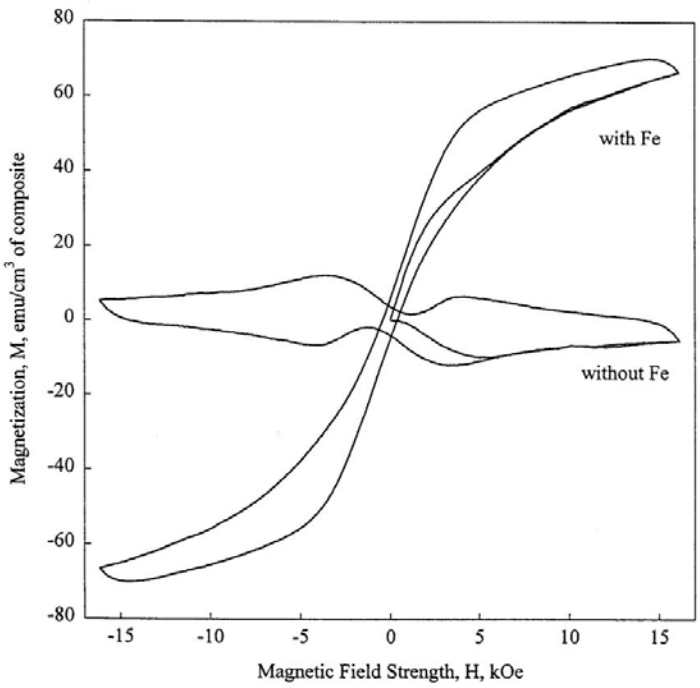

Figure 4- 34: A typical *M-H* loop of 16-filament SS/Fe/MgB_2 wire sample.

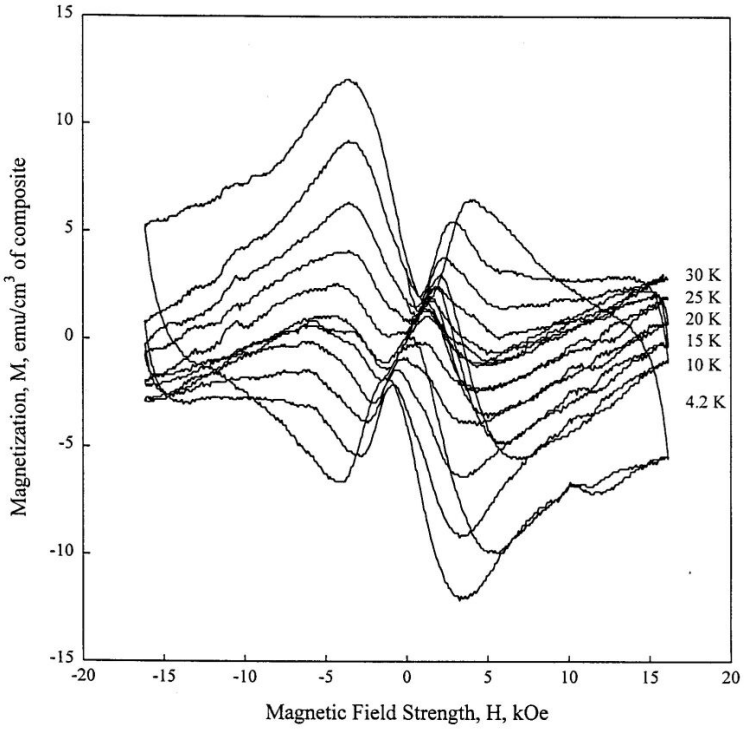

Figure 4- 35: *M-H* loops of 16-filament SS/Fe/MgB_2 wire sample at different temperatures, with the Fe contribution was removed.

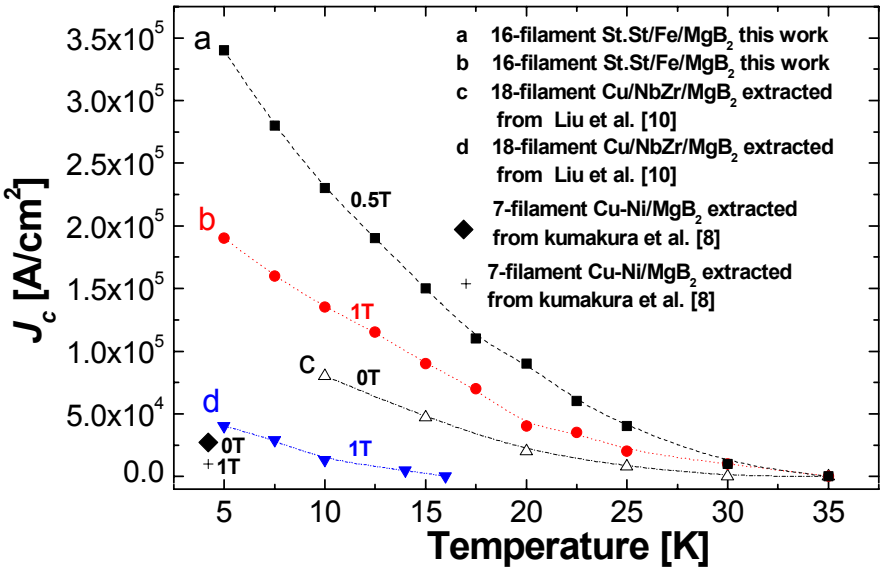

Figure 4- 36: Temperature dependence of magnetic J_c of 16-filament SS/Fe/MgB_2 wire sample at 0.5 and 1 T. The figure includes the temperature dependence of the transport J_c of 18-filament Cu/NbZr/MgB_2 tape sample at 0 and 1 T that is extracted from Liu et al. [294]. The temperature dependences of critical current density J_c of 7-filament Cu-Ni/MgB_2 wire at 0 and 1 T and 4.2 K that are extracted from Kumakura et al. [252] is also included.

4-4-4 Summary

Sixteen-filament stainless steel/Fe/MgB_2 wires were fabricated by the powder-in-tube method followed by groove rolling and heat treatment at 950 ^{o}C. The wires were characterized using SEM, and vibrating sample magnetometery. High strength sheath material results in a dense superconducting core and relatively high critical current density. Magnetic critical current densities of 3.4×10^5 A/cm^2 in 0.5 T and about 1.9×10^5 A/cm^2 in 1 T at 5 K were achieved.

4-5 Transport Critical Current of Solenoidal MgB_2/Cu Coils Fabricated Using a Wind-Reaction *In situ* Technique

4-5-1 Introduction

Since the discovery of the 39 K superconductor, MgB_2 [19], significant advances has been achieved in the fabrication of various forms of MgB_2. In particular, intensive efforts have been made in improving the critical current density (J_c) in various metal sheathed MgB_2 wires. High J_c of 10^5 – 10^6 A/cm^2 at 4 K to 30 K for MgB_2 wires and good performance of J_c in magnetic field have been reported by several groups [200-202, 233, 265, 277, 404, 423]. However, the results reported thus far have been largely limited to short samples several centimetres long. In contrast, long Bi-based HTS wires with high J_c were reported within several months time after discovery of the Bi-HTS compound [424]. For large scale applications it is essential to fabricate this material into long wires and coils. The critical challenge that remains is how much the J_c deteriorates with increasing length of the wire and whether one can wind the wire into a coil without appreciable loss of J_c. In this section, we report the fabrication and transport critical current of solenoidal MgB_2/Cu coils fabricated using a wind-reaction in-situ technique.

4-5-2 Experimental Details

Standard powder-in-tube methods were used for Cu-Fe or Cu clad MgB_2 tapes. The pure Cu or Fe tubes had an outside diameter (OD) of 10 mm, a wall thickness of 1 mm, and a length of 12 cm. One end of the tube was sealed, and the tube was filled in with magnesium (99% purity) and amorphous boron (99%) with the stoichiometry of MgB_2. The composite was drawn to 0.5, 0.7 and 1 mm diameter wires several meters long. Some wires were further rolled to ribbon over many steps. Several short samples 2 cm in length were cut from the wires and ribbons. The green wires were wound onto a ceramic tube 8 mm in diameter with both ends fixed to slots at the end of the ceramic

tube. Several coils were prepared using this procedure, and one of the coils has 100 turns and was wound using 3-meter long Cu-sheathed MgB_2 wire. These coils and some straight pieces of wires and tapes were then sintered in a tube furnace at temperatures within a range of 650-750 ^oC for 10 min. A high purity argon gas flow was maintained throughout the sintering process.

Short pieces of wires 4 mm and 30 mm long were used for magnetic and transport critical current measurements using the four probe method. For longer wire samples up to 300 mm, a number of voltage contacts were made at different distances to determine the variation of I_c with length. For the 100 turn coil two voltage contacts were made at a distance of 2 meters apart with the current contacts at the end of the coil. Transport measurements of the voltage versus current (V-I) were performed by a standard 4-probe, DC method. The measurements were performed in liquid helium. Current contacts were soldered onto the samples at least 1cm away from the voltage contacts, to allow for the heat created at the current contacts to dissipate into the liquid helium before it reached the part of the sample between the voltage contacts. The current was switched on and off gradually, to avoid damage to the sample due to the mechanical shock resulting from a fast change in the current. Each point in V-I was taken within 10 seconds, to avoid heating the sample. Magnetic measurements were performed by a Quantum Design PPMS magnetometer. Magnetic hysteresis loops were used to obtain the field dependence of the critical current density at each of the temperatures measured, by employing the critical state model. The sweep rate of the field was 50 Oe/s. The magnetic field was always applied along the sample.

4-5-3 Results and Discussions

Figure 4-37 displays 10 mm diameter MgB_2 coils of 100 turns, wound using 3 meters of Cu-sheathed single core wire and heat-treated at 700 ^oC for 10 min. The coils are reasonably flexible and can be stretched by 20% and bent to an angle of 30^o after heat treatment without degradation in I_c. Figure 4-38 shows photomicrographs of transverse and longitudinal cross-sections of a 100 turn solenoid coil (Coil-4). It is seen that the interface between the Cu and the MgB_2 core is very smooth. Although there is thin layer of MgCu formed during sintering the reaction between the Cu and the Mg is not very

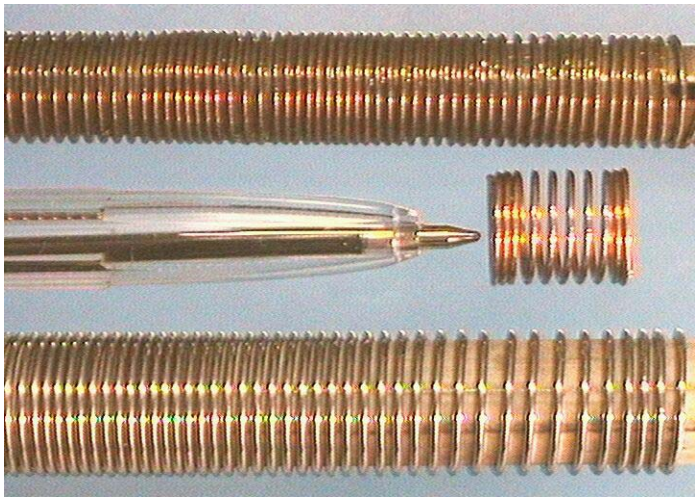

Figure 4- 37: The appearance of two 10 mm diameter MgB_2 coils of 100 turns, wound using 3 meters of Cu-sheathed single core wire and a 10 mm diameter coil of 10 turns. These coils were heat-treated at 700 ^oC for 10 min.

serious as a short reaction time (10min) and low sintering temperatures (750 ^oC) were used.

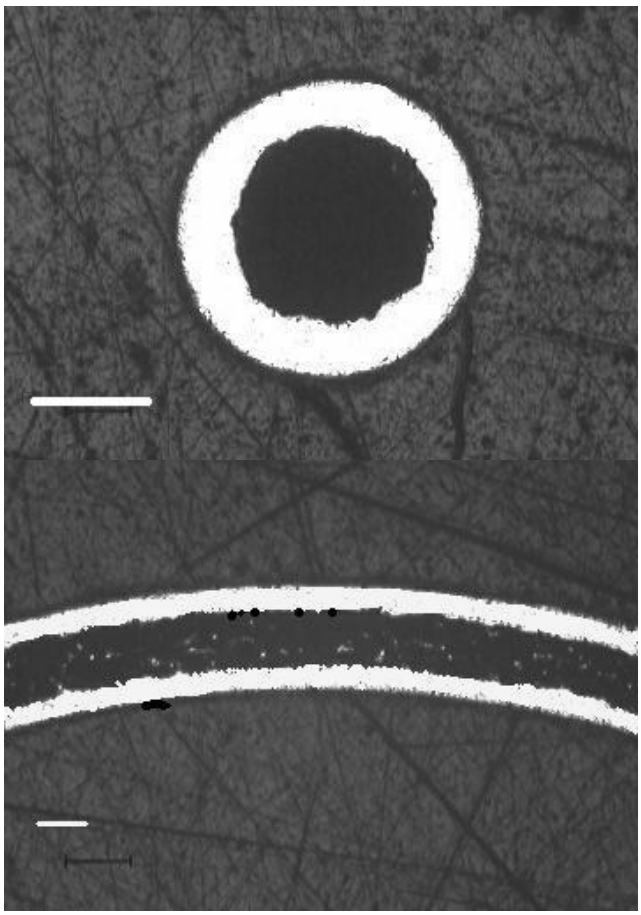

Figure 4- 38: Photomicrographs of the transverse (a) and longitudinal (b) cross-sections of the 100 turn coil-4. The scale bars represent about 300 µm.

Table 4-3 lists the parameters for samples in the form of straight wires and coils with Cu-sheaths. These results show very interesting features. Compare wire-1 and coil-1 which are made from the same green wire. The J_c is the same for both cases, indicating that (a) winding the wire into a 10 mm diameter coil does not degrade J_c and (b) the increase in distance between the two voltage contacts from 13mm to 100mm did not cause a reduction in J_c. The J_c results obtained from the straight wire (wire-2) and the 100 turn coil (coil-4) further indicate that there is no evidence of significant length dependence of J_c. For the sample wire-2, the critical current was not reached due to the limitations of contact heating. But the I_c for all three contact distances exceeds 100 A. The 6 turn coil (coil-2) and 5 turn coil (coil-3) were wound using thinner Cu-sheathed wire (OD = 0.5mm) and tape respectively. Because their core density is relatively higher, respective J_c values of 125,000 A/cm^2 and 133,000 A/cm^2 at helium temperature and self field has been achieved, suggesting that density is one of the critical factors to influence J_c.

Table 4- 3: List of various samples with description and measurement results of J_c.

Designation of samples	Sample description	Distance between voltage contacts (D, mm)	MgB_2 Core diameter (mm)	I_c (A)	J_c (A/cm^2)
Wire-1	30mm MgB2/Cu straight wire	13	0.45	105	66,000
Wire-2	200mm long MgB2/Fe-Cu straight wire	37	0.6	>100	>35,300
		80	0.6	>100	>35,300
		120	0.6	>100	>35,300
Wire Coil-1	5 turn MgB_2/Cu coil, 10mm OD	100 (3 turns)	0.45	>101	>63,500
Wire Coil-2	6 turn MgB_2/Cu coil, 10mm OD	140 (4 turns)	0.32	100	125,000
Tape Coil-3	5 turn MgB_2/Cu coil, 10mm OD	100 (3 turns)	0.055	>73	>133,000
Wire Coil-4	100 Turn MgB_2/Cu solenoid, 10mm OD	35 (1 turn)	0.45	72	45,300
		2000 (63 turns)	0.45	73	45,900

Figure 4-39 shows the characteristics of the voltage – current curves (*V-I*) for the 100 turn solenoid coil with two voltage contacts at distance of 35 mm (1 turn) and 2 meters (63 turns) apart. Despite possible inhomogeneity along the length and the low density of the core, the same value of J_c for the two very different voltage contact distances clearly indicates that the deterioration of J_c with increasing length of MgB_2 wires is insignificant. It should be pointed out that the measurement for the voltage contact distance of 35 mm was performed after several cycles of the coil between helium temperature and room temperature due to the needed to change the contact position. It is

expected that the cycling could cause some degradation in J_c as the density of the single core is low. Furthermore, a solenoid coil with 100 turns passing 73 A will generate a self-field of about 80 mT which will slightly reduce the I_c. So, the J_c for the 35mm contact distance should be higher than that with the 2 meters contact distance. Compared to sample wire-1 which was made from the same batch of green wire the J_c for the 35 mm contact distance would not be higher than that of wire-1. If the density of the wire core can be improved the thermal cycling would not have detrimental effects as has been demonstrated for Fe-sheathed wire [203].

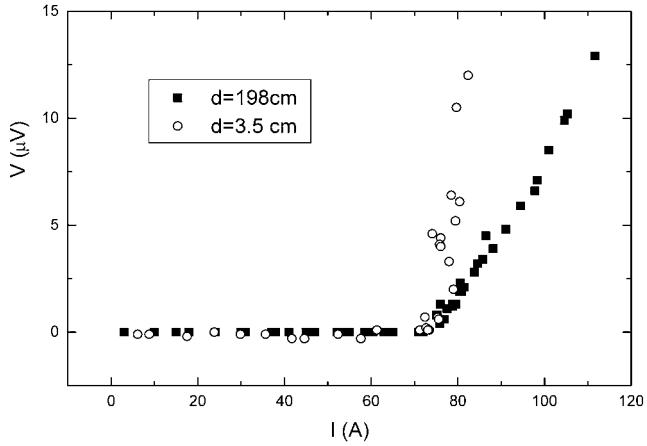

Figure 4- 39: The voltage – current curves (*V-I*) for the 100 turn solenoid coil with two voltage contacts at a distance of 35 mm (1 turn) and 2 meters (63 turns). The two current contacts were soldered at the end of each side of the solenoid coil for the latter case.

Note also from Figure 4-39 that the *V-I* curve for the contact distance of 35 mm shows a steep increase at the critical current 72 A while the voltage for the large contact distance increases more gradually. For the former the *V-I* characteristics beyond the critical current are dominated by the Cu sheath while in the latter case, there are still large segments of the coil remaining superconducting when a small section becomes normal. It is unclear that what kind of voltage criteria should be used to determine the I_c for the Cu-sheathed MgB_2 wire at this stage. In our measurements we use the same standard to determine the I_c for short straight wire and for the solenoid coils. This means that the criterion for the 100 turn solenoid coil is about 0.005 μV/cm, compared with common criterion of 1 μV/cm used in HTS wires. If we apply the 1 μV/cm criterion to the 100 turn coil the I_c will be about 200 A, estimated by extrapolating the *V-I* curve. This will

cause huge heating over normal sections of coil. Thus, the 1 μV/cm criterion may be applicable to the metal sheathed MgB_2 wire.

4-5-4 Summary

In this section, we report the results of transport J_c of solenoid coils up to 100 turns fabricated with Cu-sheathed MgB_2 wires using a wind-reaction in-situ technique. Despite the low density of the single core material and some reaction between Mg and Cu-sheath, our results demonstrate that the decrease in transport J_c with increasing length of MgB_2 wires is insignificant. Solenoid coils with diameters as small as 10 mm can be readily fabricated using a wind-reaction in-situ technique. The J_c of coils is essentially the same as for straight wires. A J_c of 133,000 A/cm^2 and 125,000 A/cm^2 at 4 K and self field has been achieved for a small coil wound using Cu-sheathed tape and Cu-sheathed wire respectively. These results indicate that MgB_2 wires have a great potential for large scale applications.

References

1. Nagamatsu, J., N. Nakagawa, T. Muranaka, Y. Zenitani and J. Akimitsu, *Superconductivity at 39 K in magnesium diboride.* Nature, 2001. **410**(6824): p. 63-64.

2. Canfield, P.C., D.K. Finnemore, S.L. Bud'ko, J.E. Ostenson, G. Lapertot, C.E. Cunningham and C. Petrovic, *Superconductivity in dense MgB_2 wires.* Physical Review Letters, 2001. **86**(11): p. 2423-2426.

3. Sumption, M.D., X. Peng, E. Lee, M. Tomsic and E.W. Collings, *Transport current in MgB_2 based superconducting strand at 4.2 K and self-field.* cond-mat/0102441, 2001.

4. Grasso, G., A. Malagoli, C. Ferdeghini, S. Roncallo, V. Braccini, A.S. Siri and M.R. Cimberle, *Large transport critical currents in unsintered MgB_2 superconducting tapes.* Applied Physics Letters, 2001. **79**(2): p. 230-232.

5. Glowacki, B.A., M. Majoros, M. Vickers, J.E. Evetts, Y. Shi and I. McDougall, *Superconductivity of powder-in-tube MgB_2 wires.* Superconductor Science & Technology, 2001. **14**(4): p. 193-199.

6. Jin, S., H. Mavoori, C. Bower and R.B. van Dover, *High critical currents in iron-clad superconducting MgB_2 wires.* Nature, 2001. **411**(6837): p. 563-565.

7. Che, G.C., S.L. Li, Z.A. Ren, L. Li, S.L. Jia, Y.M. Ni, H. Chen, C. Dong, J.Q. Li, H.H. Wen, and Z.X. Zhao, *Preparation and superconductivity of a MgB_2 superconducting tape.* cond-mat/0105215, 2001.

8. Kumakura, H., A. Matsumoto, H. Fujii and K. Togano, *High transport critical current density obtained for powder-in-tube-processed MgB_2 tapes and wires using stainless steel and Cu-Ni tubes.* Applied Physics Letters, 2001. **79**(15): p. 2435-2437.

9. Li, A.H., X.L. Wang, M. Ionescu, S. Soltonian, J. Horvat, T. Silver, H.K. Liu and S.X. Dou, *Fast formation and superconductivity of MgB_2 thick films grown on stainless steel substrate.* Physica C, 2001. **361**(2): p. 73-78.

10. Liu, C.F., S.J. Du, G. Yan, Y. Feng, X. Wu, J.R. Wang, X.H. Liu, P.X. Zhang, X.Z. Wu, L. Zhou, L.Z. Gao, K.Q. Ruan, C.Y. Wang, X.G. Li, G.E. Zhou, and Y.H. Zhang, *Preparation of 18-filament Cu/NbZr/MgB_2 tape with high transport critical current density.* Cond-mat/0106061, 2001.

11. Horvat, J., X.L. Wang, S. Soltanian and S.X. Dou, *Improvement of critical current in MgB_2/Fe superconducting wires by a ferromagnetic sheath.* Applied Physics Letters, 2002. **80**(5): p. 829-831.

12. Soltanian, S., X.L. Wang, I. Kusevic, E. Babic, A.H. Li, M.J. Qin, J. Horvat, H.K. Liu, E.W. Collings, E. Lee, M.D. Sumption, and S.X. Dou, *High-transport critical current density above 30 K in pure Fe-clad MgB_2 tape.* Physica C, 2001. **361**(2): p. 84-90.

13. Dou, S.X., X.L. Wang, J. Horvat, D. Milliken, A.H. Li, K. Konstantinov, E.W. Collings, M.D. Sumption and H.K. Liu, *Flux jumping and a bulk-to-granular transition in the magnetization of a compacted and sintered MgB_2 superconductor.* Physica C, 2001. **361**(2): p. 79-83.

14. Johansen, T.H., M. Baziljevich, D.V. Shantsev, P.E. Goa, Y.M. Galperin, W.N. Kang, H.J. Kim, E.M. Choi, M.S. Kim and S.I. Lee, *Dendritic flux patterns in MgB_2 films.* Superconductor Science & Technology, 2001. **14**(9): p. 726-728.

15. Johansen, T.H., M. Baziljevich, D.V. Shantsev, P.E. Goa, Y.M. Galperin, W.N. Kang, H.J. Kim, E.M. Choi, M.S. Kim and S.I. Lee, *Dendritic magnetic instability in superconducting MgB_2 films.* Europhysics Letters, 2002. **59**(4): p. 599-605.

16. Dhalle, M., P. Toulemonde, C. Beneduce, N. Musolino, M. Decroux and R. Flukiger, *Transport and inductive critical current densities in superconducting MgB_2.* Physica C, 2001. **363**(3): p. 155-165.

17. Grant, P.M. in *Special section on MgB_2, The American Physical Society March Meeting*. 2001. Ciatel.

18. Silver, T., S.X. Dou and J.X. Jin, Application of high temperature superconductors, EuroPhysics News, 2001.

19. Larbalestier, D.C., L.D. Cooley, M.O. Rikel, A.A. Polyanskii, J. Jiang, S. Patnaik, X.Y. Cai, D.M. Feldmann, A. Gurevich, A.A. Squitieri, M.T. Naus, C.B. Eom, E.E. Hellstrom, R.J. Cava, K.A. Regan, N. Rogado, M.A. Hayward, T. He, J.S. Slusky, P. Khalifah, K. Inumaru, and M. Haas, *Strongly linked current flow in polycrystalline forms of the superconductor MgB_2.* Nature, 2001. **410**(6825): p. 186-189.

20. Takano, Y., H. Takeya, H. Fujii, H. Kumakura, T. Hatano, K. Togano, H. Kito and H. Ihara, *Superconducting properties of MgB_2 bulk materials prepared by high-pressure sintering.* Applied Physics Letters, 2001. **78**(19): p. 2914-2916.

21. Bugoslavsky, Y., G.K. Perkins, X. Qi, L.F. Cohen and A.D. Caplin, *Vortex dynamics in superconducting MgB_2 and prospects for applications.* Nature, 2001. **410**(6828): p. 563-565.

22. Kim, M.S., C.U. Jung, M.S. Park, S.Y. Lee, K.H.P. Kim, W.N. Kang and S.I. Lee, *Prominent bulk pinning effect in the MgB_2 superconductor - art. no. 012511.* Physical Review B, 2001. **6401**(1): p. 2511-+.

23. Wen, H.H., S.L. Li, Z.W. Zhao, Y.M. Ni, Z.A. Ren, G.C. Che, H.P. Yang, Z.Y. Liu and Z.X. Zhao, *Strong quantum fluctuation of vortices in bulk samples of the new superconductor MgB_2.* Chinese Physics Letters, 2001. **18**(6): p. 816-819.

24. Kim Kijoon, H.P., W.N. Kang, M.-S. Kim, C.U. Jung, H.-J. Kim, E.-M. Choi, M.-S. Park and S.-I. Lee, *Origin of the high DC transport critical current density for the MgB2 superconductor.* cond-mat/0103176, 2001.

25. Hansen, M., in *Constitution of Binary Alloys*. 1958, McGrow-Hill: New York. p. 662-663.

26. Genenko, Y.A., A. Snezhko and H.C. Freyhardt, *Overcritical states of a superconductor strip in a magnetic environment.* Phys. Rev. B, 2000. **62**(5): p. 3453-3472.

27. Majoros, M., B.A. Glowacki and A.M. Campbell, *Magnetic screening as a possible way to decrease transport AC losses in multifilamentary superconductors — basic theoretical considerations.* Physica C: Superconductivity, 2000. **334**(3-4): p. 129-140.

28. Mager, A., *Magnetostatic shielding factors of cylinders with rectangular cross sections.* Physica B+C, 1975. **80**(1-4): p. 451-463.

29. Collings, E.W. and M.D. Sumption, *Static and dynamic parasitic magnetizations and their control in superconducting accelerator dipoles.* Physica C: Superconductivity, 2001. **354**(1-4): p. 60-65.

30. Collings, E.W., K.R. Marken Jr. and M.D. Sumption. *Advances in Cryogenic Engineering*. in *International Cryogenic Materials Conference (ICMC)*. 1990. UCLA, Los Angeles, California.

31. Collings, E.W., K.R. Marken Jr., M.D. Sumption, G. Iwaki and S. Sakai, *Design, fabrication, and properties of magnetically compensated SSC strands.* IEEE Trans. on Magn., 1991. **27**(2): p. 1787-1790.

32. Greem, M.A., E.W. Collings, K.R. Marken Jr. and M.D. Sumption, in *Supercollider 3*, J. Nonte, Editor. 1991, Plenum Press: New York. p. 365-373.

33. Wang, X.L., S. Soltanian, J. Horvat, A.H. Liu, M.J. Qin, H.K. Liu and S.X. Dou, *Very fast formation of superconducting MgB_2/Fe wires with high J_c.* Physica C, 2001. **361**(3): p. 149-155.

34. Suo, H.L., C. Beneduce, M. Dhalle, N. Musolino, J.Y. Genoud and R. Flukiger, *Large transport critical currents in dense Fe- and Ni-clad MgB_2 superconducting tapes.* Applied Physics Letters, 2001. **79**(19): p. 3116-3118.

35. Glowacki, B.A., M. Majoros, M.E. Vickers and B. Zeimetz, *Superconducting properties of the powder-in-tube Cu-Mg-B and Ag-Mg-B wires.* Physica C, 2002. **372**: p. 1254-1257.

36. Glowacki, B.A., M. Majoros, M.E. Vickers and B. Zeimetz. in *EUCAS 2001*. 2001. Copenhagen, Denmark.

37. Goldacker, W., S.I. Schlachter, S. Zimmer and H. Reiner, *High transport currents in mechanically reinforced MgB_2 wires.* Superconductor Science & Technology, 2001. **14**(9): p. 787-793.

38. Sumption, M.D., E.W. Collings, E. Lee, X.L. Wang, S. Soltanian and S.X. Dou, *Reduction and elimination of external-field AC loss in MgB_2/Fe wire by in situ magnetic shielding.* Physica C-Superconductivity and Its Applications, 2002. **378**: p. 894-898.

39. Larbalestier, D., A. Gurevich, D.M. Feldmann and A. Polyanskii, *High-T_c superconducting materials for electric power applications.* Nature, 2001. **414**(6861): p. 368-377.

40. Tenbrink, J., K. Neine, H. Krauth and M. Thonew, VDI Berichte, 1989. **733**: p. 399.

CHAPTER 5: EFFECT OF CHEMICAL DOPING ON THE CRITICAL CURRENT DENSITY AND FLUX PINNING OF MgB_2

5-1 Enhancement of the Critical Current Density and Flux Pinning of Superconductor MgB_2 by Nanoparticle SiC Doping

5-1-1 Introduction

High J_c values at a level of 10^5 A/cm^2 to 10^6 A/cm^2 at 20 K to 30 K for MgB_2 wires and tapes have been presented in previous chapter. Many groups have attempted to improve the critical current density in this superconductor as it has a lower H_{c2} and H_{irr} than the commercial low temperature superconductors Nb_3Sn and NbTi. Despite the strong link grain boundary effects on critical current density [1], the J_c drops rapidly with increasing magnetic field due to poor flux pinning. Therefore, extensive research has been done on introducing pinning centers into this superconductor.

Various mechanical deformation processes have been used either to improve the density or to introduce defects, resulting some improvements in $J_c(H)$ in hot-pressed bulk, wires and tapes [2-10]. Because the MgB_2 lattice structure is rather rigid and the number of elements in the structure is only two, the density of defects, if any, introduced by mechanical deformation is too low to provide effective pinning.

Effective pinning centers has been induced by high energy ion irradiation of MgB_2 powder [11] or by oxygen alloying in MgB_2 thin films [10]. Producing pinning centers via chemical doping is another effective method and more practical compared to physical techniques. Several attempts have been made to improve flux pinning using chemical doping. The results for doping into MgB_2 reported so far are limited to

addition rather than substitution. Additives appear to be ineffective for improving pinning at high temperatures. Zhao et al., and Feng et al. have doped MgB_2 with Ti and Zr, showing an improvement of J_c at low temperatures, attributable to the sintering aid effect of these additives [12, 13]. However, there is no evidence for improved pinning at temperatures above 10 K as the J_c drops off rapidly with increasing field ($H_{irr} \approx 4$ T at 20 K). Wang et al. doped MgB_2 using Y_2O_3 nanoparticles [14]. Their results showed a significant improvement of the irreversibility field (H_{irr}= 11.5 T) at 4.2 K for the doped sample due to the introduction of highly dispersed inclusions such as YB_4. However, the improvement in H_{irr} at 20 K is insignificant for the doped samples. Cimerle et al. found that doping with a small amount of Li, Al and Si produced some increase in J_c, but there was no improvement in H_{irr} [15] because single element doping degrades T_c dramatically at high doping levels.

Recently, using high field transport measurements, Gurevich et al. have reported the achievement of record high upper critical fields (H_{c2}) for high resistivity films and untextured bulk polycrystals [16]. They found that enhancements to the resistivity have a strong influence on H_{c2}. The observed remarkable H_{c2} enhancement to almost 50 T is a consequence of the two-gap superconductivity of MgB_2, which offers special opportunities for further H_{c2} increased by tuning the impurity scattering. In this section we present chemical doping with nanoparticle SiC into MgB_2 by means of transport and magnetic measurement evaluations in combination with TEM observations on the nanoscale-SiC doped MgB_2. We will show that SiC doping can significantly enhance J_c in high fields without a reduction in low field J_c and only a slight reduction in T_c. The results demonstrate that nanoparticle SiC doping in MgB_2 induced intra-grain defects as effective pinning centres, which are largely responsible for the improved performance of $J_c(H)$ over a wide range of temperatures.

5-1-2 Experimental Details

MgB_2 pellet samples were prepared by an in-situ reaction method, which was described in detail previously. Powders of magnesium (99% pure) and amorphous boron (99% pure) were well mixed with SiC nano-particle powder (with a particle size of 10 nm to 100 nm) with the atomic ratio of $MgB_{2-x}(SiC)_{x/2}$, where x = 0, 0.2, and 0.3. A sample with 10 wt% of SiC addition to MgB_2 was also made. Pellets 10 mm in diameter and 2

mm in thickness were made from these powders. Heat treatment was performed at a temperature of 800 ^oC for 30 min.

The magnetization of samples in magnetc fields up to 9 T was measured using a PPMS (Quantum Design) at the University of Wollongong and up to 14 T using the vibrating sample magnetometer (VSM) at the University of Wisconsin at Madison. The resistivity versus temperature curves $\rho(T)$, were measured in magnetic fields up to 9 T by a four probe method at a current density of about 1 A/cm^2 using the 9 T PPMS (Quantum Design) at the University of Wisconsin at Madison. All the samples were cut to the same size of $0.56 \times 2.17 \times 3.73$ mm^3 from as-sintered pellets. A magnetic J_c was derived using a Bean model. An empirical magnetic irreversibility field (H_{irr}) was defined as the field at which J_c falls to 100 A/cm^2. The critical temperature (T_c) was obtained as the onset of the diamagnetic transition in magnetic ac susceptibility measurements. An high-resolution transmission electron microscope (HRTEM) was employed to characterize the morphology of the samples. Electron energy loss spectroscopy (EELS) [17] was obtained using a JEOL-3000F field emission STEM/TEM, equipped with a Schottky field-emission source operated at 300 keV.

5-1-3 Results and Discussion

Fig. 5-1 shows XRD patterns for the SiC doped and non-doped samples. The XRD pattern for the non-doped sample reveals about 5% MgO, besides MgB_2 as the main phase. Doped samples consist of MgB_2 as the main phase, with Mg_2Si as the major impurity phase (crosses in Fig. 5-1) as well as small amounts of MgO and MgB_4.

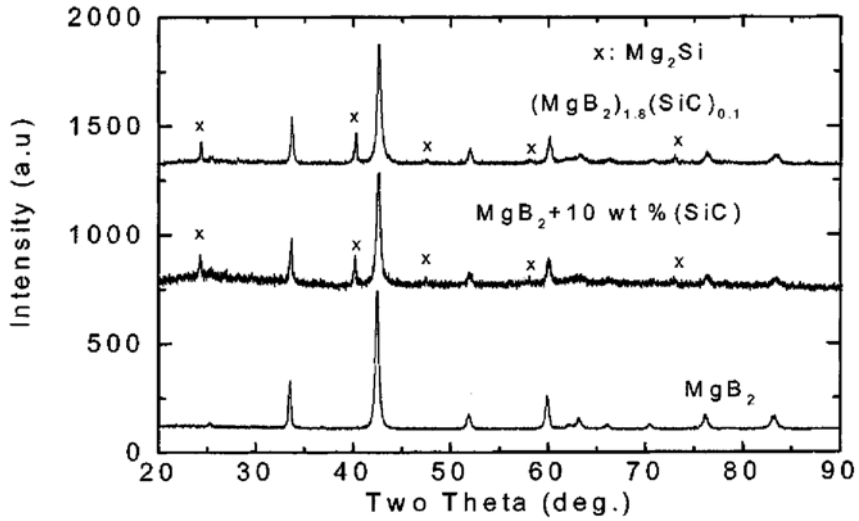

Figure 5- 1: XRD patterns for the undoped and SiC-doped samples.

Fig. 5-2 shows an SEM image of the MgB_2 + 10 wt% SiC sample. As we can see, the sample is very porous, consistent with the low mass density of the sample, about 1.3 g/cm^3 which is about 50% of the mass density of a fully dense sample. This suggests that J_c could be further improved if the density of the sample can be increased. Large numbers of spherical holes with a size of about 10-15 μm are uniformly distributed in the superconducting matrix, as can be seen in this image. The holes can be attributed to voids that were left by the melting magnesium particles. A very similar microstructure was found for all the samples without any significant differences. Further SEM examination revealed that the MgB_2 matrix consists of sub-micron grains with average grain sizes of less than 100 nm, and the homogeneity appears to be the same for all the samples with different doping levels.

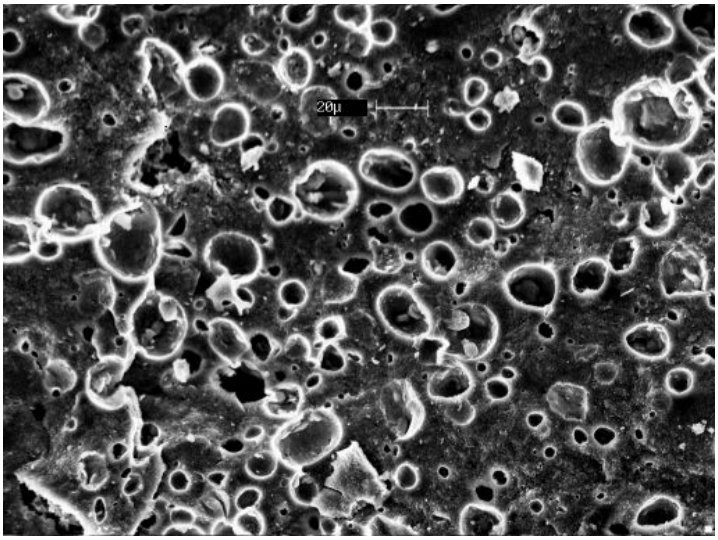

Figure 5- 2: SEM image of MgB_2 bulk sample.

Fig. 5-3 shows the transition temperature (T_c) and transition width ΔT_c for the doped and undoped samples determined by ac susceptibility measurements. The T_c onset for the undoped sample (~ 38.2 K) is almost the same as that reported by a number of groups. It shows also a sharp transition with the transition width of less than 1 K. For the doped samples, the T_c decreases with increasing doping level. It is striking to note that despite the high doping level, the T_c only drops about 0.8 K with 10 wt% of SiC doping. In contrast, T_c is depressed to about 22 K for C doped MgB_2 with the nominal stoichiometry of $Mg(B_{0.8}C_{0.2})_2$ synthesized from Mg and B_4C [18]. These results suggest that there is only a small fraction, if any, of C substituted for B in our samples.

Fig. 5-4 shows the $J_c(H)$ curves for MgB_2 doped and undoped samples at 5 K, 20 K, and 30 K. Note that all the $J_c(H)$ curves for doped samples show a crossover with the undoped samples at higher fields. Although SiC doping caused a slight reduction of J_c in low fields, it is important to note that the J_c for the doped samples drops with increasing field much more slowly than for the undoped ones.

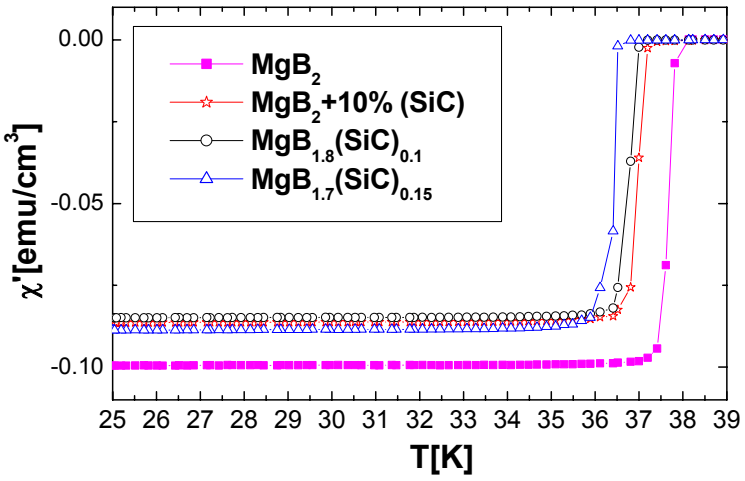

Figure 5- 3: Transition temperature (T_c) for the doped and undoped samples determined by ac susceptibility measurements (real part).

Compared to the non-doped sample, J_c for the 10 wt% doped sample increased by more than one order of magnetude at high magnetic fields. Although all the doped samples show considerably better $J_c(H)$ performance compared to the undoped sample, Fig. 5-4 shows that the sample doped with 10 wt% SiC has slightly better performance than the other samples.

Fig. 5-5 shows a comparison of $J_c(H)$ for the 10 wt% SiC doped sample at 20 K with data reported in literature. J_c for this sample exhibits better field performance and higher values of J_c in high fields than any other element doped samples [12, 14] and better than the undoped tape [19]. Our SiC doped MgB_2 samples are even better than thin film MgB_2, which has exhibited one of the strongest reported flux pinning with high J_c in high magnetic fields. At 20 K, the best J_c for the 10wt% SiC doped sample was10^5 A/cm^2 at 3 T, which exceeded J_c of the state-of-the-art Ag/Bi-2223 tapes. At 20 K and 4 T, J_c was 36,000 A/cm^2, which is twice as high as for the MgB_2 thin films [10] and an order of magnitude higher than for the state-of-the-art Fe/MgB_2 tapes [19].

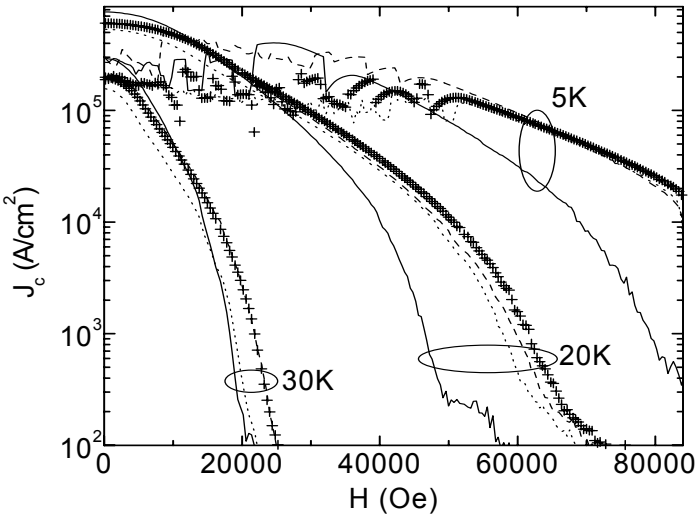

Figure 5- 4: $J_c(H)$ curves for MgB_2 doped (crosses, dashed and dotted lines for MgB_2 + 10 wt% SiC, $MgB_{1.8}(SiC)_{0.1}$, and $MgB_{1.7}(SiC)_{0.15}$ respectively) as well as undoped samples (solid lines) at 5 K, 20 K, and 30 K.

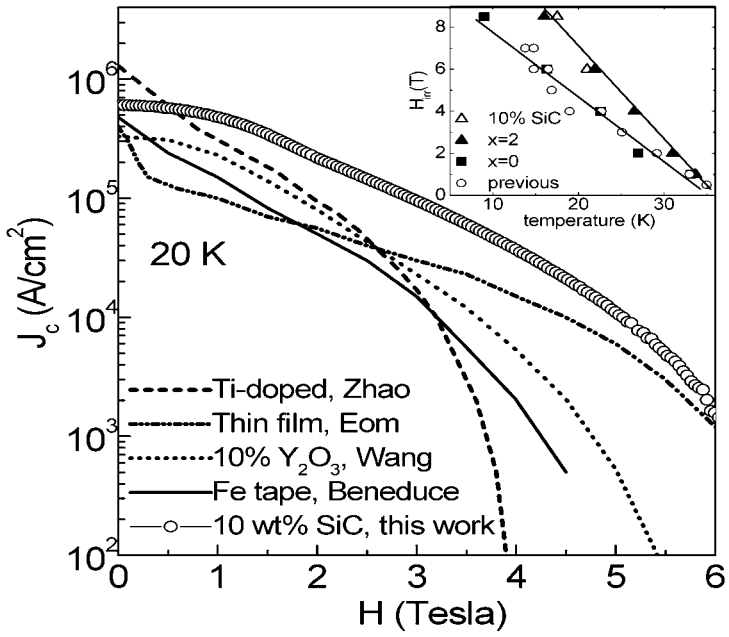

Figure 5- 5: A comparison of magnetic $J_c(H)$ at 20 K for the 10 wt % SiC-doped sample and for samples that were doped with Ti and Y_2O_3 as well as a thin film with strong pinning and Fe/MgB_2 tape. Inset: temperature dependence of the irreversibility field for SiC-doped MgB_2 with different SiC content (triangles and squares) and for previously prepared doped MgB_2 (round symbols).

The temperature dependence of H_{irr} for nano-SiC doped MgB_2, as well as for the pellets and tapes reported previously in the literature (round symbols), is shown in the inset to Fig 5-5. Apparently, H_{irr} for x=0 overlaps with H_{irr} for the previous samples, even though the latter had significantly smaller values of J_c. Doping with SiC significantly

improved H_{irr}. For example, H_{irr} for SiC doped samples reached 7.3 T at 20 K, compared to 5.7 T for the non-doped one. This is consistent with improvement of field dependence of J_c with the doping. Because H_{irr} for the undoped control sample (x=0) is the same as for the previously reported samples, the improvement of $J_c(H)$ occurred indeed because of the SiC doping and not because of improved sintering of MgB_2.

Given the ease of production of SiC-doped MgB_2, our results significantly strengthen the position of MgB_2 as a competitor to more expensive conventional superconductors and HTS. This is because SiC doping is easily achievable and results in strong improvement of flux pinning. In the present study, the density of the pellet samples is still very low, only about 1.3 g/cm^3. Thus, still higher J_c can be achieved by improving the density.

In order to confirm the results and check the reproducibility of samples, as well as achieving better understanding of the underlying mechanism responsible for the improvement in $J_c(H)$, more samples were made by doping with 10 wt% addition of SiC nano particles. The pure and doped samples have been measured in the Applied Superconductivity Center, University of Wisconsin in Madison.

Fig. 5-6 shows the resistivity versus temperature between 30 K to 300 K, for doped and undoped samples, obtained by four probe transport measurements. The onset T_c of the undoped sample was 37.5 K. For the 10 wt% SiC-doped sample, T_c decreased only by 0.6 K, consistent with the previous results. It should be note that the resistivities of the two samples are very different. The doped sample has a larger resistivity than the undoped sample over the whole temperature range. For example at 40 K, ρ is 90 μΩcm for the undoped sample and 300 μΩcm for the doped sample. However the undoped sample has a lower residual resistivity ratio (RRR) than the doped sample. Both doped and undoped samples were prepared using a reaction *in-situ* method, and they both have a low density, about 50% of theoretical density. Thus, the porosity is about the same for both samples and should not be the reason for the significant difference in the resistivity. However these results are understandable as the doped sample contains a large amount of impurity.

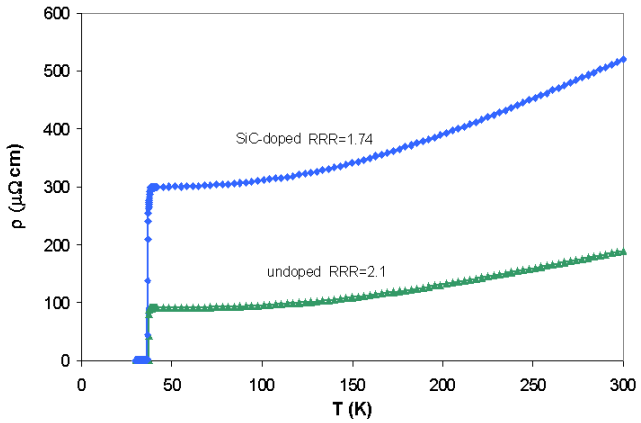

Figure 5- 6: Resistivity versus temperature between 30 K to 300 K, for doped and undoped samples, extracted from four probe transport measurements.

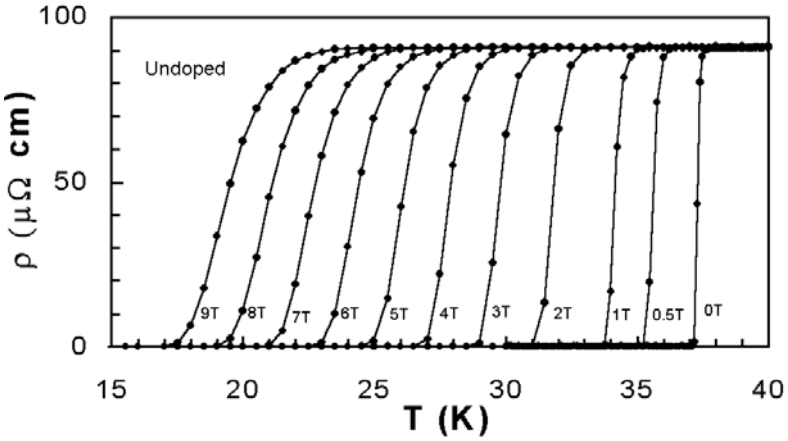

Figure 5- 7: Resistivity versus temperature curves $\rho(T)$ for the undoped sample in different magnetic fields up to 9 T.

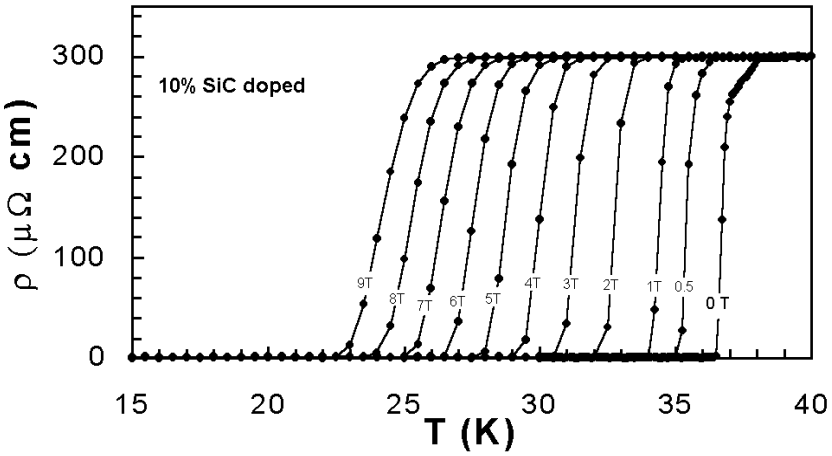

Figure 5- 8: Resistivity versus temperature curves $\rho(T)$ for the the SiC-doped sample in different magnetic fields up to 9 T.

Figs. 5-7 and 5-8 show the resistivity versus temperature curves $\rho(T)$ for the undoped (Fig. 5-7) and the SiC-doped (Fig. 5-8) samples at different magnetic fields up to 9 T. The doped sample has stronger superconductivity than the undoped, as is shown explicitly in the figures. The transition becomes broad with increasing field. The broadening of the transition for the undoped sample is more pronounced than for the nano-SiC doped sample at high field. It is also evident that the T_c was depressed much more severely with increasing applied field in the undoped sample (Fig. 5-7) than in the nano-SiC doped sample (Fig. 5-8), indicating that nano-SiC doping enhanced the flux pinning in the MgB_2.

Figs. 5-9 and 5-10 show the magnetic field dependence of J_c at 4.2 K, 10 K, 20 K and 30 K for the undoped and doped samples respectively, calculated from the dc magnetization measurements using the VSM. Note that all the $J_c(H)$ curves for doped samples show a much slower drop with increasing field compared to the undoped sample over all the measured temperature ranges, which is consistent with the previous results. The J_c for the nano-SiC doped sample is greater than 10,000 A/cm^2 at 4.2 K and 10 T, 10 K and 8 T, and 20 K and 5 T, respectively.

Figs. 5-11 and 5-12 display the comparison between the $J_c(H)$ values at 4.2 K and 20 K for the undoped and SiC-doped samples. The J_c for the doped sample increased by more than one order of magnitude at 4.2 K and above 10 T, compared to that for undoped samples. The J_c for the doped sample also increased by an order of magnitude at 20 K and 5 T compared to the undoped samples. At 20 K, the best J_c for the 10 wt% SiC doped sample achieved 10^5 A/cm^2 at 3 T which again exceeded those of the state-the-art Ag/Bi-2223 tapes and 36,000 A/cm^2 at 4 T, which is double that of the thin film and an order of magnitude high than those of the Fe/MgB_2 tapes [19].

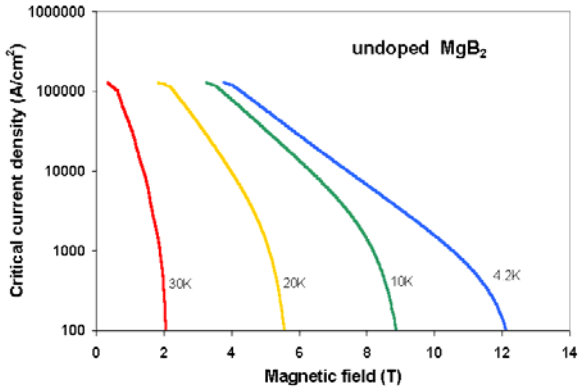

Figure 5- 9: Magnetic field dependence of J_c at 4.2 K, 10 K, 20 K and 30 K for the undoped MgB_2 sample.

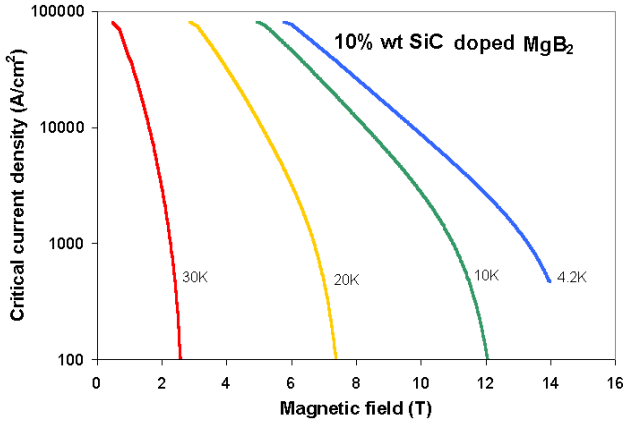

Figure 5- 10: Magnetic field dependence of J_c at 4.2 K, 10 K, 20 K and 30 K for the SiC doped MgB_2 sample.

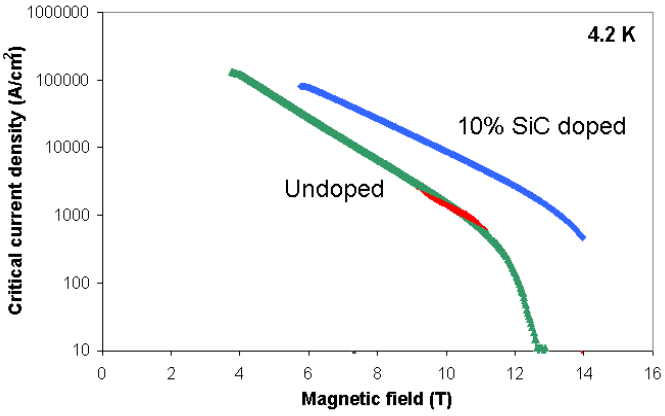

Figure 5- 11: The comparison between $J_c(H)$ of the undoped and SiC-doped samples at 4.2 K.

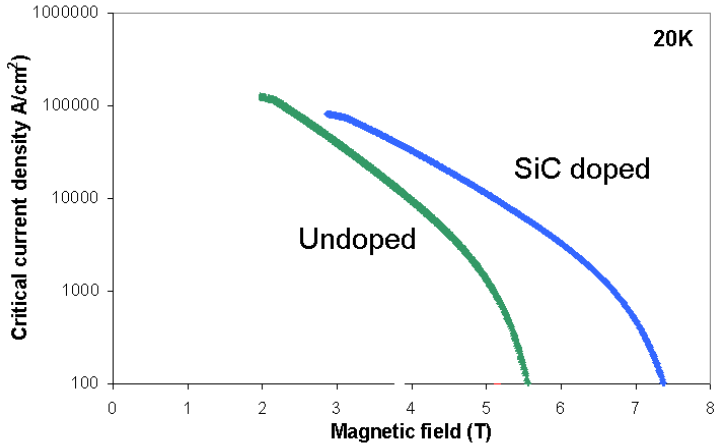

Figure 5- 12: The comparison between $J_c(H)$ of the undoped and SiC-doped samples at 20K.

Irreversibility fields (H_{irr}) for both the doped and undoped samples are shown in Fig. 5-13. The irreversibility line for the doped sample is higher than for the undoped sample over the whole temperature range. Doping with SiC significantly improved H_{irr}. For example, the H_{irr} for the SiC doped sample reached 12 T and 7.5 T, compared to 8.8 T and 5.5 T for the undoped one at 10 K and 20 K, respectively.

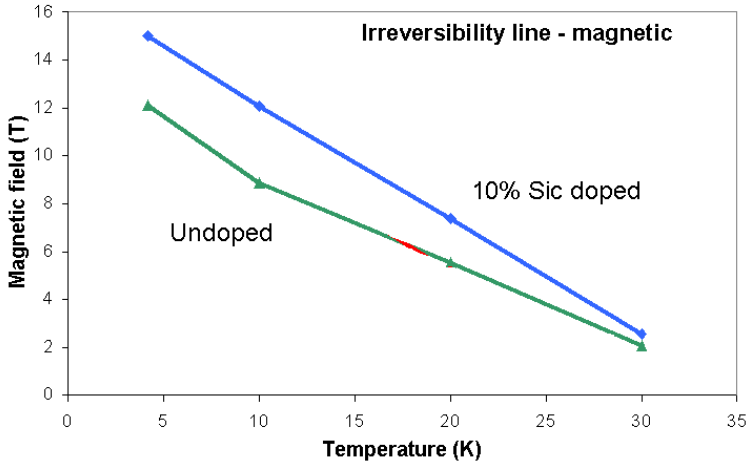

Figure 5- 13: The irreversibility field, H_{irr} versus temperature for the undoped and doped samples.

Fig. 5-14 shows the temperature dependence of the upper critical field H_{c2} determined from the resistance transition curves in Figs. 5-7 and 5-8 at a temperature where the

resistivity is 90% of the value of the resistive transition. We note that $H_{c2}(T)$ is improved for the nano-SiC doped sample. This is in agreement with the Gurevich et al. results that found the higher H_{c2} for films and untextured bulk polycrystals with higher resistivity [16]. Since H_{c2} should be directly tied to ρ it is clear that the effect of impurities must be considered to be affecting the derived values of resistivity, which are not directly interpretable as being representative of the scattering in the samples. This problem will be discussed below in connection with the effect of impurity on flux pinning.

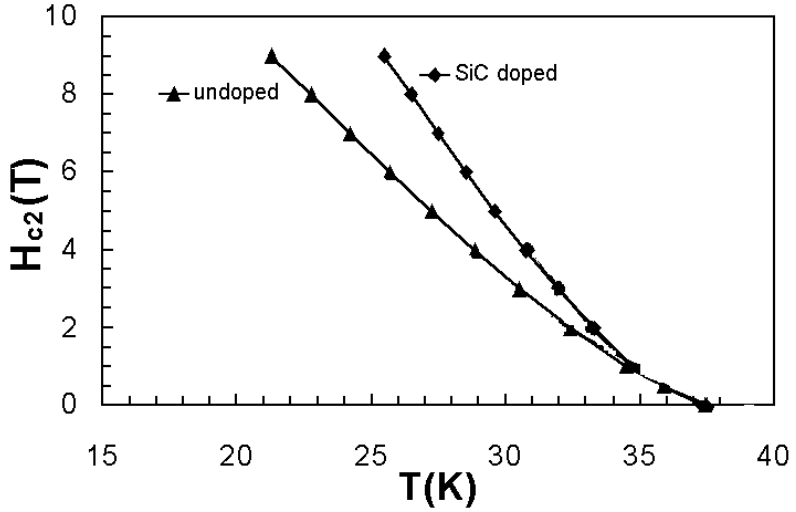

Figure 5- 14: The upper critical field (90% of the resistive transition) as a function of the temperature for the undoped and the 10 wt% SiC doped sample.

The TEM images showed a high density of dislocations and a large number of ~10nm inclusions inside the grains (Fig. 5-15 top and bottom right). EDS analysis of the grains revealed the presence of uniformly distributed Mg, B, C, Si and O (inset to Fig. 5-15 top). TEM examination revealed that there are a number of impurity phases in the form of nano-meter size inclusions inside and in between the grains in the nano-SiC doped sample. These impurities include Mg_2Si, MgB_4 and MgO detected by XRD analysis, and unreacted SiC, amorphous BO_x, $Si_xB_yO_z$ and BC detected by using the EELS technique. TEM images also show that the grain size of MgB_2 is smaller than 100nm. The Z-contrast image [20-22] of the nano-SiC doped sample, which shows a typical MgB_2 crystal in the [100] orientation, is presented in Fig. 5-15 as well (bottom left). EDX analysis shows that the Mg:Si ratio is identical across the entire sample, indicating that the phase distribution is globally homogeneous. However, nano-scale impurity phases of MgB_4 and MgO are present within the grains. The presence of oxygen within

the grains is consistent with the results obtained from an oxygen alloyed thin film with strong pinning and a resistivity of 220 μΩcm [10].

Recent work on SiC-doped MgB_2 single crystal grown under high pressure (30 kbar) and high temperature (1900-1950^{o}C) showed there was only C substitution for B with no Si detected in the crystals. These authors revealed that the C substitution for B is as high as 16%, the highest level of substitution in all the C-doping studies so far, which leads to a depression in T_c from 39 K to 9 K [23]. There is a clear trend for C substitution in MgB_2 to depress T_c in the literature data as well [24-27]. The higher the sintering temperature is, the larger the proportion of C that is substituted for B in MgB_2. As we used relatively lower sintering temperatures, ~800 ^{o}C, the C substitution for B is expected to be lower. In the SiC doped sample, it is therefore possible that the C substitution is at 1-3%, which is believed to be quite reasonable from literature on C substitution in terms of depression of T_c. However the level of C substitution could not be readily identified so far.

In addition to the high concentration of nano-inclusions, there are structural defects observed in the nano-SiC doped sample by Li et al. [28]. This kind of nano-domain structure may be the result of a small proportion of C substituted for B.

Nano-particle SiC doping into MgB_2 has a special features compared to all other doping reported so far. In this case, not only the extent of enhancement in $J_c(H)$ is very large, by more than an order of magnitude above certain fields, but also the enhancement of $J_c(H)$ occurred in all the temperatures ranges up to T_c, in contrast to most of the other doping studies, which have been effective in enhancing $J_c(H)$ only within low temperature ranges. Also in contrast to previous work on doping for improving J_c, SiC doping has no densification effect, as evidenced by the fact that the density of the doped samples is quite low and independent of the doping level.

According to two-gap superconductivity theory, the nano SiC doping could lead to two different scattering channels. First, the partial C substitution for B or the formation of alloying between B and Si, B and C and B and O in the close vicinity of B sites causes disorder on B sites which will result in *in-plane* σ scattering. The alloying phases such as BC, BO_x and $SiBO_x$ detected by the EELS analysis have dimensions well below 10nm. Their scattering will lead to an increase in dH_{c2}/dT at temperatures near T_c. The

higher H_{c2} at higher temperatures contributes to the enhancement of $J_c(H)$ at higher temperatures for the SiC doped samples. Second, the formation of nano-domain structures is due to the variation of Mg-B spacing which in turn causes disorders at B and Mg sites. These nano-domains with a size of 2-3nm are also well below the 8-10 nm coherence length of MgB_2. These extensive nano-domain defects could result in strong *in-plane* and *out-off-plane* scatterings and contribute to the increase of resistivity and H_{c2} in a wide temperature regime. This accounts for the enhancement of $J_c(H)$ over a wide temperature range for the SiC doped samples.

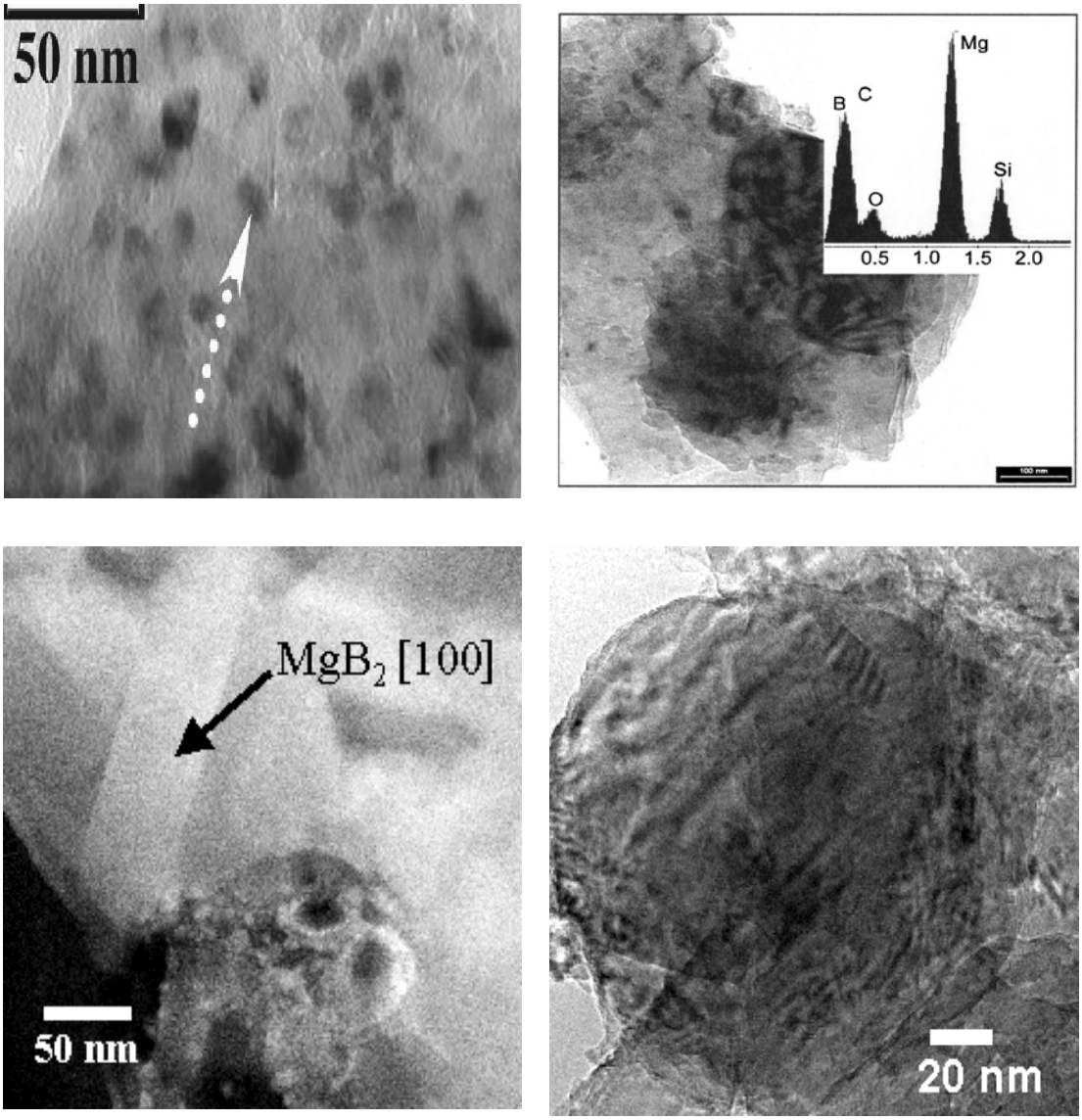

Figure 5- 15: TEM images showing the intragrain dislocations and nanoparticle inclusions within MgB_2 grains (top and bottom right). Inset: EDS element analysis of MgB_2 grains of doped sample.

On the other hand, the additional impurities at nano-scale introduced by SiC doping can serve as strong pinning centers to improve flux pinning within a certain field region.

This is clearly demonstrated by the superior J_c – H performance of the SiC doped samples.

The potential pinning centers induced by SiC doping include inclusions such as the highly dispersed $MgSi_2$, BC, BO_x and $SiBO_x$ which are all at a scale below 10nm, match the coherence length very well and can act as strong pinning centers. Some large impurity particles such as unreacted SiC would not be effective pinning centers but would act to reduce superconducting volume and thus should be eliminated in order to further improve the zero field J_c. In addition, the nano-domain defects at a scale of 2-3 nm in an extensive network would provide very effective collective pinning at all temperatures up to T_c.

5-1-4 Summary

In summary, we have demonstrated that the critical current density, irreversibility field and flux pinning properties of MgB_2 in bulk form can be significantly improved by a readily achievable and economically viable chemical doping with SiC, paving the way for MgB_2 to potentially replace the current market leader, Nb-Ti. The nano-scale SiC doping into MgB_2 enhances both H_{c2} and flux pinning through multiple scattering channels. Alloying at B and Mg sites due to C substitution and the formation of nano-domain structures will cause strong scattering over a wide range of temperatures, leading to enhancement in H_{c2}. A high concentration of various nano-scale impurity phases results in high resistivity, a low residual resistivity ratio, and a large irreversibility field and upper critical field with modest T_c reduction. The highly dispersed nano-scale precipitates $MgSi_2$, BC, BO_x, $SiBO_x$ and the extensive domain structures on a scale well below 10 nm serve as strong pinning centres. Large particle impurities such as unreacted SiC (>100 nm) increase resistivity, reduce the superconducting volume and do not help with the improvement of either flux pinning or H_{c2} and therefore should be eliminated. The doping with SiC enhances the critical current density, the irreversibility field and the upper critical field in a manner that helps make MgB_2 potentially competitive with both low and high-T_c superconductors.

5-2- Transport Critical Current Density in Fe-Sheathed Nano-SiC Doped MgB_2 Wires

5-2-1 Introduction

It has been shown that Fe is suitable sheath for fabrication of MgB_2 wire using a powder-in-tube method [7, 8] as demonstrated in the previous chapter. However, the J_c performance of wires remains unsatisfactory for many applications due to the poor pinning ability of this material. In the previous section, we showed that chemical doping with nano-particle SiC into MgB_2 can significantly enhance J_c in high fields with only slight reduction in T_c. This finding suggested that possible substitution of C for B in MgB_2 induced intra-grain defects as well as an high density of nano-inclusions as effective pinning centres, responsible for the improved performance of $J_c(H)$ over a wide range of temperatures. However, all the critical current densities presented in the previous section were limited to magnetic measurements. As the materials are far from optimum and the sample density was only about 50% of the theoretical value the current in such a porous material is highly percolative. The major concern is whether the material can carry a large transport J_c. In this section, we study the effect of the nanometer-size SiC doping on the transport critical current density and its magnetic field dependence for MgB_2 wires. Our results reveal that the nanometer size SiC-doped MgB_2/Fe wires can carry very high transport I_c and J_c in the applied magnetic fields. SiC doped MgB_2 is very promising for many applications, as this chemical doping is a readily achievable and economically viable process to introduce effective flux pinning.

5-2-2 Experimental Details

Standard powder-in-tube methods were used for the Fe clad MgB_2 tape. Powders of magnesium (99%) and amorphous boron (99%) were well mixed with 0 and 10 wt% of SiC nanoparticle powder (size of 10 nm to 20 nm) and thoroughly ground. The pure Fe tube had an outside diameter (OD) of 10 mm, a wall thickness of 1 mm, and was 10 cm long. The wire preparation procedure has been explained earlier. Short samples 2 cm in

length and 1.4 mm in diameter were sintered in a tube furnace at 800 ^oC for 30 min. A high purity argon gas flow was maintained throughout the sintering process. Transport current was measured using pulse DC method. Because the critical current for these wires was hundreds of amperes, the transport measurements had to be performed by a pulse-method, to avoid heating. A pulse of current was obtained by discharging a capacitor through the sample, a coil of thick copper wire and a non-inductive resistor connected in series. The current was measured via the voltage drop on the non-inductive resistor of 0.01 Ohm. With a proper choice of coil, the current reached its maximum value (700 A) within 1 ms. The voltage developed on the sample was measured simultaneously with the current, using a 2-channel digital oscilloscope. Because both channels of the oscilloscope had the same ground, the signal from the voltage taps was first fed to a transformer preamplifier (SR554). This decoupled the voltage taps from the resistor used for measuring the current, thereby avoiding creation of ground loops and parasitic voltages in the system, as well as of an additional current path in parallel to the sample. The transformer amplified the voltage 100 times, improving the sensitivity of the experiment. Magnetic field was produced by a 12 T superconducting magnet. Sample mounting allowed for orienting the field either perpendicular to the wire, or parallel to it. In the later case, the field was also parallel to the current passing through the sample. The sample was placed into a continuous flow helium cryostat, allowing a control of temperature to better than 0.1 K. The magnetization of samples was also measured using a PPMS (Quantum Design). The samples were in the form of bars cut from pellets which were processed under the same conditions as the wires, as explained in the previous chapter. A magnetic J_c was derived from the height of the magnetization loop using Bean's model.

5-2-3 Results and Discussion

Fig. 5-16 shows the transition temperature (T_c) for the doped and undoped samples determined by ac susceptibility measurements. The T_c obtained as the onset of magnetic screening for the undoped sample was 37.6 K. For the 10 wt% SiC doped sample, the T_c was decreased by only 0.7 K. In contrast, the T_c was depressed by almost 7 K for 10% C substitution for B in MgB_2 [27].

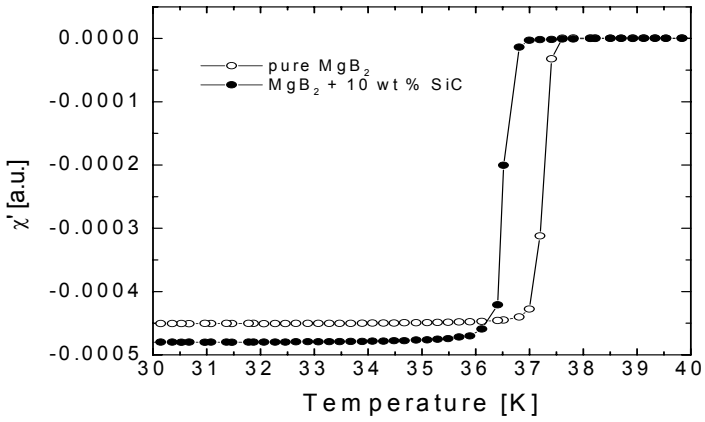

Figure 5- 16: Critical transition temperature (T_c) measured using magnetic susceptibility versus temperature for pure MgB_2 and 10wt% SiC doped MgB_2/Fe wires

As explained in the previous section, this suggests that the higher tolerance of T_c to SiC doping in MgB_2 is attributable to the low level of C substitution.

Fig. 5-17 shows a typical *V-I* characteristic for the 10 wt% SiC doped MgB_2/Fe wire. It should be noted that the self-field of the current pulse induced a voltage in the voltage taps, which gave a background voltage. It was easy to distinguish the voltage created by the superconductor on this background, because the voltage developed very abruptly when the current reached the value of I_c. It is interesting to note that the total current that the SiC doped wire can carry reached 665 A at 24 K and 1.1 T. Due to the limitations of our power source all the I_c measurements were limited to a maximum 700 A.

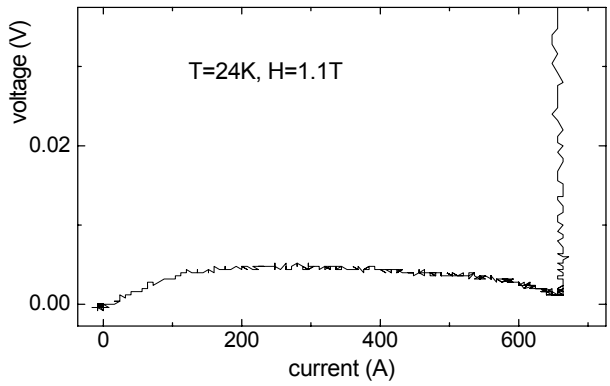

Figure 5- 17: *I-V* curves for 10 wt% SiC doped MgB_2/Fe wire. I_c = 665 A at 24 K and 1.1 T.

Fig. 5-18 shows the $J_c(H)$ curves for the undoped and the 10 wt% SiC-doped MgB_2 samples at 5 K, 10 K, and 30 K. Note that all the $J_c(H)$ values for 10 wt% SiC doped MgB_2/Fe wire are significantly higher than for the undoped sample at higher fields. The transport I_c for the 10 wt% doped MgB_2/Fe reached 140,000 A/cm^2 at 24 K and 1 T and 103,000 A/cm^2 at 20 K and 2 T (J_c). The transport J_c for the 10 wt% SiC doped MgB_2 wire increased by a factor of 6 at 5 K and 9 T and 20 K and 5 T respectively, compared to the undoped wire. These results indicate that SiC doping strongly enhances the flux pinning of MgB_2 in magnetic fields.

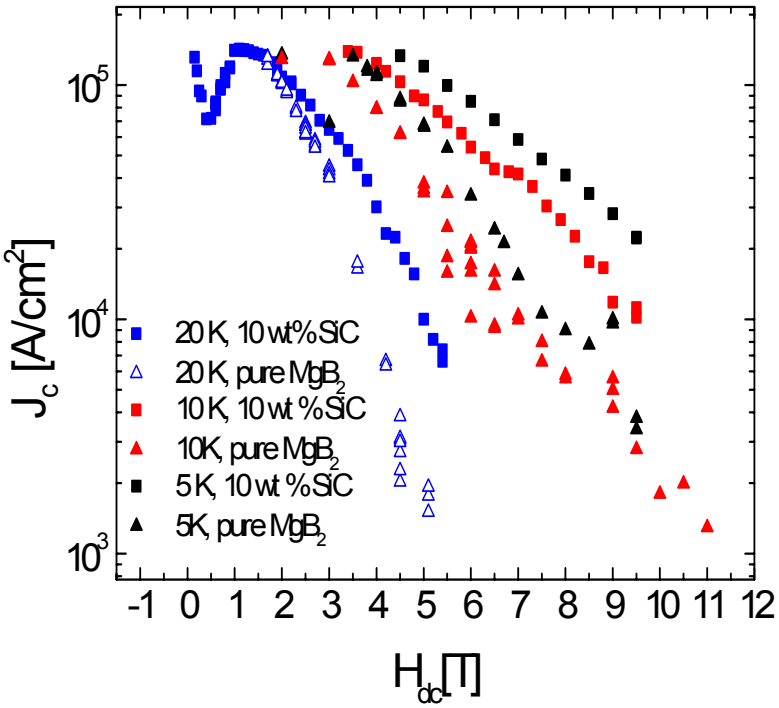

Figure 5- 18: The transport J_c – H dependence at 5 K, 10 K and 20 K for the pure MgB_2/Fe and 10 wt% SiC doped MgB_2/Fe wires.

The enhancement of pinning by SiC doping is also evident from the pinning force density versus magnetic field results shown in Fig. 5-19. The volume pinning force density of 5.5 GN/m^3 at 20 K is comparable to that of NbTi at 4.2 K. Although the maximum pinning force density only has a little shift to higher field the pinning force density for the SiC doped MgB_2/Fe wire is clearly greater than for the undoped wire at fields above 1.5 T.

Fig. 5-20 shows a comparison of the transport J_c with the magnetic J_c. Although there are quite different voltage standards for measuring the transport and magnetic J_c, due to steep characteristics, results are expected to be similar for both methods. The transport J_c for the wires is comparable to the magnetic J_c at higher fields despite the low density of the samples and percolative nature of the current. Fig. 5-20 also shows a comparison of the transport $J_c(H)$ behaviour for 10 wt% SiC doped MgB_2/Fe wire at 20 K with the thin film [8] and the Fe-sheathed MgB_2 tape [7] reported previously.

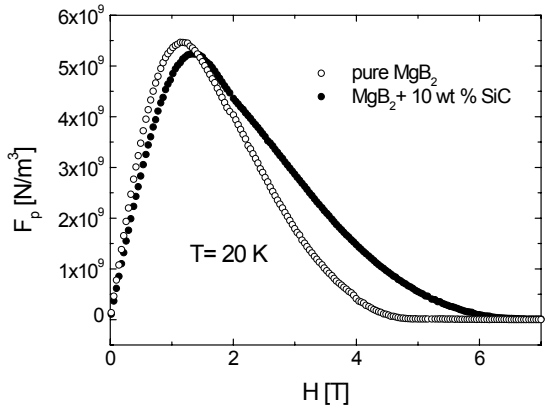

Figure 5- 19: Pinning force density versus magnetic field for the undoped and 10 wt% SiC doped MgB_2/Fe wires.

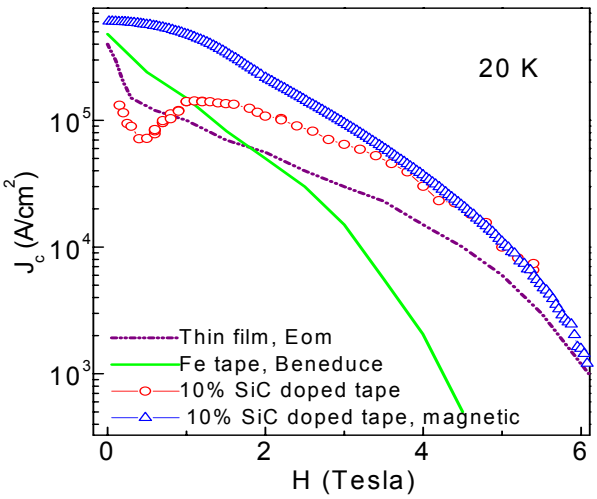

Figure 5- 20: A comparison of the transport J_c with magnetic J_c for the 10 wt% SiC doped MgB_2/Fe wire, including the best transport J_c of a strongly pinned thin film [8] and Fe-sheathed MgB_2 tape [7].

We see the J_c for the 10 wt% SiC doped wire is 30 times higher than one of the best transport J_c reported in Fe-MgB_2 tape and better than the strongly pinned thin film (magnetic J_c for the thin film).

Fig. 5-21 shows the $J_c(H)$ versus temperature for 10 wt% SiC doped wire at 1 T, 2 T and 4 T. With SiC doping, we can achieve J_c values from 50,000 A/cm^2 to 150,000 A/cm^2 over a temperature range between 15 K and 25 K and a field range of 2 T to 5 T under the total current supply limit of 700 A. Nevertheless, these results demonstrate that nano-SiC doping into MgB_2/Fe wire makes a number of applications practical, including MRI, moderate magnets, magnetic windings for energy storage, magnetic separators, transformers, levitation, motors and generators. Furthermore, the SiC substituted MgB_2/Fe wire is much more attractive from the economic point of view. The main cost for making MgB_2 conductors will be the high purity B. Because C and Si are abundant, inexpensive and readily available, by doping the superconductor with SiC, the overall cost for making MgB_2 conductors will be reduced. Furthermore, SiC doping has already been shown to enhance flux pinning, a significant benefit.

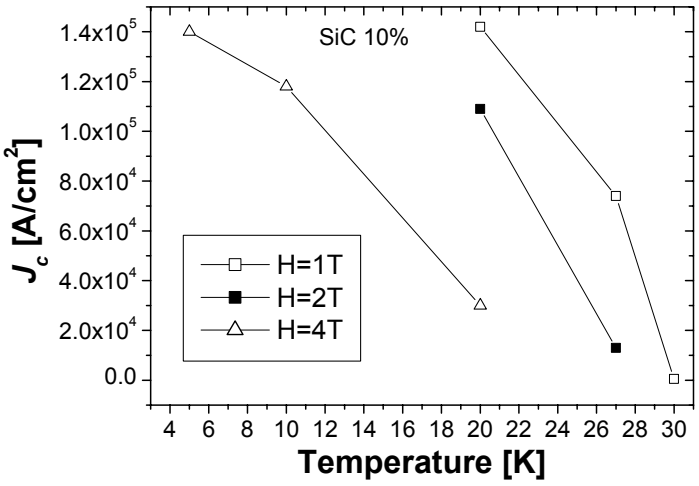

Figure 5- 21: $J_c(H)$ versus temperature for the 10 wt% SiC doped MgB_2 wire at 1 T, 2 T and 4 T.

The TEM image (Fig. 5-22) shows a high density of dislocations and massive nano-meter size inclusions inside the grains, consistent with the previous section. The density of the present Fe-sheathed MgB_2 wires is still very low, only about 1.2 to 1.3 g/cm^3. Thus, a higher J_c and better flux pinning can be achieved by further optimization of the processing conditions, as well as further improving the density of samples.

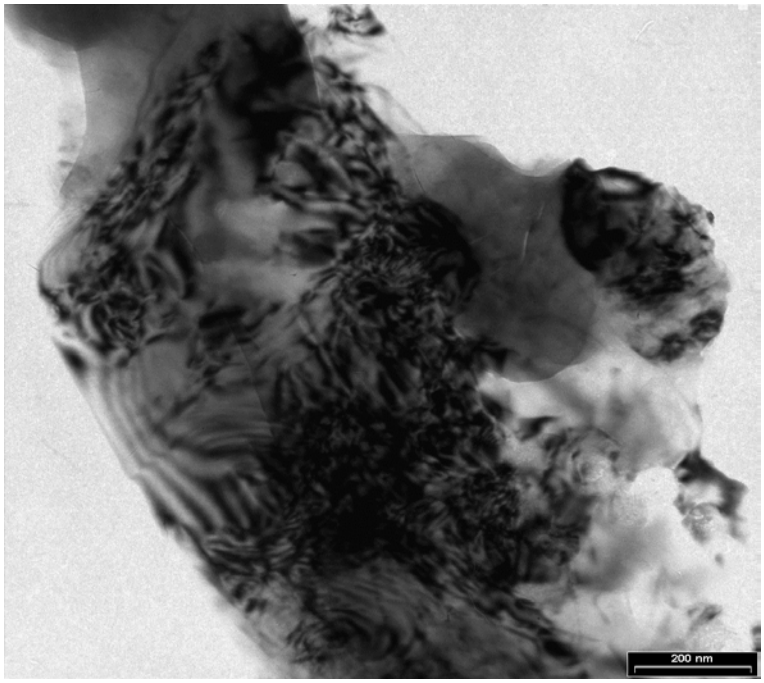

Figure 5- 22: TEM image for the 10 wt% SiC doped MgB_2/Fe wire.

5-2-4 Summary

Nano-SiC doped MgB_2/Fe wires were fabricated using a powder-in-tube method and a reaction in-situ process. The depression of T_c with increasing SiC doping level remained rather small. The transport J_c for all the wires is comparable to the magnetic J_c at higher fields despite the low density of the samples and the percolative nature of current. We have further demonstrated that a very high transport critical current and current density of Fe-sheathed MgB_2 wires can be achieved by a readily achievable and economically viable chemical doping with nano-SiC. J_c values over 100,000 A/cm^2 at 5 K and 5 T and 20 K and 2 T are comparable to NbTi and HTS respectively. High performance SiC doped MgB_2 wires will have a great potential to replace the current market leaders, Nb-Ti and HTS, for many practical applications at 5 K to 25 K up to 5 T. There is a plenty of room for further improvement in J_c as the density of the current samples is only about 50%.

5-3 Effect of Grain Size and Doping Level of SiC on the Superconductivity and Critical Current Density in MgB_2 Superconductor

5-3-1 Introduction

We have shown in the previous sections a significant improvement of J_c, H_{irr} at both high and low temperatures in nano-SiC doped MgB_2 bulk samples with only a slight reduction of T_c. It has been shown that nano-inclusions, as well as possible substitution in the crystal lattice, lead to this significant improvement. The objective of this section is to study the grain size effect of the precursor SiC on the superconductivity and flux pinning and to further investigate the enhancement in J_c field performance. It was found that the particle size of SiC plays a critical role in controlling the reaction between Mg+2B and SiC resulting in both substitution and nano-inclusions.

5-3-2 Experimental Details

MgB_2 pellet samples used in the present study were prepared by an in-situ reaction method, which has been described in detail previously. Magnesium (99%) and amorphous boron (99%) were well mixed with commercial SiC (0, 8, 10, 12, 15 wt%). Powders having three different grain sizes were used: a very fine powder with particle sizes smaller than 20 nm (powder 1), powder 2 which has particle sizes ranging up to 300 nm and powder 3, a coarse crystalline SiC with particle sizes around 35 μm. These particle sizes were determined by TEM and SEM and will be explained in the next section. Pellets 10 mm in diameter and 2 mm in thickness were prepared by sintering at 800 ^{o}C for 30 min in flowing high purity Ar. The magnetization of samples was measured using a PPMS (Quantum Design). Samples in the form of bars were cut from the as-sintered pellets. All the samples have the same size ($0.56\times2.17\times3.73$ mm^3). A magnetic J_c was derived from the height of the magnetization loop (M-H) using the Bean Model.

5-3-3 Results and Discussions

5-3-3-1 Effect of Grain Sizes of SiC

Fig. 5-23 shows the XRD patterns for the three different SiC powders used in this work. It can be seen that there are no diffraction peaks for powder 1, indicating that this powder is amorphous. Powders 2 and 3 show diffraction peaks, indicative of their crystalline natures. Powder 3 gives a strong diffraction intensity as well as sharp peaks in agreement with its bigger particle size. On the other hand, powder 2 shows a few peaks, which are wider than the equivalent peaks for powder 3, especially the $2\theta = 33.7'$ and $38'$ peaks that are very wide with low intensity. This XRD pattern indicates that powder 2 contains a wide range of particle sizes.

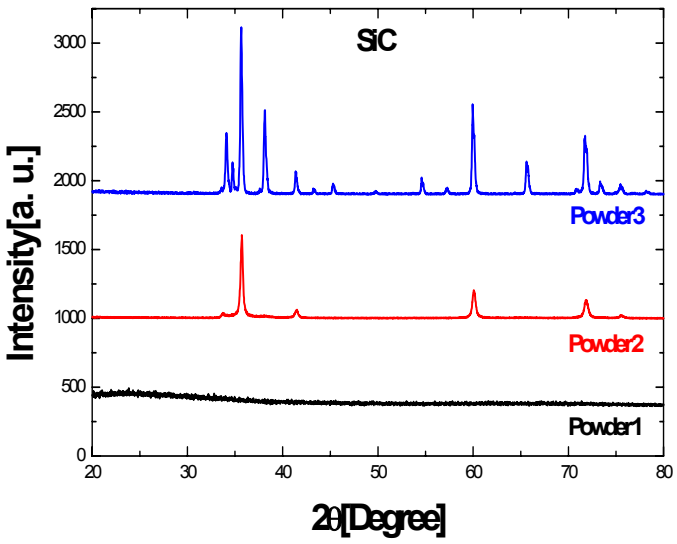

Figure 5- 23: The XRD pattern of the starting SiC powders with different grain sizes.

Figs. 5-24 to 5-26 show TEM images of powders 1 and 2 (Figs. 5-24 and 5-25) as well as a SEM image of powder 3 (Fig. 5-26). We can see that the grains of SiC in powder 1 are very fine with almost the same grain size of about 10 nm to 20 nm, (Fig. 5-24). On the other hand it can be clearly seen that powder 2 contains grains with a wide range of grain sizes from about 10 nm to about 300 nm (Fig. 5-25), consistent with its XRD pattern. The SiC particles in powder 3 are almost uniform crystalline grains with an average size of about 37 μm (Fig. 5-26).

The XRD patterns of the samples after reaction as well as the reference MgB_2 sample are shown in Fig. 5-27. All three samples were doped with 10 wt % SiC. Mg_2Si is the main impurity phase for the sample that was made using powder 1 (sample a), in agreement with previous results. However, we can still see some un-reacted SiC in the samples that were made using powders 2 and 3, samples b and c, respectively. In addition, no Mg_2Si was found in sample c. This means that only part of the SiC takes part in the reaction with Mg and B and becomes doped into MgB_2.

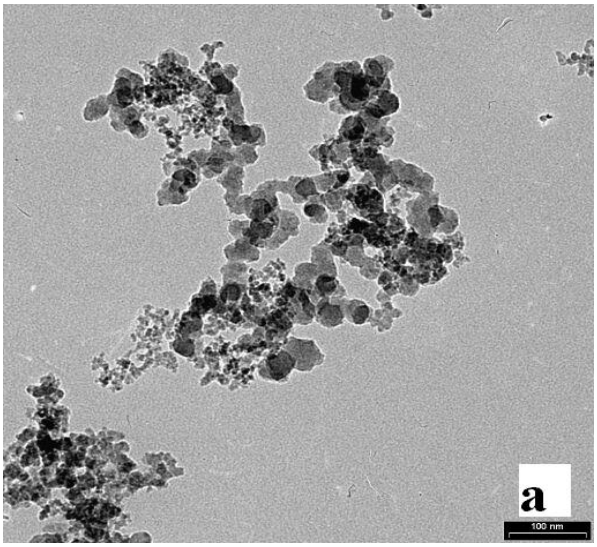

Figure 5- 24: TEM image of starting powder 1. Powder contains almost uniform particles with an average grain size of 10 nm to 20 nm.

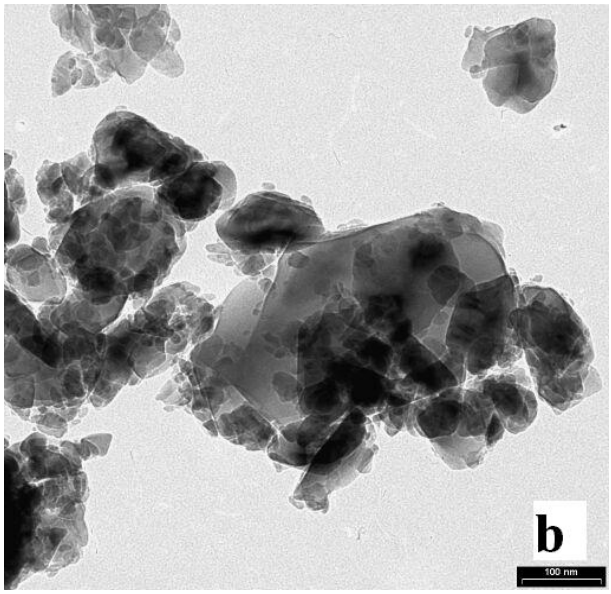

Figure 5- 25: TEM image of starting powder 2. Powder contains different particles with a wide range of grain sizes from 10 to 300 nm.

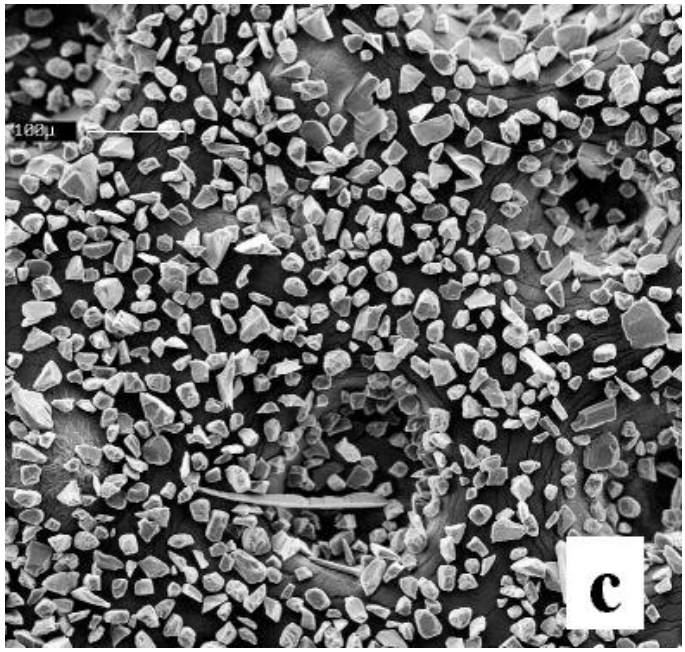

Figure 5- 26: SEM image of starting powder 3. Powder contains almost uniform particles with an average grain size of 35 μm.

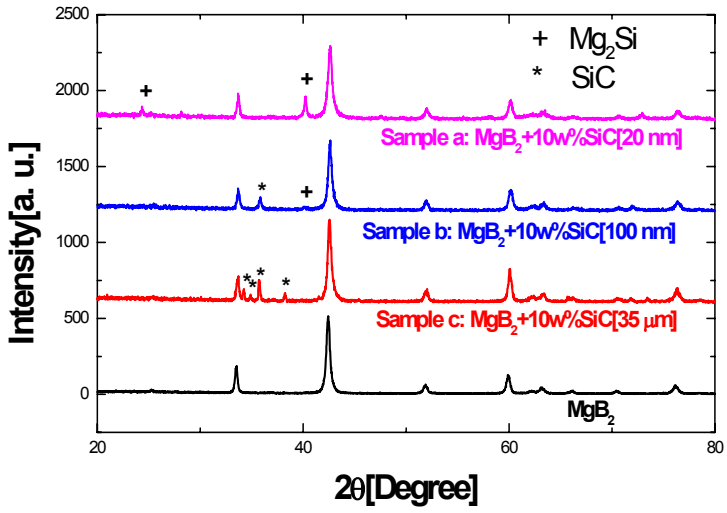

Figure 5- 27: XRD patterns of MgB_2 samples doped with 10 wt % of different SiC powders as well as the reference sample.

Fig. 5-28 shows an SEM image of sample c which was made using crystalline SiC powder (Powder 3). Big grains of un-reacted SiC can be easily seen in the MgB_2 matrix, which is in agreement with its XRD pattern. This means that the coarse SiC powder is very stable and did not react with Mg+B. Therefore; little or no substitution for B by Si and C can be expected. However, for very fine SiC powder substitutions take place as Mg_2Si was formed. This is the big difference in the phases of samples

made with coarse and fine powder. This difference is responsible for the significant difference in J_c field dependence shown below. However, this pattern does not show that all the SiC powder was consumed in sample a.

AC susceptibility measurement results for all samples are presented in Fig. 5-29. T_c values of about 37.65K, 37.5K, 37K and 36.25K were found for the reference sample, sample c, sample b and sample a respectively. The small change in T_c for such a large amount (10 wt%) of added material confirms the results presented in the previous section. Also, we can see that the smaller grain size leads to lower T_c, which is understandable, as smaller grains can react more readily than larger ones.

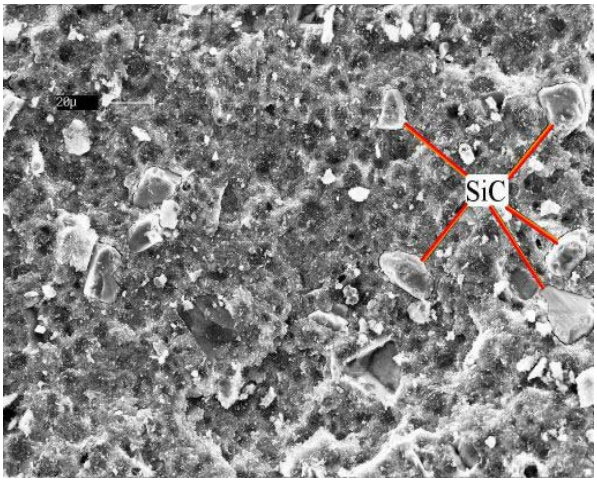

Figure 5- 28: SEM image of sample c after reaction. The large grains of un-reacted SiC can be easily seen in the MgB_2 superconductor.

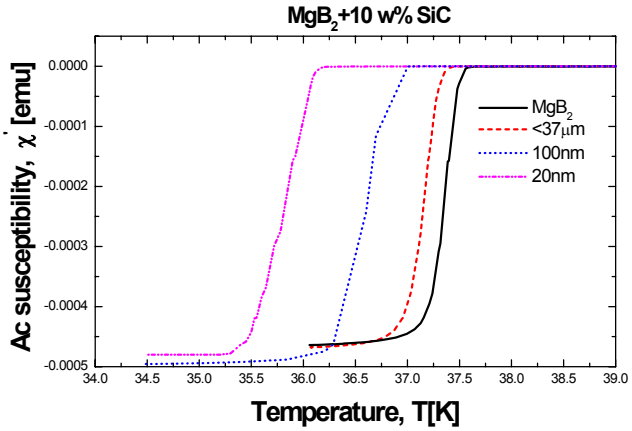

Figure 5- 29: The ac susceptibility of MgB_2 samples doped with 10 wt % of different SiC powders as well as the reference sample at different temperatures.

J_c versus field at 30, 20 and 5 K are plotted in Fig. 5-30. The performance of the J_c field dependence was improved by decreasing the grain sizes of the SiC precursor powder. The finer the SiC powders, the better the J_c field dependence is. For the coarse powders (-400 mesh), the J_c field dependence is slightly better than for the MgB_2 reference sample due to limited reaction between the particles, which can react with Mg+B. The resultant impurities or remaining SiC can embed in the MgB_2 grains acting as pinning centers. For sample a, J_c value of about 20000 A/cm^2 was achieved at 5 K and 8 T, which is more than one order of magnitude higher than that of the MgB_2 reference sample at the same field and temperature. TEM results show that there are large numbers of nano-inclusions embedded inside the MgB_2 grains. This is because the SiC is very fine, so that it can be readily form as inclusions inside the MgB_2 grains and substitute in the lattice during the formation of MgB_2 as explained in previous sections. However, the crystalline SiC powders may distribute themselves around grain boundaries acting as weak links due to their poor chemical activity.

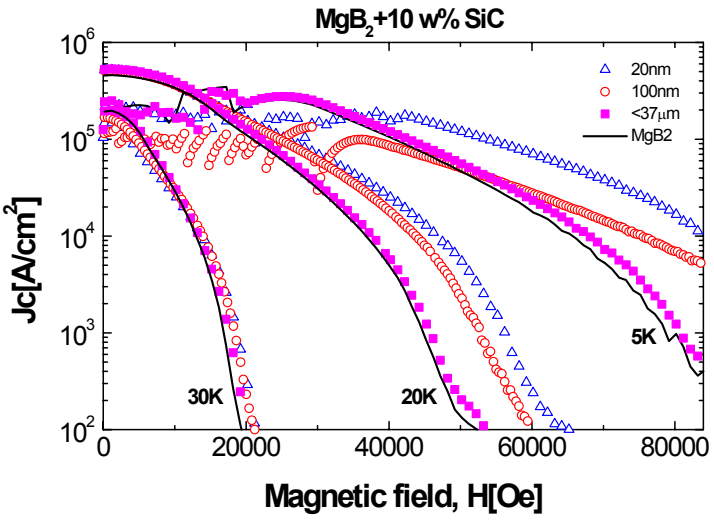

Figure 5- 30: The J_c field dependence of MgB_2 samples doped with 10 wt % of different SiC powders as well as the reference sample at different temperatures of 5, 20 and 30 K.

5-3-3-2 Effect of SiC Doping Levels

As the very fine powders of SiC (20 nm) produce the best results, we can use this fine powder to study the effect of the amount of SiC on the flux pinning in the SiC-doped MgB_2 samples in order to optimize the addition of SiC. Samples with SiC weight % of 0, 8, 10, 12, and 15 were studied in this work. The XRD patterns show that there is

almost no difference in phase purity, with only an increase of Mg_2Si when SiC increases. T_c also changed only slightly in all the samples. The J_c field dependence at different temperatures is shown in Fig. 5-31. It can be seen that all the SiC doped samples have almost the same J_c values as a function of field and temperature at all the doping levels studied. However, it seems that the sample doped by 10 wt% SiC has slightly better performance, compared to the MgB_2 reference sample. This means that the MgB_2 is very tolerant to the amount of SiC.

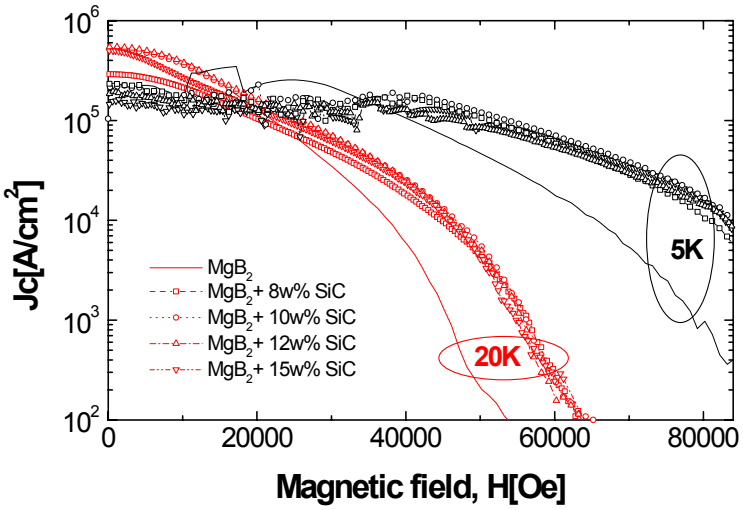

Figure 5- 31: The J_c field dependence of MgB_2 samples doped with SiC weight % of 0, 8, 10, 12, 15 at 5 K and 20 K.

5-3-4 Summary

SiC doped MgB_2 polycrystalline samples were fabricated by in-situ reaction using different grain sizes (20 nm, 100 nm, and 37 microns) of SiC and different doping levels (0, 8, 10, 12, 15 wt %). Grain sizes of the precursor SiC have a strong effect on the critical current density and its field dependence. The smaller the SiC grains are, the better the J_c field performance and H_{irr} is. It was found that very fine SiC powder plays an important role in the reaction between Mg+B and SiC. Significant enhancement of J_c and H_{irr} were revealed for all the SiC-doped MgB_2 with added levels up to 15 wt%. A J_c value as high as 20,000 A/cm^2 in 8 Tesla and 5 K was achieved for the sample doped with 10 wt% SiC having a grain size of about 20 nm. The high performance of the nano-SiC doped MgB_2 superconductor will have great potential for practical applications.

5-4 Effect of Nano-Carbon Particle Doping on the Flux Pinning Properties of MgB_2 Superconductor

5-4-1 Introduction

The effect of C-doping on superconductivity in MgB_2 compound has been studied by several groups [23-27, 29-32]. The results on C solubility and the effect of C-doping on T_c reported so far vary significantly from no substitution to 16% of B substituted by C, while the decrease in T_c ranged up to 30 K at the highest substitution level [18, 23, 33, 34]. The significant differences among the studies on C-substitution are attributable to the fabrication techniques and precursor materials used. It appears that lower sintering temperatures (e.g. 700 ^oC) and short sintering times result in an incomplete reaction and hence lower C solubility in MgB_2. The mixing procedure applied to the precursor materials may also contribute to inhomogeneity in the final product. It is difficult to precisely determine the C solubility in the lattice, as the lattice parameters can also be affected by the change of stoichiometry in MgB_2, because excess C extracts Mg and B to form MgB_2C_2. Recently, Ribeiro et al. used Mg and B_4C as precursors to synthesize C doped MgB_2 by sintering at 1200 ^oC for 24 hours [33]. Their samples appeared to be homogeneous. A neutron diffraction study confirmed that the most likely solubility of C in MgB_2 is around 10% of B positions [34]. This gives a large drop in both T_c (=22K) and the *a*-axis lattice parameter.

The studies on C doping into MgB_2 have thus far only focused on the effect on superconductivity. From the applications point of view, the effect of C doping on the flux pinning properties is also important. In this section, we explain the effects of C doping on the flux pinning and critical current density in MgB_2. It is clear from previous works that complete substitution causes a drastic depression in T_c, which is very undesirable for improving J_c at high temperatures. In order to explore the potential applications of MgB_2 at around 20 K or above, it is essential to maintain the T_c and, at the same time, to enhance the J_c performance in magnetic fields. Therefore, we

designed synthesis conditions that limit the degree of C substitution, but can introduce effective pinning centers into MgB_2.

5-4-2 Experimental Details

Polycrystalline samples of $MgB_{2-x}C_x$ were prepared through a reaction in-situ process as explained earlier. High purity powders of magnesium (99%), amorphous boron (99%) and carbon nano-particles (with a particle size of about 20 nm) were weighed out according to the nominal atomic ratio of $MgB_{2-x}C_x$ with x = 0, 0.05, 0.1, 0.2, 0.3, 0.4 and well mixed through grinding. The heat treatment was performed at 770 ^oC for 30 min in flowing high purity Ar. An un-doped sample was also made under the same conditions for use as a reference sample. The magnetization was measured using a PPMS (Quantum Design). The magnetic J_c was calculated from the height ΔM of the magnetization loop (*M-H*) using the Bean model. The T_c was determined by measuring the real part of the ac susceptibility at a frequency of 117 Hz and an external magnetic field of 0.1 Oe. T_c was defined as the onset of the diamagnetism.

5-4-3 Results and Discussion

Fig. 5-32 shows the XRD patterns of $MgB_{2-x}C_x$ samples for x=0, 0.05, 0.1, 0.2, 0.3 and 0.4 as well as the XRD pattern of the starting C powder. An Si standard was used for all runs. It can be seen that there are no diffraction peaks for C powder, indicating that this powder is amorphous. Thus, there is no peak related to C in the XRD patterns of the C-doped samples, and the amount of the un-reacted C powder is not clear. The undoped samples consist of a main phase, MgB_2, with minor phases of MgO (<5%) and MgB_4. In the C-doped samples extra peaks appear as impurity phases. These peaks can be indexed as Mg_2C_3 and MgB_2C_2, and they increase as the doping level increases.

More accurate XRD examinations were performed to evaluate the lattice parameters. The XRD patterns are shown in Fig. 5-33. Note that the position of the (100) peak shifts continuously to higher angles with increasing C doping level, indicating a decrease in the a-axis lattice parameter. However the position of the (002) peak remains unchanged with increasing C-doping level, indicating that C-doping does not affect the c axis.

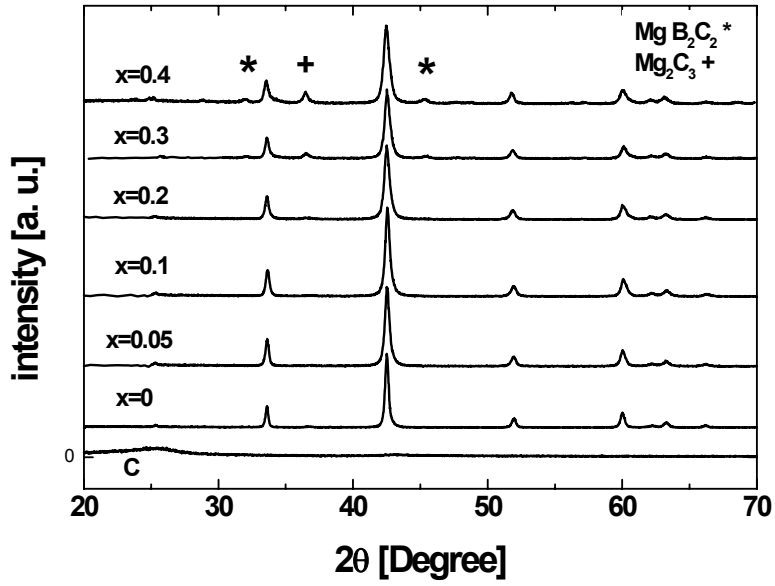

Figure 5- 32: XRD patterns of $MgB_{2-x}C_x$ composition for x=0, 0.05, 0.1, 0.2, 0.3 and 0.4 as well as the XRD pattern of the starting C powder.

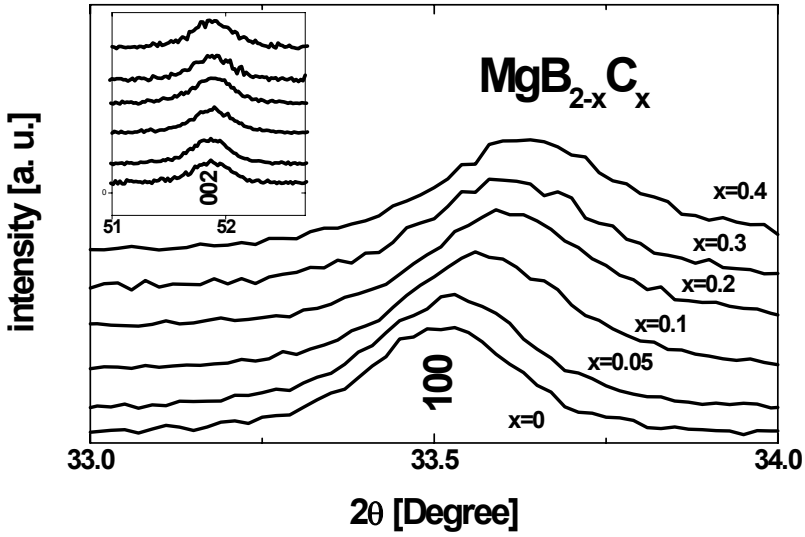

Figure 5- 33: The (100) and (002) (inset) Bragg reflections for $MgB_{2-x}C_x$ composition with x= 0, 0.05, 0.1, 0.2, 0.3, and 0.4

The changes in crystal lattice parameters deduced from the x-ray diffraction patterns of the samples as well as the lattice parameters extracted from the previously published studies by Maurin et al. [25] and Avdeev et al. [34] are shown in Fig. 5-34. As can be seen, the in-plane (*a* axis) lattice parameter decreases monotonically as the C doping level decreases from 3.087A^o to 3.076A^o at x=0 and x=0.4 respectively. This is

understandable because the average size of the C ion (0.077 nm) is smaller than the B (0.082 nm). However, we are unable to see any significant change in the inter layer (*c*-axis) lattice parameter. This is in agreement with recent work, indicating that carbon is substituted in the boron honeycomb layer and does not change the interlayer distance in the MgB_2 crystal. However, the change in the *a* lattice parameter even for x=0.4 is considerably less than the *a* axis contraction from 3.085 to 3.052 due to 10% carbon doping [34]. This indicates that the carbon powder in our samples is only partially substituted in the B position due to the low sintering temperature and short sintering time. The C mostly reacted with Mg and B to form Mg_2C_3 and MgB_2C_2 or remained in an un-reacted form.

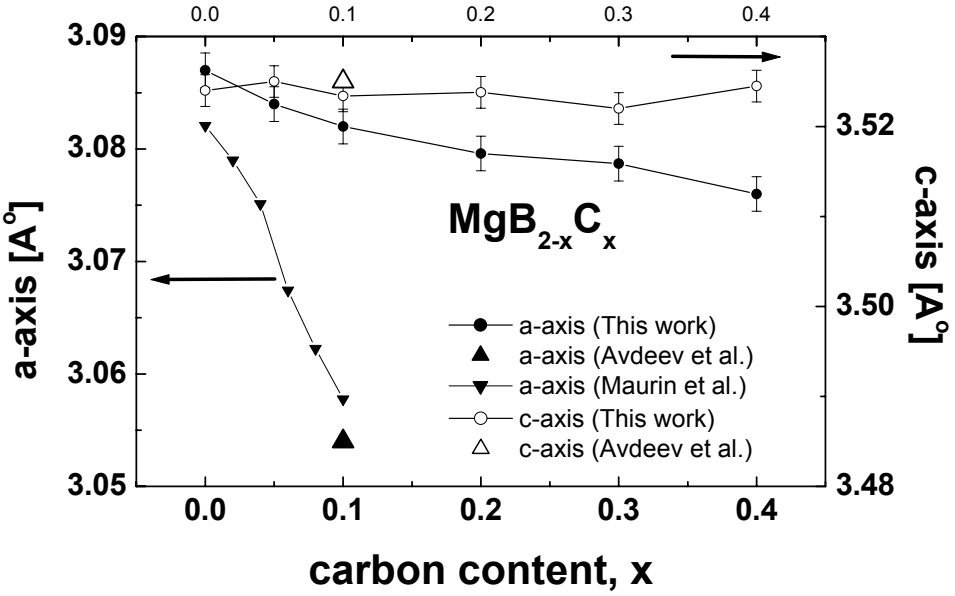

Figure 5- 34: Change in the *a* and *c* lattice parameters in $MgB_{2-x}C_x$ as a function of the nominal C content x. The lattice parameters extracted from the previously published studies by Maurin et al. [25] and Avdeev et al. [34] are also included.

Fig. 5-35 shows the transition temperature (T_c) for the doped and undoped samples determined by ac susceptibility measurements. The T_c onset for the undoped sample (~ 38.5 K) is almost the same as that reported by a number of groups. For the doped samples, the T_c decreases with increasing doping level. Despite the large amount of non-superconducting phases present, the T_c only drops slightly, 2.7 K at a high C doping level of x=0.4 (which represents 20% C doping). This result is in contrast to the previously reported results in which the T_c was depressed about 17 K in the 10% C

substituted sample, as we can see in the inset of Fig. 5-35 [34]. Once again, these results suggest that only a small amount of C powder was substituted in the B position in our samples, consistent with the lattice contraction. Because the C doping has little effect on the T_c, the partial substitution and partial addition of nano-carbon particles may enhance flux pinning over a wide range of temperatures.

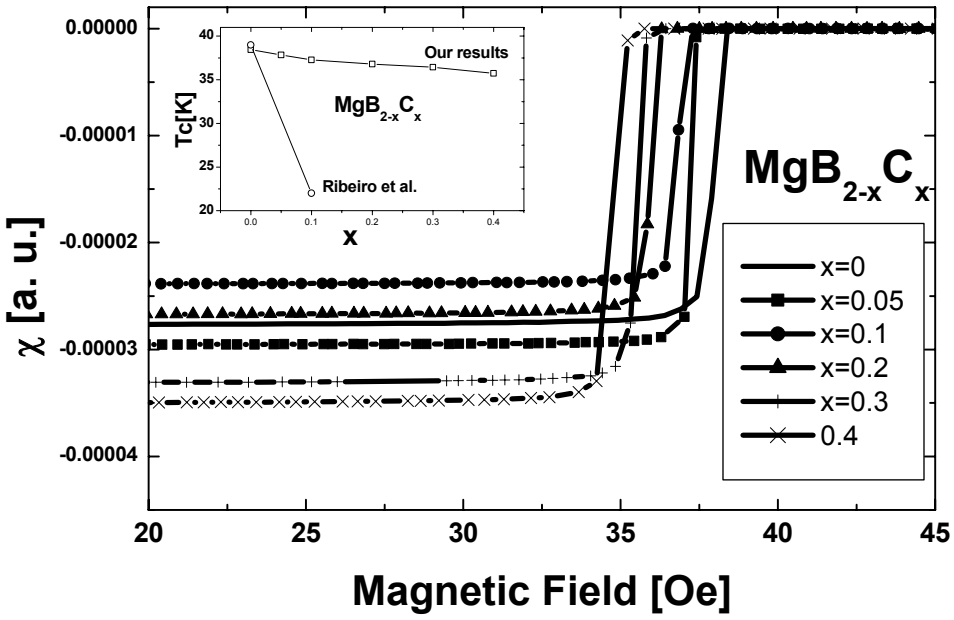

Figure 5- 35: AC susceptibility (real part) vs. magnetic field for different nominal C content x for $MgB_{2-x}C_x$. The inset shows the T_c changes with x for the same composition including for x=0.1, reported by Ribeiro et al. [18].

Fig. 5-36 (a-d) shows the $J_c(H)$ curves for MgB_2 doped and undoped samples at 5 K, 10 K, 20 K and 30 K. It should be noted that at 5 K, 10 K and 20 K, all the $J_c(H)$ curves for doped samples show a crossover with the undoped sample at higher fields except for the sample doped with x=0.4 at 20 K. Because the C doping reduces T_c, only the $J_c(H)$ curve for the C-doped sample with x=0.05 shows the crossover with the undoped sample at 30 K.

Fig. 5-37 shows the irreversibility field, H_{irr} versus temperature for all the doped and undoped samples. Here, we defined H_{irr} as the field where J_c drops to 100 A/cm^2. The improvement in H_{irr} for all the C doped samples is consistent with the $J_c(H)$.

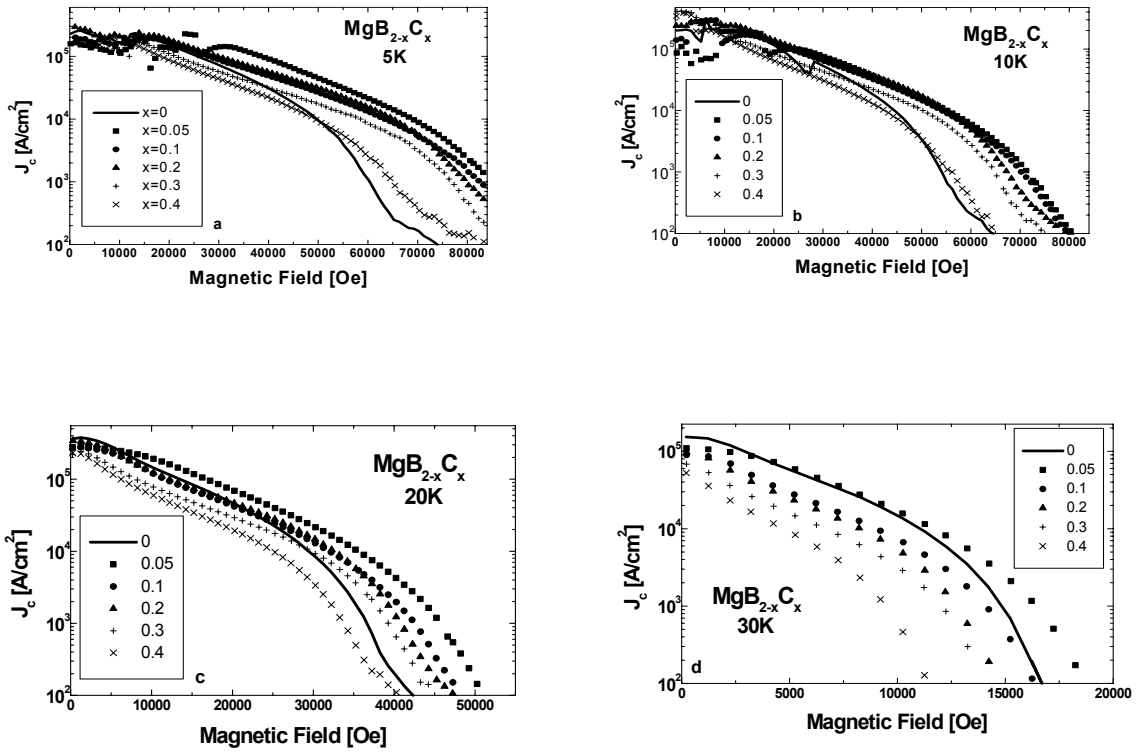

Figure 5- 36: The J_c field dependence of $MgB_{2-x}C_x$ composition for x=0, 0.05, 0.1, 0.2, 0.3 and 0.4 at 5 K, 10 K, 20 K and 30 K.

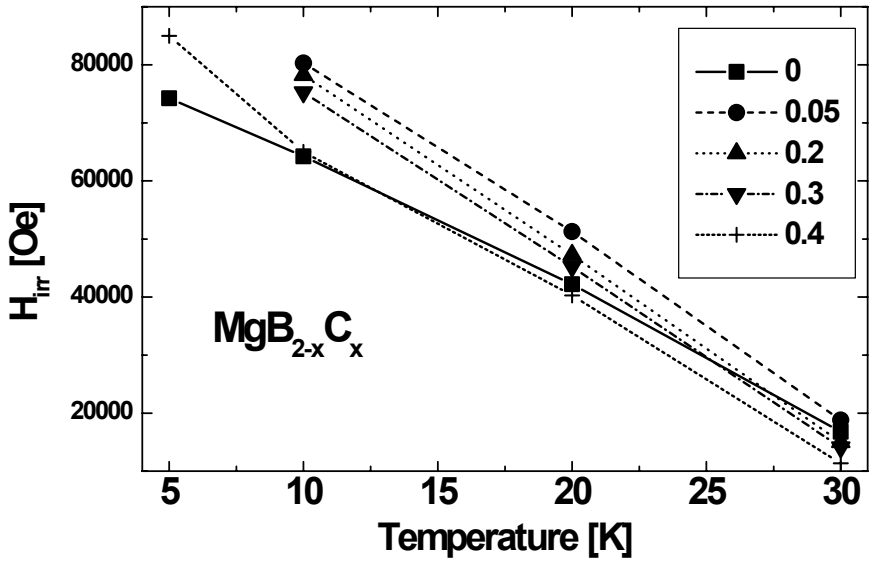

Figure 5- 37: Irreversibility lines for $MgB_{2-x}C_x$ composition for x=0, 0.05, 0.1, 0.2, 0.3 and 0.4.

In order to understand the mechanisms for the enhancement of flux pinning in the nano-C doped samples a TEM study was performed. Fig. 5-38 shows a typical TEM image for the C-doped sample at x=0.05 (Fig. 7(a)) and x=0.1 (Fig.7 (b)). Note that the MgB_2 grains are approximately 100 –200 nm long and 50-100 nm wide. It is evident that although the doping levels of x=0.05 and x=0.1 are well below the C solubility limit, there are noticeable amounts of precipitates which may be unreacted C and the impurity phases Mg_2C_3 and MgB_2C_2. These precipitates are uniformly distributed within the matrix and have a diameter of 5nm to 10nm. Many are included in the grains as fine inclusions. The density and amount of these inclusions increase with increasing doping level. The size of these inclusions matches the coherence length of MgB_2 very well. Thus, it is believed that the high density of nano-inclusions is responsible for the enhanced flux pinning in the C-doped samples.

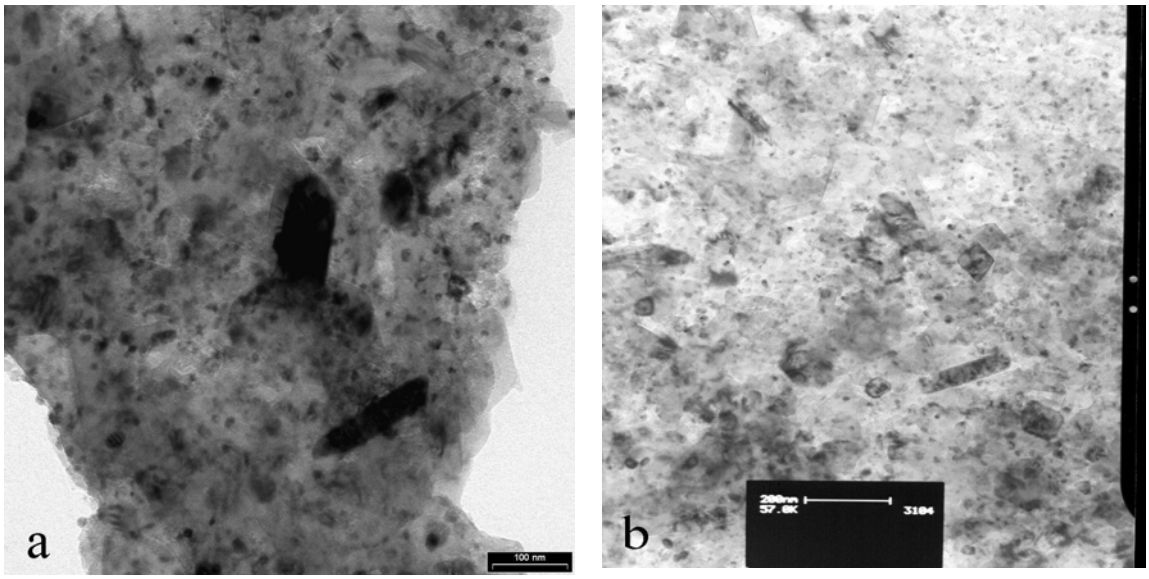

Figure 5- 38: TEM images for C doped $MgB_{2-x}C_x$ composition at x=0.05 (a) and 0.1 (b).

In previous sections, we presented the effect of nano-SiC doping into MgB_2. Compared to the un-doped sample, J_c for the 10wt% SiC-doped sample increased by more than an order of magnitude in higher magnetic fields. It was also confirmed that nano-Si particle doping shows a pinning enhancement, but not as strong as with SiC [35]. Fig. 5-39 compares the normalized $J_c(H)$ and H_{irr} for nano-SiC, nano-Si [35] and nano-C doped MgB_2 at 20 K. Note that C and Si doping gave almost the same level of enhancement over the undoped sample, while SiC-doped MgB_2 remained the best of all the forms of MgB_2.

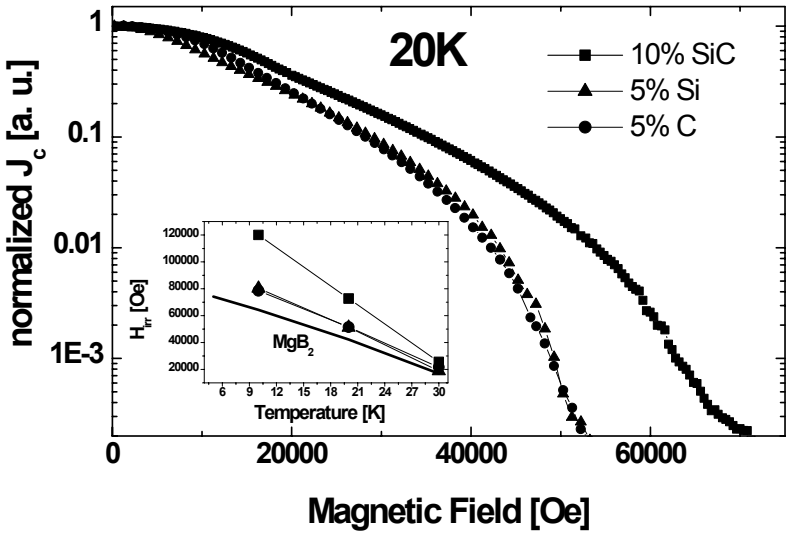

Figure 5- 39: A comparison of $J_c(H)$ and H_{irr} for SiC, C and Si doped MgB_2.

5-4-4 Summary

The effect of C doping on lattice parameters, T_c, J_c and flux pinning in MgB_2 was investigated under the conditions of limited C substitution for B. It was found that both the *a*-axis lattice parameter and the T_c decreased monotonically with increasing doping level. For the sample doped with the highest nominal composition of x=0.4 the T_c dropped only 2.7 K. The nano-C-doped samples showed an improved field dependence of the J_c over a wide temperature range compared with the undoped sample. X-ray diffraction and TEM studies indicate that C reacted with Mg to form Mg_2C_3 and MgB_2C_2 with nano-dimensions. Nano-particle inclusions and substitution, both observed by transmission electron microscopy, are proposed to be responsible for the enhancement of flux pinning in high fields.

References

1. Larbalestier, D.C., L.D. Cooley, M.O. Rikel, A.A. Polyanskii, J. Jiang, S. Patnaik, X.Y. Cai, D.M. Feldmann, A. Gurevich, A.A. Squitieri, M.T. Naus, C.B. Eom, E.E. Hellstrom, R.J. Cava, K.A. Regan, N. Rogado, M.A. Hayward, T. He, J.S. Slusky, P. Khalifah, K. Inumaru, and M. Haas, *Strongly linked current flow in polycrystalline forms of the superconductor MgB_2.* Nature, 2001. **410**(6825): p. 186-189.

2. Dou, S.X., X.L. Wang, J. Horvat, D. Milliken, A.H. Li, K. Konstantinov, E.W. Collings, M.D. Sumption and H.K. Liu, *Flux jumping and a bulk-to-granular transition in the magnetization of a compacted and sintered MgB_2 superconductor.* Physica C, 2001. **361**(2): p. 79-83.

3. Goldacker, W., S.I. Schlachter, S. Zimmer and H. Reiner, *High transport currents in mechanically reinforced MgB_2 wires.* Superconductor Science & Technology, 2001. **14**(9): p. 787-793.

4. Suo, H.L., C. Beneduce, M. Dhalle, N. Musolino, J.Y. Genoud and R. Flukiger, *Large transport critical currents in dense Fe- and Ni-clad MgB_2 superconducting tapes.* Applied Physics Letters, 2001. **79**(19): p. 3116-3118.

5. Grasso, G., A. Malagoli, C. Ferdeghini, S. Roncallo, V. Braccini, A.S. Siri and M.R. Cimberle, *Large transport critical currents in unsintered MgB_2 superconducting tapes.* Applied Physics Letters, 2001. **79**(2): p. 230-232.

6. Glowacki, B.A., M. Majoros, M. Vickers, J.E. Evetts, Y. Shi and I. McDougall, *Superconductivity of powder-in-tube MgB_2 wires.* Superconductor Science & Technology, 2001. **14**(4): p. 193-199.

7. Jin, S., H. Mavoori, C. Bower and R.B. van Dover, *High critical currents in iron-clad superconducting MgB_2 wires.* Nature, 2001. **411**(6837): p. 563-565.

8. Soltanian, S., X.L. Wang, I. Kusevic, E. Babic, A.H. Li, M.J. Qin, J. Horvat, H.K. Liu, E.W. Collings, E. Lee, M.D. Sumption, and S.X. Dou, *High-transport critical current density above 30 K in pure Fe-clad MgB_2 tape.* Physica C, 2001. **361**(2): p. 84-90.

9. Takano, Y., H. Takeya, H. Fujii, H. Kumakura, T. Hatano, K. Togano, H. Kito and H. Ihara, *Superconducting properties of MgB_2 bulk materials prepared by high-pressure sintering.* Applied Physics Letters, 2001. **78**(19): p. 2914-2916.

10. Eom, C.B., M.K. Lee, J.H. Choi, L.J. Belenky, X. Song, L.D. Cooley, M.T. Naus, S. Patnaik, J. Jiang, M. Rikel, A. Polyanskii, A. Gurevich, X.Y. Cai, S.D. Bu, S.E. Babcock, E.E. Hellstrom, D.C. Larbalestier, N. Rogado, K.A. Regan, M.A. Hayward, T. He, J.S. Slusky, K. Inumaru, M.K. Haas, and R.J. Cava, *High critical current density and enhanced irreversibility field in superconducting MgB_2 thin films.* Nature, 2001. **411**(6837): p. 558-560.

11. Bugoslavsky, Y., L.F. Cohen, G.K. Perkins, M. Polichetti, T.J. Tate, R. Gwilliam and A.D. Caplin, *Enhancement of the high-magnetic field critical current density of superconducting MgB_2 by proton irradiation.* Nature, 2001. **411**(6837): p. 561-563.

12. Zhao, Y., Y. Feng, C.H. Cheng, L. Zhou, Y. Wu, T. Machi, Y. Fudamoto, N. Koshizuka and M. Murakami, *High critical current density of MgB_2 bulk superconductor doped with Ti and sintered at ambient pressure.* Applied Physics Letters, 2001. **79**(8): p. 1154-1156.

13. Feng, Y., Y. Zhao, Y.P. Sun, F.C. Liu, B.Q. Fu, L. Zhou, C.H. Cheng, N. Koshizuka and M. Murakami, *Improvement of critical current density in MgB_2 superconductors by Zr doping at ambient pressure.* Applied Physics Letters, 2001. **79**(24): p. 3983-3985.

14. Wang, J., Y. Bugoslavsky, A. Berenov, L. Cowey, A.D. Caplin, L.F. Cohen, J.L.M. Driscoll, L.D. Cooley, X. Song and D.C. Larbalestier, *High critical current density and improved irreversibility field in bulk MgB_2 made by a scaleable, nanoparticle addition route.* Applied Physics Letters, 2002. **81**(11): p. 2026-2028.

15. Cimberle, M.R., M. Novak, P. Manfrinetti and A. Palenzona, *Magnetic characterization of sintered MgB_2 samples: effect of substitution or 'doping' with Li, Al and Si.* Superconductor Science & Technology, 2002. **15**(1): p. 43-47.

16. Gurevich, A., S. Patnaik, V. Braccini, K.H. Kim, C. Mielke, X. Song, L.D. Cooley, S.D. Bu, D.M. Kim, J.H. Choi, L.J. Belenky, J. Giencke, M.K. Lee, W. Tian, X.Q. Pan, A. Siri, E.E. Hellstrom, C.B. Eom, and D.C. Larbalestier, *Very high upper critical fields in MgB_2 produced by selective tuning of impurity scattering.* cond-mat/0305474, 2003.

17. Egerton, R.F., *Electron Energy Loss Spectroscopy in the electron microscope*. 1986, New York: Plenum Press.

18. Ribeiro, R.A., S.L. Bud'ko, C. Petrovic and P.C. Canfield, *Carbon doping of superconducting magnesium diboride.* Physica C-Superconductivity and Its Applications, 2003. **384**(3): p. 227-236.

19. Beneduce, C., H.L. Suo, P. Toulemonde, N. Musolino and R. Flukiger, *Transport critical current, anisotropy, irreversibility fields and exponential n factors in Fe sheathed MgB_2 tapes.* cond-mat/0203551, 2002.

20. James, E.M. and N.D. Browning, *Practical aspects of atomic resolution imaging and analysis in STEM.* Ultramicroscopy, 1999. **78**(1-4): p. 125-139.

21. Browning, N.D., M.F. Chisholm and S.J. Pennycook, *Atomic-Resolution Chemical Analysis Using a Scanning Transmission Electron Microscope.* Nature, 1993. **143**: p. 366.

22. Duscher, G., N.D. Browning and S.J. Pennycook, *Atomic Column Resolved Electron Energy-Loss Spectroscopy.* physica status solidi (a), 1998. **166**(1): p. 327-342.

23. Kazakov, S.M., J. Karpinski, J. Jun, P. Geiser, N.D. Zhigadlo, R. Puzniak and A.V. Mironov, *Single crystal growth and properties of MgB_2 and $Mg(B_{1-x}C_x)_2$.* cond-mat/0304656, 2003.

24. Cheng, Z.H., B.G. Shen, J. Zhang, S.Y. Zhang, T.Y. Zhao and H.W. Zhao, *Superconductivity of $Mg(B_{1-x}C_x)_2$ ternary compounds.* Journal of Applied Physics, 2002. **91**(10): p. 7125-7127.

25. Maurin, I., S. Margadonna, K. Prassides, T. Takenobu, Y. Iwasa and A.N. Fitch, *Carbon miscibility in the boron layers of the MgB_2 superconductor.* Chemistry of Materials, 2002. **14**(9): p. 3894-3897.

26. Takenobu, T., T. Ito, D.H. Chi, K. Prassides and Y. Iwasa, *Intralayer carbon substitution in the MgB_2 superconductor - art. no. 134513.* Physical Review B, 2001. **6413**(13): p. 4513-+.

27. Mickelson, W., J. Cumings, W.Q. Han and A. Zettl, *Effects of carbon doping on superconductivity in magnesium diboride - art. no. 052505.* Physical Review B, 2002. **6505**(5): p. 2505.

28. Li, S., T. White, K. Laursen, T.T. Tan, C.Q. Sun, Z.L. Dong, Y. Li, S.H. Zho, J. Horvat and S.X. Dou, *Intense vortex pinning enhanced by semicrystalline defect traps in self-aligned nanostructured MgB_2.* Applied Physics Letters, 2003. **83**(2): p. 314-316.

29. Paranthaman, M., J.R. Thompson and D.K. Christen, *Effect of carbon-doping in bulk superconducting MgB_2 samples.* Physica C, 2001. **355**(1-2): p. 1-5.

30. Bharathi, A., S.J. Balaselvi, S. Kalavathi, G.L.N. Reddy, V.S. Sastry, Y. Hariharan and T.S. Radhakrishnan, *Carbon solubility and superconductivity in MgB_2.* Physica C, 2002. **370**(4): p. 211-218.

31. Ahn, J.S. and E.J. Choi, *Carbon substitution effect in MgB_2.* cond-mat/0103169, 2001.

32. Maurin, I., S. Margadonna, K. Prassides, T. Takenobu, T. Ito, D.H. Chi, Y. Iwasa and A. Fitch, *Phase separation in carbon-doped MgB_2 superconductors.* Physica B, 2002. **318**(4): p. 392-397.

33. Ribeiro, R.A., S.L. Bud'ko, C. Petrovic and P.C. Canfield, *Effects of boron purity, Mg stoichiometry and carbon substitution on properties of polycrystalline MgB_2.* Physica C-Superconductivity and Its Applications, 2003. **385**(1-2): p. 16-23.

34. Avdeev, M., J.D. Jorgensen, R.A. Ribeiro, S.L. Bud'ko and P.C. Canfield, *Crystal chemistry of carbon-substituted MgB_2.* Physica C-Superconductivity and Its Applications, 2003. **387**(3-4): p. 301-306.

35. Wang, X.L., S.H. Zhou, M.J. Qin, P.R. Munroe, S. Soltanian, H.K. Liu and S.X. Dou, *Significant enhancement of flux pinning in MgB_2 superconductor through nano-Si addition.* Physica C-Superconductivity and Its Applications, 2003. **385**(4): p. 461-465.

CHAPTER 6: STUDY OF AC SUSCEPTIBILITY, MAGNETIC SHIELDING AND SAMPLE SIZE EFFECT IN MgB_2 SUPERCONDUCTOR

6-1 Flux Dynamics of MgB_2 Superconductor by ac Susceptibility Measurement

6-1-1 Introduction

The critical current density, one of the most important parameters in considering superconductors for practical applications, has been determined to be quite high in MgB_2 as we have shown in the last chapters. Although the zero field values of J_c are quite exciting compared to the high temperature superconductors, we have seen in previous chapters that they decrease rapidly with the applied magnetic field. The critical current density is determined by the pinning properties of the sample as well as by the flux motion, because the motion of the vortices over pinning centres (flux creep) in the superconductor induces dissipation and reduces the critical current density J_c. It is the flux creep that sets the limiting critical current density in superconductors. It is thus essential to study the activation energy against flux motion, in order to understand the underlying mechanism resulting in the rapid decreasing relationship between the critical current density and magnetic field, and therefore to enhance the current carrying capacity of this material. In this section, we investigate the flux creep activation energy in MgB_2, and determine its dependence on the current density, the magnetic field, and the temperature by measuring the real $\chi'(T)$ and imaginary $\chi''(T)$ parts of the ac susceptibility at different ac field amplitudes, frequencies and dc magnetic fields. The irreversibility line is obtained using the third harmonic ac susceptibility technique.

6-1-2 Experimental Details

All measurements were performed on a MgB_2 bulk sample (T_c= 38.6 K, ΔT_c<1 K by ac susceptibility in an ac field of 1 G and frequency 117 Hz.). The sample preparation has been explained in the previous chapters. A sample with dimension of $2.18\times2.76\times1.88$ mm^3 was cut from the as sintered pellet. Phase purity was determined by XRD and grain size by SEM. The ac susceptibility measurements were carried out using a Quantum Design PPMS.

6-1-3 Results and Discussion

Figure 6-1 shows the effects of the dc magnetic field B_{dc} on the ac susceptibility of the MgB_2 bulk sample. As B_{dc} is increased from 0.5 T to 3 T, the transition temperature shifts to lower temperatures and the transition width broadens. Although the transition width is slightly changed from about 3 K at 0.5 T to 6 K at 3 T, the transition temperature is greatly depressed by the dc field from about 35 K at 0.5 T to 27 K at 3 T, while in Y-Ba-Cu-O, the depression in T_c is quite small [1, 2]. As the transition temperature under a dc magnetic field is an indication of the irreversibility line (IL), this result indicates that the IL in the pure MgB_2 bulk sample is rather low in the *H-T* plane, as has been obtained by dc magnetization measurements [3, 4] and confirmed by our results explained in previous chapters. The inset of Fig. 6-1 shows the IL of the MgB_2 sample determined by the onset temperature of the ac susceptibility at high frequency and low ac field amplitude, which is higher than the ILs obtained by dc measurements [1, 2]. The reason is that the IL determined by ac measurement is frequency and ac field amplitude dependent. This has been discussed in detail by Deak *et al.* [5].

Typical $\chi'(T)$ and $\chi''(T)$ curves for the MgB_2 bulk sample at B_{dc}=*1 T* are shown in Fig. 6-2. The frequency f =1117 Hz, and different ac field amplitudes B_{ac} are indicated in this figure. As B_{ac} is increased, the transition shifts to lower temperatures accompanied by an increasing transition width. The effects of the frequency on the ac susceptibility of this MgB_2 sample is shown in Fig. 6-3. In contrast to the effects of B_{ac}, the transition shifts to higher temperatures and the transition width broadens as f is increased. All the characteristics shown in Figs. 6-1 to 6-3 for the MgB_2 sample are similar to what have

been observed in high temperature superconductors [1, 2] and predicted from theoretical calculations [6]. This is understandable, because ac susceptibilities at different dc magnetic fields, ac field amplitudes and frequencies reflect a common phenomenon, i.e. flux dynamics in type-II superconductors.

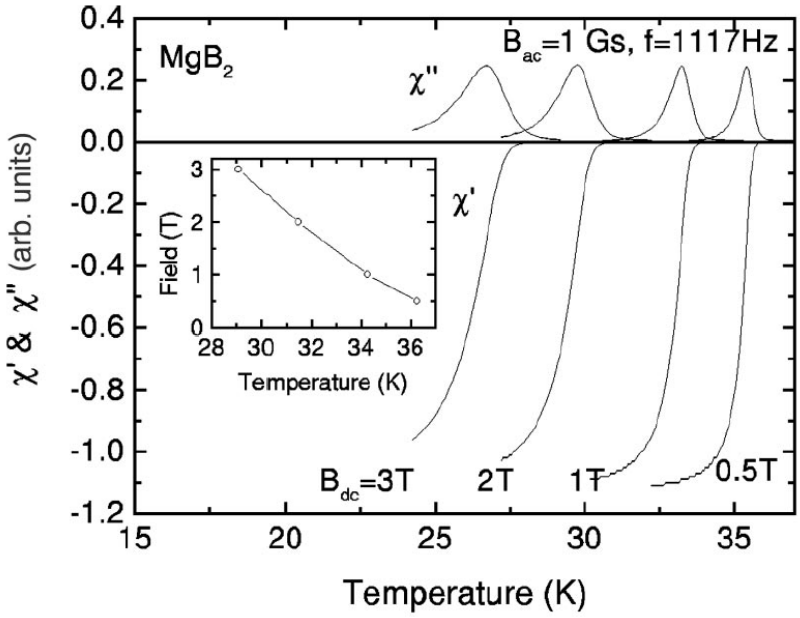

Figure 6- 1: $\chi'(T)$ and $\chi''(T)$ curves of the MgB_2 bulk sample at B_{ac}= 1 G, f = 1117 Hz, and B_{dc} = 0.5, 1, 2, 3 T. Inset shows the irreversibility line (solid line is just a guide to the eye).

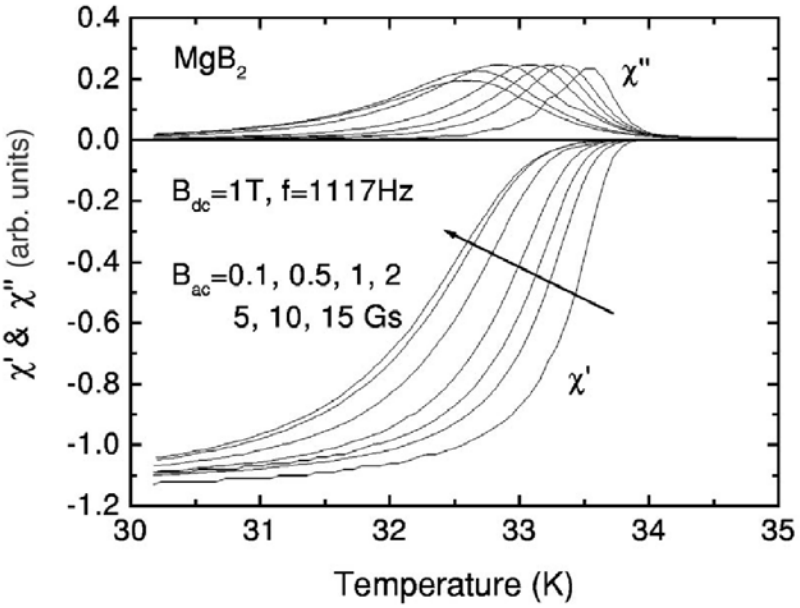

Figure 6- 2: $\chi'(T)$ and $\chi''(T)$ curves of the MgB_2 sample at B_{dc} =1 T, f =1117Hz and B_{ac} = 0.1, 0.5, 1, 2, 5, 10, 15 G (from right to left).

A measurement of the superconducting transition by means of the ac susceptibility $\chi = \chi' + i\chi''$ typically shows a sharp decrease in the real part of the susceptibility χ', just below the critical temperature T_c, a consequence of diamagnetic shielding, and a peak in the imaginary part of the susceptibility χ'', representing losses. The peak in χ'' will occur when the flux front reaches the centre of the sample. It follows that the position of the peak in χ'' will also strongly depend on temperature, dc field, ac field amplitude and frequency. The criterion for the peak in χ'' is [7]:

$$U(T_p, B_{dc}, J)=U(T_p)U(B_{dc})U(J)=k_B T_p \ln\frac{1}{f_{peak} t_0} \qquad (6\text{-}1)$$

where the time scale $t_0 = 4\pi\mu_0 H_{ac}^2 / \rho_0 J^2(\omega)$ [7], ρ_0 is the prefactor in the Arrhenius law $\rho = \rho_0 \exp[-U(J)/K_B T]$, T_p is the peak temperature in the $\chi''(T)$ curve and k_B is the Boltzmann constant.

It has been shown [6] by numerical calculation that during the penetration of the ac magnetic field into a superconductor, the magnetic field profile can be regarded as a straight line. Therefore, at the peak temperature, the current density can be approximated as

$$J = \frac{H_{ac}}{d} \qquad (6\text{-}2)$$

where d is the sample size.

Since

$$\frac{U(T)}{K_B T} U(J, B_{dc}) = -\ln(f) - \ln(t_0) \qquad (6\text{-}3)$$

a plot of - $\ln f_{peak}$ versus $U(T_p)/k_B T_p$ should be a straight line with the slope of $U(J,B_{dc})$. We can derive the current density dependence of the activation energy $U(J)$ by varying the ac amplitude and then using equation (6-2) to determine the current density. Using the ac method the usual difficulty in conventional relaxation measurements of having

only a very limited time window (1~10^4 s) can be overcome by extending the latter to smaller values of 10^{-5} ~10^{-3} s (f =100 kHz -1 kHz) [1, 2].

In order to account for the explicit temperature dependence of the activation energy, we choose a form of temperature scaling function

$$U(T) = [1 - (T / T_x)^2]^2 \qquad (6\text{-}4)$$

where T_x=36.3, 34.3, 31.5, 29.1 K for B_{dc}=0.5, 1, 2, 3 T, respectively, is a characteristic temperature, which is taken from the irreversibility line. $U(T)$ changes slightly with temperature for $T \ll T_x$ and drops rapidly as T approaches T_x. A detailed discussion on choosing the function $U(T)$ has been given by McHenry et al. [8].

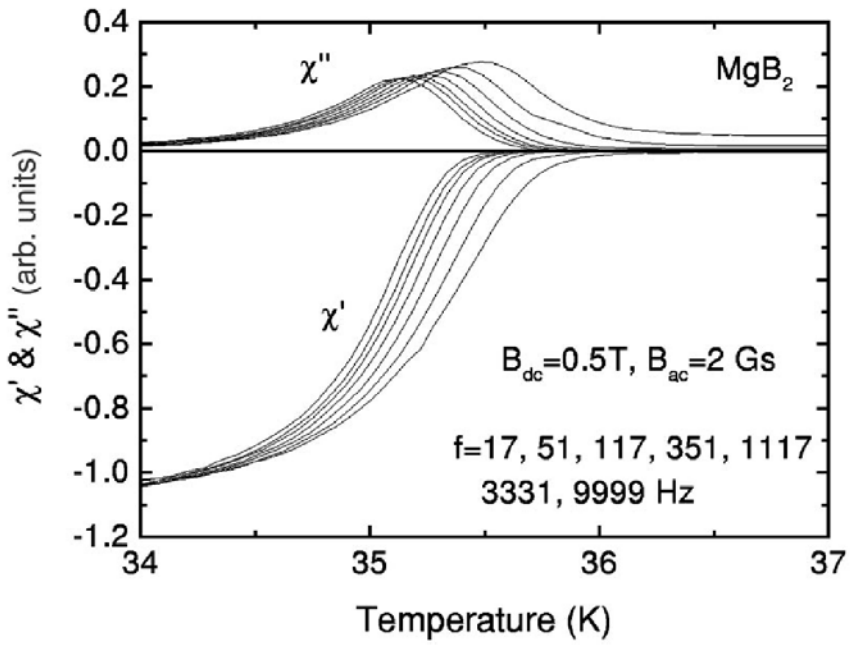

Figure 6- 3: $\chi'(T)$ and $\chi''(T)$ curves of the MgB_2 sample at B_{dc} = 0.5 T, B_{ac} =2 G, and f =17, 51, 117, 351, 1117, 3331, 9999 Hz (from left to right).

Fig. 6-4 shows -lnf_{peak} versus $U(T_p)/k_BT_p$ curves at B_{dc} =0.5 T and various current densities. The experimental data can be fitted very well by straight lines [Eq. (6-3)], shown assolid lines in Fig. 6-4. We can then derive the activation energy U (J, B_{dc} = 0.5 T) from the slopes of the straight lines. $U(J,B_{dc})$ at other dc magnetic fields have also been derived, and the results are summarized in Fig. 6-5, where the activation energy $U(J) \propto U(J, B_{dc}) \times B^{1.3}$ is plotted as a function of the current density for the MgB_2 bulk sample at various dc magnetic fields. As can be seen from Fig. 6-5, we have obtained a

universal curve $U(J)$ by scaling the data by $B^{1.3}$. The slight scattering at low current density may result from the field-dependent critical current density $J_c(B)$. Note that B_{ac} has been changed to J by using Eq. (6-2), where d is the sample size rather than the grain size, because it has been reported [3] that current flow in MgB_2 is strongly linked. The current density J obtained here is also very close to what has been derived using magnetization measurements [9].

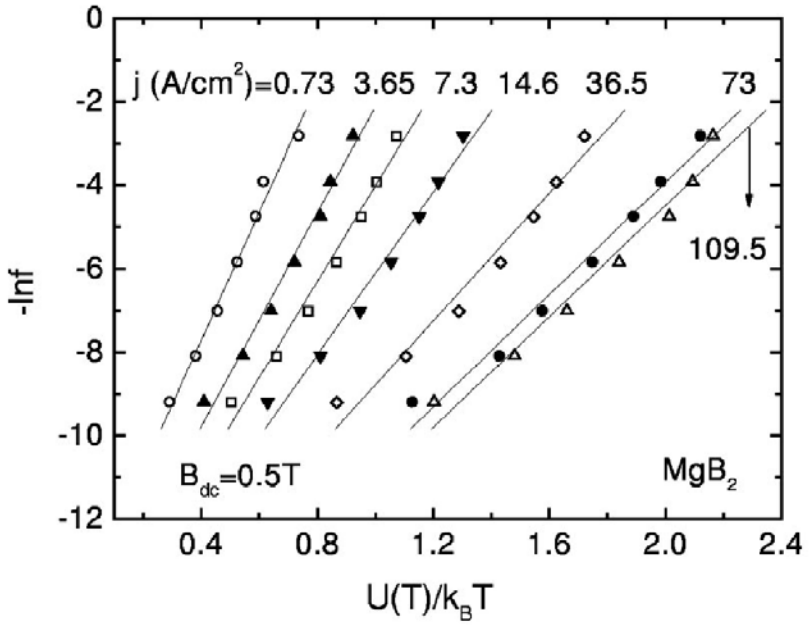

Figure 6- 4: -Ln f_{peak} versus $U(T_p)/k_BT_p$ of the MgB_2 sample at various current densities indicated by different symbols. Solid lines are linear fits calculated from Eq. (3).

From the best fit of the data in Fig. 6-5, we derived the current density dependent activation energy $U(J) \propto J^{-0.2}$, which is highly non-linear. This result suggests that the $I-V$ curve of MgB_2 should also be highly non-linear, because using the Arrhenius rate equation, we have $E = Bv_0 \exp[-U(J)/k_BT] \propto \exp(-J^{-\mu})$. Non-linear $I-V$ characteristics have been experimentally observed in MgB_2 [10]. On the other hand, the relaxation of the current density or the magnetization can be derived from equation (6-1) as $J(t) \propto [\ln(t/t_0)]^{-1/\mu}$, which is also a non-linear function of $\ln(t/t_0)$.

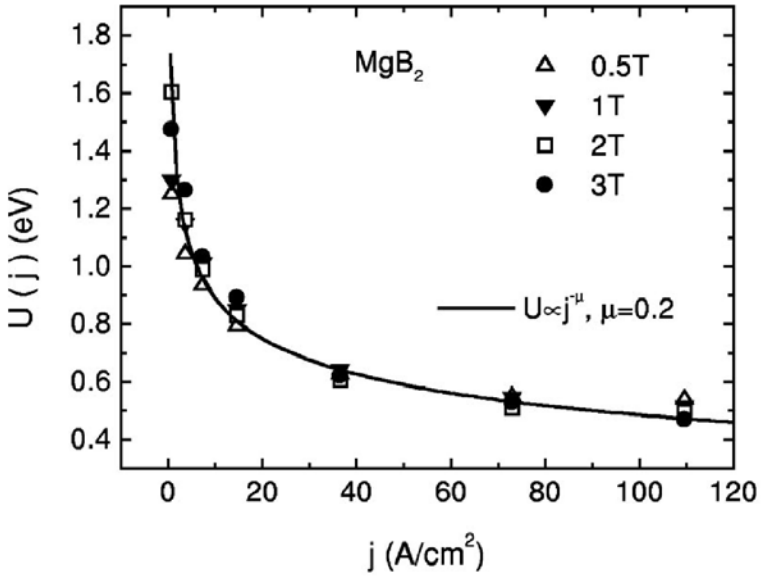

Figure 6- 5: Activation energy $U(J) \sim U(J, B_{dc}) \times B^{1.3}$ as a function of the current density for the MgB_2 sample at various dc magnetic fields. Solid line is the fitting curve $U(J) \sim J^{-0.2}$.

As can be seen from equation (6-3), we can also derive the activation energy as a function of the dc magnetic field $U(B)$ by fixing the current density J. The results are summarized in Fig 6-6, where the activation energy $U(B) \propto U(J, B_{dc}) \times J^{0.21}$ is plotted as a function of the magnetic field for the MgB_2 sample at various current densities. As can be seen from Fig. 6-6, by scaling the data by $J^{0.21}$, we have also obtained a universal curve. This current density dependence is consistent with the one derived in Fig. 6-5. Since the scaling factor B_0 [see Eq. (6-5) below] for B is current density independent, we can see that the scaling of $U(B)$ is much better than that of $U(J)$ shown in Fig. 6-5. The solid line in Fig. 6-6 is a fit to the power law $U(B) \propto B^{-1.33}$. The obtained $U(B)$ is also consistent with the one derived from scaling in Fig. 6-5. The self-consistent scaling of $U(J,B)$ shown in Fig. 6-5 and Fig. 6-6 suggests that the separation of the activation energy $U(J,B,T)$ to $U(J)U(B)U(T)$ in Eq. (6-1) is quite reasonable. The final expression for the temperature-, field- and current density- dependent activation energy is given by

$$U(T,B,J) = U_0\left[1-\left(\frac{T}{T_x}\right)^2\right]^2\left(\frac{B}{B_0}\right)^{-n}\left(\frac{J_0}{J}\right)^{\mu} \qquad (6\text{-}5)$$

where, U_0, B_0 and J_0 are scaling values, and the exponents n and μ are determined to be 1.33 and 0.2 respectively.

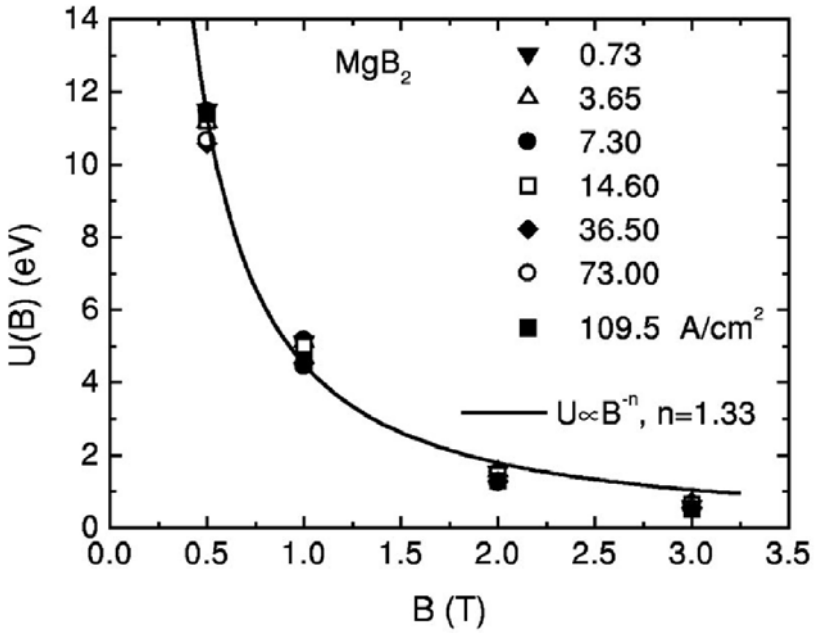

Figure 6- 6: Activation energy $U(J) \propto U(J, B_{dc}) \times J^{0.21}$ as a function of the magnetic field for the MgB_2 sample at various current densities. The solid line is the fitting curve $U(J) \propto B^{-1.33}$.

As for the magnetic field dependence of the activation energy, a B^{-1} dependence has been previously derived using the Anderson-Kim model of the activation energy combined with the Ginzburg-Landau expressions for the coherence length, thermodynamic critical field, depairing critical current density, etc. [11, 12]. Such a B^{-1} dependence has been observed in a $La_{1.86}Sr_{0.14}CuO_4$ single crystal with weak pinning centres by McHenry et al. [8]. For $YBa_2Cu_3O_x$ samples with strong pinning centres, such as twin planes, stacking faults or Y_2BaCuO_5 inclusions, a $U(B) \sim B^{-0.5}$ has been derived by both ac susceptibility [2] and dc magnetization measurements [13, 14].

On the other hand, for the new superconductor MgB_2 we find a $U(B) \propto B^{-1.33}$ dependence showing that the activation energy decreases even faster with increasing magnetic field, compared to weakly pinning high temperature superconducting $La_{1.86}Sr_{0.14}CuO_4$ single crystal. The weakening of the activation energy with increasing magnetic field is probably the reason why the critical current density drops steeply as the magnetic field increases, as has been observed by dc magnetization measurements [3, 4, 15, 16].

6-1-4 Summary

In summary, a systematic ac susceptibility measurements have been performed on a MgB_2 bulk sample. The magnetic-field- and current-density-dependent flux creep activation energy has been determined to be $U(J,B) \propto J^{-0.2}B^{-1.33}$. Compared to high-temperature superconductors $U(B) \propto B^{-1}$ for a weakly pinned $La_{1.86}Sr_{0.14}CuO_4$ single crystal and $U(B) \propto B^{-0.5}$ for strongly pinned $YBa_2Cu_3O_x$, the steeply declining dependence $U(B) \propto B^{-1.33}$ results in a steep drop in J_c with magnetic field and suggests that pinning in pure MgB_2 is quite weak, as can also be seen from the low irreversibility field.

6-2 Improvement of Critical Current in Fe/MgB_2 Superconducting Wires by a Ferromagnetic Sheath

6-2-1 Introduction

As we saw in the previous chapters, Fe sheathed MgB_2 wire is currently one of the most promising conductors for practical application. In addition to providing a medium for obtaining MgB_2 in a chemical reaction at high temperature and ensuring the mechanical strength of the wires, iron is a ferromagnetic material which can be utilized to magnetically shield the superconductor from the external field. This could be very effectively employed for decoupling the superconducting filaments in a multifilamentary MgB_2/Fe wires, substantially lowering the AC loss in the wires. Majoros et al. theoretically predicted that magnetic shielding could lead to a decrease in transport ac loss [17]. A model by Genenko et al.[18] predicted either a suppression or enhancement of the loss-free transport current of a superconducting strip in magnetic surroundings. Earlier measurements [19] indicated the existence of magnetic shielding in MgB_2/Fe tapes, suppressing the ac loss. In chapter 4 we have also shown that the critical current density of Fe/MgB_2 tape can be affected by magnetic shielding. In this section, we present more detailed measurements of the field dependence of transport J_c, influenced by magnetic shielding and the interaction between the Fe sheath and the superconductor in round MgB_2/Fe wires.

6-2-2 Experimental Details

Fe/MgB_2 wire samples were prepared through the powder in tube and reaction in situ techniques. Measurements were performed on three superconducting round wires The zero field critical current density (J_{c0}) at 32 K as well as the dimensions of the samples are given in Table 6-1. The critical temperature of all the samples obtained from the measurements of magnetic ac susceptibility was found to be almost 38.5 K. The mass density of the samples was almost the same for all the samples within experimental uncertainty (5%), about 60%. However, we expect S3 to have slightly higher mass density because it was drawn to the smaller diameter and had the highest value of J_{c0} as

can be seen in Table 6-1. SEM images showed that all three samples had the same average grain size of about 100nm.

Voltage-current characteristics were measured using a 6 milliseconds long pulse of current. The current was swept at a constant rate, with the maximum current 250 A. The signal from the voltage taps was filtered by a low-pass filter and pre-amplified by a SR560 preamplifier. The current through the wire was measured via the voltage drop on a non-inductive resistor, connected in series to the wire and current source. Both voltage and current signals were fed into a digital oscilloscope. The measured data were transferred into a computer for analysis. Using a high enough cut-off frequency of the low-pass filter prevented distortions of the voltage signal and the phase shift between the current and voltage signals.

The measured MgB_2/Fe wire was placed in a continuous flow cryostat, with temperature control better than 0.1 K. The cryostat was placed in an electromagnet on a rotating base, enabling the angle between the field and long axis of the wire to be changed. Measurements were limited to the temperature range between 32 and 35 K, due to the limitations of the current source. $V(I)$ measurements showed a very sharp increase in the voltage at the critical current (I_c).

6-2-3 Results and Discussion

Figure 6-7 shows the angular dependence of I_c for S1, at 33.7 K and 400 mT. The θ = 90° represents the magnetic field perpendicular to the long (cylindrical) axis of the wire. As we can see, critical current shows a maximum value of 99 A for θ = 90°. The I_c value is decreased by about 75% of its maximum value within 30°. However, for the remaining 60°, only a negligible change in I_c was observed (Fig. 6-7). These measurements helped to accurately align the field into a perpendicular orientation. Fig. 6-8 shows the temperature dependence of I_c for S1 in zero field. The zero field critical current value (I_{c0}) decreased almost linearly with temperature between 32 and 36 K, at a rate of 46.4 A/K. For higher temperatures, I_{c0} decreased more gradually, approaching zero at about 38.5 K.

Table 6- 1: Dimensions of the samples measured; d_o, d_i, and l are outer diameter, inner diameter and length, respectively. J_{c0} is the critical current density in zero external field, at a temperature of 32 K.

Sample	d_o (mm)	d_i(mm)	l(mm)	J_{c0}(A/cm^2)
S1	1.50	0.85	14	38,700
S2	1.52	0.95	14	21,000
S3	1.30	0.65	13	53,300

The magnetic field dependence of I_c for sample S3 at 32 K is shown in Fig. 6-8. The solid and open symbols correspond to $\theta = 90°$ and $\theta = 0°$, respectively. In the latter case, the field is parallel to the long wire axis, and therefore to the current. The solid line shows the value of the self-field produced by the critical current at the surface of the superconducting core. For $\theta = 0°$, I_c does not change with the field up to about 0.03 T (open symbols in Fig. 6-9). For higher fields, an exponential decrease in I_c is obtained: $I_c = I_{c0} \exp(-H/H_0)$. For all the samples measured, $H_0 \approx 0.35$ T at 32 K.

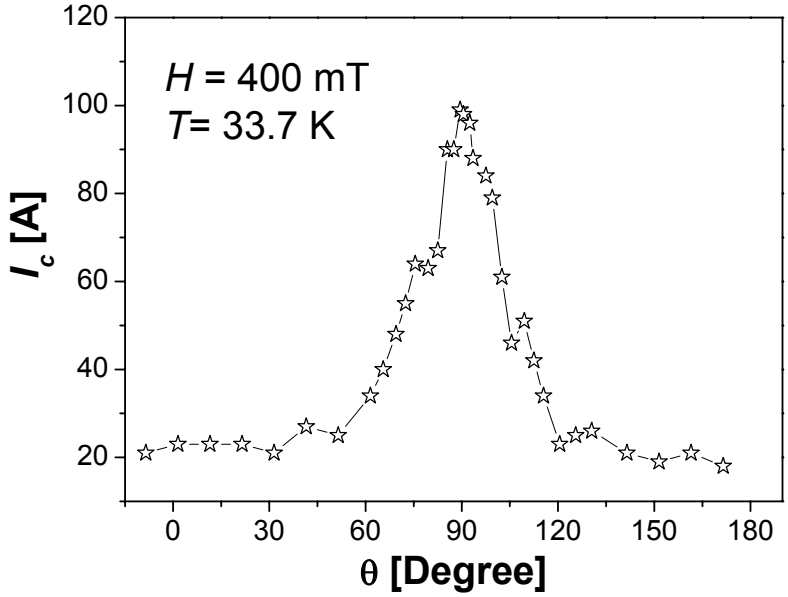

Figure 6- 7: Angular dependence of critical current for Fe/MgB_2 wire sample S1 at 33.7 K and 0.4 T.

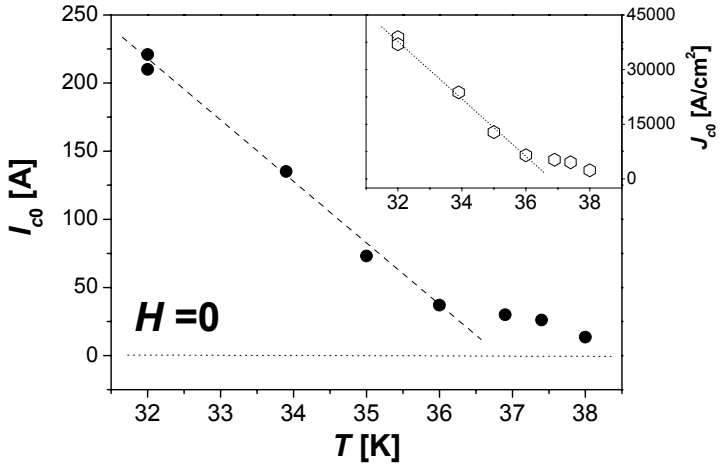

Figure 6- 8: Temperature dependence of critical current in zero field for Fe/MgB_2 wire sample S1. Inset is the critical current density versus temperature for this sample. Lines are just guides to the eye.

For $\theta = 90°$, the field dependence of I_c is the same as for $\theta = 0°$ with H>0.6 T. However, for 0.2 T < H < 0.6 T, there is a plateau in I_c(H), where I_c decreases with the field by less than 5% of I_{c0} (Figure 6-9). For H< 0.2 T, I_c decreases with the field by about 20% of I_{c0}. The inset to Fig. 6-9 shows that the experimental points for the two field orientations overlap by adding 0.38 T to the parallel field.

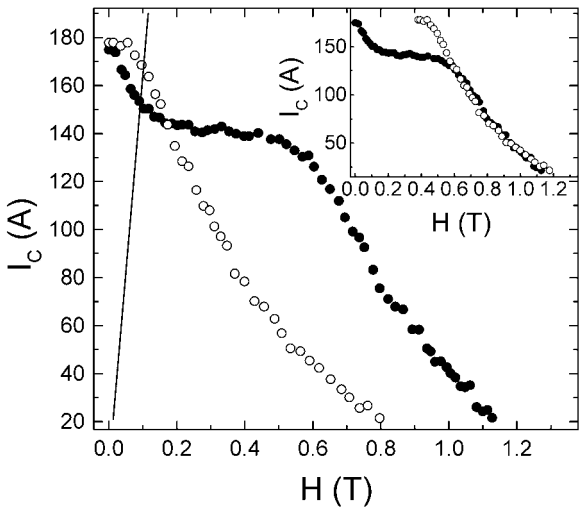

Figure 6- 9: Field dependence of critical current for sample S3 at 32 K. The solid and open symbols are for perpendicular and parallel field (i.e. $\theta = 90°$ and 0°), respectively. The solid line is the self-field produced on the surface of the superconductor by the critical current. Inset: The same, with 380 mT added to the parallel field.

The same results were obtained for the other samples measured, except for the difference in I_{c0} and the field by which I_c(H) for $\theta = 0°$ had to be shifted to obtain overlapping with I_c(H) for $\theta = 90°$ (Inset to Fig. 6-9). The values of this field for S1 and S2 were 0.39 T and 0.33 T, respectively.

The results shown in Fig. 6-9 are affected by the magnetic shielding due to the Fe sheath, as well as by the interaction between the sheath and superconductor. To identify the effects of shielding only, the field inside and outside the sheath was measured, with the MgB_2 removed. This was performed by inserting tiny pick-up coils into the sheath and using an external ac magnetic field with frequencies between 20 and 60 Hz, and a field amplitude up to 0.6 T. The length of the coils corresponded to the distance between the voltage contacts when measuring I_c(H). Comparing the results for different frequencies, we found that the dynamic effects (eddy currents) were negligible below 30 Hz.

Fig. 6-10 shows the magnetic field inside the Fe sheath against the external magnetic field for $\theta = 90°$ (open symbols). The solid symbols were measurements with the sheath removed from the pick-up coil ($H_{in}=H_{out}$) and the solid line shows theoretical shielding for an infinite cylinder of the same dimensions and magnetic susceptibility as our Fe sheath [20].

For H<0.2 T, the shielding from the external field was almost total, with H_{in}= 0.04 H_{out} at 0.2 T (Fig. 6-10). For higher fields, the shielding rapidly weakened and for H>0.4 T the entire external field additional to 0.4 T was passed through the Fe sheath, i.e. H_{in} against H_{out} was parallel to the data with no shield for H>0.4 T. These measurements are in good quantitative agreement with calorimetric measurements of ac loss in a similar MgB_2/Fe wire [19]. However, the measured shielding is better than that given by the analytical expression for an infinite cylindrical shield of the same thickness and magnetic permeability [20] (solid line in Fig. 6-10). Still, extrapolation of the experimental results to high fields is in agreement with the theoretical prediction. The discrepancy at low fields is probably due to the finite length of the measured sheath.

The inset to Fig. 6-10 shows the measured shielding for $\theta = 0°$. The dashed line represents $H_{in}=H_{out}$. The shielding was almost total for H< 0.02 T. For H>0.025 T, the

entire field higher than 0.025 T was passed through the shield. The hysteresis was due to magnetic hysteresis of the iron.

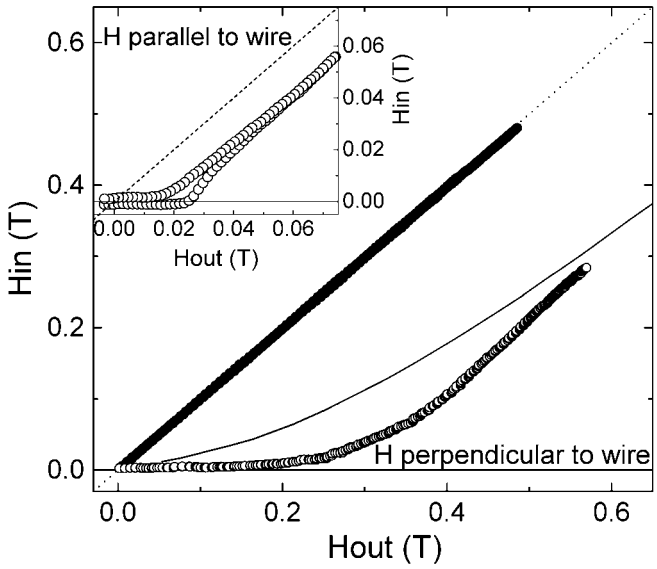

Figure 6- 10: The magnetic field inside the iron sheath, H_{in}, plotted against the external field, H_{out}, for perpendicular field, $\theta = 90°$ (open symbols). When the iron sheath is removed, $H_{in}=H_{out}$ (solid symbols). The solid line shows theoretical H_{in} against H_{out}. Inset: H_{in} against H_{out} for a parallel field, $\theta = 0°$ (solid symbols). The dashed line shows $H_{in}=H_{out}$.

$I_c(H)$ for $\theta = 0°$ can be explained by the shielding effect. The initial plateau is a consequence of complete shielding from the external field. Above 0.025 T, $I_c(H)$ is the same as with no shield, except for about 0.025 T which is screened out by the shield. The same is obtained for $\theta = 90°$ and H>0.6 T, except that the value of the screened-out field is about 0.3 T (Fig. 6-10). However, $I_c(H)$ for H<0.6 T cannot be explained by simple screening. Instead of the expected constant I_c with the external field fully screened out for H<0.2 T, I_c actually decreases with the field (Fig. 6-9). For 0.2 T <H<0.6 T, I_c decreases very little with field (Fig. 6-9), despite the full penetration of field through the Fe sheath (Fig. 6-10).

Overlapping of $I_c(H)$ for $\theta = 0°$ and $\theta = 90°$ above 0.6 T (Inset to Fig. 6-9) shows that the current does not flow through the wires in a straight line. If that were the case, $I_c(H)$ corrected for the shielding of the iron sheath would differ for the two orientations of the field. This is because $I_c(H)$ is defined by the Lorentz-like force on magnetic vortices [21]. This force is proportional to $H \times \sin\theta$. Therefore, for $\theta = 0°$, Lorentz force would always be zero and I_c would not depend on the field. This is in contrast to the experimental results in the Inset to Fig. 6-9. These results suggest that the current

meanders between the superconducting grains, resulting in a variation of local θ. Averaging over the whole sample volume gives the same $I_c(H)$ for $\theta = 90°$ and 0° after shifting of $I_c(H)$ by 0.38 T along H-axis (the shift is needed to account for the shielding by the iron sheath). The decrease in I_c for $H<0.2$ T cannot be ascribed to weak links, because such a decrease was not also observed for the case $\theta = 0°$ (Fig. 6-9).

6-2-4 Summary

In conclusion, transport critical current (I_c) was measured for Fe-sheathed MgB_2 round wires. A critical current density of 5.3×10^4 A/cm^2 was obtained at 32 K. Strong magnetic shielding by the iron sheath was observed, resulting in a decrease in I_c by only 15% in a field of 0.6 T at 32 K. In addition to shielding, interaction between the iron sheath and the superconductor resulted in a constant I_c between 0.2 and 0.6 T. This was well beyond the maximum field for effective shielding of 0.2 T. This effect can be used to substantially improve the field performance of MgB_2/Fe wires at fields at least 3 times higher than the range allowed by mere magnetic shielding by the iron sheath. The dependence of I_c on the angle between the field and the current showed that the transport current does not flow straight across the wire, but meanders between the grains.

6-3 Effect of Sample Size on the Magnetic Critical Current Density in Nano-SiC Doped MgB_2 Superconductors

6-3-1 Introduction

Improving the critical current density (J_c) is one of the most important issues so far as applications are concerned. Results presented in chapter 5 show that SiC doped MgB_2 superconductor is one of candidates for high field applications. In contrast to the direct transport J_c measurements used for tapes and wires, for bulk samples one has to calculate magnetic J_c from the dc magnetization using the Bean model. It has been shown that magnetic J_c strongly depends on the sample size [22]. In contrast to the high T_c superconductor materials [23] it was observed that in pure MgB_2 bulk samples H_{irr} decreased as the sample volume decreased. Due to the dependence of J_c on sample size, for a reliable comparison of J_c values derived from magnetic measurements, sample size has to be carefully taken into account. Some explanations have been presented to explain this behavior. Jin et al. suggested a linear dependence of the activation energy on the J_c and gave an explanation for the J_c dependence on the sample size [24]. They proposed that in a cylindrical MgB_2 sample, vortices are remarkably rigid in small samples up to 1mm long, while they behave as individual segments for longer samples. Horvat et al. qualitatively explain this phenomenon by considering the different coupling between the grains at different length scales [22]. Very recently Qin et al. established a new model to explain this effect [25]. Based on this model the magnetic J_c depends on sample size as $J_c \propto R^{\frac{1}{n}}$ where R is the radius of a cylindrical sample and n is the n-factor characterizing the E-J curve $E = E_c(J/J_c)^n$. They proposed that the low n factor at high magnetic fields is the reason for the significant sample size effect for pure MgB_2 superconductors. As the nano-SiC doped sample exhibited much stronger flux pinning than the pure MgB_2, we intend to investigate the size effect in the strong pinning samples and compare them with pure MgB_2 samples. A detailed study with the aim of further understanding the sample size effect in both pure and doped MgB_2 superconductor is presented in this section.

6-3-2 Experimental Details

Two groups of polycrystalline MgB_2 and MgB_2 +10% SiC samples were synthesized from high purity Mg and B and nano-SiC powders using the Hot Isostatic Pressing (HIP) method. An MgB_2 pellet was prepared by reacting magnesium and boron powders at 850°C under isostatic pressure of 150 MPa for 1 hour. The magnetization was measured over a temperature range of 5 K to 30 K using the Quantum Design PPMS. Bar shaped samples were cut and dry polished from each pellet for magnetic measurements. The shiny polished surface was golden and black for the pure and doped samples respectively. The sample volume was decreased about 75% through sawing and dry polishing after each measurement. To avoid any geometrical effect on the results each dimension reduced by a factor of about 0.35% (i.e. the ratio of a:b:c remains constant) before each subsequent measurement. The sample information is presented in Table 6-2. The magnetic measurements were performed by applying the magnetic field parallel to the longest sample axis. The magnetic J_c was calculated using the Bean model. The T_c was determined to be 38.6 K and 37.5 K for the pure and doped samples respectively using the ac susceptibility measurement. A small bar shaped sample of the same size as sample 4, was directly cut from the same batch and given a J_c measurement. No significant difference was found between the results for this sample and for sample 4, indicating that the repeated polishing and measurements had no effect on the samples.

Table 6- 2: The dimensions of samples prepared for magnetic measurements. Each dimension was reduced by about 35% before each subsequent measurement. The magnetic field was applied parallel to the c axis.

	Undoped				Doped			
Sample	*a* (mm)	*b* (mm)	*c* (mm)	*V* (mm^3)	*a* (mm)	*b* (mm)	*c* (mm)	*V* (mm^3)
1	1.07	3.27	7.15	25.01	1.12	2.98	6.95	23.2
2	0.7	2.12	4.65	6.9	0.7	2.12	4.62	6.82
3	0.46	1.34	2.92	1.78	0.45	1.34	2.9	1.75
4	0.29	0.85	1.87	0.46	0.3	0.85	1.81	0.45

6-3-3 Results and Discussion

The field dependence of J_c for SiC doped and undoped MgB_2 samples at 5 K, 20 K and 30 K for samples of different sizes are presented in Fig. 6-11 and Fig. 6-12 respectively. It can be clearly seen that in both doped and undoped samples the J_c field performance strongly depends on the sample size. At high field, J_c significantly decreased as a function of the magnetic field as the sample size decreased. On the other hand the low field J_c increased as the sample size decreased in both pure and doped samples. These changes in either low fields or in high fields are stronger in the lower temperature regime. Flux jumping was observed in both pure and doped samples but flux jumps occurred at higher fields for bigger samples. Flux jumping was also found to be less serious in the doped samples. For sample 1 flux jumping was observed up to 3.9 T for the doped sample, but in the pure sample flux jumping can be seen even at 5 T. Flux jumping also occurred in the pure samples 1 and 2 at 20 K, but no flux jumping was observed in the doped samples at 20 K.

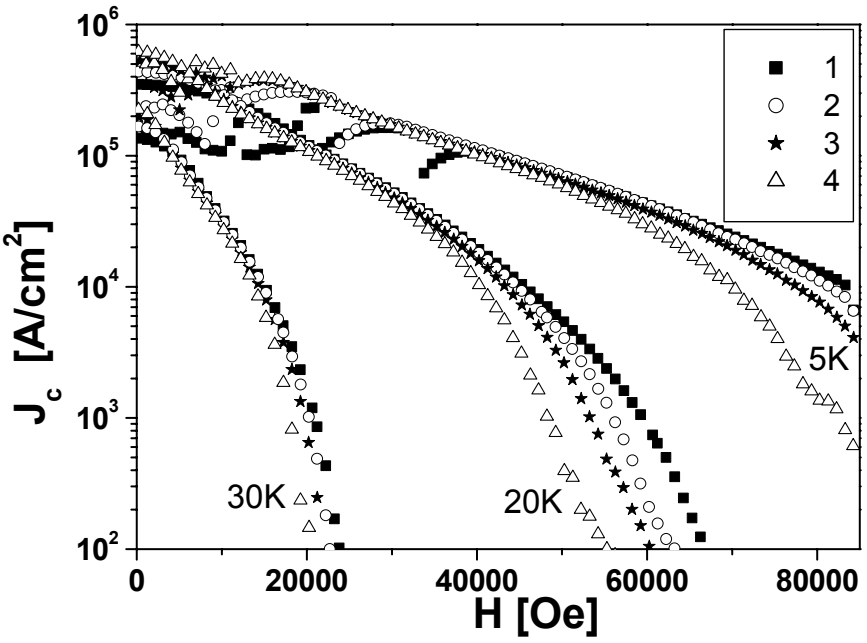

Figure 6- 11: Magnetic J_c field dependence of MgB_2 + 10% SiC samples of different sizes (Table 6-2) at 5 K, 20 K and 30 K.

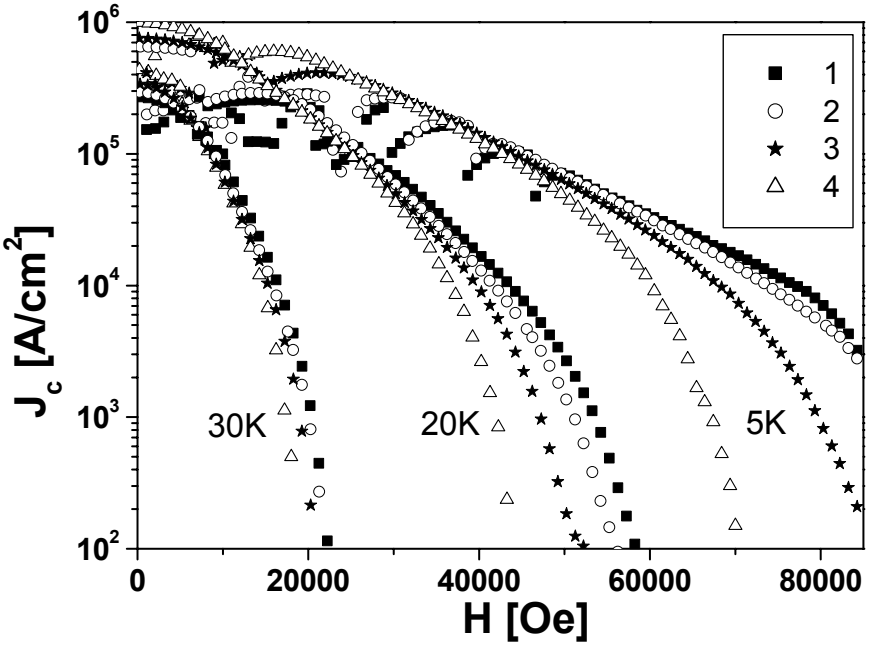

Figure 6- 12: Magnetic J_c field dependence of pure MgB_2 samples of different sizes (Table 6-2) at 5 K, 20 K and 30 K.

The ratio of J_{c1}/J_{c4} for samples 1 and 4 between 5 T and 8.5 T for both pure and doped samples at 5 K are presented in Fig. 6-13. For both samples the larger the sample, the higher the J_{c1}/J_{c4} ratio. However, the sample size dependence is much more pronounced in the undoped sample. At 6.5 T and 5 K J_{c4} is lower than J_{c1} by a factor of 1.8 for the doped samples. However, under the same conditions, J_{c4} is more than one order of magnitude lower than J_{c1} in the pure samples. The J_c field dependences of the doped samples at low magnetic fields and 20 K are shown in the inset of Fig. 6-13. As we can see, the zero field J_c increases as the sample size decreases. However, the differences between the J_c values of all the samples are reduced by increasing the magnetic field. The J_c field dependence curve of sample 1 crosses over the J_c curves of the smaller samples at a magnetic field of about 1 T. The same behavior was also found in the pure samples.

The dependence of the irreversibility field H_{irr} on the volume of pure and doped samples at 20 K is shown in a semi-logarithmic plot in Fig. 6-14. H_{irr} was determined from J_c–H curves using the criterion of 100 A/cm^2. Some points for the pure samples were extracted from reference [4]. As we can see, H_{irr} decreases logarithmically as the

sample volume decreases. The irreversibility field H_{irr} versus the sample volume is plotted in the inset with linear scaling, showing a gradual saturation behavior as the sample volume increases. Almost the same trend was found at other temperatures as well.

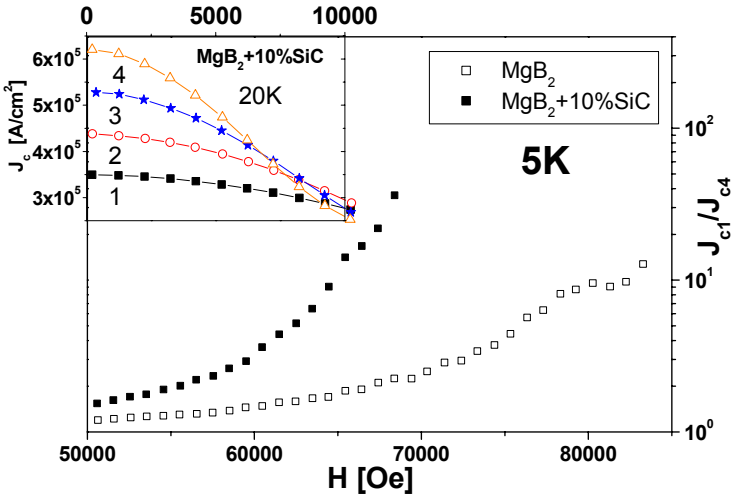

Figure 6- 13: The ratio of J_{c1}/J_{c4} between 50000 Oe and 85000 Oe for both pure and doped samples at 5 K. The J_c field dependence of doped sample at low magnetic fields at 20 K is shown in the inset.

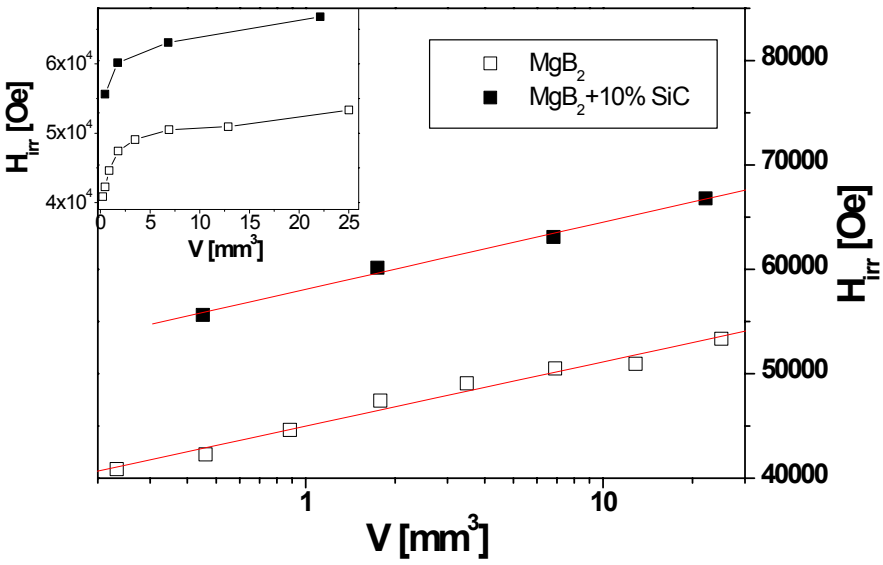

Figure 6- 14: The dependence of H_{irr} samples on the sample volume of pure and doped MgB_2 at 20 K in a semi-logarithmic plot. H_{irr} versus the volume with linear scaling is shown in the inset.

Fig. 6-15 shows the dependence of the zero field critical current (J_{c0}) on the sample volume of pure and doped samples at 20 K and 30 K. Some points for pure samples were extracted from reference [4]. All J_{c0} values were normalized to the J_{c0} value of the biggest sample. Over all temperature ranges the smaller samples had a higher J_{c0}. For pure samples the normalized J_{c0} increases slightly as the sample volume decreases down to 7 mm^3, followed by a faster increase for smaller sample volumes. J_{c0} can also be very well scaled for both 20 K and 30 K with the same curve. However for doped samples, J_{c0} increases more gradually than for the pure samples as the sample size decreases. Moreover the J_{c0} values for 20 K and 30 K cannot be scaled using the same curve. The difference between the normalized J_{c0} values for 20 K and 30 K is increased by decreasing the volume. The lower the temperature is, the faster J_{c0} increases. The absolute value of J_{c0} versus the sample volume for pure and doped samples at 20 K is plotted on a logarithmic scale in the inset. The curves can be fitted as an exponential decay function as is shown in the figure (lines).

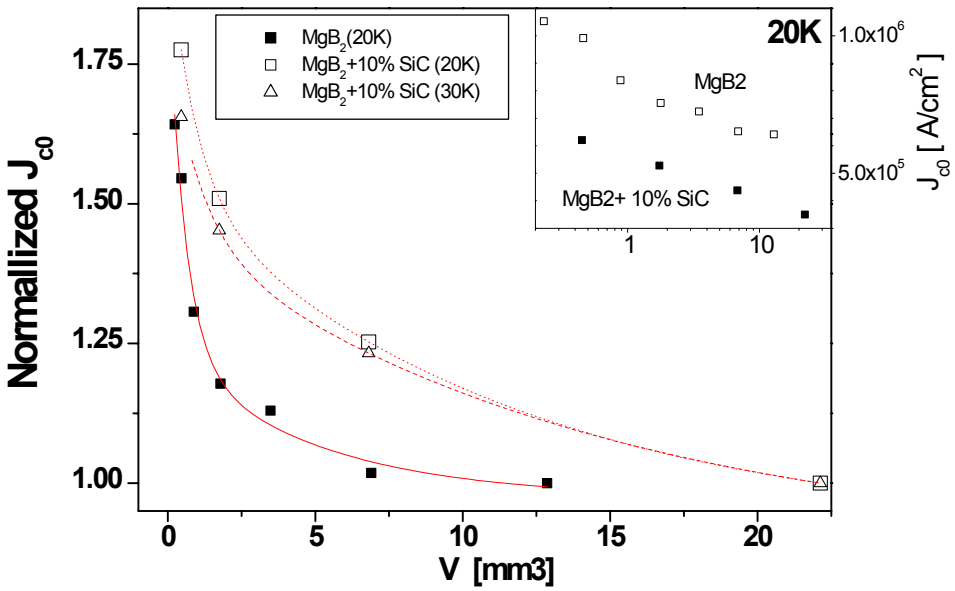

Figure 6- 15: The dependence of the zero field J_c (J_{c0}) on the sample volume of pure and doped samples at 20 K and 30 K. In the inset the dependence of J_{c0} on the volume at 20 K is plotted on a logarithmic scale.

Based on Qin's method we have plotted $\ln(J_c)$ versus $\ln[ab/(a+b)]$ for the doped samples at 20 K and at 3 T, 4 T, 5 T, and 6 T in Fig. 6-16. Similar curves at 5 K and 30 K for different magnetic fields are presented in the insets of this figure. The solid lines are the best linear fittings between $\ln(J_c)$ and $\ln[ab/(a+b)]$. The inverses of the slopes give the *n* factors. Calculated *n* factors for the SiC doped samples are shown in Fig. 6-17 at 5 K, 20 K and 30 K. The *n* factors of pure samples are also included as open squares and open triangles for 5 K and 20 K respectively. The solid lines are just guides to the eye.

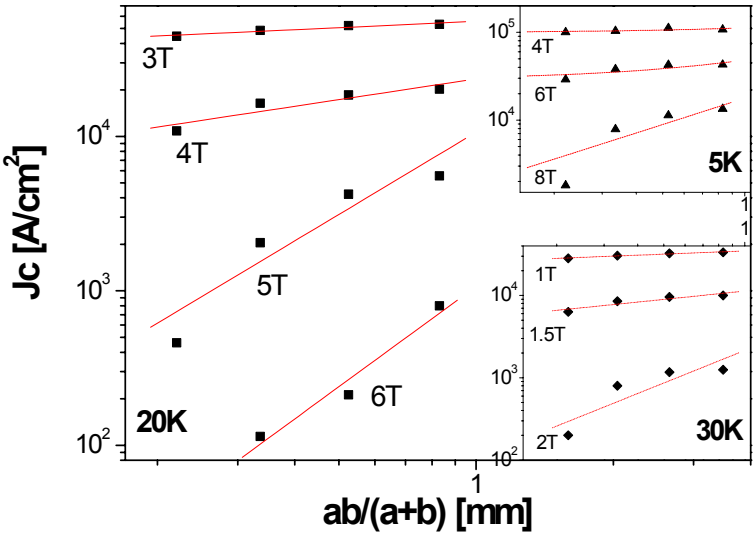

Figure 6- 16: The sample size dependence of J_c for doped MgB_2 samples at 20 K. The same dependence is plotted in the insets for 5 K and 30 K. The solid lines are linear fits to the data.

As the *n*-factor is the exponent characterizing the *E-j* curve $E = E_c(j/j_c)^n$, a large *n*-factor will lead to a sharp *E-j* curve. On the other hand, the *n*-factor can be calculated as $n = U_0/kT$ [25], where U_0 is the energy scale for the current density dependent activation energy $U(j) = U_0 \log(j_c/j)$ with k the Boltzmann constant. Therefore a large *n* indicates a stronger pinning effect. Moreover, the dependence of the current density on the sample size has been derived to be $j \propto R^{1/n}$, indicating that a large *n* will give rise to less sample size dependence. It can be seen from Fig. 6-16 that the *n*-factors of the doped samples are much higher than those of the pure samples, indicating that strong pinning centers have been introduced into the MgB_2 samples by means of SiC doping.

Fig. 6-17 also explains the observed lesser sample size effect in the SiC doped samples shown in Figs. 1–3.

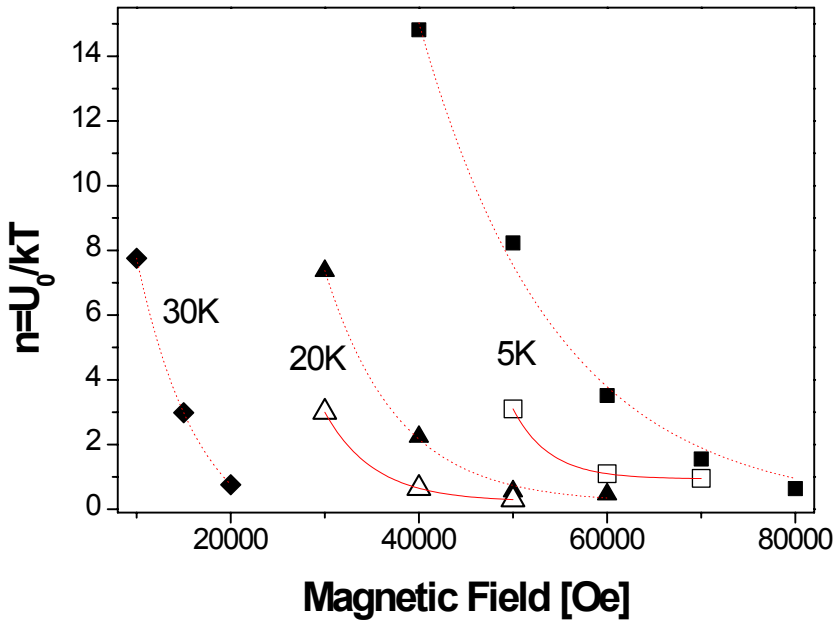

Figure 6- 17: The *n* factor versus applied magnetic field for the doped MgB_2 samples at 5 K, 20 K and 30 K (solid symbols). The *n* factor of pure samples are also included (open symbols). The solid lines are only guides to the eye.

6-3-4 Summary

In conclusion we have studied the sample size effect in pure and SiC doped MgB_2 samples and derived the *n*-factors for both samples. The doped samples show a larger *n*-factor and less sample size dependence, indicating a stronger pinning effect by SiC doping in MgB_2 samples. The irreversibility field H_{irr} was found to increase with increasing sample volume as a logarithmic function. The zero field J_c decreased with decreasing sample volume as an exponential decay function. A systematic shift in the pinning force density was found in both pure and doped samples as the sample volume decreased.

References

1. Ding, S.Y., G.Q. Wang, X.X. Yao, H. T. Peng, Q.Y. Peng and S.H. Zhou, *Magnetic relaxation and the flux diffusion barrier for $TlSr_2Ca_2Cu_3O_y$ doped with Pb and Ba determined by complex ac susceptibility measurements.* Physical Review B, 1995. **51**(14): p. 9107-9110.

2. Qin, M.J., S.Y. Ding, C. Ren, X.X. Yao, Y.X. Fu, C.B. Cai, T.S. Shi and G.Y. Wang, *Logarithmic U(J) relationship in melt-textured growth $YBa_2Cu_3O_{6+x}$ by AC susceptibility measurements.* Physica C-Superconductivity and Its Applications, 1996. **262**(1-2): p. 127.

3. Larbalestier, D.C., L.D. Cooley, M.O. Rikel, A.A. Polyanskii, J. Jiang, S. Patnaik, X.Y. Cai, D.M. Feldmann, A. Gurevich, A.A. Squitieri, M.T. Naus, C.B. Eom, E.E. Hellstrom, R.J. Cava, K.A. Regan, N. Rogado, M.A. Hayward, T. He, J.S. Slusky, P. Khalifah, K. Inumaru, and M. Haas, *Strongly linked current flow in polycrystalline forms of the superconductor MgB_2.* Nature, 2001. **410**(6825): p. 186-189.

4. Wen, H.H., S.L. Li, Z.W. Zhao, H. Jin, Y.M. Ni, Z.A. Ren, G.C. Che and Z.X. Zhao, *Flux dynamics and vortex phase diagram of the new superconductor MgB_2.* Physica C, 2001. **363**(3): p. 170-178.

5. Deak, J., M. McElfresh, J.R. Clem, Z. Hao, M. Konczykowski, R. Muenchausen, S. Foltyn and R. Dye, *Irreversibility line in $YBa_2Cu_3O_7$ thin films: Correlation of transport and magnetic behavior.* Physical Review B, 1994. **49**(9): p. 6270-6279.

6. Qin, M.J. and X.X. Yao, *ac susceptibility of high-temperature superconductors.* Physical Review B, 1996. 54(10): p. 7536-7544.

7. Blatter, G., M.V. Feigel'man, V.B. Geshkenbein, A.I. Larkin and V.M. Vinokur, *Vortices in high-temperature superconductors.* Review of modern physics, 1994. **66**(4): p. 1125-1388.

8. McHenry, M.E., S. Simizu, H. Lessure, M.P. Maley, J.Y. Coulter, I. Tanaka and H. Kojima, *Dependence of the flux-creep activation energy on the magnetization current for a $La_{1.86}Sr_{0.14}CuO_4$ single crystal.* Physical Review B, 1991. **44**(14): p. 7614-7624.

9. Dou, S.X., X.L. Wang, J. Horvat, D. Milliken, A.H. Li, K. Konstantinov, E.W. Collings, M.D. Sumption and H.K. Liu, *Flux jumping and a bulk-to-granular transition in the magnetization of a compacted and sintered MgB_2 superconductor.* Physica C, 2001. **361**(2): p. 79-83.

10. Kim, K.H.P., W.N. Kang, M.-S. Kim, C.U. Jung, H.-J. Kim, E.-M. Choi, M.-S. Park and S.-I. Lee, *Origin of the high DC transport critical current density for the MgB_2 superconductor.* cond-mat/0103176, 2001.

11. Yeshurun, Y. and A.P. Malozemoff, *Giant flux creep and irreversibility in an Y-Ba-Cu-O crystal: An alternative to the superconducting-glass model.* Physical Review Letters, 1988. **60**(21): p. 2202-2205.

12. Tinkham, M., *Resistive transition of high-temperature superconductors.* 61, 1998. 14(1658-1661).

13. Kung, P.J., M.P. Maley, M.E. McHenry, J.O. Willis, J.Y. Coulter, M. Murakami and S. Tanaka, *Magnetic hysteresis and flux creep of melt-powder-melt-growth $YBa_2Cu_3O_7$ superconductors.* Physical Review B, 1992. **46**(10): p. 6427-6434.

14. Kung, P.J., M.P. Maley, M.E. McHenry, J.O. Willis, M. Murakami and S. Tanaka, *Flux pinning by Y_2BaCuO_5 precipitates and field- and temperature-driven pinning centers in melt-powder-melt-growth processed $YBa_2Cu_3O_7$.* Physical Review B, 1993. **48**(18): p. 13922–13938.

15. Bugoslavsky, Y., G.K. Perkins, X. Qi, L.F. Cohen and A.D. Caplin, *Vortex dynamics in superconducting MgB_2 and prospects for applications.* Nature, 2001. **410**(6828): p. 563-565.

16. Finnemore, D.K., J.E. Ostenson, S.L. Bud'ko, G. Lapertot and P.C. Canfield, *Thermodynamic and transport properties of superconducting $Mg^{10}B_2$.* Physical Review Letters, 2001. **86**(11): p. 2420-2422.

17. Majoros, M., B.A. Glowacki and A.M. Campbell, *Magnetic screening as a possible way to decrease transport AC losses in multifilamentary superconductors — basic theoretical considerations.* Physica C-Superconductivity and Its Applications, 2001. **334**(3-4): p. 129-140.

18. Genenko, Y.A., A. Snezhko and H.C. Freyhardt, *Overcritical states of a superconductor strip in a magnetic environment.* Phys. Rev. B, 2000. **62**(5): p. 3453-3472.

19. Sumption, M.D., E.W. Collings, E. Lee, X.L. Wang and S.X. Dou. *Suppression of AC (hysteretic) loss by magnetic shielding of MgB_2/Fe superconductors: the pseudo-Meissner effect*. in *ICMC 2001 Conference*. 2001. Madison, Wisconsin.

20. Rikitake, T., *Magnetic and Electromagnetic shielding*. 1987, Tokyo: Terra Scientific Publishing Co. 43.

21. Friedel, J., P.G. de Gennes and J. Matricon, Applied Physics Letters, 1963. **2**: p. 119.

22. Horvat, J., S. Soltanian, X.L. Wang and S.X. Dou, *The effect of sample size on field dependence of J_c for MgB_2 superconductor.* cond-mat/0304004, 2003.

23. Oussena, M., P.A.J. de Groot, S.J. Porter, R. Gagnon and L. Taillefer, *Vortex channeling along twin planes in $YBa_2Cu_3O_{7-x}$.* Physical Review B, 1995. **51**(2): p. 1389-1392.

24. Jin, H., H.H. Wen, H.P. Yang, Z.Y. Liu, Z.A. Ren, G.C. Che and Z.X. Zhao, *Rigid vortices in MgB_2.* Applied Physics Letters, 2003. **83**(13): p. 2626-2628.

25. Qin, M.J., S. Keshavarzi, S. Soltanian, X.L. Wang, H.K. Liu and S.X. Dou, *On the sample size dependence of the critical current density in MgB_2 superconductors- art. no. 012507.* Physical Review B, 2004. **69**.

CHAPTER 7: CONCLUSION

Fe-clad MgB_2 tapes made by powder-in tube technique show a superconducting core with large clusters of grains about 100 μm in size. They reveal a sharp transition with a transition width ΔT_c of 0.2 K and transition temperature T_{c0} of 37.5 K. A transport critical current density of 1.7×10^4 A/cm^2 for both 29.5 K in 1 T and for 33 K in null field has been obtained. The effects of sintering time and temperature on the critical current densities of Cu, Ag and Fe-clad MgB_2 wires have been also investigated. It was found that a short time heat treatment in the fabrication of Cu and Ag clad MgB_2 wires can markedly enhance the critical current density. A total sintering time of several minutes is enough to form nearly pure MgB_2 with high performance characteristics. The Cu and Ag clad MgB_2 wire samples which were sintered for 6 minutes are better than those sintered for longer times. J_c of 1.2×10^5 A/cm^2 in zero field and above 10^4 A/cm^2 in 2 T at 20 K have been achieved for Ag-clad MgB_2 wire sintered for a short period of time. Moreover, it is evident that long MgB_2 wires and solenoid coils can be fabricated using the wind-reaction *in-situ* technique with little J_c degradation over the entire length, paving the way for design and fabrication of the magnetic windings and magnets which are the central element for many large scale applications.

We demonstrated that a very high critical current density can be achieved by a readily achievable and economically viable chemical doping with nano-C or nano-SiC. By studying the SiC doped samples, it was found that there are two closely related but distinguishable mechanisms: H_{c2} and flux pinning that jointly control the performance of $J_c(H)$. Nano-scale SiC doping into MgB_2 enhances both H_{c2} and flux pinning. Alloying at B and Mg sites due to C substitution and the formation of nano-domain structures will cause strong scattering over a wide range of temperatures, leading to enhancement in H_{c2}. A high concentration of various nano-scale impurity phases results in high resistivity, a low residual resistivity ratio and a large irreversibility field and upper critical field with modest T_c reduction. The highly dispersed nanoscale precipitates $MgSi_2$, BC, BO_x, and $SiBO_x$ and the extensive domain structures at a scale well below 10 nm both serve as strong pinning centres. Large particle impurities such as

unreacted SiC (>100nm) increase resistivity, reduce superconducting volume and do not help the improvement of either flux pinning or H_{c2}. They should therefore be eliminated. The doping with SiC gives enhancements to the critical current density, the irreversibility field and the upper critical field in a manner that helps make MgB_2 potentially competitive with both low and high-T_c superconductors. In Fe-sheathed MgB_2 wire we have further demonstrated that J_c field performance can be significantly improved by nano-SiC doping. J_c values over 100,000 A/cm^2 at 5 K and 5 T and 20 K and 2 T were obtained for Fe clad wire, comparable to both NbTi and HTS. High performance SiC doped MgB_2 wires will have a great potential to replace the current market leaders, Nb-Ti and HTS, for many practical applications at 5 K to 25 K up to 5 T. It was also found that the grain sizes of the precursor SiC have a strong effect on the critical current density and its field dependence. The smaller the SiC grains are, the better the J_c field performance and H_{irr} is. It was found that very fine SiC powder plays an important role in the reaction between Mg+B and SiC. Significant enhancements of J_c and H_{irr} were revealed for all the SiC-doped MgB_2 with added levels up to 15 wt%. A J_c value as high as 20,000 A/cm^2 in 8 Tesla and 5 K was achieved for the sample doped with 10 wt% SiC, which had grain sizes of about 20 nm. The high performance of the nano-SiC doped MgB_2 superconductor will have great potential for practical applications

The effect of nano-particle C doping on the lattice parameters, T_c, J_c and flux pinning in MgB_2 was investigated as well. It was found that both the *a*-axis lattice parameter and the T_c decreased monotonically with increasing doping level. For the sample doped with the highest nominal composition of x=0.4 the T_c dropped only 2.7 K. The nano-C-doped samples showed an improved field dependence of the J_c over a wide temperature range compared with the undoped sample. X-ray diffraction and TEM studies indicate that C reacted with Mg to form Mg_2C_3 and MgB_2C_2 with nano-dimensions. Nano-particle inclusions and substitution, both observed by transmission electron microscopy, are proposed to be responsible for the enhancement of flux pinning in high fields. Although a significant improvement in MgB_2 performance has been obtained by nano-SiC and C doping, there is still no evidence for Si doping whether in Mg or B sites. It is still not clear whether substitution or inclusion is the more effective way to improve the properties of samples. More work is necessary to elucidate the mechanism of flux pinning in the doped samples. There is also a lot of room for further study of nano

particle doping effects on the mechanical properties and stability of samples exposed to water. It is also needs to be pointed out that the fabrication process needs to be optimized in order to achieve better performance for practical applications.

In the final part of the thesis, we performed systematic ac susceptibility measurements on a MgB_2 bulk sample. The magnetic-field- and current-density-dependent flux creep activation energy has been determined to be $U(J,B) \propto J^{-0.2}B^{-1.33}$. Compared to high-temperature superconductors ($U(B) \propto B^{-1}$ for a weakly pinned $La_{1.86}Sr_{0.14}CuO_4$ single crystal and $U(B) \propto B^{-0.5}$ for strongly pinned $YBa_2Cu_3O_x$), the steeply declining dependence $U(B) \propto B^{-1.33}$ results in a steep drop in J_c with magnetic field and suggests that pinning in MgB_2 is quite weak. We also demonstrate by direct transport measurements of I_c that an iron sheath can be used as a very effective magnetic shield with MgB_2 superconducting wires. The initial decrease in I_c with field and the plateau in intermediate fields is a newly observed effect, originating in an interaction between the Fe sheath and the superconductor. Better understanding of this effect can lead to extending the plateau to higher fields and improving the field performance of MgB_2/Fe wires further. It was also shown that the current path in the wires meanders between the grains.

The sample size effect in pure and SiC doped MgB_2 samples has been studied, and the n-factor for both samples was also derived. The doped samples show a larger n-factor and less sample size dependence, indicating a stronger pinning effect by SiC doping in MgB_2 samples. The irreversibility field H_{irr} was found to increase with increasing sample volume as a logarithmic function. The zero field J_c also decreased with decreasing sample volume. More work is needed to clearly understand the mechanism underlying this effect.

Publication During the PhD Study

M. J. Qin, S. Keshavarzi, **S. Soltanian**, X. L. Wang, H. K. Liu, S. X. Dou, *"On the sample size dependence of the critical current density in MgB_2 superconductor"*, Physical Review B, 69 (2004) 012507.

S. Keshavarzi, M. J. Qin, **S. Soltanian**, H. K. Liu, and S. X. Dou, *"Vortex dynamics in pure and SiC-doped MgB_2"*, Physica C in press.

X.L. Wang, J. Horvat, **S. Soltanian**, M.J. Qin, H.K. Liu and S.X. Dou, *"Significant enhancement of critical current density and effective pinning centers in MgB_2 with nano sized SiC, Si and C addition"*, Physica C in press.

S. Soltanian, M. J. Qin, S. Keshavarzi, X. L. Wang, and S. X. Dou, *"Effect of sample size on the magnetic critical current density in nano-SiC doped MgB_2 superconductor"*, Physical Review B, 68 (2003) 134509.

S. Soltanian, J. Horvat, X.L. Wang, M. Tomsic and S.X. Dou, *"Transport critical current of Solenoidal MgB_2/Cu Coils Fabricated Using a Wind-Reaction In-situ Technique"*, Superconductor Science and Technology (Rapid Communication), 16 (2003) L4-L6.

S. Soltanian, X. L. Wang, J. Horvat, M. J. Qin, H. K. Liu, P. R. Munroe, S. X. Dou, *"Effect of grain size and doping level of SiC on the superconductivity and critical current density in MgB_2 superconductor"*, IEEE, Transaction on Applied Superconductivity, 13 (2003) 3273.

S. Soltanian, J. Horvat, X. L. Wang, P. R. Munroe, S. X. Dou, *"Effect of nano-carbon particle doping on the flux pinning properties of MgB_2 superconductor"*, Physica C 390 (2003) 185.

J. Horvat, **S. Soltanian**, X. L. Wang, S. X. Dou, *"Magnetic shielding in MgB_2/Fe superconducting wires"*, IEEE, Trans. on Applied Superconductivity, 13 (2003) 3324.

S. X. Dou, J Horvat, **S. Soltanian**, X. L. Wang, S. H. Zhou, H. K. Liu, P. R. Munroe, *"Transport critical current density in Fe-sheathed nano-SiC doped MgB_2 wires"*, IEEE, Transaction on Applied Superconductivity, 13 (2003) 3199.

A. H. Li, X. L. Wang, **S. Soltanian**, M. Ionescu, J. Horvat, H. K. Liu, and S. X. Dou, *"Effect of sintering temperature on the microstracture and critical current density of nanocrystalline MgB_2 thick films prepared using very fast formation method"*, Journal of Metastable and Nanocrystalline materials, 15-16

(2003) 349-354.

H. K. Liu, S. H. Zhou, **S. Soltanian**, J. Horvat, A. Pan, M. J. Qin, X. L. Wang, M. Ionescu, S. X. Dou, *"Effect of nano-SiC and nano-Si doping on critical current density of MgB_2 superconductor"* Tsinghua Science and Technology, pp307-315. Vol.8, No3. June 2003.

X.L. Wang, S. H. Zhou , M. J. Qin, P. R. Munroe, **S. Soltanian**, H.K. Liu, S.X. Dou, *"Significant enhancement of flux pinning in MgB_2 superconductor through nano-Si addition"*, Physica C, 385 (2003) 461.

E. W. Collings, E. Lee, M. D. Sumption, M. Tomsic, X. L. Wang, **S. Soltanian**, and S. X. Dou, *"Continuous- band batch-processed MgB_2/Fe strands--transport and magnetic properties"* Physica C, 386 (2003) 555.

S. Soltanian, X.L. Wang, J. Horvat, T. Silver, H.K.Liu and S.X. Dou, *"Effects of grain size and grain boundaries on the transport and magnetic properties of charge-ordered $Nd_{0.5}Sr_{0.5}MnO_3$ material"*, Superconductor Science and Technology, 15 (2002) 423.

S. Soltanian, X.L. Wang, A.H. Li, E.W. Collings, K. Lee, M. Sumption, E Lee, H. K. Liu, and S.X. Dou, *"Fabrication and critical current density in 16-filament stainless steel/Fe/MgB_2 square wire"*, Solid State Communications, 124 (2002) 59.

S. Soltanian, X.L. Wang, J. Horvat, T. Silver, H.K.Liu and S.X. Dou, *"Improvement of critical current density in the Cu/MgB_2 and Ag/MgB_2 superconducting wires using fast formation method"*, Physica C 382 (2002) 187.

S.X. Dou, **S. Soltanian**, J. Horvat, X.L. Wang, S.H. Zhou, M. Ionescu , H.K. Liu, *"Enhancement of the critical current density and flux pinning of superconductor MgB_2 by nanoparticle SiC doping"*, Applied Physics Letters, 81 (2002) 3419.

J. Horvat, X. L. Wang, **S. Soltanian**, and S. X. Dou, *"Improvement of critical current in MgB_2/Fe superconducting wires by a ferromagnetic sheath"*, Applied Physics Letters, 80 (2002) 829.

S. Li, O. Prabhakai, T.T. Tan, C.Q. Sun, X.L. Wang, **S. Soltanian**, J. Horvat, and S.X. Dou *"Intrinsic Nanostructural Domains: Possible Origin of Weaklinkless Superconductivity in the Quenched Reaction Product of Mg and Amorphous B"*, Applied Physics Letters, 81 (2002) 874.

M. Qin, X. L. Wang, **S. Soltanian**, H. K. Liu, and S. X. Dou, *"Flux dynamics of MgB_2 superconductor by AC susceptibility measurements" Proc. Int. Cryogenic Mat. Conf.* 16-20/7/01, Eds: B. Balachandran, D. Gruber and K.T. Hartwig, 795-802 (2002).

M. D. Sumption, E. W. Collings, E. Lee, X. L. Wang, **S. Soltanian**, and S. X. Dou, *"Reduction and Elimination of External Field Ac Loss in MgB_2/Fe wire by in-situ Magnetic Shielding"*, Physica C, 378-381 (2002) 894.

M.D. Sumption , E.W. Collings, E. Lee, X.L. Wang, **S. Soltanian**, S.X. Dou, and M. Tomsic, *"Real and apparent loss suppression in MgB_2 superconducting composites"*, Physica C, 382 (2002) 98.

S. Soltanian, X.L. Wang, I. Kusevic, E. Babic, A.H. Li, M.J. Qin, J. Horvat, E.W. Collings, K. Lee, M. Sumption, H. K. Liu, and S.X. Dou, *"High-transport critical current density above 30K in pure Fe-clad MgB_2 tape "*, Physica C, 361 (2001) 84.

S. Soltanian, X.L. Wang, H.K.Liu, J. Horvat, T. Silver, and S.X. Dou, *"Effects of Cr doping on the structure, charge-ordering, transport and spin ordering state in $Nd_{0.5}Sr_{0.5}Mn_{1-x}Cr_xO_3$",* Physica C, 364-365 (2001) 343.

X.L. Wang, **S. Soltanian**, J. Horvat, M.J. Qin, H.K. Liu and S.X. Dou, *"Very fast formation of superconducting MgB_2/Fe wires with high J_c "*, Physica C, 361 (2001) 149.

M.J. Qin, X.L. Wang, **S. Soltanian**, A. H. Li, H.K. Liu, and S.X. Dou, *"Dependence of the flux creep activation energy on current density and magnetic field for MgB_2 superconductor"*, Physical Review B, 64 (2001) R060505.

A.H. Li, X.L. Wang, M. Ionescu, **S. Soltanian**, J. Horvat, T. Silver, H.K. Liu, and S.X. Dou, *"Fast formation and superconductivity of MgB_2 thick films grown on stainless steel substrate"*, Physica C, 361 (2001) 73.